9th Workshop on Three-Dimensional Modelling of Seismic Waves Generation, Propagation and their Inversion

22 September - 4 October, 2008

A strategy to optimize the resolving power of non-linear inversion of surface waves dispersion relations

G.F. Panza

Dept. of Earth Sciences/ICTP, Trieste

panza@dst.units.it

A strategy to optimize the resolving power of non-linear inversion of surface waves dispersion relations.

Giuliano F. Panza
Dipartimento di Scienze della Terra – Universita' di Trieste
SAND group – ICTP

1. Introduction

Geophysics is a branch of physics that deals with a wide number of topics ranging from the study of the physical properties of the Earth, as a basis to infer its structure, to the investigation of static and dynamic processes in the Earth. Even if we limit our considerations to the part of geophysics that studies the spatial distribution of physical properties of the materials, there are a great number of problems, relevant to different and unconnected parts of this science, which have to be analysed. All these problems are characterized by a common method of investigation that consists in the observation, on the Earth's surface, of some geophysical fields (seismic, gravity, electromagnetic, …) due to physical properties of the Earth's interior. Conclusions on the structure of the Earth's interior are validated from the field observed at the Earth's surface, as a result of the spatial distribution of the material properties in the deeper part.

It is possible to predict theoretically the values of geophysical fields expected from a given distribution of corresponding physical properties of the material. Such problems, called as *forward problems of geophysics*, are solved by methods depending on the field's nature.

Estimation of physical parameters of the Earth's material from the values of the field observed in some part of the medium is the *inverse problem of geophysics* (Fig.1.1).

At the first developing stages of geophysics the inverse problems were formulated and solved rather primitively. They were reduced to a choice of one from two or few models, for which the calculated characteristics of the field were in better agreement with the observed values. For this aim, for example, different characteristic of the seismic field (e.g. travel-time curves, dispersion curves of surface waves, periods of free oscillation of the Earth, …) were calculated for the selected models, and compared with corresponding observations. There are many disadvantages in using this approach. First of all, there is no guarantee that among the

alternative models there is the one, which reflects the true Earth's structure. Moreover, there are many unsolved questions concerning the resolving power of observations as well as the errors of unknown models, the search of the optimal model consistent with the observation, etc.
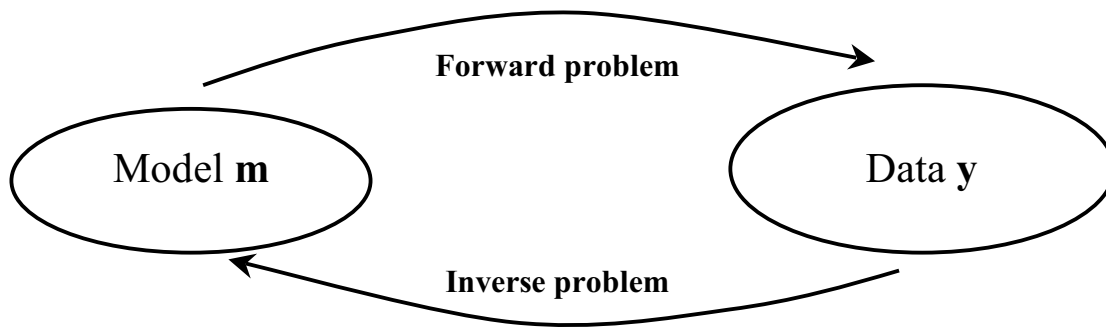

Fig. 1.1: Forward and inverse problem

The need to answer to those and other questions led to the development of methods for solving the inverse problem. In general inverse problems can be formulated as follows:

Given are: the values of some characteristics of the geophysical fields obtained directly from observations, or from preliminary processing (for example the dispersion curves obtained from recorded seismograms). The values are generally discrete and form a data set y_i (i = 1,2,…,n) which we refer to as n-dimensional vector **y**. The observations contain errors, which can also be regarded as the initial data for the inverse problem.

Known is a relationship between the fields and the physical parameters of the Earth's material. Since the properties of the Earth's material are varying from point to point, the physical parameters, describing the correspondent properties, are functions of the coordinates. In general we can introduce the vector **m** whose components represent different physical parameters of the medium, which influence the correspondent geophysical field. We call the vector **m** as the *Earth model*. Different models describing different physical properties of the Earth are, obviously, studied in different problems. In each case an operator should be known in order to calculate the values of the field **y** from the given model **m**:

$$\mathbf{y} = \mathbf{\Phi}\, \mathbf{m} \tag{1.1}$$

the operator **Φ** is called *forward operator*.

Theoretically it would be desirable to construct an operator inverse to Φ, which allows us to find **m** from **y**. However, in a realistic experiment the amount of data that can be used for the determination of the model is usually finite. A simple count of variables shows that the data cannot carry sufficient information to determine the model uniquely.

Observation **y** can be regarded as an element of the space **Y,** and the model **m** as an element of the space **M**. The operator Φ transforms the space **M** into the space **Y**. This transformation is always single-valued. The inverse problem can be considered as the construction of an inverse operator Φ^{-1} transforming the space **Y** into the space **M**. This transformation is not, generally, single-valued. If we display schematically this consideration, then only one point **y** in the space domain **Y** corresponds to a point **m** in the space **M**, whereas a certain domain *m* in the space **M** may correspond to a point **y**; in general the domain *m* may be disconnected (not simply connected) as shown in Fig. 1.2.
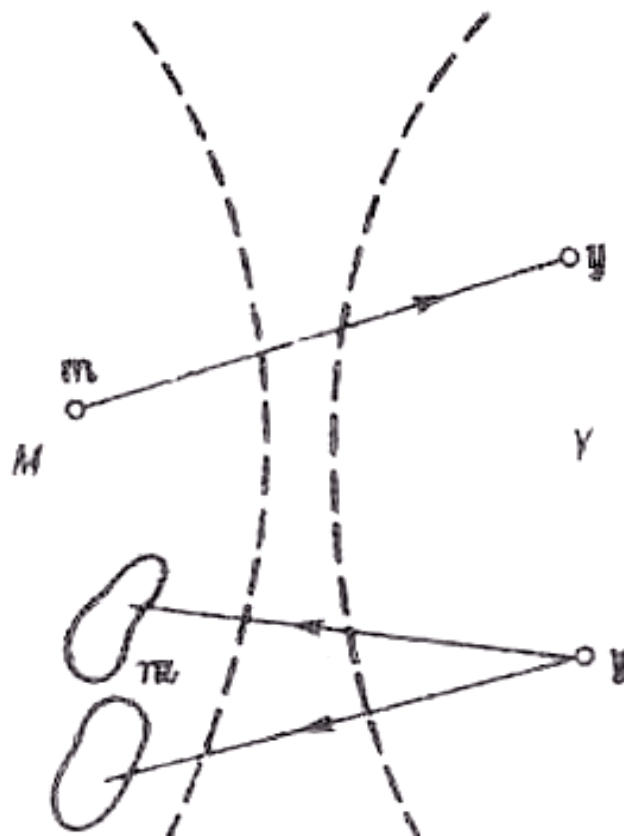

Fig. 1.2: Relation between models space **M** and observations space **Y** (from Yanovskaya, 2003)

For geophysical studies it is important to obtain a set of solutions corresponding to given observations. It is desirable to find such characteristics, which would specify all the models

belonging to the set of solutions. This can be made in two different ways. One way is a priori averaging the model: it means that instead of a true model we estimate some of its average properties. Usually the estimation is performed by the partitioning of the medium into layers (blocks) and by estimating average values of the unknown physical parameters in each layer. In principle, this approach allows us to achieve a one-to-one correspondence between the model and the observations, but the practice is not so easy.

If the averaging is insufficient, we still remain in the situation described above, when to one point from the space **Y** corresponds a domain in the space **M**. On the contrary, if the averaging is too strong, we face the opposite problem: a given point in the space **Y** does not correspond to any point from the space **M.**

The other way is to choose a method for averaging the model directly on the basis of the observations used. Since each data set fixes a corresponding domain in the model space, a method of averaging should be determined by the data set.

Thus, in solving the inverse problem, we may meet both with the non-uniqueness of the solution and with the absence of the exact solution.

For realistic problems the inversion consists in two steps. Let the true model be denoted by m and the data by y. From the observations y, an estimated model $\hat{m}$, consistent with the data, can be reconstructed, and this is called the *estimation problem*. The next step is to determine what properties of the true model are recovered by the estimated model and what errors are attached to it. This step is called the *appraisal problem*. By the end we can say that *inversion = estimation + appraisal* (Fig.1.3).
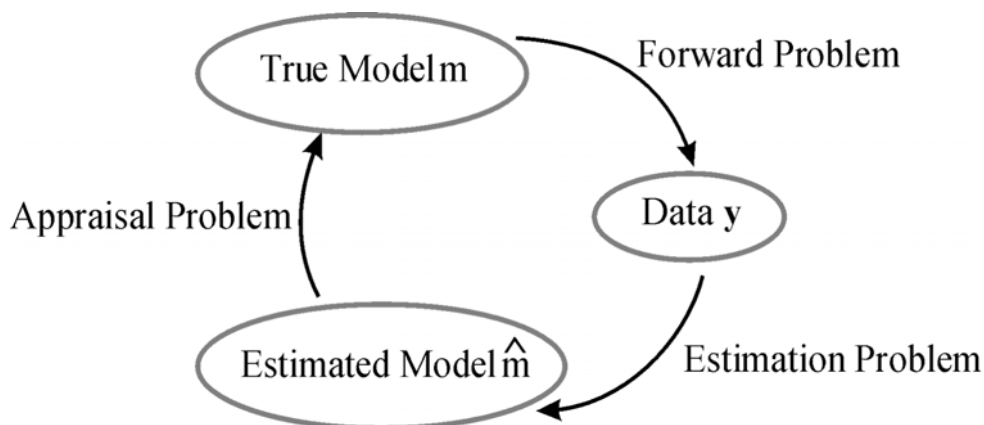

Fig. 1.3: The inverse problem viewed as a combination of the estimation problem plus the appraisal problem.

The determination of the shear wave velocity-depth curve from surface wave phase and group velocity dispersion curves is a severely non-linear problem.

The used approach for facing this non-linearity is based on two steps. The first step constructs surface wave tomography maps; the second makes a non-linear inversion of the dispersion curves extracted from tomographic maps, to obtain shear wave velocity (Vs) models of the Earth interior (crust and upper mantle).

The recording and, to a large extent, the processing of the data to obtain phase and group velocities is a relatively straight-forward procedure. To draw inferences from these velocities about the physical properties of the Earth is, however a much more equivocal process involving serious questions of non uniqueness.

Two different approaches to inversion are used mainly at present. The first can be traced back to the linearized inversion formulated by Backus and Gilbert (1968, 1970). The method is essentially based on the iterative procedure of refining the Earth model by small disturbances of an initial a priori, assumed known, Earth structure. Therefore the linearized inversion strongly depends upon the initial model. The second approach combines different trial-and-error techniques, searching for fitting the observational data among a predetermind set of possible Earth models; the well-known Monte Carlo random search (Keilis-Borok and Yanovskaya, 1967; Press 1968) or the "Hedgehog" random-deterministic search (Valyus, 1972; Valyus et al., 1969, Knopoff, 1972, Panza, 1981) fall into this category. By its nature the non-linear inversion does not depend from the initial model.

To define a set of possible Earth models it is necessary to describe them by a limited number of parameters. Such a parametrization of the Earth is to be based on a priori knowledge of some features of seismic velocities and density distribution within the Earth and the resolving power of the inverted data set.

Results of both approaches to inversion are thus essentially dependent on a priori information.

Very useful textbooks about geophysical inverse theory have been published (e.g. Tarantola 1987; Parker, 1994; Moritz, 1995; Zhdanov, 2002; Yanovskaya, 2003).

2. Parametrization and flow of cross-sections

This step involves the representation of the cross-section through a finite number of numerical parameters and the indication of a priori limits for them. A convenient approach is

the division of the structure into layers and the approximation of each physical function in each layer. The parameters of the structure are thus the parameters of the approximating functions in each layer as well as the depth of the layer boundaries. The physical function in each layer can be approximated by a constant, a straight-line, a parabola or some higher polynomial in z, where z is the depth.

The choice of parameters may be decisive for the success of inversion, since too simple or too complicated an approximation of the structure can produce absolutely meaningless results. It is important to keep the number of parameters, N, as small as possible, for an easy understanding and geological interpretation of the inversion results, but, if the number of parameters is too small, the result is too rough an approximation of the reality, and possibly some of its interesting features are missed. The choice of the parameters must be correlated with the task of inversion. If, for example, a search is made to find out whether some elements of the structure exist, like a wave-guide, a discontinuity within some depth interval, then the assumed set of parameters has to allow the structure both with these elements and without them, and the probability of meeting the considered element by random choice should be about ½. Finally the information really contained in the given observations is the decisive factor in the parametrization.

As a result of the parametrization the cross-section is represented as a point in the space of its unknown parameters, indicating their limits, thus determining the region in which the point lies. Limits can also be imposed on the values of parameters and on any function of them. The problem of inversion is to narrow this region as far as the observations allow. A set of combinations of the unknown parameters has to be found for which the discrepancy between observations and the computed properties is sufficiently small.

The lack of a general theory of solution of this problem makes the following empirical method the simplest and the only one absolutely reliable. The investigated multidimensional region is divided by a net, in each knot of the net the function of parameters is computed and finally the points are chosen in which the misfit function is sufficiently small. For model spaces with more than a few parameters, it is more economical to select points in the model space randomly, than to define a regular grid dense enough to ensure that at least one point will be in the optimal area.

Any method which uses a random (or pseudo-random) generator at any stage is named Monte Carlo. The interest of these methods of inversion is that they can solve problems of relatively large size in a fully non-linear form and independently from the initial guess.

3. The hedgehog non-linear inversion method

The Hedgehog random-deterministic search (Valyus et al, 1969; Valyus, 1972; Knopoff, 1972; Panza, 1981) is one type of approach to the inversion, that fall into the category that combines different trial-and-error techniques, searching for fitting the observation data among a predetermined set of possible Earth models. In fact, this inversion method represents an optimized Monte Carlo search to find velocity-depth distributions consistent with the experimental observations, in such a way to solve problems of relatively large size.
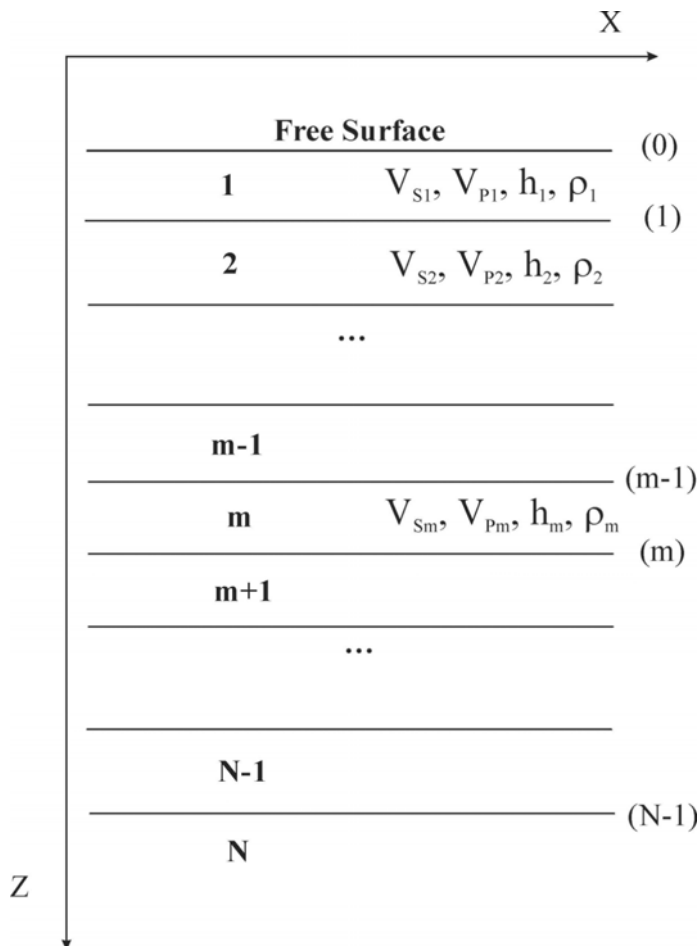
Fig. 3.1: Structural model is modeled as a stack of N homogeneous isotropic layers, each one defined by compressional (V_p) and shear (V_s) wave velocities, thickness (h) and density (ρ). Boundaries between two layers are indicated with (m).

It is "optimized" because guided methods for the research of the minimum are used, resolving the disadvantage of the Monte Carlo method for which the results of the trials already made are not used in the next trial. The solutions retrieved are independent from the starting model. This procedure can be briefly described as follows.

Let $x(P_1, P_2, \ldots, P_N)$ be a single point of the minimum region, where P_i are the parameters of the structure, found by the Monte Carlo search. Then the neighboring points x' are tried:

$$x'(P_i + a_i \delta P_i), \text{ with } i = 1, \ldots, N \text{ and } a_i = 0 \text{ or } 1, \tag{3.1}$$

and certain combinations of a_j are picked in turn. Points, which fall within this minimum region, are selected.
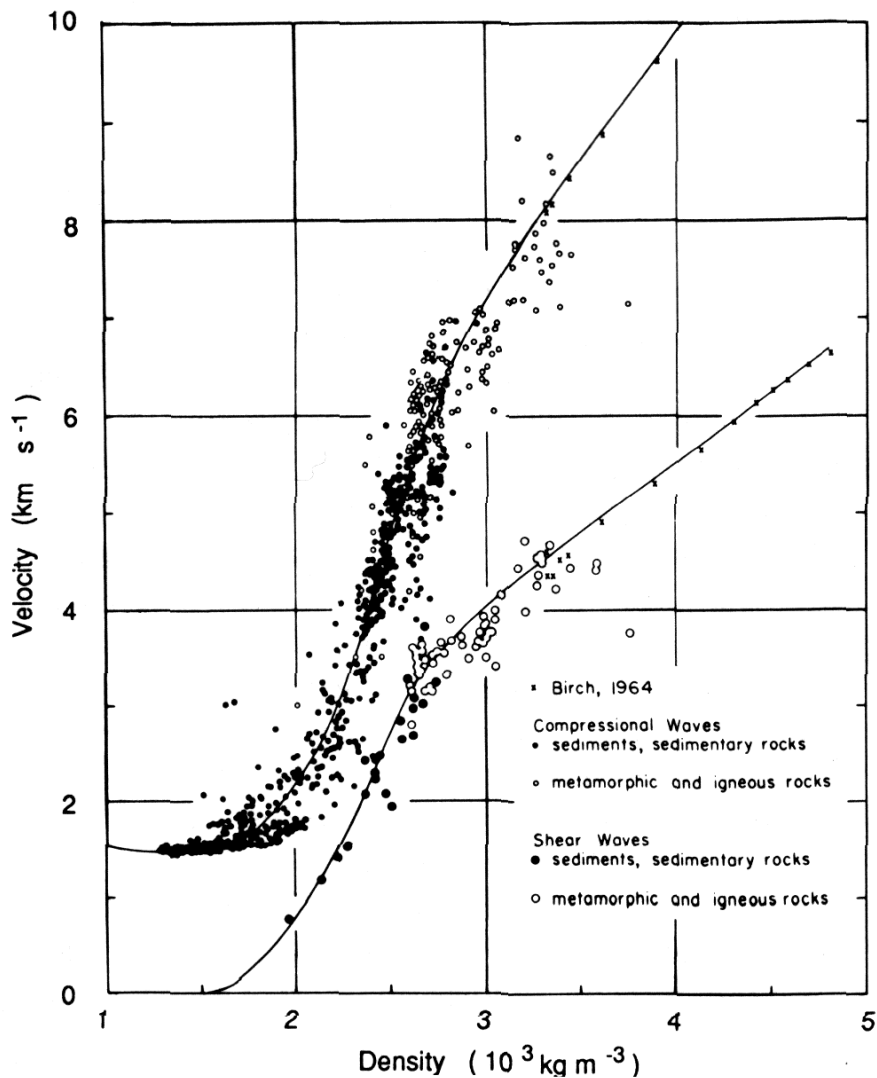
Fig. 3.2: Nafe and Drake curve (e.g. Fowler, 1995; Ludwig et al., 1970) that connects seismic velocities and density.

The same procedure is applied to every selected point until the whole region is covered. Upon this, return is made to the Monte Carlo technique, another minimum region is reached and so on.

The surface wave velocity (the phase velocity appropriately reduced for sphericity) curves are the data used to perform this non-linear inversion method to define average models of the shear wave velocity distribution within the crust and the upper mantle.

Since the unknown Earth model is replaced by a set of parameters and the determination of the structure is reduced to the determination of numerical values of the parameters, in the elastic approximation, the structure is modeled as a stack of N homogeneous isotropic layers (Fig. 3.1), each one defined by compressional and shear wave velocities, thickness and density. The structure is parametrized and each parameter can be fixed (during the inversion the parameter is held constant accordingly to independent geophysical evidences), independent (the variable parameters that can be well resolved by the data) or dependent (the parameter has a fixed relationship with an independent parameter). The variable range limits of the independent parameters, i.e. the region where the real structure exists, must be indicated.

For the choice of the parameterization and of the ranges of variability of the velocity and thickness parameters, we take into account the resolving power of the data (Knopoff and Panza, 1977; Panza 1981) and relevant petrological information that allow us to fix upper and lower limits to the upper mantle V_s.

The available interpretations of the seismic profiles that cross the study area and other information available from literature are used to fix the thickness and the V_p of the uppermost crustal layers, the ones not sampled by the available data set. These layers are, as a rule, assumed to be formed by Poissonian solids, while the density is estimated from the Nafe-Drake relation (e.g. Fowler, 1995, and Ludwig et al., 1970; see Fig. 3.2) that connects seismic velocities and density. The same relation between V_p and V_s and density has been used for all the dependent parameters in the inversion. More recently Yanovskaya and Kozhevnikov (2003) have proposed similar relations consistent with PREM model (Dziewonski and Anderson, 1981), as shown in Fig. 3.3.
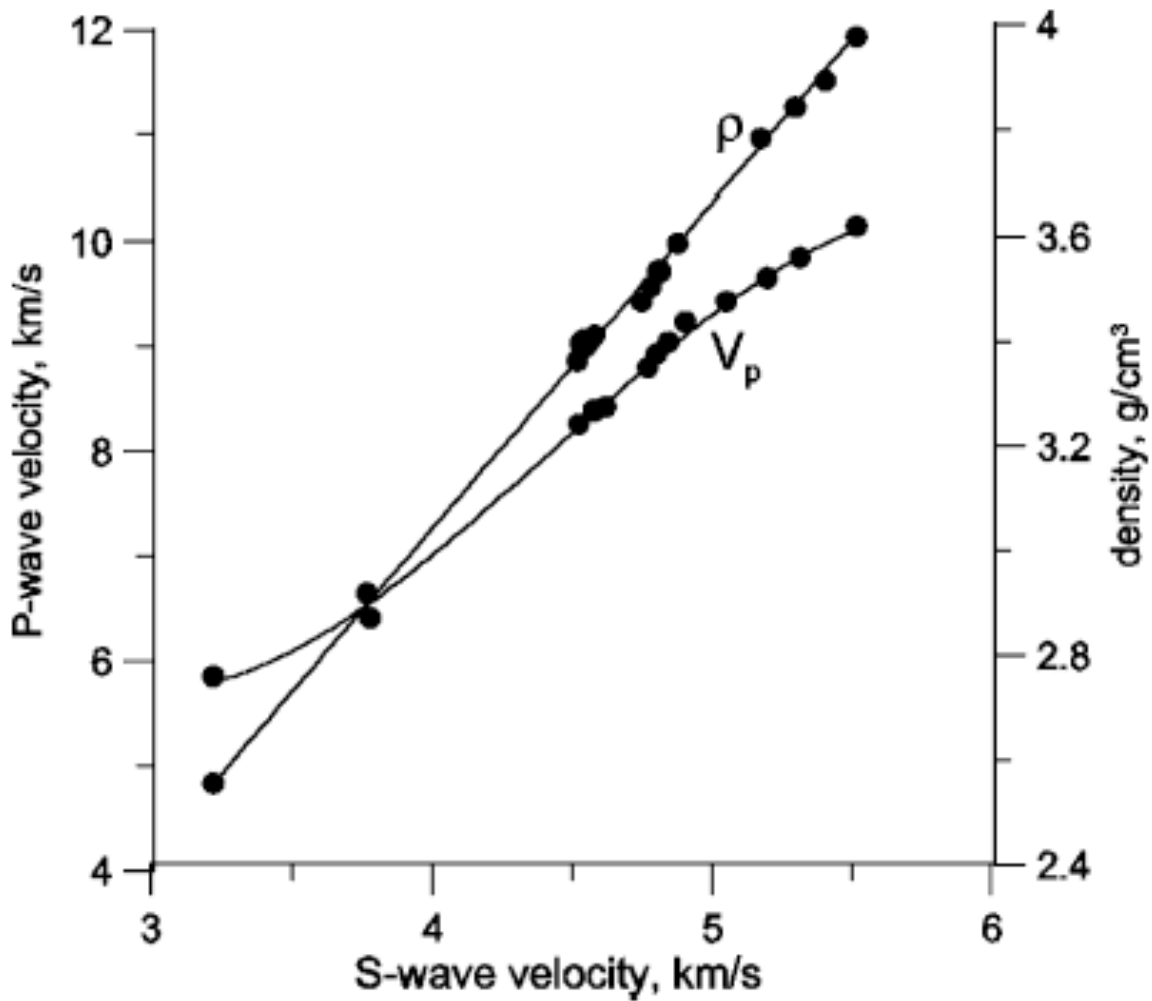
Fig. 3.3: Relationship between P-wave velocity, density and S-wave velocity for PREM. Points represent the PREM (Dziewonski and Anderson, 1981) data, lines represent a possible approximation of the data to be used in inversion studies (from Yanovskaya and Kozhevnikov, 2003)

As a result of the parameterization, any structural model is a point in the space of the unknown parameters. For each structural model in the parameters space, surface wave velocity curves are computed and if, at each period, the difference, $\hat{d}_i$, between the computed and the experimental values (obtained from tomography), is less than the measurement error, and if the r.m.s. of the differences is less than a chosen fraction (usually about 60%) of the average between the error values, the model is accepted (Panza, 1981). The problem is not unique, thus a set of accepted structures is defined. In Fig. 3.4 an example of a six dimensional model space and of the acceptable solutions is plotted.
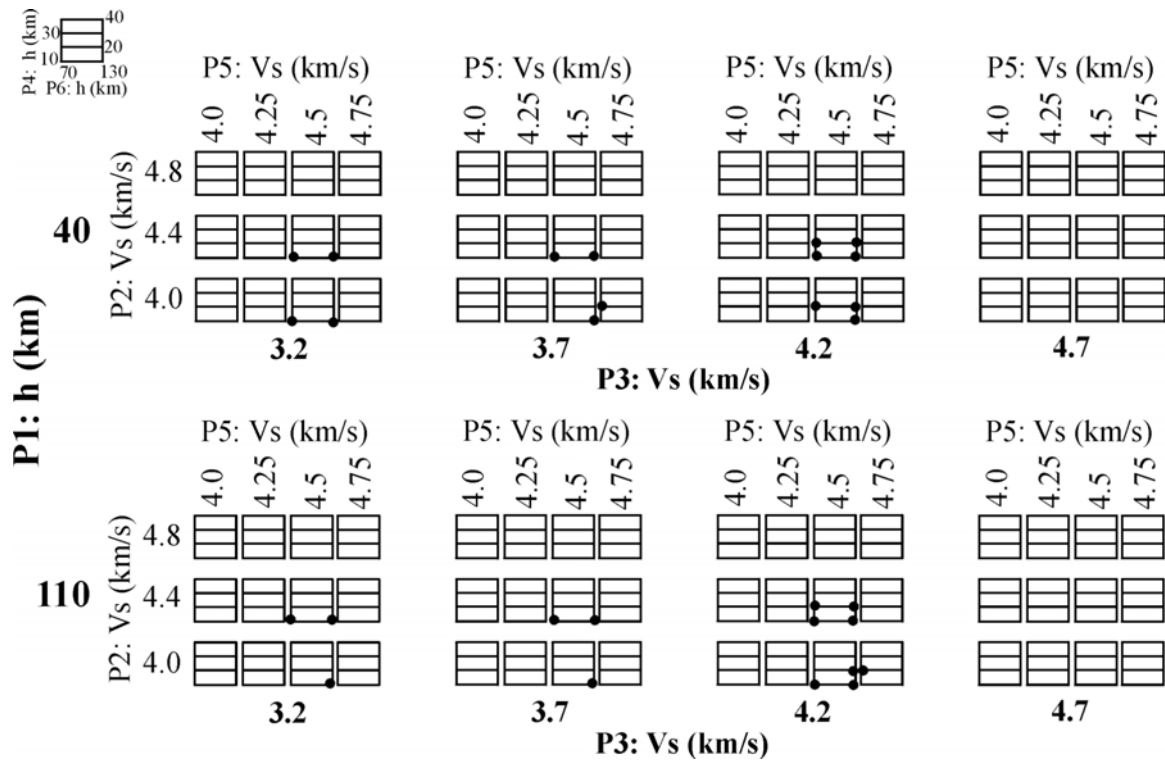
Fig. 3.4: An example of a six dimensional model space of acceptable solutions (the black dots) for the inversion of surface-wave velocity. Thickness and V_s are inverted for three layers (the parameters P1-P2, P4-P3 and P6-P5 are the three couples thickness-V_s for the three layers). The main horizontal scale (bold number) is for P3 parameter (velocity); the main vertical scale (bold number) is for P1 parameter (thickness); the horizontal and vertical scales for each composite sketch are for P5 and P2 velocity parameters, respectively. Each little sketch (in the frame) is bi-dimensional, for P4 (vertical) and P6 (horizontal) thicknesses.

From the experiments of Panza (1981) on the resolving power of dispersion measurements with respect to structural parameters in the crust and in the upper mantle, for a given error, Rayleigh wave group velocities lead, in general, to a better resolution as compared with Rayleigh wave phase velocities. The results of the inversion experiments (Panza, 1981) clearly indicate that the sub-Moho V_s can be determined with a rather good accuracy using indifferently phase or group velocity data, while crustal parameters are better resolved by group velocities.

4. The resolution

The choice of the parameters and of their steps, which, as shown by (4.4), can be used to represent the uncertainty of the inverted parameters, has to be related to the description of the

data variances in the M-dimensional parameter space. Therefore the partial derivatives of the dispersion curves with respect to the considered parameter (Rodi et al., 1975; Urban et al., 1993) have to be calculated, for an average representative structure (e.g. continental, oceanic, rift), at all the periods of the experimental data. The resolving power, which is quantified by the partial derivatives controls the suitable steps that are used in the inversion. The following formulation is due to Panza (1981).

For a known structural model the fundamental mode dispersion relation of group, $U(T)$, and phase, $c(T)$, velocities are computed at selected periods T_i. The velocity $U(T_i)$ and $c(T_i)$ are assumed to have the standard deviations $\sigma_U(T_i)$ and $\sigma_c(T_i)$ respectively. Let the parameters P_j (with j=1, … N) be layer's velocities and/or thicknesses. A description of model variance corresponding to the data variances, in a N-dimensional parameter space, requires the specification of a large number of values. To simplify this task, it is possible to choose to list the diagonal elements of the model error matrix[1], which are the intercepts of the solution ellipsoid with the parameter axes P_j:

$$\left[\frac{1}{N} \sum_{i=1}^{N} \left(\frac{\partial V(T_i)}{\partial P_j} \right)^2 \sigma^{-2}(T_i) \right]^{-\frac{1}{2}} \tag{4.1}$$

where $V(T_i)$ and $\sigma(T_i)$ are considered equal to $U(T_i)$ and $\sigma_U(T_i)$ for the group velocity case, or equal to $c(T_i)$ and $\sigma_c(T_i)$ for the phase velocity case. If the parameter P_j is allowed to vary by an amount δP_j from its starting value, while the others are held fixed at the starting value, then the r.m.s. difference between the exact result and the model result is:

$$\left[\frac{1}{N} \sum_{i=1}^{N} \left(\frac{\partial V(T_i)}{\partial P_j} \right)^2 \right]^{\frac{1}{2}} \delta P_j \tag{4.2}$$

which can be set equal to the pre-assigned value σ. The quantities given by (4.1) can be equalized to the standard deviation in the parameters P_j for the case in which all the other parameters P_i (i ≠ j) are kept fixed at their starting values. Thus the tabulation of the items (4.1) does give some rough information regarding the resolution of the parameter P_j by the data set and the quantities (4.1) can be called the resolution, despite the fact that this

---

[1] i.e. the covariance matrix multiplied by σ^{-2}

definition is inconsistent with other usages in the literature (Knopoff and Panza, 1977; Panza, 1981).

It follows that the proper use of the results given by (4.1) is their application as guiding criteria in the structure parametrization to be used with the hedgehog inversion procedure.

In his experiments, Panza (1981) considers the problem of searching for the most suitable data set for the determination of any given model parameter. If the premise is correct, namely that the inclusion of too much data is deleterious to the program of optimizing resolution, then the problem of finding the proper subset of data can be approached rejecting those data which make the largest contributions to the estimate of (4.1). Thus the maximum resolution for a given model parameter, P_j, could be achieved by retaining only one datum, $V(T_i)$, specifically that for which it is satisfied the condition:

$$\text{Min}\left[\left(\frac{\partial V(T_i)}{\partial P_j}\right)^{-1}\sigma(T_i)\right]. \tag{4.3}$$

This criterion is valid only if all the parameters, except the selected datum, are held fixed and known during the exploration for the optimum value of the parameter. But, since none of the parameters is known, we must take into account the feature that the partial derivative curves often have large wings remote from the peaks (different parameters are correlated). In this case, the variation of the values of phase velocities with respect to one parameter in the neighbourhood of, let's say, a peak in the partial derivative curve, influences the value of variation in the phase velocity in the neighbourhood of partial derivative with respect to the other parameter. Thus the two parameters are not independent, the resolution of each is poorer than the values obtained by (4.3) and the full problem requires the determination of the period for which the quantities δP_j are minima subject to the condition:

$$\sum_j\left(\frac{\partial V(T_i)}{\partial P_j}\right)\delta P_j = \sigma(T_i). \tag{4.4}$$

In applying the hedgehog inversion procedure, the parameterization for the inversion is defined so that the parameter steps are minima, subject to the condition (4.4). Therefore for all the solutions of the Hedgehog inversion, the step associated to each parameter P_j is such that in (3.1) $a_j=\pm 1$ or 0, at the end of the inversion. In this way each parameter step represents a satisfactory estimate of the uncertainty affecting each parameter.

The depth resolution of our dataset is determined by the partial derivatives of the dispersion curves of the Rayleigh wave fundamental mode with respect to the shear-wave velocity at different periods. The vertical resolution of the considered dispersion measurements is consistent with the steps given in Tab. 4.2 and extends to depth of the order of 250 km.

The lateral resolution of the dispersion measurements (phase and group velocities) performed is about 2°x2°. In fact, the grouping of group velocity dispersion relations has allowed identifying areas with similar dispersion properties, but not necessarily with laterally homogeneous structures. The resolution of dispersion measurements is, in fact, only indirectly connected with the lateral structural resolution: to a given dispersion relation can correspond different structural models, depending upon the a priori information used to constrain the inversion.

In the following we present three numerical tests to investigate the effect of different constraints in the fixed structure and of different parameterizations in the inversion.

In TEST-1 we show that the inversion of the same phase velocity dispersion curve but group velocity dispersion curves that differ for $T \leq 25$ s (Fig. 4.1-b1 and Tab. 4.1), can be consistent with significantly different models, depending on the constraints imposed by the a priori knowledge, about the uppermost structure. In this test the non-linear inversion is performed considering different crustal models, e.g. oceanic-like and continental-like: in cases 1 and 3 the uppermost part of the crustal model contains a water layer (1 km and 2.4 km thick, respectively) that is absent in case 2. The parameterization used in the three cases (Tab. 4.2) allows us investigating the parameters of 5 layers below the uppermost fixed structure but the starting values (in parenthesis in Tab. 4.2) of the parameters (or initial structure) and the variability range as well as the steps are different in each case. In Fig. 4.1-a1 the sets of solutions obtained for each case, are shown. The bold line is the structure with the r.m.s. values closest to the average values. Even if the a priori constraint is limited to the uppermost crust, a clear cut differentiation in the lower crust and upper mantle structural properties extends to about 50 km, and the retrieved differences tend to fade out only at depths greater than 100 km. Thus, even if different cells are characterised by equal phase velocities, but by slightly different group velocities and by different a priori constraints at crustal level, the set of solutions of the inverse problem can be quite different even at mantle depths. In other words, the introduction of independent a priori information about the crustal parameters

improves the resolving power of our tomography data at greater depths (e.g. Chimera et al., 2003).

Tab. 4.1: Group (U) and phase (C) velocity values at different periods (from 10 s to 35 s and from 25 s to 100 s, respectively) with the single point error (ρ_U , ρ_C) and the r.m.s. values used in tests 1, 2 and 3. For Test 1 and Test 3, C at all the periods and U at the periods of 30 and 35 s have the same values; the slightly different U values, in the period range 10-25 s, are shaded. Test 2 uses for the three cases the same dispersion curves for U and C.

	TEST 1 and TEST 3												TEST 2			
	Case 1				Case 2				Case 3				Cases 1, 2, 3			
T	U	ρ_U	C	ρ_C	U	ρ_U	C	ρ_C	U	ρ_U	C	ρ_C	U	ρ_U	C	ρ_C
(s)	(km/s)	(km/s)	(km/s)	(km/s)	(km/s)	(km/s)	(km/s)	(km/s)	(km/s)	(km/s)	(km/s)	(km/s)	(km/s)	(km/s)	(km/s)	(km/s)
10	2.16	0.1			2.12	0.1			2.16	0.1			2.16	0.1		
15	2.39	0.08			2.32	0.08			2.29	0.08			2.29	0.08		
20	2.62	0.07			2.54	0.07			2.46	0.07			2.46	0.07		
25	2.87	0.07	3.65	0.11	2.8	0.07	3.65	0.11	2.76	0.07	3.65	0.11	2.76	0.07	3.69	0.22
30	3.07	0.08	3.72	0.09	3.07	0.08	3.72	0.09	3.07	0.08	3.72	0.09	3.07	0.08	3.72	0.18
35	3.26	0.16	3.76	0.08	3.26	0.16	3.76	0.08	3.26	0.16	3.76	0.08	3.26	0.16	3.76	0.16
50			3.85	0.06			3.85	0.06			3.85	0.06			3.85	0.12
80			3.92	0.06			3.92	0.06			3.92	0.06			3.92	0.12
100			3.98	0.06			3.98	0.06			3.98	0.06			3.98	0.12
r.m.s.		0.07		0.55		0.07		0.55		0.07		0.55		0.07		0.09

TEST 1

Grey area

	Case 1			Case 2			Case 3		
	h (km)	vs (km/s)	vp (km/s)	h (km)	vs (km/s)	vp (km/s)	h (km)	vs (km/s)	vp (km/s)
	1	0.0	1.52	4	2.5	4.3	2.4	0.0	1.52
	2	2.6	4.5	9	2.85	4.9	2.1	2.1	3.63
							0.7	2.25	3.9
							2.8	3.25	5.62
	P1	P6	P6x1.73	P1	P6	P6x1.73	P1	P6	P6x1.73
	P2	P7	P7x1.73	P2	P7	P7x1.73	P2	P7	P7x1.73
	P3	P8	P8x1.73	P3	P8	P8x1.73	P3	P8	P8x1.73
	P4	P9	P9x1.73	P4	P9	P9x1.73	P4	P9	P9x1.73
	P5	P10	P10x1.73	P5	P10	P10x1.73	P5	P10	P10x1.73

White area

	Case 1			Case 2			Case 3		
h (km)	δPi (km)	Range (km)		δPi (km)	Range (km)		δPi (km)	Range (km)	
P1(14)	4	2-22	P1(16)	4	8-16	P1(24)	4	12-32	
P2(4)	10	4-24	P2(12.5)	5	12.5-27.5	P2(40)	20	20-40	
P3(15)	10	5-35	P3(10)	20	10-30	P3(35)	20	15-55	
P4(110)	25	60-110	P4(125)	50	25-125	P4(50)	50	50-100	
P5(130)	60	70-130	P5(70)	60	70-130	P5(105)	25	55-105	
vs (km/s)	δPi (km/s)	Range (km/s)	vs (km/s)	δPi (km/s)	Range (km/s)	vs (km/s)	δPi (km/s)	Range (km/s)	
P6(2.75)	0.15	2.3-4.55	P6(3.6)	0.15	2.4-4.5	P6(3.3)	0.1	2.4-4.5	
P7(4.35)	0.2	3.15-4.75	P7(3.85)	0.15	3.25-4.75	P7(4.55)	0.1	3.35-4.75	
P8(3.5)	0.2	3.1-4.7	P8(4.65)	0.4	3.05-4.65	P8(4.5)	0.2	3.7-4.7	
P9(4.6)	0.2	4.0-4.8	P9(4.6)	0.2	4.0-4.8	P9(4.6)	0.2	4.0-4.8	
P10(4.25)	0.25	4.0-4.75	P10(4.0)	0.25	4.0-4.75	P10(4.0)	0.25	4.0-4.75	

TEST 2

Grey area

	Case 1			Case 2			Case 3		
	h (km)	vs (km/s)	vp (km/s)	h (km)	vs (km/s)	vp (km/s)	h (km)	vs (km/s)	vp (km/s)
				1	0.0	1.52			
				2	2.6	4.5			
	P1	P6	P6x1.73	P1	P5	P5x1.73	P1	P7	P7x1.73
	P2	P7	P7x1.73	P2	P6	P6x1.73	P2	P8	P8x1.73
	P3	P8	P8x1.73	P3	P7	P7x1.73	P3	P9	P9x1.73
	P4	P9	P9x1.73	P4	P8	P8x1.73	P4	P10	P10x1.73
	P5	P10	P10x1.73				P5	P11	P11x1.73
							P6	P12	P12x1.73

White area

	Case 1			Case 2			Case 3		
h (km)	δPi (km)	Range (km)		δPi (km)	Range (km)		δPi (km)	Range (km)	
P1(14)	4	2-22	P1(14)	4	2-22	P1(14)	4	2-22	
P2(4)	4	4-28	P2(4)	8	4-28	P2(4)	8	4-28	
P3(15)	10	5-35	P3(15)	5	5-35	P3(15)	20	15-35	
P4(110)	50	60-110	P4(210)	25	60-210	P4(60)	30	30-60	
P5(70)	60	70-130				P5(50)	25	25-50	
						P6(70)	60	70-130	
vs (km/s)	δPi (km/s)	Range (km/s)	vs (km/s)	δPi (km/s)	Range (km/s)	vs (km/s)	δPi (km/s)	Range (km/s)	
P6(2.75)	0.15	2.3-4.25	P5(2.7)	0.1	2.3-4.25	P7(2.75)	0.3	2.15-4.25	
P7(4.35)	0.4	3.15-4.75	P6(4.35)	0.2	3.15-4.75	P8(4.35)	0.4	3.15-4.75	
P8(3.5)	0.2	3.1-4.7	P7(3.6)	0.2	3.1-4.7	P9(3.5)	0.2	3.1-4.7	
P9(4.6)	0.2	4.0-4.8	P8(4.5)	0.1	4.0-4.8	P10(4.6)	0.2	4.0-4.8	
P10(4.25)	0.25	4.0-4.75				P11(4.6)	0.2	4.0-4.8	
						P12(4.25)	0.25	4.0-4.75	

TEST 3

Grey area

	Case 1			Case 2			Case 3		
	h (km)	vs (km/s)	vp (km/s)	h (km)	vs (km/s)	vp (km/s)	h (km)	vs (km/s)	vp (km/s)
	1	0.0	1.52	4	2.5	4.3	2.4	0.0	1.52
	2	2.6	4.5	9	2.85	4.9	2.1	2.1	3.63
							0.7	2.25	3.9
							2.8	3.25	5.62
	P1	P6	P6x1.73	P1	P6	P6x1.73	P1	P6	P6x1.73
	P2	P7	P7x1.73	P2	P7	P7x1.73	P2	P7	P7x1.73
	P3	P8	P8x1.73	P3	P8	P8x1.73	P3	P8	P8x1.73
	P4	P9	P9x1.73	P4	P9	P9x1.73	P4	P9	P9x1.73
	P5	P10	P10x1.73	P5	P10	P10x1.73	P5	P10	P10x1.73

White area

h (km)	δPi (km)	Range (km)
P1(12)	2	6-20
P2(12)	8	4-44
P3(20)	10	10-30
P4(100)	25	50-125
P5(100)	30	40-100
vs (km/s)	δPi (km/s)	Range (km/s)
P6(3.15)	0.3	2.25-4.35
P7(4.05)	0.2	3.85-4.65
P8(3.8)	0.4	3.2-4.6
P9(4.6)	0.2	4.0-4.8
P10(4.0)	0.2	4.0-4.8

Tab. 4.2: Parameterization used in tests 1, 2 and 3. *Grey area*: h (thickness), v_s and v_p of each layer. The variable parameters are Pi, with i = 1, …, 5 for thickness and i = 6, …, 10 for v_s for tests 1 and 3. In Test 2 the number of parameters Pi is different in each case. *White area*: step (δPi), variability range and starting value (in parenthesis) of each parameter Pi. Test 1: the uppermost layers are fixed differently for the three cases, as well as δPi, the variability range and the starting value of the parameters, but the number of parameters is the same; Test 2: the uppermost layers are the same, but the parameterization that follows has different number of parameters (10, 8, 12); Test 3: the uppermost layers are fixed differently (as in Test 1) but the remaining parameterization (δPi, number, variability range and starting value of the parameters) is the same.

Fig. 4.1: Results of tests 1, 2 and 3. (a1, a2, a3) Sets of solutions (thin lines) obtained through the non–linear inversion of the dispersion relations shown in (b1, b2, b3). The investigated parameter's spaces (grey zones) and the chosen solutions (bold lines) are shown as well. The parameterization used in the inversion is given in Tab. 4. (b1, b2, b3) Group (U) and phase (C) velocity curves used in the tests (see Tab. 3).

17

To distinguish the effect of a different parametrization from that of a difference in the data two further tests have been made. In TEST-2 we perform the inversion of the same dispersion curves (Fig. 4.1-b2 and Tab. 4.1) whilst three different parameterizations are used (Tab. 4.2). In the three cases we use the same uppermost fixed structure and the thickness and velocity of 5 layers are inverted in case-1, of 4 layers in case-2 and of 6 layers in case-3. The result of the inversion (Fig. 4.1-b1) shows that the parameterization does not affect the uppermost structure (a low velocity layer is present in all the cases). It also shows, from the number of the obtained solutions (20, 10 and 40 respectively) and from the type of solutions obtained, that 5 layers (10 parameters) is the right number of layers to invert in the depth interval that we are investigating: at depth larger than 100 km the structures in case-1 and 3 have very similar trend, whilst the rough parametrization in case-2 misses a relevant feature like the mantle lvz seen in case 1 and case 3.

In TEST-3 the dispersion curves (Tab. 4.1 and Fig. 4.1-b3) and the parameterization used for the three cases are the same as in TEST-1 but starting values, variability ranges and steps of the parameters (Tab. 4.2) are the same for the three cases. This test, as well as TEST-1, shows in Fig. 4.1-a3 that the sets of structures are quite different also at mantle depths even if the inversion is performed for the same phase velocities and same parameterization but by slightly different group velocities and different a priori constraints at crustal level. Furthermore, a comparison between the sets of solutions of TEST-1 and TEST-3 shows that if the result is not so different for case-2, it is different at crustal and uppermost mantle depths for cases 1 and 3. Thus, not only the number of layers inverted but also the values of the incremental step of the parameters are important, and they must be chosen accordingly to condition (4.4).

5. The choice of the representative solution

The "Hedgehog" inversion produces a set of acceptable models compatible with the data, but, in order to summarize and interpret the results, it is often necessary to identify a representative model. There are two typical approaches: the first one consists in choosing the 'Median Model' of all the solutions (Shapiro and Ritzwoller, 2002) as the representative model; with the second approach the model chosen is that model characterized by the minimum r.m.s.. Both approaches are not fully acceptable in our opinion. In the first case the

'Median Model' may not represent a formally acceptable solution of the inversion process and may indicate a vertical resolving power better than the real one. In the second case the solution with the minimum r.m.s. is the most affected by the presence of possible systematic errors. In alternative, among all the solutions we select that with the r.m.s for phase and group velocities closest to the average r.m.s. for all the solutions; in this way it is possible to reduce the projection of possible systematic errors (Panza, 1981) into the structural model. We tested that, if a median of all solutions in a set is used as representative, the resulting picture is not significantly different from our selected solution.

The parameterization for the inversion is defined so that the parameter steps are minima, subject to the condition (4.4). An example of a set of solutions derived accordingly to (4.4) is given in Table 5.1. For all the solutions the variation of all parameters is no more than $\pm\delta P_i$.

Tab. 5.1: n=order number of solution; P_i, inverted parameters. A good approximated rule is that the number of solutions obtained, n, is comparable with the number of inverted parameters, N, i.e. $n \leq N$.

n	P1	P2	P3	P4	P5	P6	P7	P8	P9	P10	P11	P12
1	0	0	1	0	0	0	0	1	1	1	-1	0
2	1	-1	-1	1	0	-1	0	0	-1	0	-1	-1
3	1	-1	-1	1	0	-1	0	0	-1	1	-1	-1
4	1	-1	-1	1	0	-1	0	0	-1	1	-1	-1
5	0	0	1	-1	1	-1	1	1	1	1	0	1
6	0	-1	1	-1	1	-1	1	0	1	0	0	1
7	0	-1	1	-1	1	-1	0	0	0	0	0	1
8	0	-1	1	-1	1	-1	1	0	1	1	0	1
9	0	-1	1	-1	1	-1	0	0	0	1	0	1
10	0	0	0	-1	1	-1	1	1	-1	0	1	1
11	0	0	0	-1	1	-1	1	1	-1	1	1	1

In Tab. 5.2 the representative solution (i.e. the one corresponding to the average r.m.s.) of the set obtained by the hedgehog inversion is shown with the uncertainty for each of the inverted parameters, according to condition (4.4). For each inverted parameter, we consider the range $[P^r_i \pm \delta p_i/2]$, where P^r_i is the value of the *i*-th inverted parameter of the representative solution and δp_i is the *i*-th step used for the inversion. If the value $P^r_i \pm \delta p_i/2$ falls out of the a priori defined variability range for the hedgehog inversion, the value $P^r_i \pm \delta p_i/2$ is replaced by the extreme value of the variability range. Tab. 5.2 reports the thickness (km) and the shear velocity (km/s) up to the layer following the last inverted layer. As a rule the inverted

quantities are rounded off to 0.05km/s for velocities and to 0.5 km for thickness, if $T_i \geq 10s$. If $T_i \leq 10s$ the rounding of the thickness can be 0.05 km. The thickness marked by * is not a truly inverted parameter, but it satisfies the condition that the total thickness from the free surface to the top of the first fixed layer is equal to a predefined quantity H.

The following form for the table and its caption should be used to represent the results of the Hedgehog inversion:

Cell A2 (12.5; 40.5)		Cell A3 (13.5; 40.5)		Cell A4 (14.5; 40.5)	
h	V_S	h	V_S	h	V_S
(km)	(km/s)	(km)	(km/s)	(km)	(km/s)
3	0.00	1.5	0.00	0.5	0.00
0.7	1.20	2.2	1.20	1	2.60
1	3.45	1	3.45	1.5	3.00
2	4.00	2	4.00	3	3.35
8-12	4.15-4.45	5-9	3.8-4.2	7-11	2.65-2.85
10-15	3.0-3.4	5.5-9	3.22-3.47	6-10	4.0-4.5
10-30	3.95-4.35	20-35	3.45-3.85	10-16	3.1-3.6
55-80	4.07-4.22	15-38	4.37-4.62	50-78	4.37-4.62
105-140	4.15-4.45	100-130	4.1-4.3	60-95	4.12-4.37
*	4.60	*	4.60	*	4.60
44	4.90	44	4.90	44	4.90

Tab. 5.2: Range of variability of the parameters h (thickness) and Vs for each layer of the chosen solution. In the table the inverted quantities are rounded off to 0.5 km or to 0.05 km/s and we take into account the a priori information used to constrain the inversion, therefore the chosen solution does not necessarily fall in the center of the range that can be smaller than the step used in the inversion. The thickness marked by * is not a truly inverted parameter, but it satisfies the condition that the total thickness from the free surface to the top of the fixed upper mantle is equal to a predefined quantity H (In this case: H=350 km). The structure deeper that H has been fixed accordingly with already published models (Du et al, 1998).

6. Optimization of the results of non-linear inversion

In the early fourteenth century William of Occam wrote "it is vain to do with more what can be done with fewer" (see Russell, 1946, ch.14). What has become known as Occam's razor has also become fundamental in the modern science, i.e. hypothesis should be neither unnecessarily complicated nor unnecessarily numerous. Therefore, the problem arisen from

the multi-valued inversion of surface waves dispersion data is considered in order to identify a representative model between all the equally-probable solutions.

The aim is to construct a three-dimensional velocity model in a certain domain Ω.

The domain Ω is covered by an ε-set, i.e. Ω is divided into many four-sided polygons δ_{ij} (cells). Using *hedgehog* method (Valyus, 1972; Valyus et al., 1969; Knopoff, 1972) the inverse problem is solved in a non-linear way, in each cell. The inversion gives as solution a set of equally probable models among which, for seek of simplicity, a representative one has to be chosen.

The purpose is to aid the choice of one single model in each cell, providing an objective, formally defined method for the selection, that satisfies Occam criterion.

Taking into account the geophysical origin of the problem (surface waves tomography, an intrinsically smoothing technique), the developed criteria of optimization consists in finding, for each cell, the representative solution so that the lateral velocity gradient between neighbouring cells is minimized, this means that the local shape of the physical field has to be as smooth as possible.

One motivation for using the smoothness criteria is that we want to avoid the introduction of heterogeneities that can arise from a subjective choice. In fact because of the well-known non uniqueness of the inverse problem, a set of models fits the observational data with an equivalent level of reliability even though some of them could be only mathematical solutions but could not be acceptable from the physical point of view.

A second matter that has to be considered is that, when we build a 3D velocity model in the studied domain (assembling a number of cells) we insert boundaries between cells. In such a way we force the introduction of new boundary conditions in the wave-velocity equations, which have been solved in each cell, to obtain a lateral homogeneous (1D) layered model.

 Three criteria have been developed, all aimed to minimize the lateral velocity gradient in the studied domain:

1.   the GFO (*Global Flatness Optimization*). It defines the optimized global solution of the inverse problem with respect to the flatness criterion, i.e. it identifies, for each cell, the solution which gives the smoothest picture by calculating all possible combinations between all solutions of all the cells covering the domain Ω. Let us define the set of all global combinations by $G(\Omega)$.

2.   the LSO (*Local Smoothness Optimization)*. Optimized local solution of the inverse problem is the one that is searched, cell-by-cell, considering the neighbors only of the selected cell and fixing the solution as the one that minimizes the lateral velocity gradient in between such neighbors. Starting from the search of the representative solution in one cell (called *starting cell*) we look for the representative solution in all the other cells of the studied domain Ω, following the criteria of maximum local smoothness, i.e. between neighboring cells.

3.   the GSO (*Global Smoothness Optimization*). It is based on the idea of close neighbors, extended to the whole study domain. The method consists of two steps: the first one is to extract a subset Γ(Ω) of G(Ω) such that Γ(Ω) contains all global combinations with close neighboring components along an entire row or column; the second is to minimize the lateral velocity gradient in between contiguous subsets Γ(Ω), following the criteria of maximum smoothness as in the case of LSO method.

Here we focus on the LSO method, used to construct the 3D velocity model for the studied area starting from the results of the *Hedgehog* inversion.

The use of LSO is justified by two reasons, a physical and mathematical one. From the physical point of view we do not want to introduce, between the layers of neighboring cells, unnecessary discontinuities in the physical parameters (in our case shear-wave velocities). From the mathematical point of view we have to face the problem that the hedgehog inversion gives, as result, a one-dimensional model, i.e. a laterally infinite and homogeneous layered model. When the cells are put in contact we force the appearance between them of a vertical boundary, which in principle invalidates the inversion, i.e. the lateral infinity of the model's layers. Therefore the choice of the smoothest solutions is needed also to keep the final result as close as possible to the inversion validity conditions

7. The LSO optimization algorithm

Let us subdivide the studied domain, Ω, with a rectangular-shaped grid G_{NM} with N rows and M columns. G_{NM} is an NxM matrix, so we use both "grid" and "matrix" words to indicate the same object. In case Ω is odd-shaped the same notation convention is kept for convenience and the presence of empty cells is allowed.

Let be **n** the dimension of the model vectors (i.e. **n** is the number of layers in each cell).

Definition 1: Let $\mathbf{w}, \mathbf{v} \in \mathbb{R}^n$ be the solutions of the inverse problem in two neighboring cells (i.e. cells with a side in common). The *distance* between $\mathbf{w}$ and $\mathbf{v}$, or the *divergence* of $\mathbf{w}$ and $\mathbf{v}$, is the standard Euclidean norm:

$$\left\| \vec{w} - \vec{v} \right\| = \left(\sum_{i=1}^{n} \left(w_i - v_i \right)^2 \right)^{1/2} \tag{7.1}$$

where w_i and v_i are the components of $\mathbf{w}$ and $\mathbf{v}$, respectively.

	$\mathbf{u}_{i,j-1}$	
$\mathbf{u}_{i-1,j}$	$\mathbf{u}_{i,j}$	$\mathbf{u}_{i+1,j}$
	$\mathbf{u}_{i,j+1}$	

Fig. 7.1: Representations of solutions in cell δ_{ij} and its neighbours

Definition 2: Let $\delta_{i,j}$ be one cell from the grid covering Ω. By $u_{i,j}^k$ we denote the kth *solution* of the inverse problem in the cell $\delta_{i,j}$. The notation $u_{i,j}$ is used in case that $u_{i,j}^k$ belongs to the set of the solutions in the cell $\delta_{i,j}$, since the exact order number k of the solution is not important.

Definition 3: The set

$$u_l(i,j) = \{u_{i,j}, u_{i,j+1}, u_{ij-1}, u_{i+1,j}, u_{i-1,j} \, ; \, i = 1 \dots N, j = 1 \dots M\} \tag{7.2}$$

is called *local combination* associated to one cell $\delta_{i,j}$. We take one representative solution of the cell $\delta_{i,j}$ and one representative solution for each of its neighbours and we compose u_l as the union of these representatives.

The LSO algorithm is described in the following three steps:

1.   **the data pre-processing** in which the different layering of the models of each cell and, therefore, of the whole domain, is considered and equalized;

2.   **the choice of the starting cell** among all the cells of the domain;

3.   **the optimization algorithm** in which the final method is described and some definition are given.

8. Data pre-processing for LSO

Every solution can be represented as a double column matrix whose row elements are the Vs-wave velocity of each layer and the correspondent layer thickness.

The optimization aim is to minimize the lateral gradient of the velocity field so it is necessary to compare the velocity values of layers with equal thickness and occupying equal depth range.

Therefore the first step of the problem consists in "*matching*" all the layers of all the structures, retrieved with the inversion, for the whole domain Ω. This means that the kth layer's thickness, present at a certain depth, has to be the same for all the models we are dealing with. This is done by adding "virtual" layers into the original structure without changing the velocity value retrieved for it.

An example of original and "matched" models, for two different solutions of the same cell, is given in Fig. 8.1.
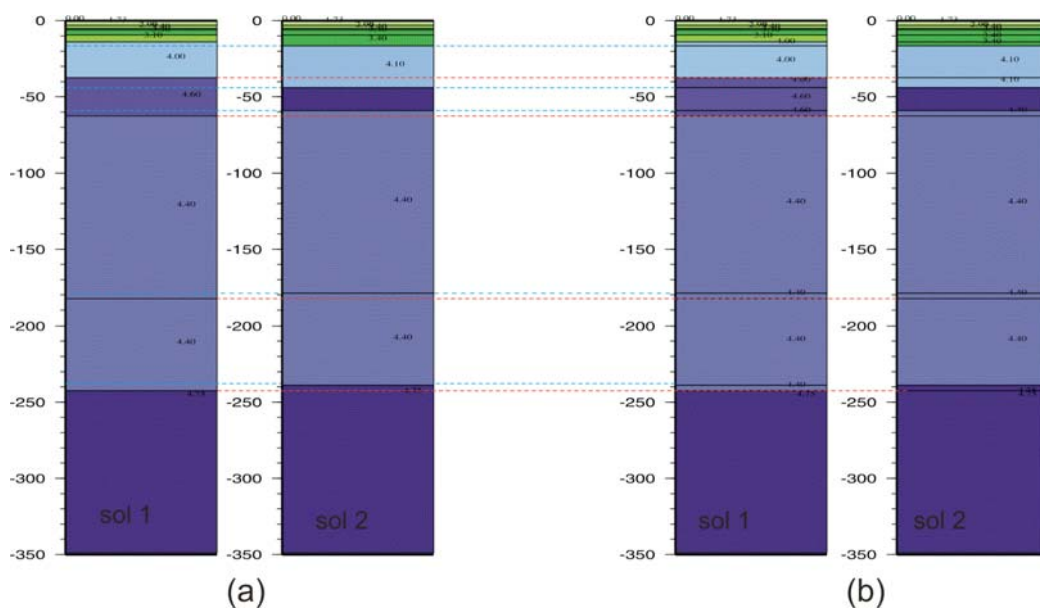
Fig. 8.1: (a) Two different models (sol 1 and sol 2), retrieved by the inversion, for the same cell with the original layering obtained by the inversion; (b) Models after matching. The red dotted lines represent the "virtual layers" added in sol 2 from sol 1 and the blue dotted lines represent the "virtual layers" added in sol 1 from sol 2.

To take into account the contribution of the kth layer thickness, each velocity value has been weighted with the ratio given by the correspondent layer thickness over the total thickness of the structure i.e. in the kth layer the weighted velocity is:

$$V_{wk} = V_k = V_{Sk} \cdot \frac{h_k}{H} \qquad (8.1)$$

where V_{Sk} is the shear-wave velocity in the kth layer, h_k is its thickness and H is the total thickness of the structure:

$$H = \sum_k h_k \qquad \text{and} \qquad \sum_k \frac{h_k}{H} = 1 \qquad (8.2)$$

At the end of this step, each model is represented by a single vector whose elements are weighted velocities V_k.

9. Choice of the starting cell for LSO

Next problem to solve is the choice of the starting cell (*SC*).

Obviously it is possible, for the user, to choose the *SC*. For example one may prefer to start from the cell in the centre of the studied domain Ω, taking into account the fact that in the centre of the area, generally, the resolving power of the data is the best. Another possibility is to start from a cell for which a priori geophysical and geological information is available.

In absence of any a priori constraint it is preferable to have objective criteria in the choice. For this reason it is important to find one discriminator, i.e. a parameter that characterizes each cell and allows us to make a formally defined selection of the initial one.

After the first step, each model is characterized by a vector whose elements are weighted velocities. The entire domain is thus represented by a matrix $\mathcal{E}_{NxM}$ whose elements are:

$$\varepsilon_{ij} = \begin{cases} N_{sol_{ij}} \\ 0 \end{cases} \qquad (9.1)$$

where $N_{sol_{ij}}$ is the number of solutions retrieved for cell δ_{ij}, while 0 means that in the cell the inversion has not been performed. Each solution can be identified by an order number which follows the sequence of the hedgehog results.

According to the definition of the *distance* given by equation 7.1, if $\mathbf{V}_1$ and $\mathbf{V}_2$ are the vectors representing two different models in the same cell, then the distance between them is:

$$d = \left\| \vec{V}_1 - \vec{V}_2 \right\| = \sqrt{\sum_{k=1}^{n} \left[V_{1k} - V_{2k} \right]^2} \qquad (9.2)$$

In each cell δ_{ij}, the distance between any possible couple of its solutions is calculated and the average $\widetilde{d}_{ij}$ of all these distances is the value used to characterize the cell δ_{ij}. The parameter $\widetilde{d}_{ij}$ is the searched discriminator. It is proportional to the variance of the solutions and it gives an estimation of the density of the solutions in the parameter space.

Therefore, as *SC* it has been decided to choose the one with the minimum $\widetilde{d}_{ij}$, i.e. the dependence of the smoothing process on the initial solution is minimized.

In choosing the *SC* a matrix Λ_{NxM}, whose elements are $\widetilde{d}_{ij}$, is computed. The elements of this matrix are subsequently used to define the direction followed to reach the final smoothest picture. The next cell, in which the representative solution has to be defined, is the one, among the neighbours of the last analyzed cell, with the smaller $\widetilde{d}_{ij}$.

10. LSO optimization algorithm

The first iteration, of the optimization algorithm, consists in the determination of a representative solution for the *SC* and, then, iteratively, for all the other cells.

Therefore, let $\delta_{i,j}$ be the *SC*, for this cell the local combination $u_l(i, j)$ such that:

$$\text{norm}_{i,j} = \min_{k}\left(\alpha_1 \left\| u^k_{i,j} - u_{i,j-1} \right\| + \alpha_2 \left\| u^k_{i,j} - u_{i,j+1} \right\| + \alpha_3 \left\| u^k_{i,j} - u_{i-1,j} \right\| + \alpha_4 \left\| u^k_{i,j} - u_{i+1,j} \right\| \right) \quad (10.1)$$

is searched and the solution $u^k_{i,j}$ for the cell $\delta_{i,j}$ is fixed.

The constants $\alpha_i = 1$ if the neighbouring cell contains solutions, while $=0$ if the cell has not been explored (i.e. if no solutions are available).

At the end of the first iteration a matrix Φ_i (NxM) is generated with elements such that:

· $\varphi_{l,m} = 0$ defines cells for which the representative solution has still to be searched

· $\varphi_{l,m} = -1$ defines not explored cells

· $\varphi_{i,j} =$ is the order number of the chosen solution for the *SC*

An example of such a matrix is given in Tab. 10.1.

The second iteration starts once a representative solution is found in the SC. The next cell, in which the representative solution is searched (*new cell*), is, among the SC neighbours ($\delta_{i\pm1,j}$ or $\delta_{i,j\pm1}$), the one with the minimum $\widetilde{d}$ between $\widetilde{d}_{i\pm1,j}$ and $\widetilde{d}_{i,j\pm1}$.

```
-1  -1  -1  -1  -1  -1  -1  -1  -1  -1  -1  -1  -1  -1  -1  -1
-1  -1  -1   0   0   0   0   0  -1  -1  -1  -1  -1  -1  -1  -1
-1  -1   0   0   0   0   0   0   0  -1  -1  -1  -1  -1  -1  -1
-1   0   0   0   0   0   0   0   0   0   0  -1  -1  -1  -1  -1
-1   0   0   0   0   0   0   0   0   3   0   0   0   0  -1  -1
-1  -1  -1  -1  -1   0   0   0   0   0   0   0   0   0  -1  -1
-1  -1  -1  -1  -1   0   0   0   0   0   0   0   0   0  -1  -1
-1  -1  -1  -1  -1  -1   0   0   0   0   0   0   0   0   0  -1
-1  -1  -1   0   0   0   0   0   0   0   0   0   0   0   0  -1
-1  -1  -1   0   0   0   0   0   0   0   0   0   0   0   0  -1
-1  -1  -1  -1  -1  -1   0   0   0   0   0   0   0   0   0  -1
-1  -1  -1  -1  -1  -1   0   0   0   0   0   0   0   0   0  -1
-1  -1  -1  -1  -1  -1  -1  -1  -1  -1  -1  -1  -1  -1  -1  -1
```

Tab. 10. 1: Output matrix (Φ_i) of the first iteration of LSO. The chosen solution (order number marked in red) has been identified in the SC. The elements $\varphi_{l,m} = 0$ define cells for which the representative solution has still to be searched while $\varphi_{l,m} = -1$ defines not explored cells.

This procedure is applied to any new cell which is individuated as the "more stable" among the neighbours of the last explored cell. This means that the local optimization follows, in the progressive searching of representatives $u^k_{i,j}$, the direction of "maximum stability".

By the end of the second iteration the matrix Φ_f is generated where its elements are the order number of the selected solutions and, the "-1", still defines not explored cells. An example of matrix Φ_f is given in Tab. 10.2.

```
-1  -1  -1  -1  -1  -1  -1  -1  -1  -1  -1  -1  -1  -1  -1  -1
-1  -1  -1   3  14   7   9  10  -1  -1  -1  -1  -1  -1  -1  -1
-1  -1   3   7  13   4   5   6   1  -1  -1  -1  -1  -1  -1  -1
-1   9   8  10  24   1  15   4   5   4   3  -1  -1  -1  -1  -1
-1   7   6  15  17   3   6   3   2   3   9   1  11  13  -1  -1
-1  -1  -1  -1  -1   4  11   7  13   5   4   2   6   4  -1  -1
-1  -1  -1  -1  -1   4   4  14   2   5   9   3   6   3  -1  -1
-1  -1  -1  -1  -1  -1   2   7  13   4   9   6   4   4  13  -1
-1  -1  -1   2   9   4   9  11   8   4   9   8   3   7   2  -1
-1  -1  -1   6   3  15  10   3   1   7  17   1   5  11   8  -1
-1  -1  -1  -1  -1  -1   4   2   7   1   2   8   5   9   9  -1
-1  -1  -1  -1  -1  -1   1   5   3   4  10   4  12   7   1  -1
-1  -1  -1  -1  -1  -1  -1  -1  -1  -1  -1  -1  -1  -1  -1  -1
```

Tab 10.2: Output matrix (Φ_f) of the second iteration of LSO. Elements $\varphi_{l,m} = -1$ define not explored cells, while the others represent, the order number of the selected solution. The chosen solution in the SC is identified by the order number marked in red).

At the end of this step, the optimization algorithm LSO may select, in some cells, a model not fully consistent with existing well accepted models and/or observations. In each of these

cells, it is possible to choose the representative solution according to independent information, to fix the order number of the solution in matrix Φ_i and to run again a second iteration, that now satisfies existing well accepted models and/or observations.

To summarize: a first iteration identifies the representative solution for the *SC* and a second iteration (with or without a priori constraints) identifies the representative solutions for all the other cells.

A rough estimation of the number of computation can be given by formula:

$$c = \left(4n - 1\right)\tilde{c}$$

where $\tilde{c}$ is the average number of solutions per cell and n is the number of cells in the studied domain. However, the real number of computations depends strongly on the initial cell and the direction of the choice for the next cell.

Once the solution for each cell is chosen, as we have just illustrated, to each of the inverted parameters it is reasonable to assign an uncertainty equal to its inversion step. However, if, as in Tab A2.2 (Appendix II) the inverted quantities are rounded off to 0.5 km or to 0.05km/s and we take into account the a priori information used to constrain the inversion, therefore the chosen solution does not necessarily fall in the centre of the range that can be smaller than the step used in the inversion.

11. The cellular models of the lithosphere-asthenosphere system in the Italian region

11.1. Introduction. The present day geologic and geomorphologic setting of the Italian peninsula and surrounding areas is controlled by a complex system of geodynamic processes. This setting is marked by two orogens, the Alps to the north, and the Apennines along the peninsula and Sicily, as described by Carminati et al., (2004) in their interpretation of the Italian geodynamics (Fig. 11.1). Few areas have not been involved by the two orogenic waves, i.e. the Puglia region, part of the Iblean Plateau (SE-Sicily), and a few areas in the Po and Venetian plains. These foreland areas underwent subsidence or uplift movements connected to the migration of the Alpine or Apenninic fronts. The actual Apenninic foredeep can be followed on the external side of the Apenninic chain from Southern Apennines to the Po Plain where it interferes with the older Southalphine foredeep. Furthermore, the Apennines are characterized on their west side by the presence of a back-arc basin, the Tyrrhenian Sea, developed from the Miocene times. Moreover, other geodynamic processes must be taken into account, as described by Meletti et al. (2000) in their seismotectonic model of the Italian peninsula and surrounding areas. These processes are: the anticlockwise rotation of the Adria microplate versus Europe with the rotation pole located in Northern Italy; the shallow asthenospheric wedges in the Northern Apenninic Arc and Calabrian Arc; the Alps-Dinarides joint with the development of compressive-transpressive features along the plate margin; the compression fronts of the Adria-verging outer thrust systems (Southern Alps and Dinarides); the compression fronts of the Adria-verging inner thrust systems (Northern Apenninic Arc and Calabrian Arc) and the inactive compression front in the Southern Apennines; the extensional young fault system between Adria and Europe in the Southern Apennines; the Wadati-Benioff zone of the Southern Tyrrhenian Sea.

Tomographic methods applied to dispersion measurements are often used in studies of the crust and upper mantle in tectonically comples domains (e.g. Yanovskaya et al., 1988; Martinez et al., 1997, 2000 and 2001; Ritzwoller et al., 1998; Yanovskaya et al., 1998; Vuan et al., 2000; Yanovskaya and Antonova, 2000; Yanovskaya et al., 2000; Pasyanos et al., 2001; Karagianni et al., 2002; Panza and Pontevivo, 2004; Pontevivo and Panza, 2006). Here we focus on the Italian peninsula, its bordering seas (Southern Tyrrhenian Sea, Adriatic Sea, and Ionian Sea), the Alpine region and the area of the Dinarides chain, to delineate the gross features of the crust, lid and asthenosphere – the lithosphere-asthenosphere system - as defined by the V_s distribution versus depth. This modelling can be well integrated and refined by direct gravity modelling.
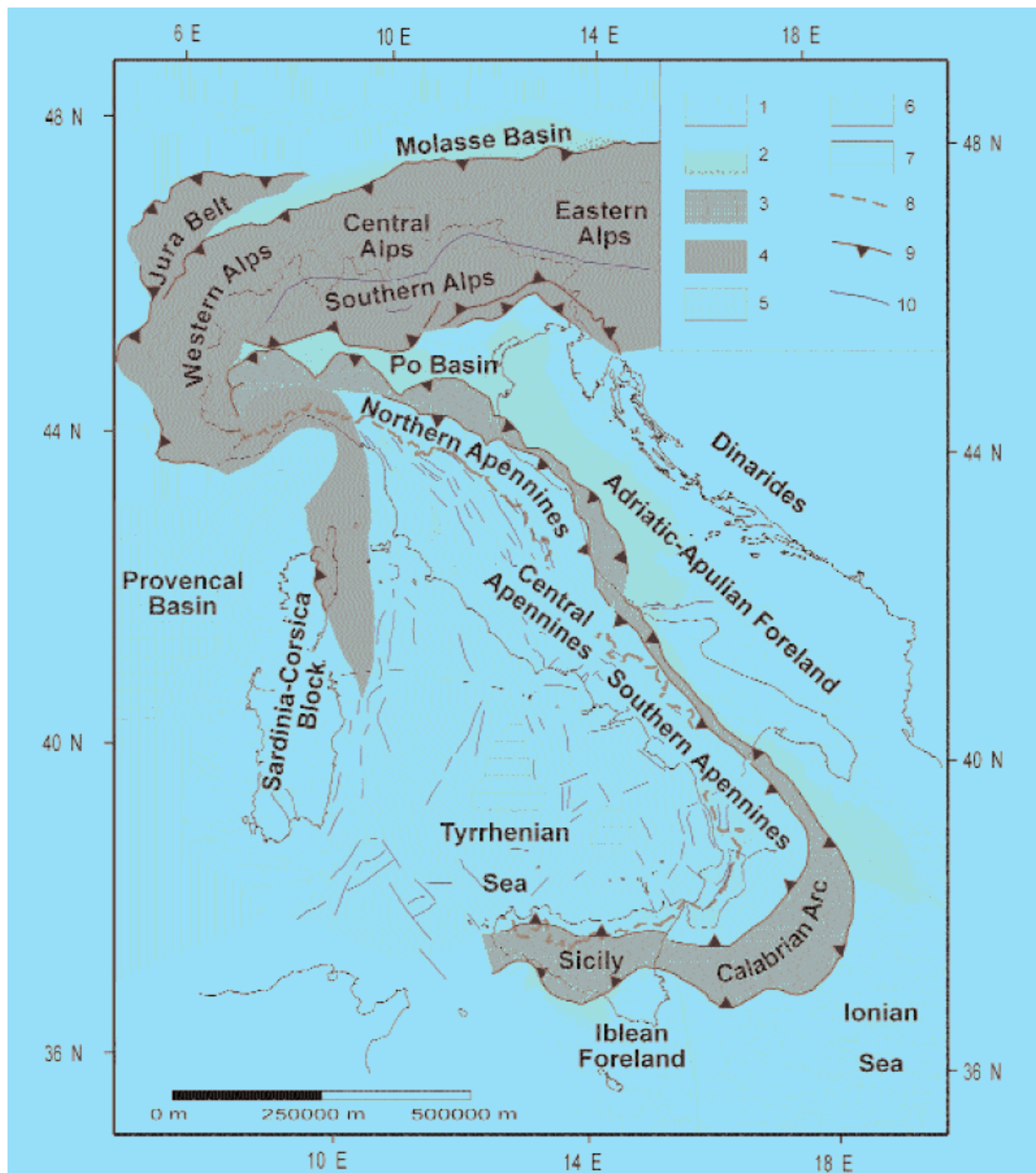
Fig. 11.1: Synthetic tectonic map of Italy and surrounding regions, (Carminati et al., 2004). 1) foreland areas; 2) foredeep deposits (delimited by the -1000 m isobath); 3) domains characterized by a compressional tectonic regime in the Apennines; 4) thrust belt units accreted during the Alpine orogenesis in the Alps and in Corsica; 5) areas affected by extensional tectonics: these areas can be considered as a back-arc basin system developed in response to the eastward roll-back of the west-directed Apennines subduction; 6) outcrops of crystalline basement (including metamorphic alpine units); 7) regions characterized by oceanic crust: an oceanic crust of new formation has been recognized in the Provençal Basin (Miocene in age) and in the Tyrrhenian sea (Plio-Pleistocene in age) while an old Mesozoic oceanic crust could be inferred for the Ionian Basin; 8) Apennines water divide; 9) thrust front; 10) faults.

11.2. The data. To determine the S-wave velocity structure, a set of sequential steps has been followed, as shown in Fig. 11.2.
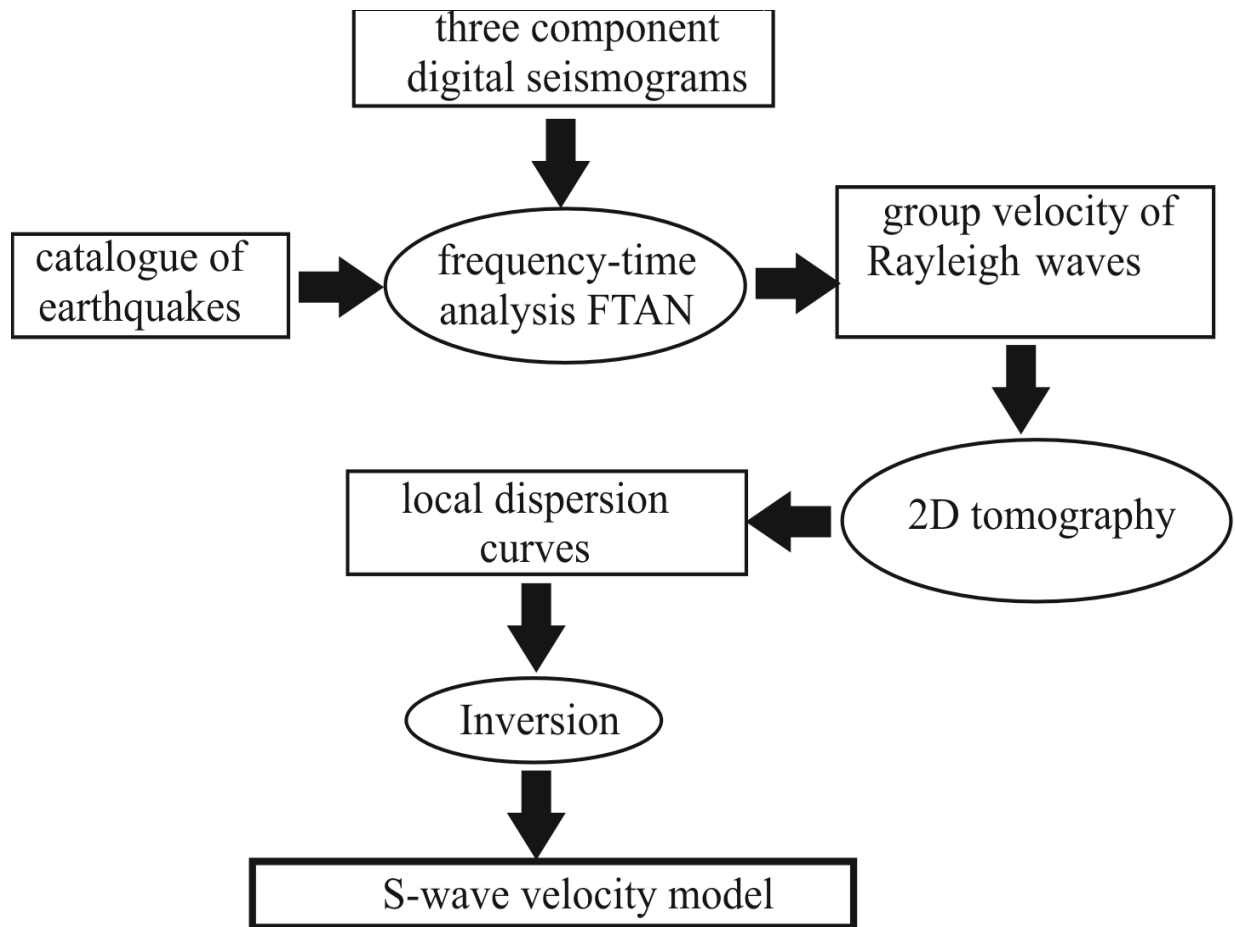
Fig. 11.2: Block-diagram of the methodology used to obtain S-wave velocity models.

The available surface waves dispersion curves at regional scale (Pontevivo and Panza, 2002; Pontevivo, 2003), determined by the two-stations method (Panza, 1976) or by the Frequency Time Analysis (Levshin et al., 1972; 1992) have been used to obtain tomography maps, using the two-dimensional tomography algorithm developed by Ditmar and Yanovskaya (1987) and Yanovskaya and Ditmar (1990). The database of the group velocity dispersion curves and tomography maps (Pontevivo and Panza, 2006) have recently been reviewed and improved (Raykova et al., 2004). More than 600 3-component digital seismograms recorded at the stations located in the Italian peninsula and bordering areas - Adriatic, Ionian and Tyrrhenian seas, Greece, Croatia, Slovenia and Albania - have been analyzed. The period range of the group velocity dispersion curves derived from the records collected at regional distances (300 km – 4000 km) is between 7 and 80 sec, while longer period group velocity data, collected from global studies, available at the Center for Imaging

the Earth's Interior in the University of Colorado at Boulder (http://ciei.colorado.edu/~nshapiro/MODEL/index.html), have been used to extend the period range up to 150 sec, see also (Ritzwoller and Levshin, 1998; Shapiro and Ritzwoller, 2002). Therefore the database is suitable to explore the S-wave velocity structure down to a depth of about 300 km.

The lateral resolving power of the available dispersion data is of about 200 km (Pontevivo and Panza, 2002); however the availability of a priori independent geological and geophysical information, about the uppermost part of the crust, improves the lateral resolving power and justifies the choice to perform the non-linear inversion of dispersion curves averaged over cells of a 1°x1° grid (Pontevivo, 2003; Panza et al., 2003a, b; Panza and Pontevivo, 2004).

In Fig. 3.3 (a, b) the distributions of the seismic paths used to obtain phase and group velocity tomography maps, respectively, are shown.

(a)

(b)
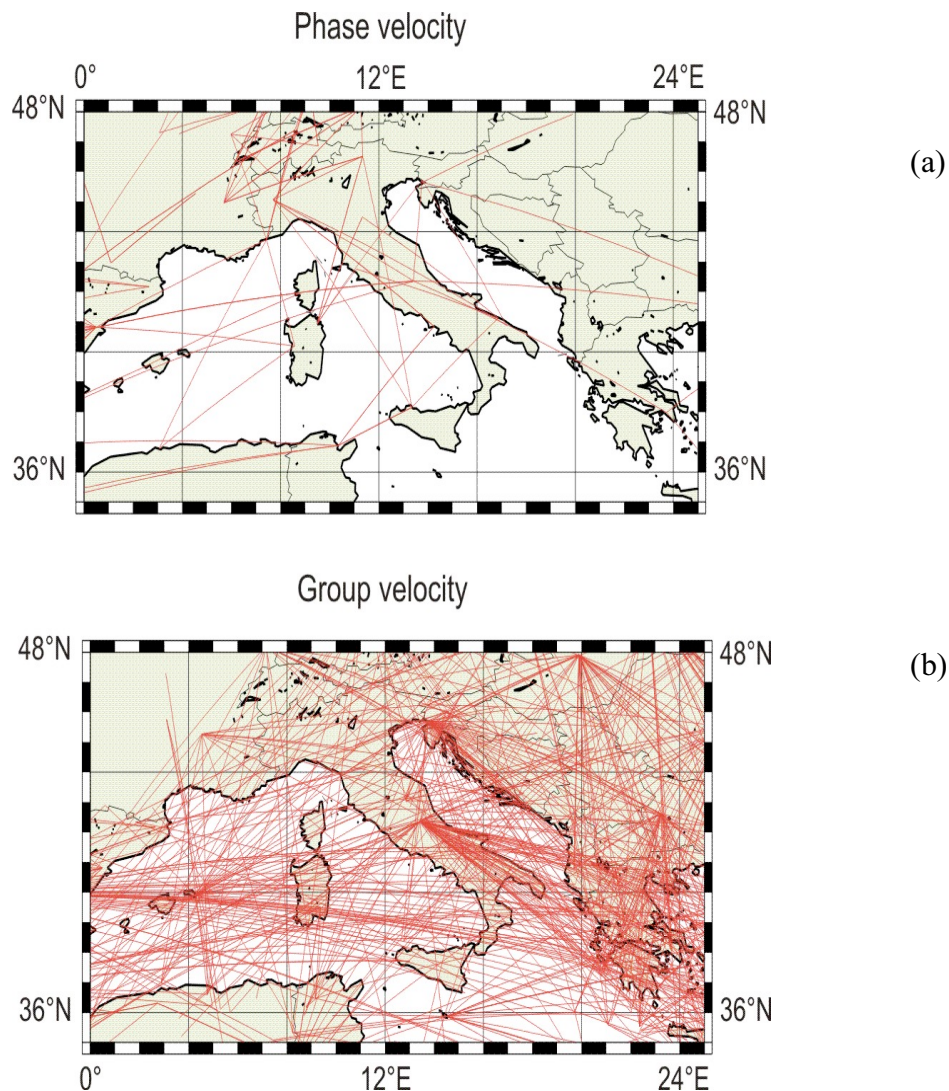
Fig. 11.3: (a) Analyzed paths for the Phase velocity tomography; (b) Analyzed paths for the Group velocity tomography

In Fig. 11.4 a, b tomographic maps at different periods for group and phase velocity, respectively, are shown. In each map of Fig 11.4a and Fig. 11.4b the percent deviation with respect to the mean group velocity U_{mean}, and the mean phase velocity C_{mean}, respectively, calculated over the whole area at the fixed period specified in each map, is identified by Ref:.

The percent deviation, at period T, in the (x, y) point is defined by:

$$\left(\frac{dV(x,y)}{V(x,y)} \right)_T = \left(\frac{V_{mean} - V(x,y)}{V(x,y)} \right)_T \qquad\qquad (11.1)$$

where V = U, for group velocity and V = C, for phase velocity.

The group velocity maps, that are consistent with that of Martinez et al. (1997 and 2000), particularly at T=30s, reveal significant lateral variation at all shown periods, T. The period range from T=10s to T=35s samples the depth interval from about 5 km to about 50 km, as can be estimated from the analytical partial derivatives of group velocity of Rayleigh waves with respect to the structural parameters (Urban et al., (1993). The tomography maps at the shortest periods, from 10s to 20s, show the main features of the major sedimentary deposits (Lake and Masters, 1997), in particular those in the Southern Adriatic Sea (sediments thickness grater than about 9-10 km) and Ionian Sea (sediment thickness greater than about 7 km).

In the map at T=10s, a negative anomaly, trending NW-SE, can be clearly seen. It corresponds to the thick sedimentary layer present in the Southern Adriatic Sea. The anomaly increases at T=15s and T=20s and starts to decrease at T=25s becoming positive at longer periods. Similar characteristics can be seen in the Ionian Sea, showing the NW-SE trend of the variation of the sediment thickness in this area. The negative anomalies detected at shorter periods along the Apennines chain, are not associated with the presence of thick sediments but, more realistically, they represent low velocity crustal material, which is the result of the inherited compressional tectonics on the ongoing extensional deformation (e.g. Chimera et al., 2003).

The phase velocity maps do not reveal very strong lateral variations in the considered period range (from 30s to 150s). The most evident is the negative anomaly, visible at T=30s, along the Apennines chain and the Alps. At T=50s it is possible to see a negative anomaly in the Southern Tyrrhenian basin in correspondence of the Tyrrhenian volcanoes.
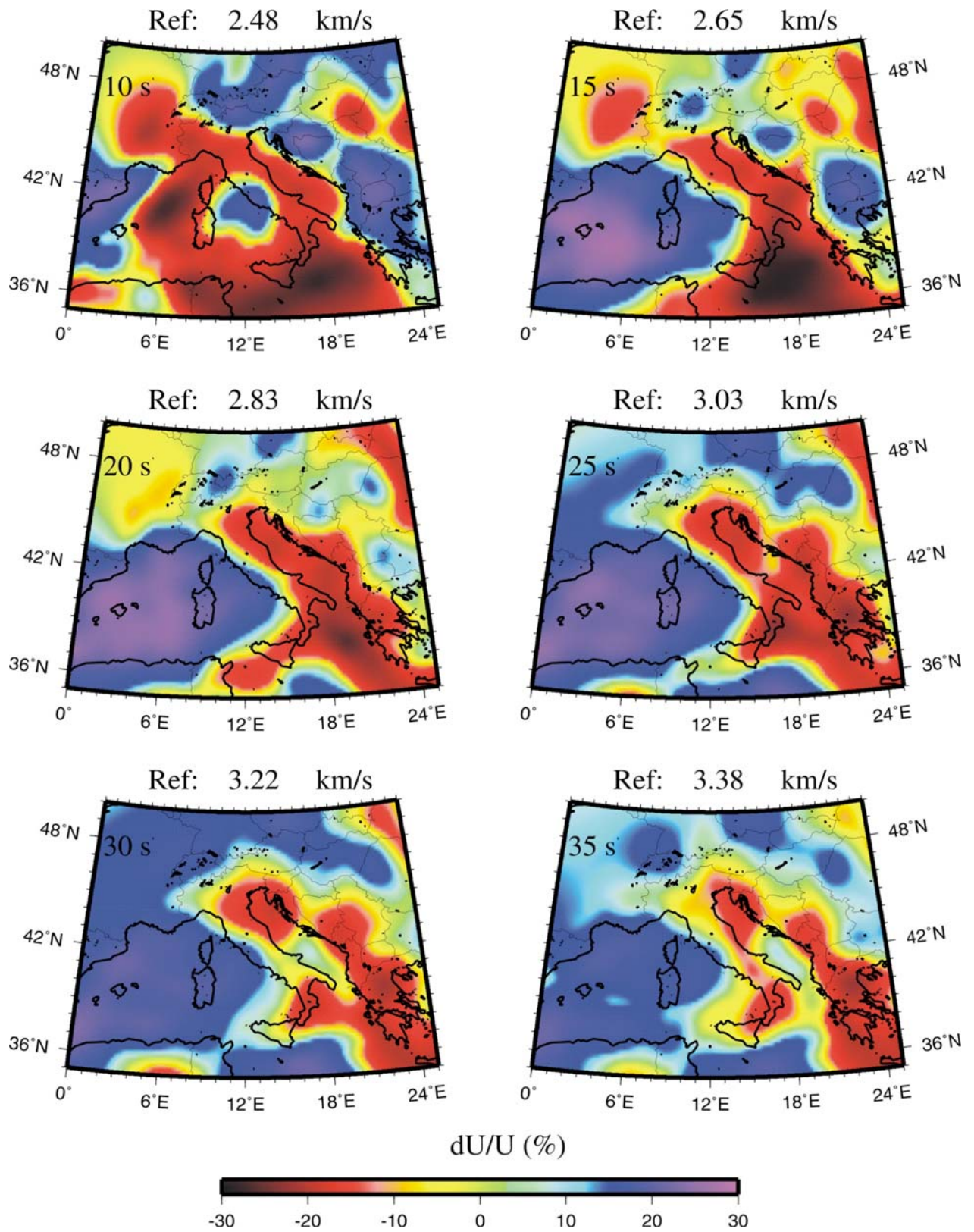
Fig. 11.4a: Group velocity tomography maps at periods ranging from 10s to 35s. The mean velocity with respect the percent variation is calculated has been indicated, in each map, by *Ref:*. In the bottom of the picture the scale of the velocity variation is presented.
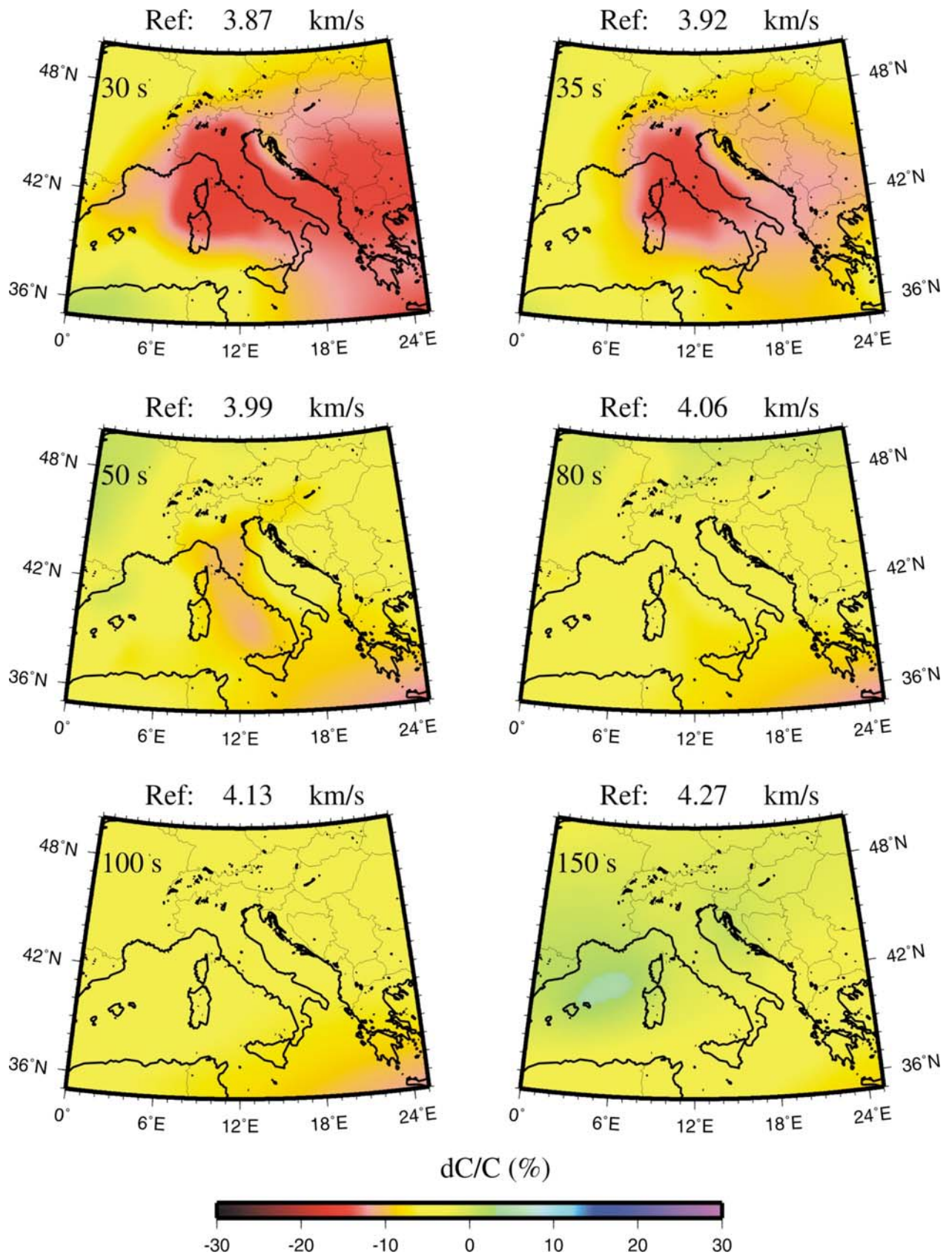
Fig. 11.4b: Phase velocity tomography maps at periods ranging from 10s to 35s. The mean velocity with respect the percent variation is calculated has been indicated, in each map, by *Ref:*. In the bottom of the picture the scale of the velocity variation is presented.

11.3. Non-linear inversion. The determination of the shear-wave velocity-depth curve from surface wave dispersion curves is a severely non-linear problem. The first step of inversion is the construction of surface wave tomography maps; the second is to perform the non-linear inversion of the dispersion curves extracted from tomographic maps, to obtain shear wave velocity (Vs) models of the crust and upper mantle. This can be done superimposing to the tomography maps a grid with mash comparable to the resolving power of the data (1°x1° in our case), thus covering with contiguous cells the study domain Ω (see Fig. 11.5).
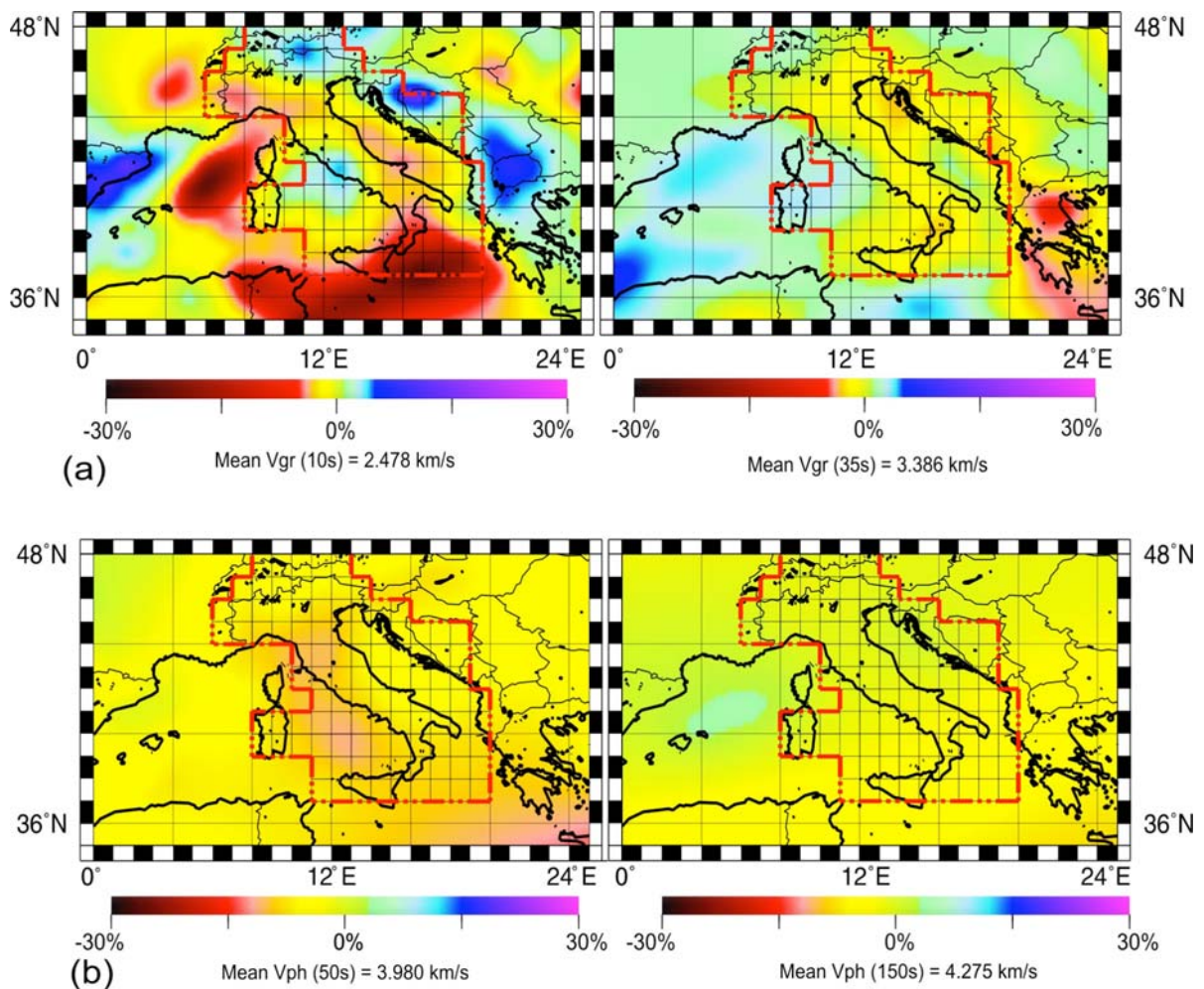
Fig. 11.5: examples of tomography maps with the superimposed grid: a) group velocity, b) phase velocity

Each cell of the grid can be characterised by local dispersion curves (see Fig. 11.6) computed as the average of the values read from the relevant tomography maps at the four knots of each 1°x1° cell.
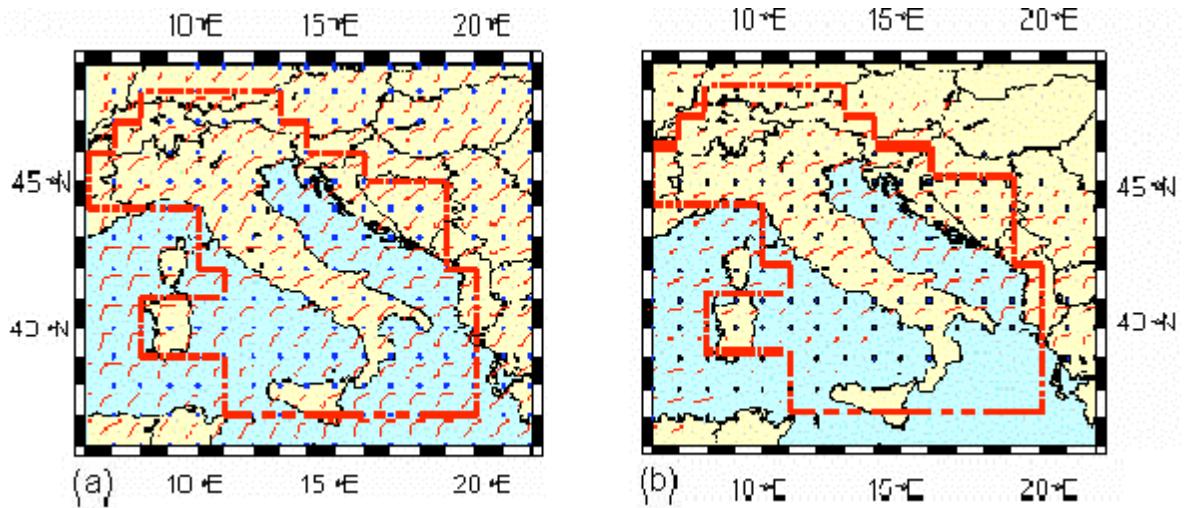
Fig. 11.6: Local dispersion curves for group (a) and phase (b) velocity derived from tomographic maps. The studied region is contoured by a red bold line

Each 1° x 1° cell is defined by the couple of coordinates of its centre and it is identified by one letter and one number, as showed in Fig. 11.7. The cellular dispersion values and related errors, given in Tab. A1.1 (Appendix I) have been inverted using the hedgehog non-linear inversion (Valyus et al., 1969; Valyus, 1972; Knopoff, 1972; Panza, 1981), therefore, contrary to any linearized inversion, the solutions retrieved in such a way are independent from the initial guess.

One of the key parameters in the inversion is the absolute value of the single point error at each specified period. The single error is estimated as the sum of the r.m.s. of the measurement error and the standard deviation of the cellular dispersion curve at each period. The measurement error is determined as the standard deviation of the measurements of group velocity along similar wave paths. The r.m.s. value for the whole dispersion curves is estimated as 65 % of the single error's sum at all specified periods. The value of the group velocity at 80 s is the average between our measurements at this period and global published measurements. The single point error at this period is the r.m.s. of the error of both measurements.

The structure parameterization has been chosen taking into account the resolving power of the data (Knopoff and Panza, 1977; Panza 1981) and relevant petrological information (e.g. Ringwood, 1966; Graham, 1970; Ahrens, 1973; Bottinga and Steinmetz, 1979; Della Vedova et al., 1991). In such a way we have fixed the upper limit of V_s, for the sub-Moho mantle, at 4.90 km/sec, and the lower limit of V_s at 4.00 km/sec for the asthenosphere at depths greater than about 60 km. The thickness and the P-wave velocity of the uppermost crustal layers, assumed to be formed by Poissonian solids, has been fixed using the available interpretations of the seismic profiles, that cross most of the peninsula and adjacent seas, and other information available from literature (Bally et al., 1986; Barchi et al., 1998; Finetti and Del Ben, 1986; Calcagnile et al., 1982; Mantovani et al.,

A-2: 4
A-1: 4
A0: 4
A1: 20, 38
A2: 20, 38
A3: 20, 30, 38
A4: 11, 14, 30
A5: 23, 30
A6: 23, 30
A7: 30 39
A8: 39
A9: 39
B-2: 4
B-1: 4
B0: 4
B1: 20, 27, 38
B2: 20, 27, 38
B3: 20, 27, 38
B4: 20, 27, 38
B5: 20, 24, 28, 38
B6: 20, 24, 29, 30, 38
B7: 10, 29
B8: 39
B9: 39
C1: 6, 33
C2: 6, 33
C3: 27, 33
C4: 27, 29, 30, 38
C5: 27, 29, 30, 38
C6: 18, 20, 27, 38
C7: 7, 19, 20, 38
C8: 7, 19
C9: 7, 8, 19
D1: 38
D2: 6, 30, 38
D3: 6, 30, 38
D4: 38
D5: 12, 15
D6: 7, 8, 15, 16, 18, 38
D7: 7, 15, 19
D8: 7, 12, 15, 19
D9: 7, 12, 15, 19

a1: 39
a2: 30, 38
a3: 30, 38
a4: 23, 30, 31
a5: 23, 30, 35
a6: 39
a7: 39
a8: 39
a9: 24, 39
b0: 2, 9, 22, 27, 30
b1: 2, 9, 22, 27, 30
b2: 2, 9, 22, 30
b3: 2, 9, 22, 30, 35, 38
b4: 8, 22, 39
b5: 39
b6: 39
b7: 26, 39
b8: 39
c0: 30, 34
c1: 2, 30, 34
c2: 2, 9, 27, 30
c3: 2, 9, 27
c4: 21
c5: 21
c6: 3, 26
c7: 3, 26
c8: 3, 26
d-4: 32
d-3: 32
d-2: 34, 37
d-1: 34, 37
d0: 30, 35, 38
d1: 30, 35, 38
d2: 1, 39
d3: 1, 21, 39
d4: 1, 39
d5: 3, 26, 39
d6: 3
d7: 3
d8: 3

Legend:
- Inactive compression front
- Transfer zone
- European plate, including the Corsica-Sardinia block, the Western Mediterranean and the Tyrrhenian backarc basins
- Southern Tyrrhenian Basin
- Compression front
- Wadati-Benioff zone
- Continental-Oceanic crustal transition
- Study area bordering
- Recent volcanoes

e-4: 32
e-3: 32, 34
e-2: 34, 37
e-1: 34, 37
e0: 37
e1: 28, 35, 38
e2: 17, 28, 35, 32
e3: 28, 17, 39
e4: 3, 17
e5: 3

f-3: 34
f-2: 34
f-1: 34, 37
f0: 37
f1: 37, 39
f2: 17, 28
f3: 17, 28

g-2: 34
g-1: 34, 37
g0: 37
g1: 37, 39
g2: 28, 39
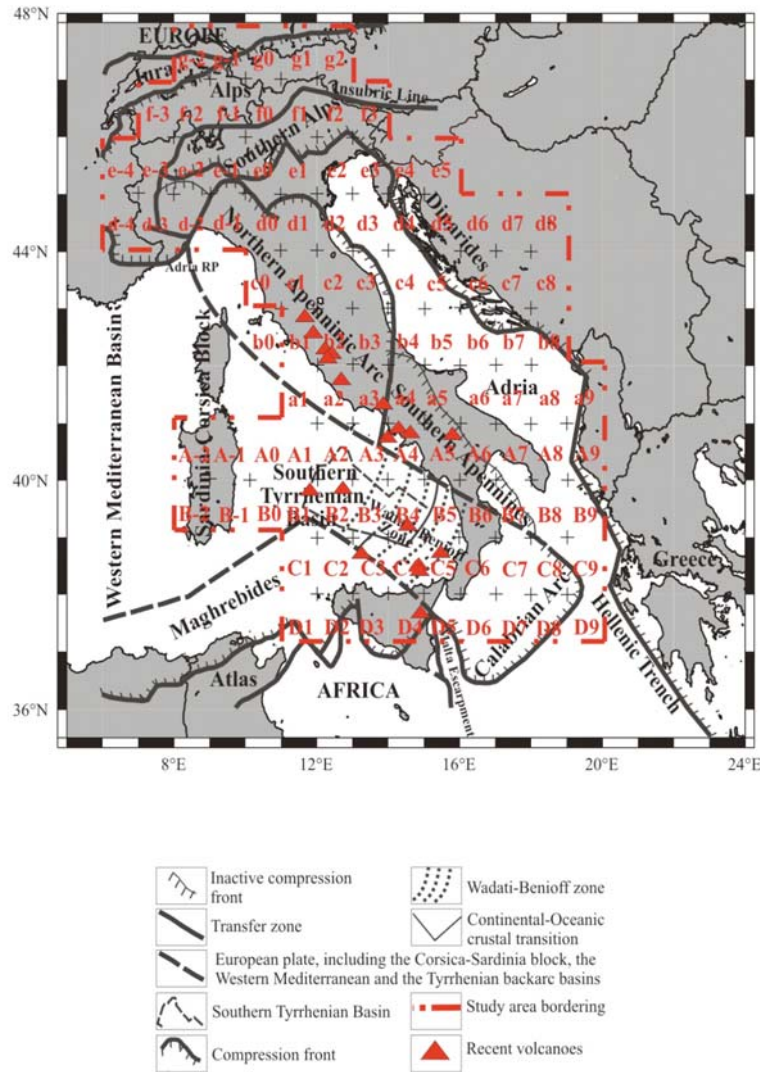
Fig. 11.7: Structural-kinematic model of the study area, modified from Meletti et al. (2000) and, for each cell, the order number of the references (reported in Tab. 11.1) used to fix the upper crust parameters in the inversion.

1	Aljinovic, B., and Blaskovic, I., 1987.
2	Bally, A.W., Burbi, L., Cooper, C., and Ghelardoni, R., 1986.
3	Bondar, I., Zoltan, B., Zivcic, Z., Costa, G., and Levhin, A., 1995.
4	Blundell, D., Freeman, R. St. Mueller, 1992. A continental revealed.
5	Calcagnile, G., D'Ingeo, F., Farrugia, P., and Panza, G.F., 1982.
6	Catalano, R., Di Stefano, P., Sulli, A., And Vitale, F.P., 1996.
7	Catalano, R., Doglioni, C., and Merlini, S., 2001.
8	Cernobori, L., Hirn, A., McBride, J.H., Nicolich, R., Petronio, L., Romanelli, M., and STREAMERS/PROFILES Working Groups, 1996.
9	Chimera, G., Aoudia, A., Saraò, A., and Panza, G.F., 2003.
10	Cristofolini, R., Ghisetti, F., Scarpa, R., And Vezzani, L., 1985.
11	De Gori, P, Cimini, G.B., Chiarabba, C., De Natale, G., Troise, C., and Deschamps, A., 2001.
12	Della Vedova, B., Pellis, G., and Pinna, E., 1989.
13	Della Vedova, B., Marson, I., Panza, G.F., and Suhadolc, P., 1991.
14	De Matteis, R., Latorre, D., Zollo, A., and Virieux, J., 2000.
15	De Voggd, B., Truffert, C., Chamot-Rooke, N., Huchon, P., Lallermant, S. and Le Pichon, X., 1992.
16	Doglioni, C., Innocenti, F., and Mariotti, G., 2001.
17	Fantoni., R., Della Vedova,B., Giustiniani, M., Nicolich, R., Barbieri, C., Del Ben, A., Finetti, I., and Catellarin, A., 2003
18	Ferrucci, F., Gaudiosi, G., Hirn, A., and Nicolich, R., 1991.
19	Finetti, I., 1982.
20	Finetti, I., and Del Ben, A., 1986.
21	Finetti, I., Bricchi, G., Del Ben, A., Pipan, M., and Xuan, Z., 1987.
22	Finetti, I.R., Boccaletti, M., Bonini, M., Del Ben, A., Geletti, R., Pipan, M., and Sani, F., 2001.
23	Improta, L., Iannaccone, G., Capuano, P., Zollo, A., and Scandone, P., 2000.
24	Kern, H., And Schenk, V., 1988.
25	Mantovani, E., Nolet, G., and Panza, G.F., 1985.
26	Markusic, S., Herak, D., Ivancic, I., Sovic, I., Herak, M., and Prelogovic, E., 1998.
27	Marson, I., Panza, G.F., and Suhadolc, P., 1995.
28	Merlini, S., Doglioni, C., Fantoni, R., and Ponton, M., 2002.
29	Morelli, C., 1998.
30	Mostaanpour, M.M., 1984.
31	Panza, G.F., 1981.
32	Paul, A., Cattaneo, M., Thouvenot, F., Spallarossa, D., Béthoux, N., Fréchet, J., 2001.
33	Pepe, F., Bertotti, G., Cella, F., and Marsella, E., 2000.
34	Pfiffnerr, O.A., Schlunegger, F., and Buiter, S.J.H., 2002
35	Pialli, G., Alvarez, W., and Minelli, G., 1995.
36	Scarascia, S., and Cassinis, R., 1992.
37	Scarascia, S., and Cassinis, R., 1997
38	Scarascia, S., Lozej, A., and Cassinis, R., 1994.
39	Transalp Working Group, 2002
40	Venisti, N., Calcagnile, G., Pontevivo, A., and Panza, G.F., 2005.

Tab. 11.1: The references used to fix the upper crust in the parameterization for the non-linear inversion. The numbers associated to each cell in Fig. 3.7 correspond to those indicated on the left in the table.
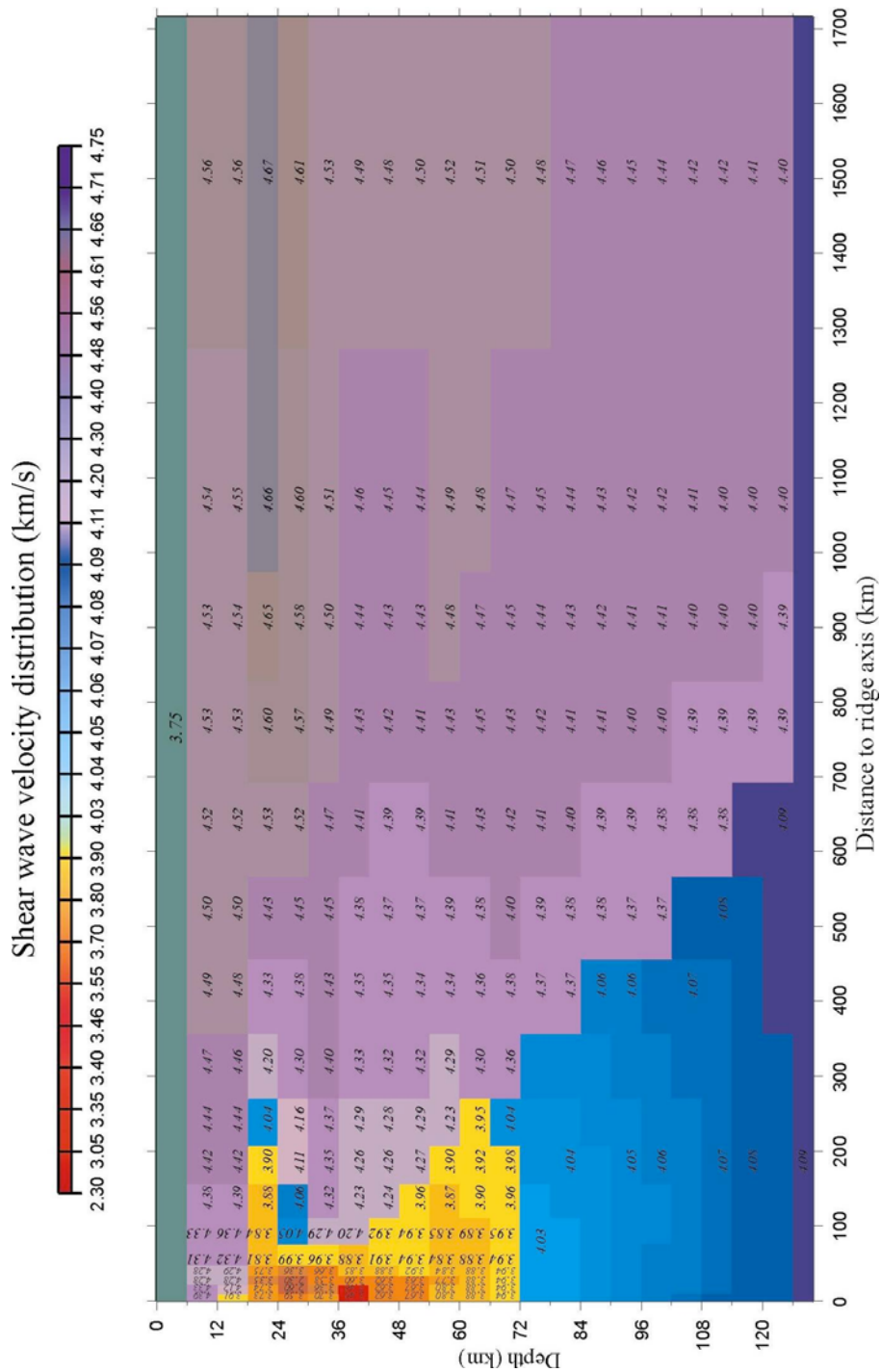
Fig 11.8 Representation of the geophysical, geochemical and petrological model of Bottinga and Steinmetz (1979): shear wave velocity distribution (km/s) in the submarine upper mantle. The relation of the thickness of the thermal boundary layer versus the age of the lithosphere is expressed by: $z(km) \cong 10\sqrt{age(Ma)}$ (Turcotte and Schubert, 1982).

1985; Bondar et al., 1996; Zivcic et al., 2000; Catalano et al., 2001). The density is estimated from the Nafe-Drake relation (e.g. Fowler, 1995; Ludwig et al., 1970) that connects seismic velocities and density (see Fig. 3.2). The step used in the parameterization of the structure roughly represents the

uncertainty of each solution (see eq. 4.4). The thickness of the water layer is chosen according to the standard bathymetric maps. In most of the cells of the study area, one and the same relation between V_s, V_p and the density has been used for all the dependent parameters in the inversion. In cells A2, A3, B1, B2, B3 and B4 (see Fig. 11.7), the value of $V_p/V_s = 2.0$ has been used (see Table A2.1 in Appendix II), in agreement with the geophysical, geochemical and petrological model of the submarine lithosphere proposed by Bottinga and Steinmetz (1979) (see Fig. 11.8). According to the results of Panza (1981) a high V_p/V_s is more consistent with the data than a "standard" one, since in these cells the number of solutions, all ranges and steps of the other inversion parameters remaining fixed, increases when from $\left(V_p/V_s = \sqrt{3} \right)$ we increase the ratio to 2.0.

In Fig. 11.7 the cells grid and indentification are shown. For each cell the used literature (the a priori information), listed in Tab. 11.1 is indicated. In Table A2.1 (Appendix II) the fixed V_p, V_s and h of the upper crustal layers are reported for each cell. The deeper structure, below the inverted layers, is the same for all the considered cells and it has been fixed according to already published data (Du et al., 1998).

11.4. The local smoothing optimization (LSO). For each cell, because of the well-known non-uniqueness of the inverse problem, a set of models fits the observational data, with an equivalent level of reliability. To choose one representative model for each cell, the LSO (Local Smoothing Optimization) method, based on operational research theory (Bryson et al., 1975; De Groot-Hedlin and Constable, 1990), has been applied to the whole area. The method starts from the search of the *starting cell* (*SC*). In order to minimize the dependence of the smoothing process on the initial solution, as *SC* it is chosen the one with the minimal divergence between the accepted velocity models (minimum $\tilde{d}_{ij}$), i.e. inside *SC* the solutions are the densest in the parameter space. In choosing the SC a matrix Λ_{NxM}, whose elements are $\tilde{d}_{ij}$, is computed. The matrix is reported in Tab.11.2. Its elements are the quantities $\tilde{d}_{ij}$ that give, for each cell, an estimation of the stability of the solutions. In the case reported in Tab. 11.2, which covers the entire study area, the *SC* is cell d4 (see Fig 11.7).

Applying the first iteration of LSO, the solution for the SC is chosen such that (10.1) is satisfied, as described in section 10, and the matrix Φ_i (NxM), which is shown in Tab. 11.3, is construcuted. The not explored cells (cells with no data) are identified with -1, while the cells, for which the representative solution has still to be searched, are indicated with 0. The *SC* is identified by the order number of the solution corresponding to the chosen one.

```
       col-4  col-3  col-2  col-1  col 0  col 1  col 2  col 3  col 4  col 5  col 6  col 7  col 8  col 9
0.0000 0.0000 0.0000 0.0000 0.0000 0.0000 0.0000 0.0000 0.0000 0.0000 0.0000 0.0000 0.0000 0.0000 0.0000 0.0000
0.0000 0.0000 0.0000 0.0040 0.0046 0.0041 0.0043 0.0033 0.0000 0.0000 0.0000 0.0000 0.0000 0.0000 0.0000 0.0000 row g
0.0000 0.0000 0.0040 0.0049 0.0037 0.0053 0.0042 0.0048 0.0051 0.0000 0.0000 0.0000 0.0000 0.0000 0.0000 0.0000 row f
0.0000 0.0050 0.0064 0.0052 0.0047 0.0062 0.0055 0.0048 0.0044 0.0054 0.0053 0.0000 0.0000 0.0000 0.0000 0.0000 row e
0.0000 0.0050 0.0048 0.0047 0.0055 0.0050 0.0058 0.0064 0.0051 0.0018 0.0045 0.0055 0.0042 0.0046 0.0000 0.0000 row d
0.0000 0.0000 0.0000 0.0000 0.0000 0.0048 0.0052 0.0047 0.0040 0.0059 0.0050 0.0045 0.0049 0.0041 0.0000 0.0000 row c
0.0000 0.0000 0.0000 0.0000 0.0000 0.0035 0.0043 0.0050 0.0051 0.0045 0.0045 0.0043 0.0045 0.0045 0.0000 0.0000 row b
0.0000 0.0000 0.0000 0.0000 0.0000 0.0000 0.0037 0.0060 0.0044 0.0053 0.0049 0.0030 0.0028 0.0065 0.0049 0.0000 row a
0.0000 0.0000 0.0000 0.0000 0.0000 0.0041 0.0057 0.0062 0.0046 0.0046 0.0052 0.0043 0.0034 0.0062 0.0048 0.0000 rwo A
0.0000 0.0000 0.0000 0.0000 0.0000 0.0000 0.0043 0.0043 0.0044 0.0057 0.0057 0.0057 0.0041 0.0037 0.0066 0.0000 rwo B
0.0000 0.0000 0.0000 0.0000 0.0000 0.0000 0.0047 0.0043 0.0033 0.0054 0.0037 0.0043 0.0044 0.0057 0.0038 0.0000 rwo C
0.0000 0.0000 0.0000 0.0000 0.0000 0.0000 0.0024 0.0025 0.0038 0.0046 0.0045 0.0049 0.0036 0.0045 0.0044 0.0000 rwo D
0.0000 0.0000 0.0000 0.0000 0.0000 0.0000 0.0000 0.0000 0.0000 0.0000 0.0000 0.0000 0.0000 0.0000 0.0000 0.0000
```

Tab. 11.2: Λ_{NxM} matrix. Each element $\tilde{d}_{ij}$ of the matrix is related to a single studied cell. For an easier reading of the matrix, each column is indicated by a number and each row by a letter maintaining the same notation used in Fig 3.7. In red it is marked the minimum $\tilde{d}_{ij}$, which identifies the SC. Zeroes indicate cells with no data.

```
col-4  col-3 col-2 col-1 col 0 col 1 col 2 col 3 col 4  col 5 col 6  col 7  col 8  col 9
 -1    -1    -1    -1    -1    -1    -1    -1    -1    -1    -1    -1    -1    -1    -1    -1
 -1    -1    -1     0     0     0     0     0    -1    -1    -1    -1    -1    -1    -1    -1   row g
 -1    -1     0     0     0     0     0     0     0    -1    -1    -1    -1    -1    -1    -1   row f
 -1     0     0     0     0     0     0     0     0     0     0    -1    -1    -1    -1    -1   row e
 -1     0     0     0     0     0     0     0     0     3     0     0     0     0    -1    -1   row d
 -1    -1    -1    -1    -1     0     0     0     0     0     0     0     0     0    -1    -1   row c
 -1    -1    -1    -1    -1     0     0     0     0     0     0     0     0     0    -1    -1   row b
 -1    -1    -1    -1    -1    -1     0     0     0     0     0     0     0     0     0    -1   row a
 -1    -1    -1     0     0     0     0     0     0     0     0     0     0     0     0    -1   row A
 -1    -1    -1     0     0     0     0     0     0     0     0     0     0     0     0    -1   row B
 -1    -1    -1    -1    -1    -1     0     0     0     0     0     0     0     0     0    -1   row C
 -1    -1    -1    -1    -1    -1     0     0     0     0     0     0     0     0     0    -1   row D
 -1    -1    -1    -1    -1    -1    -1    -1    -1    -1    -1    -1    -1    -1    -1    -1
```

Tab.11.3 Output matrix (Φ_i) of first iteration of LSO identifying the chosen solution (order number marked in red) for SC. For an easy reading of the matrix, each column is indicated by a number and each row by a letter maintaining the same notation used in Fig 11.7.

In the second iteration the search continues through the whole considered region in a sequence that points to the neighboring not-explored cell with the densest set of models.

The new cell, for which the solution has to be found, is selected among the neighbours of *SC* (i.e. cells e4, d3, d5, c4) as the one with the smaller $\tilde{d}_{ij}$, i.e. cell c5 (see Tab. 11.2) and, for this cell, the representative solution is chosen that satisfies the maximum local smoothness criterion (see section 10). The procedure continues until the representative solutions, for all cells, are chosen. The result

of this unconditioned search is given in Tab. 11.4, where in each cell is given the order number of the chosen solution.

	col-4	col-3	col-2	col-1	col 0	col 1	col 2	col 3	col 4	col 5	col 6	col 7	col 8	col 9		
-1	-1	-1	-1	-1	-1	-1	-1	-1	-1	-1	-1	-1	-1	-1	-1	
-1	-1	-1	3	14	7	9	10	-1	-1	-1	-1	-1	-1	-1	-1	row **g**
-1	-1	3	7	13	4	5	6	1	-1	-1	-1	-1	-1	-1	-1	row **f**
-1	9	8	10	24	1	15	4	5	4	3	-1	-1	-1	-1	-1	row **e**
-1	7	6	15	17	3	6	3	2	**3**	9	1	11	13	-1	-1	row **d**
-1	-1	-1	-1	-1	4	11	7	13	5	4	2	6	4	-1	-1	row **c**
-1	-1	-1	-1	-1	4	4	14	2	5	9	3	6	3	-1	-1	row **b**
-1	-1	-1	-1	-1	-1	2	7	13	4	9	6	4	4	13	-1	row **a**
-1	-1	-1	2	9	4	9	11	8	4	9	8	3	7	2	-1	row **A**
-1	-1	-1	6	3	15	10	3	1	7	17	1	5	11	8	-1	row **B**
-1	-1	-1	-1	-1	-1	4	2	7	1	2	8	5	9	9	-1	row **C**
-1	-1	-1	-1	-1	-1	1	5	3	4	10	4	12	7	1	-1	row **D**
-1	-1	-1	-1	-1	-1	-1	-1	-1	-1	-1	-1	-1	-1	-1	-1	

Tab. 11.4 Output matrix (Φ_f) of second iteration of LSO. In red the solution for the SC is marked. For an easy reading of the matrix, each column is identified by a number and each row by a letter maintaining the same notation used in Fig 11.7.

At the end of this procedure, the optimization algorithm LSO may select as representative model a model not fully consistent with existing well accepted models or observations. The first example of this situation is given by cell C5 (Southern part of the studied region, see Fig. 11.7). In the solution chosen by LSO the uppermost mantle, with Vs of about 4.30 km/s, overlies a fast lid, reaching a depth of about 170 km and with Vs ~ 4.70 km/s. The thick lid is sitting on a well developed asthenosphere (Vs~4.35 km/s) that reaches a depth of more than about 280 km. In this depth range, for a single layer mantle of simple composition Vs values around 4.30 km/s are close to the 0.1% H_2O pyrolite solidus (e.g. Della Vedova et al., 1991). Therefore the asthenosphere with Vs of about 4.35 km/s could have a relatively plastic behavior which is not in agreement with the hypocenters distribution, obtained using the ISC catalogue, which suggests the presence of brittle material at those depth.

In Fig 11.9 the earthquakes distribution, for two different hypocenters ranges (A: 0-500 km and B: 50-500km) is shown.

Therefore, among the hedgehog solutions for this cell, we choose the one, which agrees best with the distribution of the intermediate-depth seismicity falling in this cell. Thus in cell C5 a high velocity lid, with Vs of about 4.60 km/s sits on a fast asthenosphere, with Vs of about 4.50 km/s reaching a depth of about 200 km, where a fast mantle, with Vs of about 4.70 km/s is seen down to a depth of more than 300 km.

With this solution fixed, we run the optimization again.
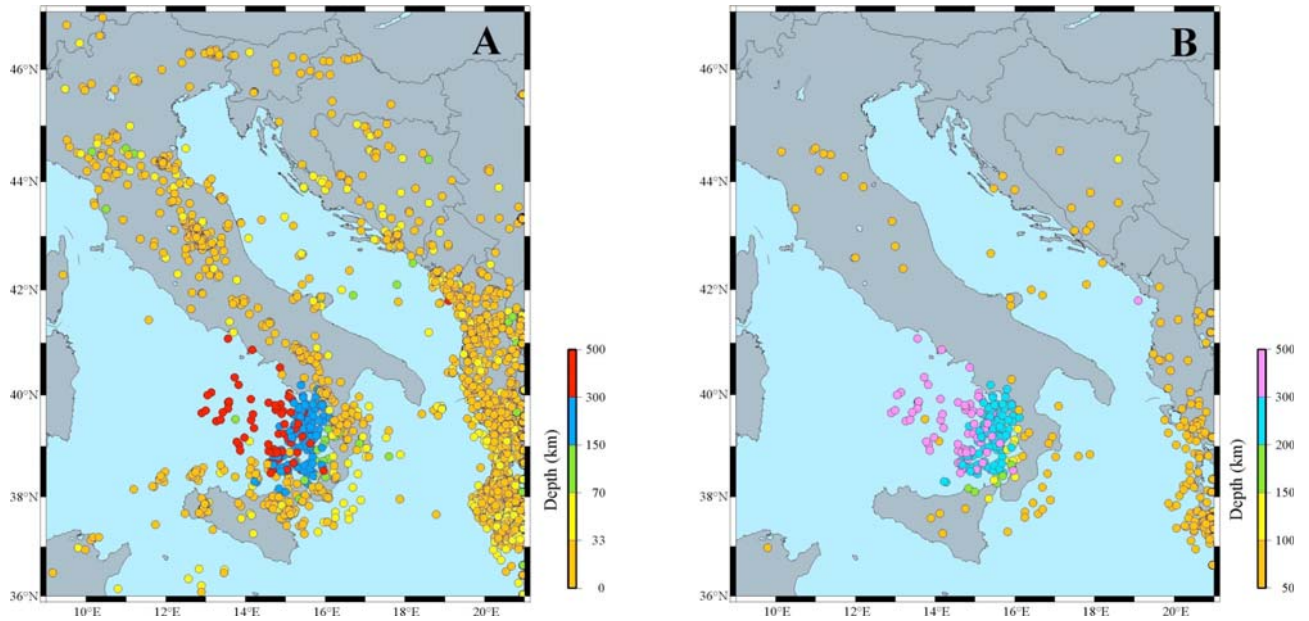
Fig. 11.9: ISC epicentres, plotted for different ranges of the hypocentres (km). A: 0-500km and B: 50-500km.

In Fig 11.10 the hypocentres distribution is plotted on the two structural models: (a) the one retrieved applying LSO, without any a priori constraint and (b) the one more consistent with the intermediate-depth seismicity.
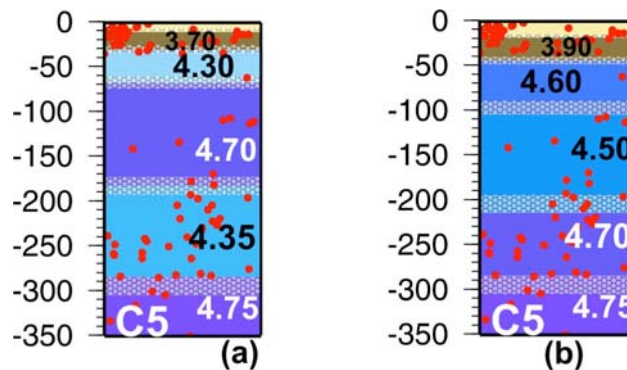
Fig 11. 10: Hypocenter distribution versus depth for the earthquakes falling in cell C5. (a) Seismic velocities (km/s) are given for the LSO solution; (b) seismic velocities (km/s) are given for the solution more consistent with seismicity distribution.

For cell C5, in Fig. 11.11a, the cellular group velocity values (dots with error bars), the dispersion relations computed for all the solutions (black lines) and the one corresponding to the chosen solution (solid red line) are shown. In Fig. 11.11b, the grey area outlines the sampled part of the parameter's space.

longitude 15.5 latitude 38.5 sol 12
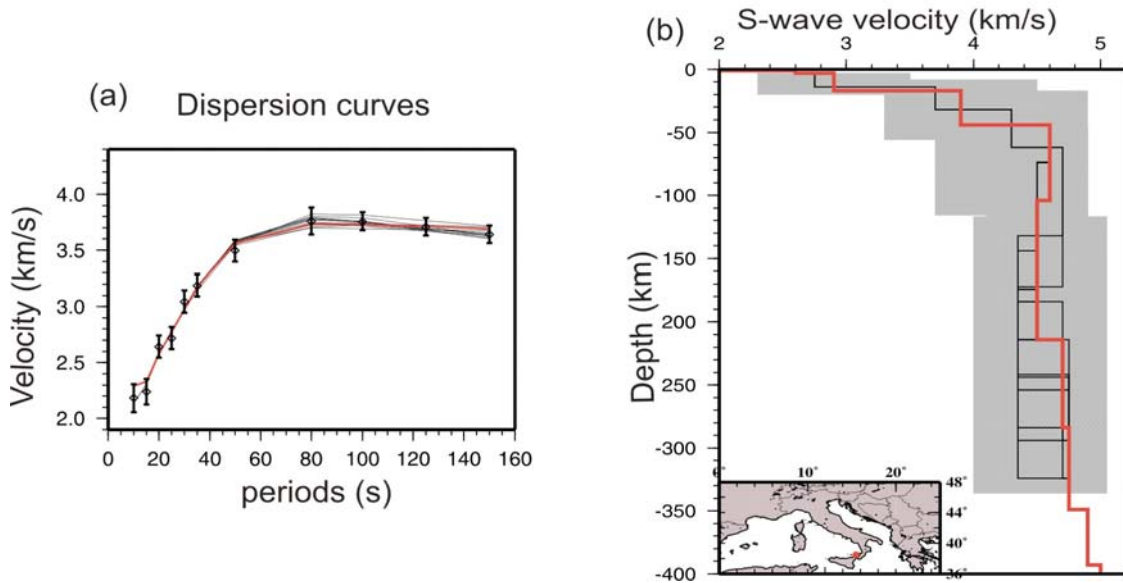
Fig. 11.11: Cell C5: (a) observed (black dots) dispersion measurements (vertical bars represent measurement errors), compared with the group velocity (red dispersion curve) computed for the chosen S-wave solution shown as solid red line in (b), where the grey area delimits the portion of the solution's space, sampled by the non-linear inversion of group velocity of Rayleigh waves. In (a) and (b) the black lines refer to the other hedgehog solutions.

Thus, once the solution for cell C5 is chosen and the matrix Φ_i is suitably modified, so that the solution of the *SC* and the solution in cell C5 are fixed a priori, the optimization algorithm starts again from the second iteration.

In Tab. 11.5 the matrix Φ_f, obtained after the second iteration of LSO, is reported. Only in three cells, neighboring C5, the solution is different with respect to that chosen without any a priori constraint. This is not surprising since LSO does not extend to the entire domain a local perturbation.

The LSO is followed by a further analysis of the chosen models (i.e. laterally *smoothest solutions*), for every cell, to see if all of them are fully consistent with a priori well established and accepted information. From this analysis it appears that the models for cells c4 and b3 are not consistent with other independent observations (seismic refraction data of Nicolich and Dal Piaz, 1990 and local, regional and teleseimic study of Marone et al. 2003, 2004).

In Fig. 11.12 the uppermost 100 km are shown for the, so far chosen, solutions of cells b3 and c4.

The crust for cell b3 is as thin as about 15 km, while the Moho depth is estimated as deep as about 30 km (Nicolich and Dal Piaz, 1990; Marone et al. 2003, 2004, Dèzes and Ziegler, 2001). Therefore, among the hedgehog solutions we choose the one with thicker crust and mantle layering as similar

as possible to the one of the solution choosen by LSO. In the solution obtained in this way a lower crust appears with graben-like character (e.g. Muller, 1978).

col-4	col-3	col-2	col-1	col 0	col 1	col 2	col 3	col 4	col 5	col 6	col 7	col 8	col 9	
-1	-1	-1	-1	-1	-1	-1	-1	-1	-1	-1	-1	-1	-1	
-1	-1	3	14	7	9	10	-1	-1	-1	-1	-1	-1	-1	row g
-1	3	7	13	4	5	6	1	-1	-1	-1	-1	-1	-1	row f
9	8	10	24	1	15	4	5	4	3	-1	-1	-1	-1	row e
7	6	15	17	3	6	3	2	3	9	1	11	13	-1	row d
-1	-1	-1	-1	4	11	7	13	5	4	2	6	4	-1	row c
-1	-1	-1	-1	4	4	14	2	5	9	3	6	3	-1	row b
-1	-1	-1	-1	-1	2	7	13	4	9	6	4	4	13	row a
-1	-1	2	9	4	9	11	8	4	9	8	3	7	2	row A
-1	-1	6	3	15	10	3	1	7	13	1	5	11	8	row B
-1	-1	-1	-1	-1	4	2	7	5	12	8	5	9	9	row C
-1	-1	-1	-1	-1	1	5	3	4	10	1	12	7	1	row D
-1	-1	-1	-1	-1	-1	-1	-1	-1	-1	-1	-1	-1	-1	

Tab. 11.5: Output matrix Φ_f of the last running of LSO. The order number of the chosen solution for the SC is marked in red, the order number of the solution fixed for cell C5 is marked in yellow, the solutions that are different from the ones obtained with the run without any a priori constraint are marked in grey. For an easy reading of the matrix, each column is indicated by a number and each row by a letter maintaining the same notation used in Fig 3.7.
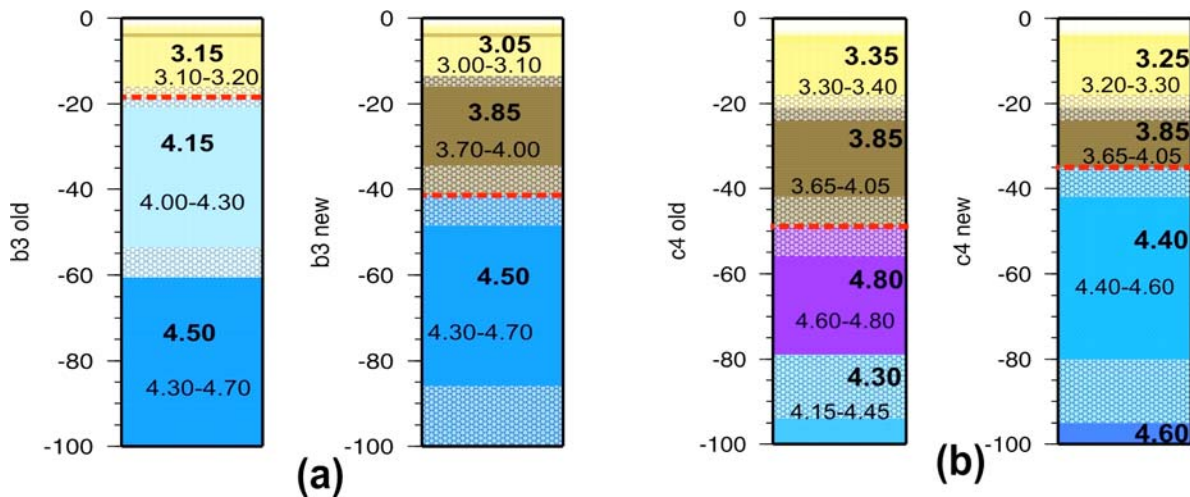
Fig. 11.12: Cells b3 (a) and c4 (b) - Uppermost 100 km of the models chosen by LSO (old) and of those selected among hedgehog solutions (new), in order to be as close as possible to accepted models given in the literature.

The crust for cell c4 is as deep as about 49 km, while the Moho depth, in this region, is estimated to be at a depth of about 30-35km (Nicolich and Dal Piaz, 1990; Marone et al. 2003, 2004, Dèzes and Ziegler, 2001). Therefore, among the hedgehog solution we choose the one with a crustal thickness of about 35 km and mantle layering as similar as possible to the one of the solution choosen by LSO.

The new matrix Φ_i, with the solution fixed in cells C5, c4 and b3, is shown in Tab. 11.6.

	col-4	col-3	col-2	col-1	col 0	col 1	col 2	col 3	col 4	col 5	col 6	col 7	col 8	col 9		
-1	-1	-1	-1	-1	-1	-1	-1	-1	-1	-1	-1	-1	-1	-1	-1	
-1	-1	-1	0	0	0	0	0	-1	-1	-1	-1	-1	-1	-1	-1	row g
-1	-1	0	0	0	0	0	0	0	-1	-1	-1	-1	-1	-1	-1	row f
-1	0	0	0	0	0	0	0	0	0	-1	-1	-1	-1	-1	-1	row e
-1	0	0	0	0	0	0	0	0	3	0	0	0	0	-1	-1	row d
-1	-1	-1	-1	-1	0	0	0	0	3	0	0	0	0	-1	-1	row c
-1	-1	-1	-1	-1	0	0	0	1	0	0	0	0	0	-1	-1	row b
-1	-1	-1	-1	-1	-1	0	0	0	0	0	0	0	0	0	-1	row a
-1	-1	-1	0	0	0	0	0	0	0	0	0	0	0	0	-1	row A
-1	-1	-1	0	0	0	0	0	0	0	0	0	0	0	0	-1	row B
-1	-1	-1	-1	-1	-1	0	0	0	0	12	0	0	0	0	-1	row C
-1	-1	-1	-1	-1	-1	0	0	0	0	0	0	0	0	0	-1	row D
-1	-1	-1	-1	-1	-1	-1	-1	-1	-1	-1	-1	-1	-1	-1	-1	

Tab. 11.6: Matrix Φ_i before the second iteration of LSO for the whole domain and after fixing the solutions in cells c4 and b3 (evidenced in yellow). The order number of the chosen solution for the SC is marked in red, the order number of the solution fixed for cell C5 is marked in yellow. For an easy reading of the matrix, each column is indicated by a number and each row by a letter maintaining the same notation used in Fig 3.7.

As a result we obtain in all other cells, with the exception of one of them (cell c3), the same models as in the previous iteration, i.e. that with fixed solution only in cell C5, which is a nice indication of the robustness of our model of the entire study area. The order number of the chosen solution of each cell is shown in Tab. 11.7.

	col-4	col-3	col-2	col-1	col 0	col 1	col 2	col 3	col 4	col 5	col 6	col 7	col 8	col 9		
-1	-1	-1	-1	-1	-1	-1	-1	-1	-1	-1	-1	-1	-1	-1	-1	
-1	-1	-1	3	14	7	9	10	-1	-1	-1	-1	-1	-1	-1	-1	row g
-1	-1	3	7	13	4	5	6	1	-1	-1	-1	-1	-1	-1	-1	row f
-1	9	8	10	24	1	15	4	5	4	3	-1	-1	-1	-1	-1	row e
-1	7	6	15	17	3	6	3	2	3	9	1	11	13	-1	-1	row d
-1	-1	-1	-1	-1	4	11	7	7	3	4	2	6	4	-1	-1	row c
-1	-1	-1	-1	-1	4	4	14	1	5	9	3	6	3	-1	-1	row b
-1	-1	-1	-1	-1	-1	2	7	13	4	9	6	4	4	13	-1	row a
-1	-1	-1	2	9	4	9	11	8	4	9	8	3	7	2	-1	row A
-1	-1	-1	6	3	15	10	3	1	7	13	1	5	11	8	-1	row B
-1	-1	-1	-1	-1	-1	4	2	7	5	12	8	5	9	9	-1	row C
-1	-1	-1	-1	-1	-1	1	5	3	4	10	1	12	7	1	-1	row D
-1	-1	-1	-1	-1	-1	-1	-1	-1	-1	-1	-1	-1	-1	-1	-1	

Tab. 11.7: Output matrix Φ_f of the last run of LSO obtained fixing the solutions in cells C5, c4, and b3. The order number of the chosen solution for the SC is marked in red, the order number of the solutions fixed for the other cells is marked in yellow and the order number of the solutions changed with respect to the previous run is marked in grey.
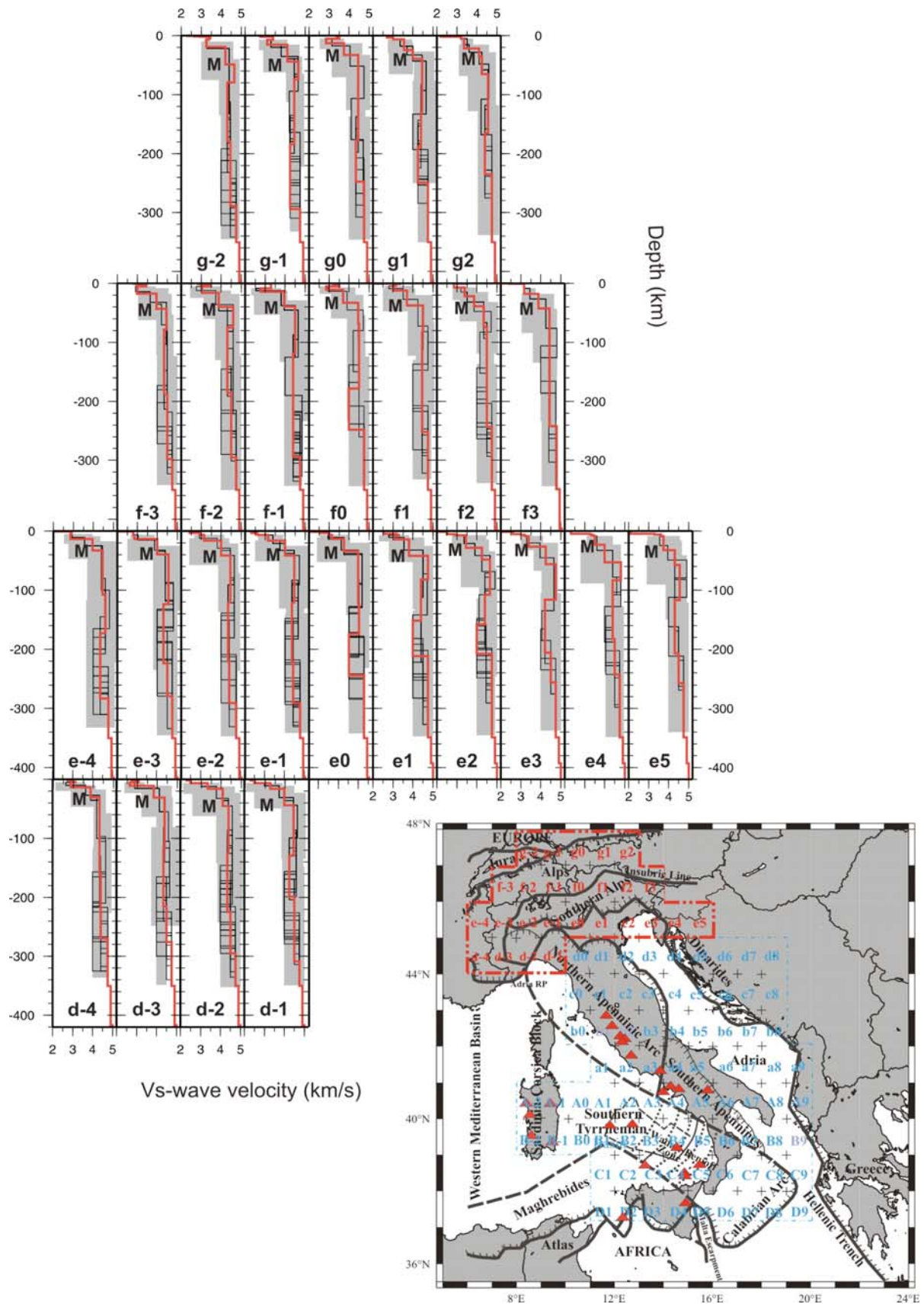
Fig. 11.13a: The set of solutions obtained through the non–linear inversion of the dispersion relations of each cell in the area indicated by the red dashed line in the insert. The investigated parameter's space (grey zone) is shown. The Moho is marked with M. In the insert, the recent volcanoes in the study area are plotted as triangles.
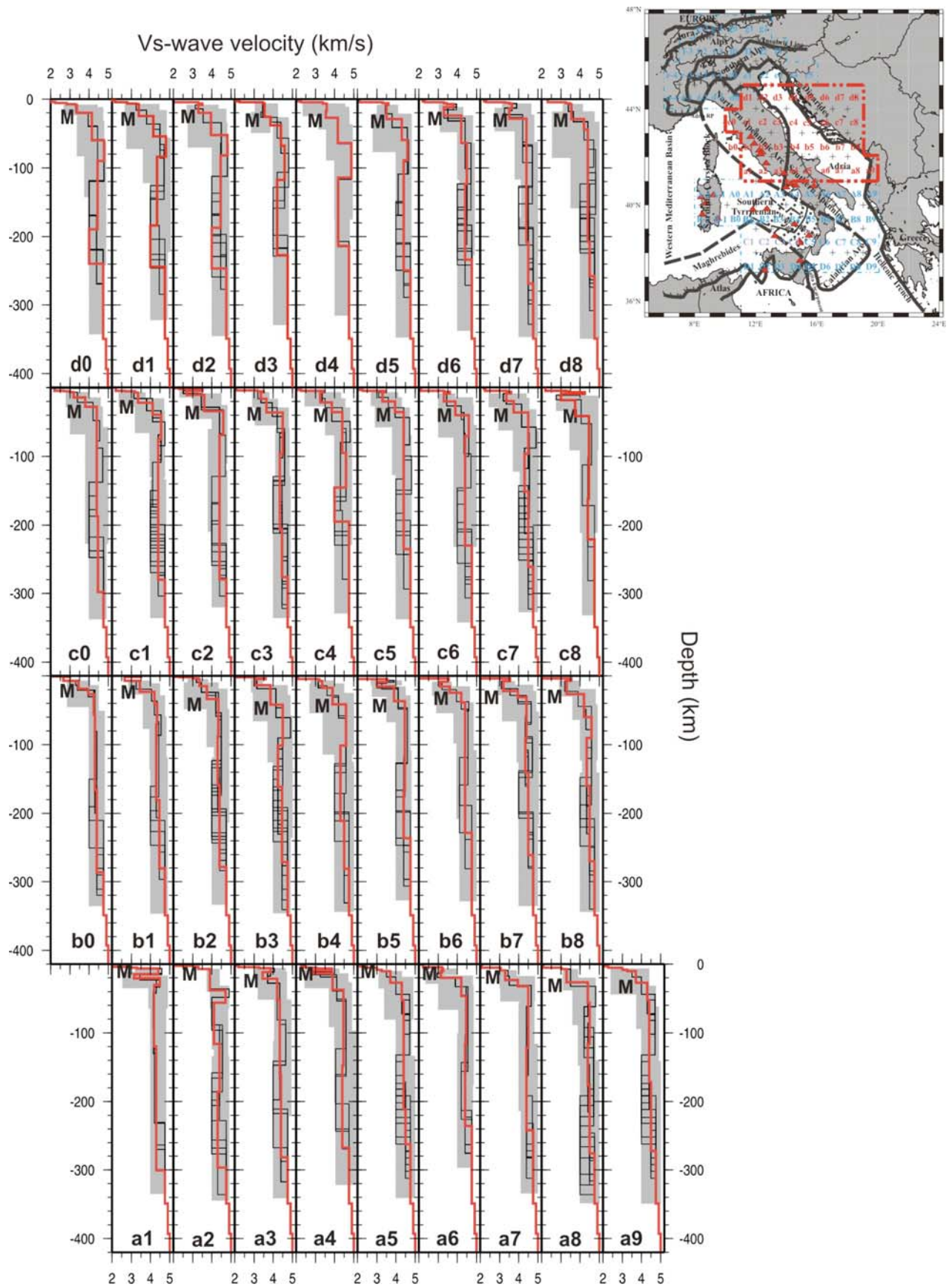
Fig. 11.13b: As in Fig. 11.13a for cells in the area indicated by the red dashed line in the insert.
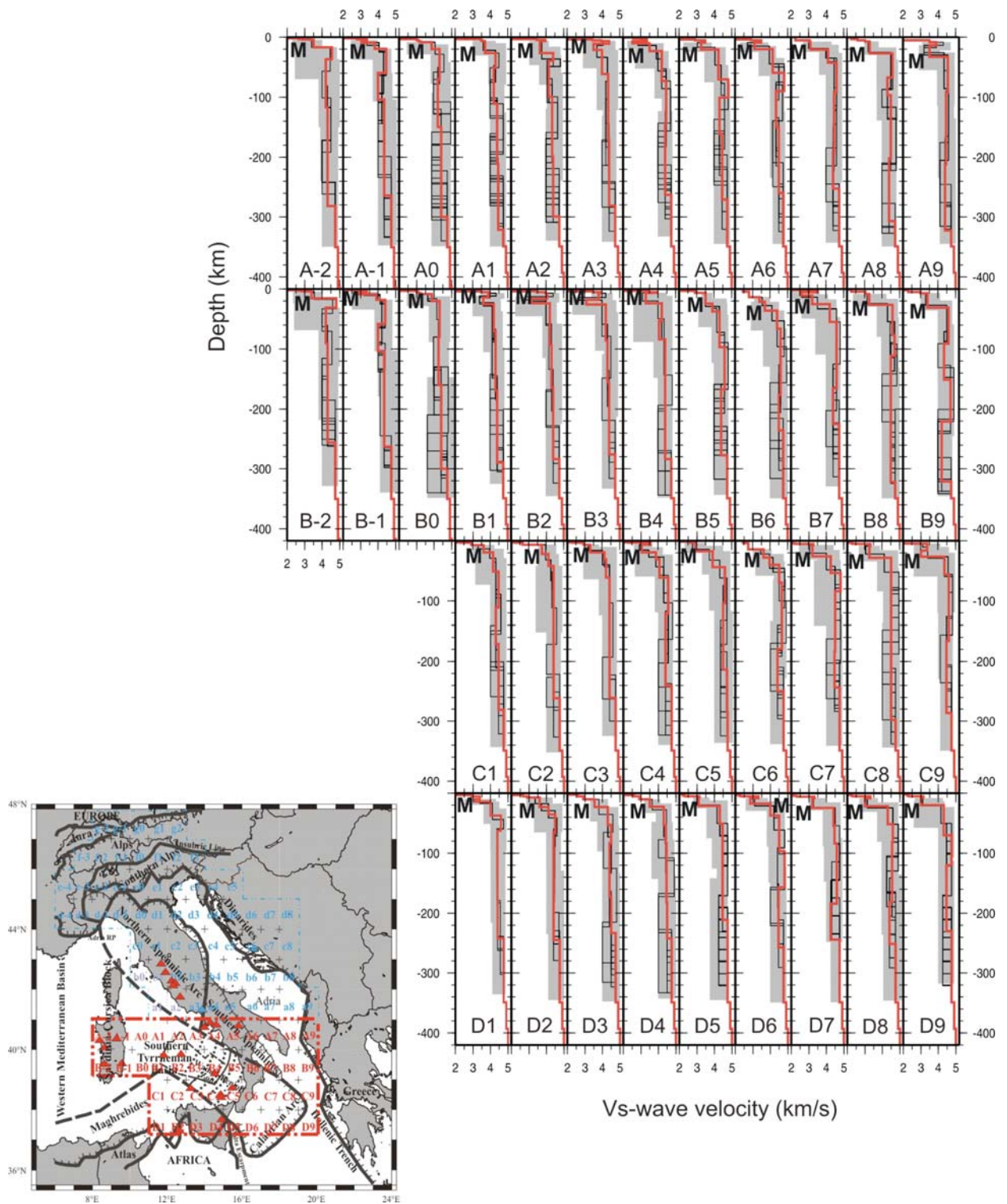
Fig. 11.13c: As in Fig. 11.13a, b for cells in the area indicated by the red dashed line in the insert.

A further analysis of these solutions evidences that there is no need for any further LSO run with additional constraints. Therefore the final inversion result differs from the unconstrained one only in seven cells, out of the 105 considered.
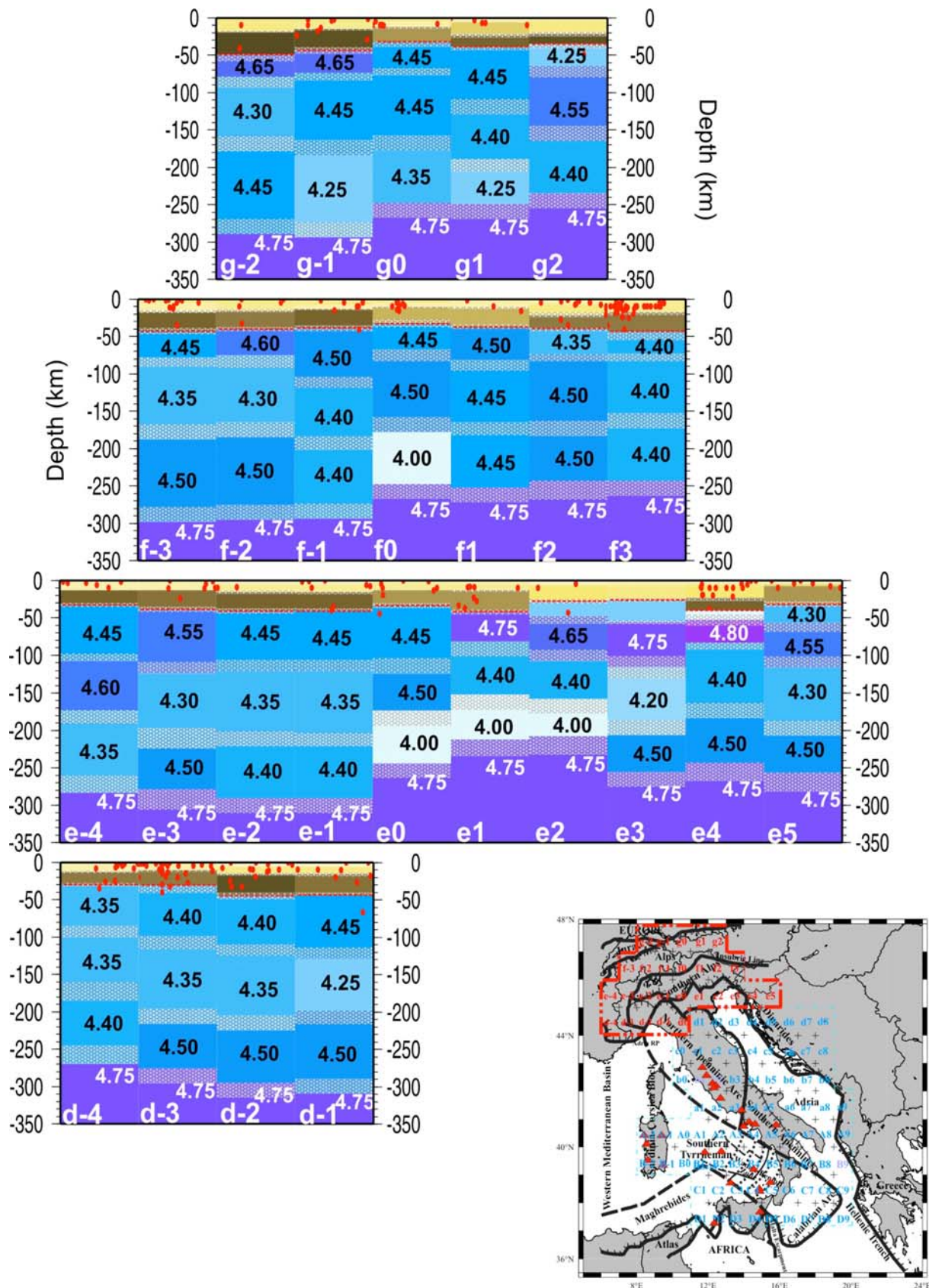
Fig. 11.14a: Structural models, chosen by LSO, for each cell of the area marked with a red line in the insert. The models are represented in the depth range 0-350 km and the range of variability of the inverted layers' thickness is shown as shadowed area; in each cell the Moho is marked by a red dashed line. The distribution of hypocentres of the events with magnitude greater than 3, collected from ISC on-line bulletin for the period 1904-2004, is shown for each cell.

Fig. 11.14 b: Zoom of Fig. 11.14 a in the depth range 0-100 km.
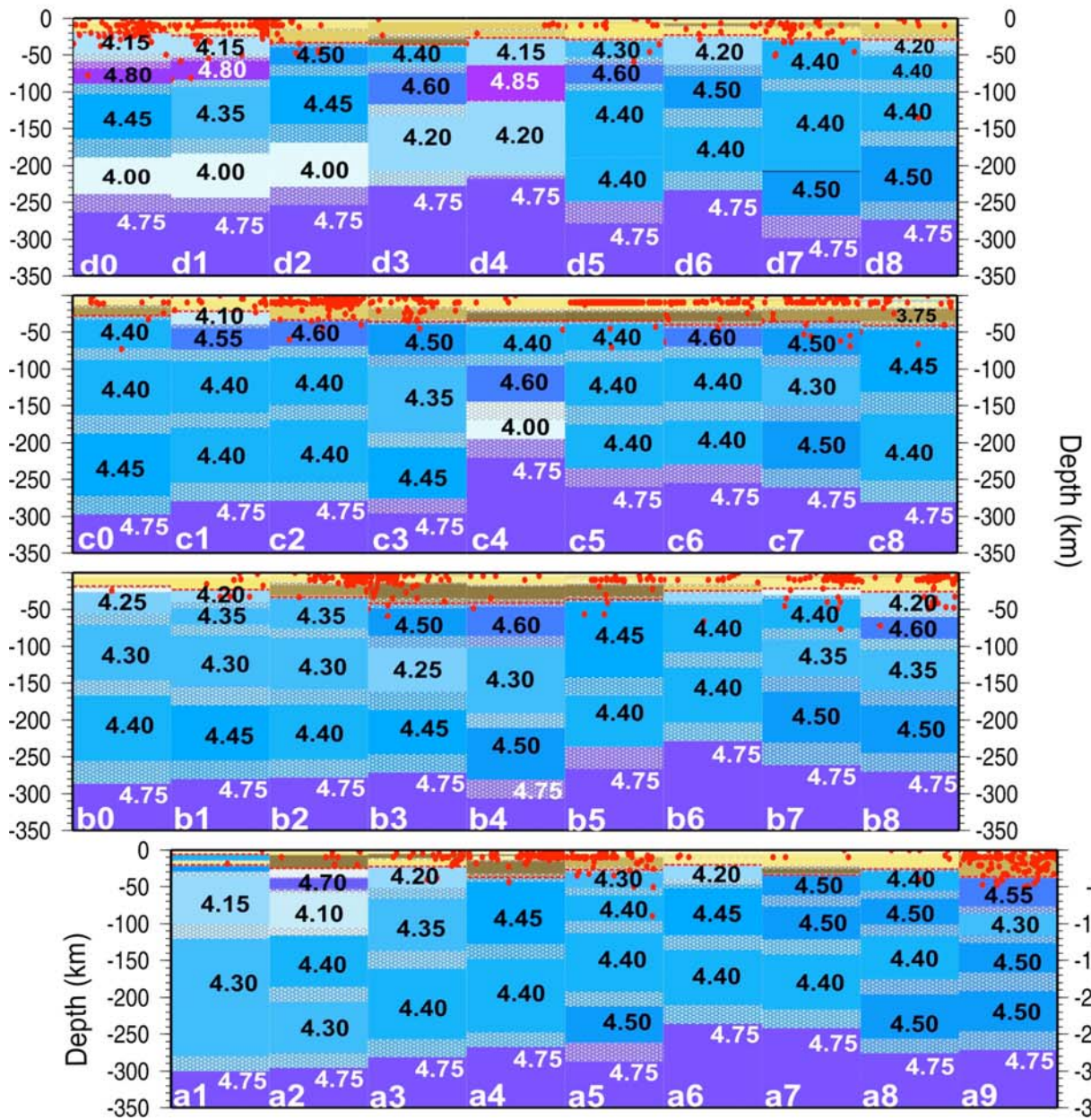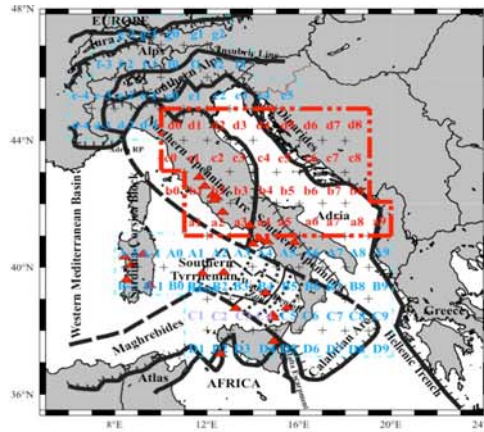
Fig. 11.14 c: Structural models, chosen by LSO, for each cell of the area marked with a red line in the insert. The models are represented in the depth range 0-350 km and the range of variability of the inverted layers' thickness is shown as shadowed area; in each cell the Moho is marked by a red dashed line. The distribution of hypocentres of the events with magnitude greater than 3, collected from ISC on-line bulletin for the period 1904-2004, is shown for each cell.
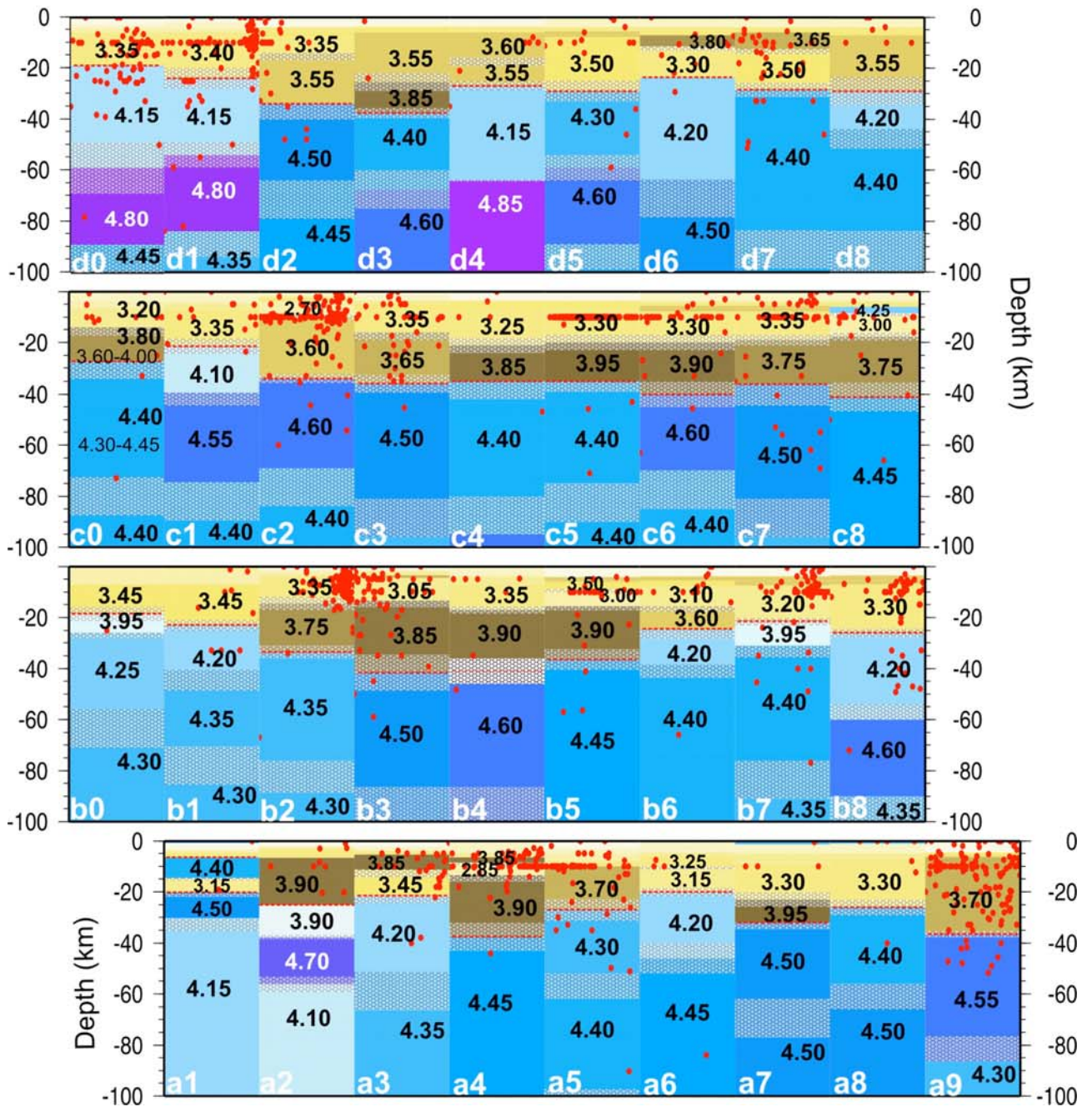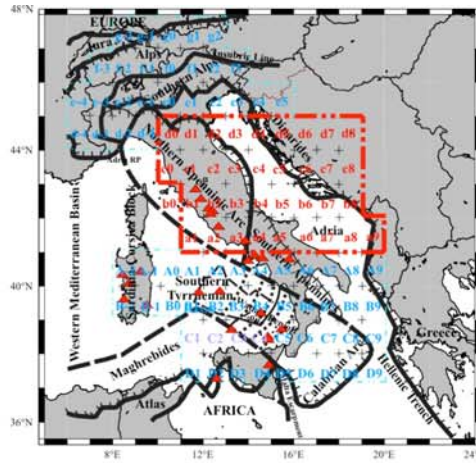
Fig. 11.14 d: Zoom of Fig. 11.14 c in the depth range 0-100 km.
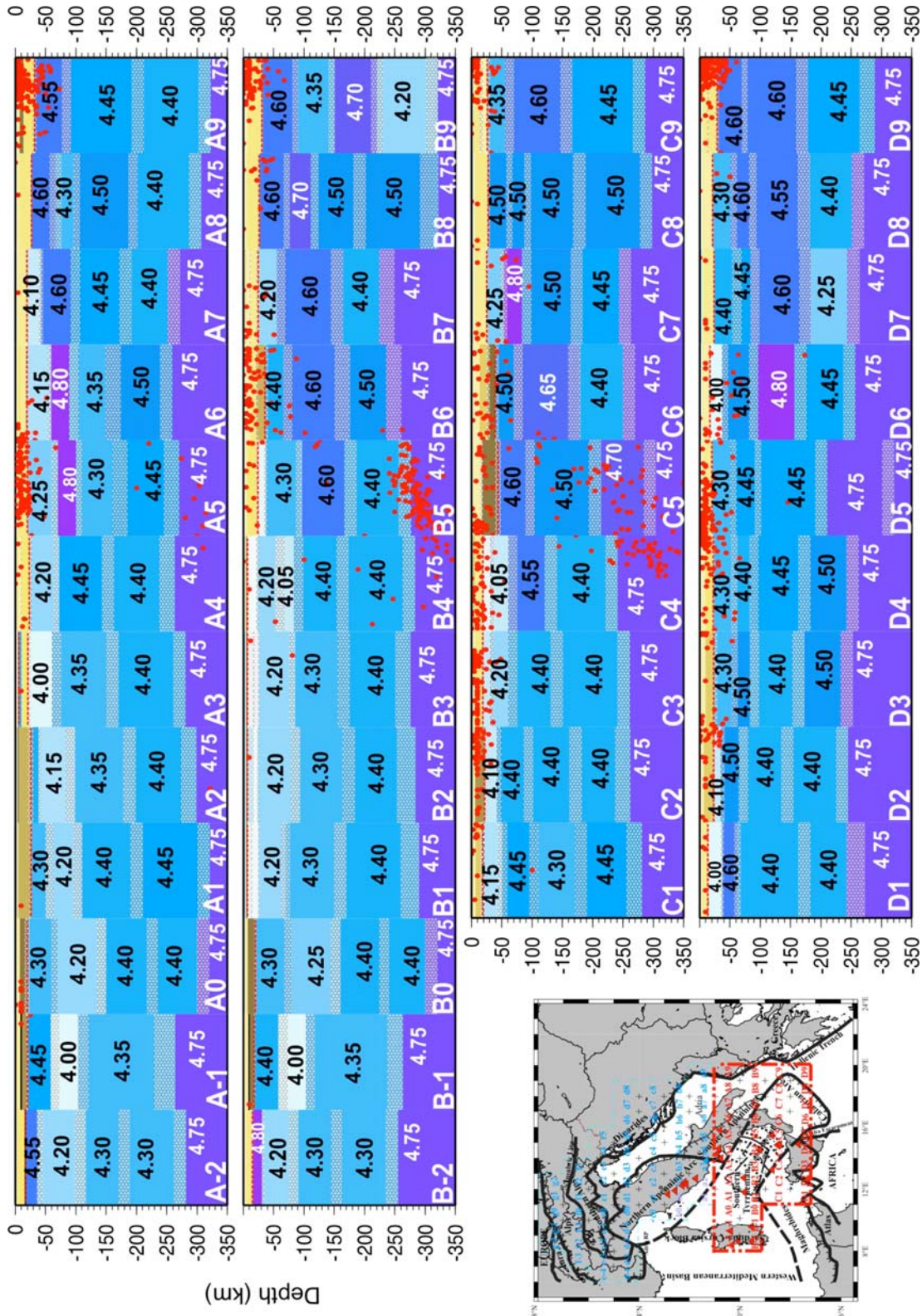
Fig. 11.14 e: Structural models, chosen by LSO, for each cell of the area marked with a red line in the insert. The models are represented in the depth range 0-350 km and the range of variability of the inverted layers' thickness is shown as shadowed area; in each cell the Moho is marked by a red dashed line. The distribution of hypocentres of the events with magnitude greater than 3, collected from ISC on-line bulletin for the period 1904-2004, is shown for each cell.
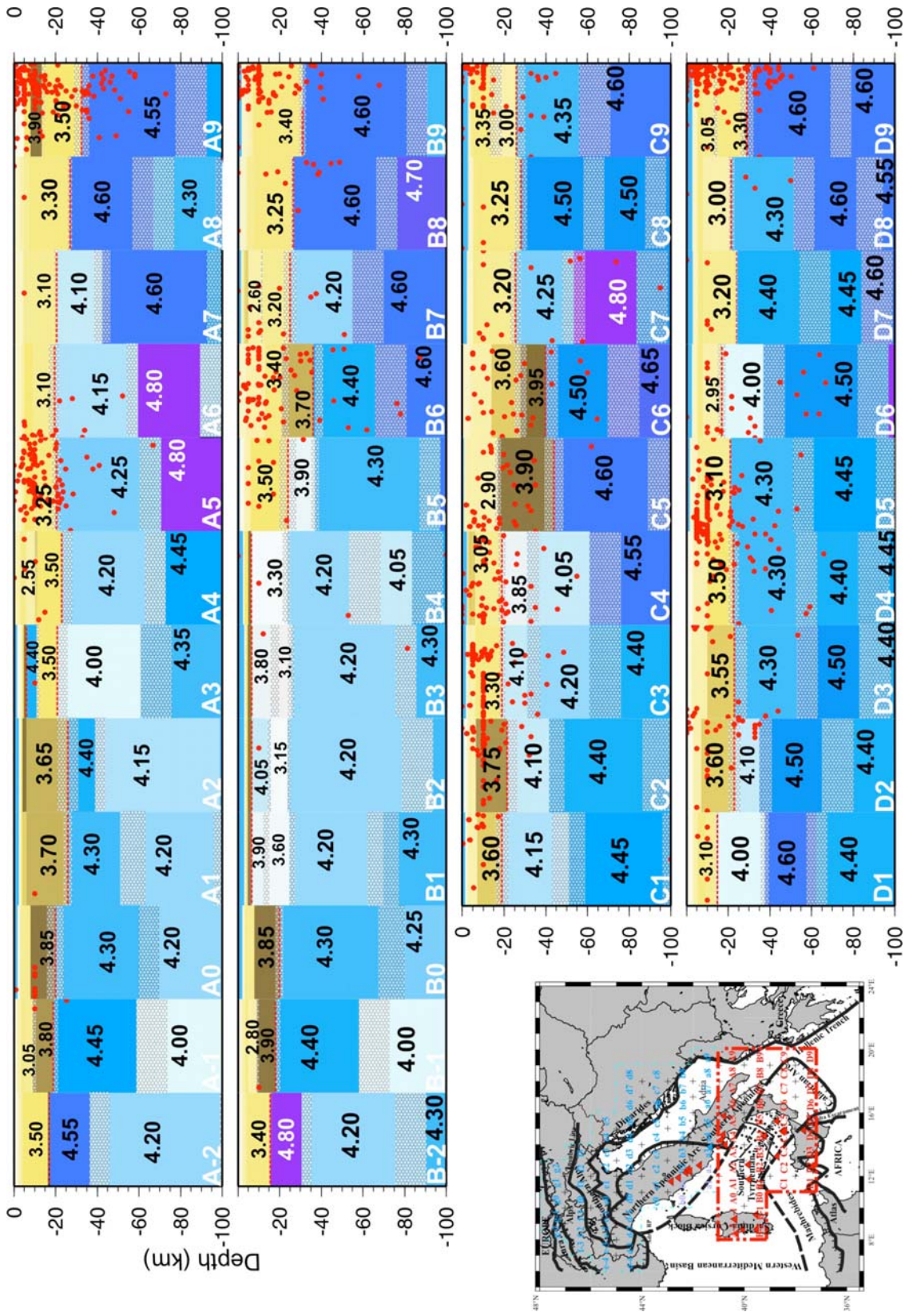
Fig. 11.14 f: Zoom of Fig. 11.14 e in the depth range 0-100 km.

The results of the optimization are summarized in Fig. 11.13a, b, c and in Table A2.2 (Appendix II). For each cell the depth of the Mohorovicic discontinuity (M), the selected solution (red line) and the explored parameter's space (grey area) are indicated.

The velocity structures are parameterized in the depth range from 6-13 km to 350 km, in agreement with the resolving power of our data set, estimated from the depth distribution of the partial derivatives (Urban et al., 1993) of the group velocity curves with respect to the shear-wave velocity. The deeper structure is fixed accordingly with already published models (Du et al., 1998).

The chosen structural models, for each cell, are shown in Fig. 11.14 (a, b, c, d, e, f) from the surface to the maximum investigated depth (i.e. 350 km) and for the uppermost 100 km. In each cell, the distribution of hypocentres of events with magnitude greater than 3, collected from ISC on-line bulletin for the period 1904-2004, is shown and, for each inverted layer, the retrieved velocity value is specified. The range of variability of the thickness of the inverted layers is represented, for each cell, by the shadowed area, and this representation is used to evidence that the boundaries between layers can well be transition zones in their own right. In Appendix II, Fig II (a, b, c, d, e) the same models are shown with the velocity range of variability, specified both for crustal and mantle layers.

12. The Crust.

In the description that follows we will refer to the models shown in Fig. 11.14(a, c, e) and to their range of variability, as given in table A2.2 (Appendix II). The complexity of the studied region is well marked by the heterogeneities visible both for the crust and the whole lithosphere-asthenosphere system. The location of the Moho depth is, defined, for each cell, within a few kilometres (the variability range of the thickness of the retrieved solution for the crustal layers is shown in Fig 11.14a, b, c, d, e, f and Tab. A2.2).

The Alpine region (fig. 11.14 a) is characterized by a thick crust with the Moho depth ranging between a minimum of about 25 km to a maximum of more than 45 km, well in agreemetn with Nicolich and Dal Piaz (1990) (see Fig. 12.1), Panza (1980a), Marone et al. (2003, 2004) (see Fig. 12.2) and the map of the European Moho compiled by Dèzes and Ziegler (2001) (see Fig. 12.3).

To the West of the Molasse Basin, cells g-2 and g-1 are characterized by a positive velocity gradient in the sediments, till a depth of about 7 km where Vs is about 3.40 km/s (see Tab. A2.2). At this depth it observed a relatively low velocity layer (Vs in the range 3.10-3.25 km/s), about 10-15 km thick, overlying a high velocity lower crust with an average Vs of about 4.10 km/s, reaching a depth of about 45 km. More to the east, in the Molasse Basin, in cell g0, starting at a depth of about 5 km,
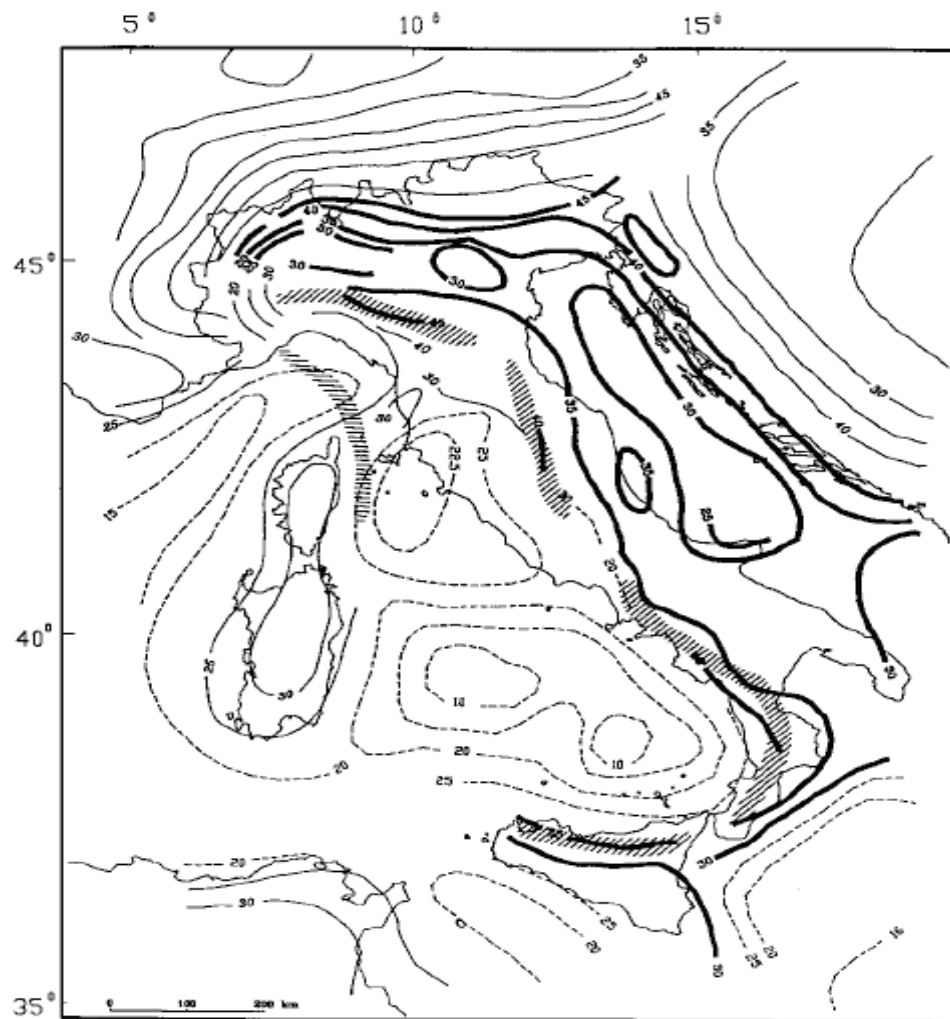
Fig. 12.1: Isobaths of the European (thin), Adriatic (thick) and tyrrhenian (dashes) Mohos produced from DSS profiles (Nicolich and Dal Piaz, 1988)
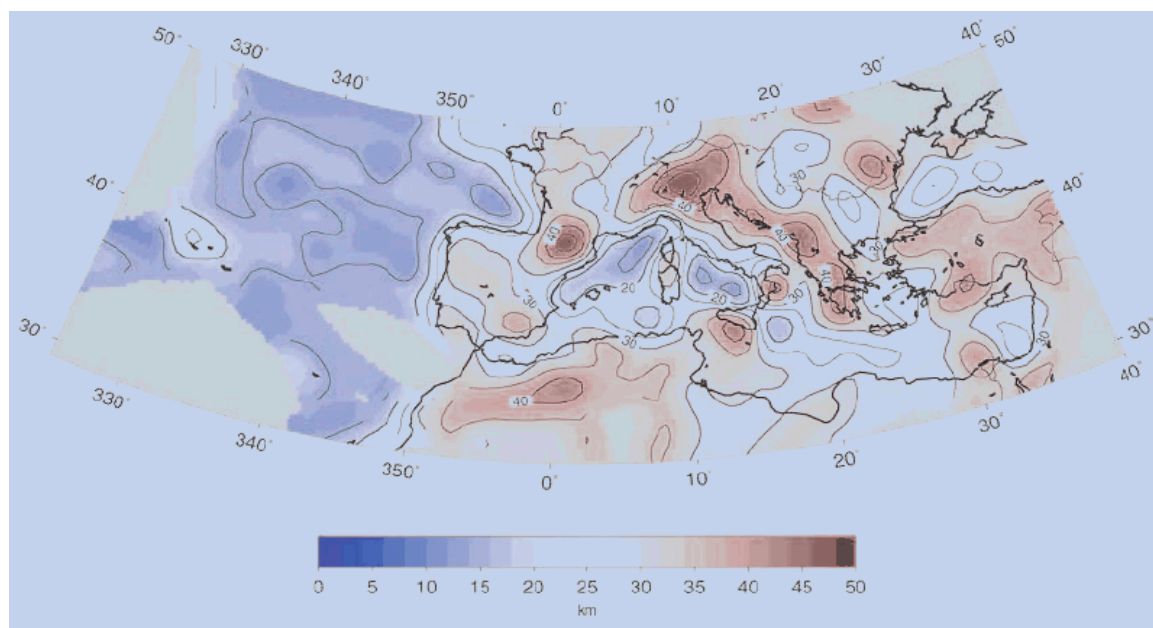
Fig. 12.2: Map of Moho depth (EAMO2) obtained in the 3-D inversion of local, regional and teleseismic data (Marone et al., 2003)
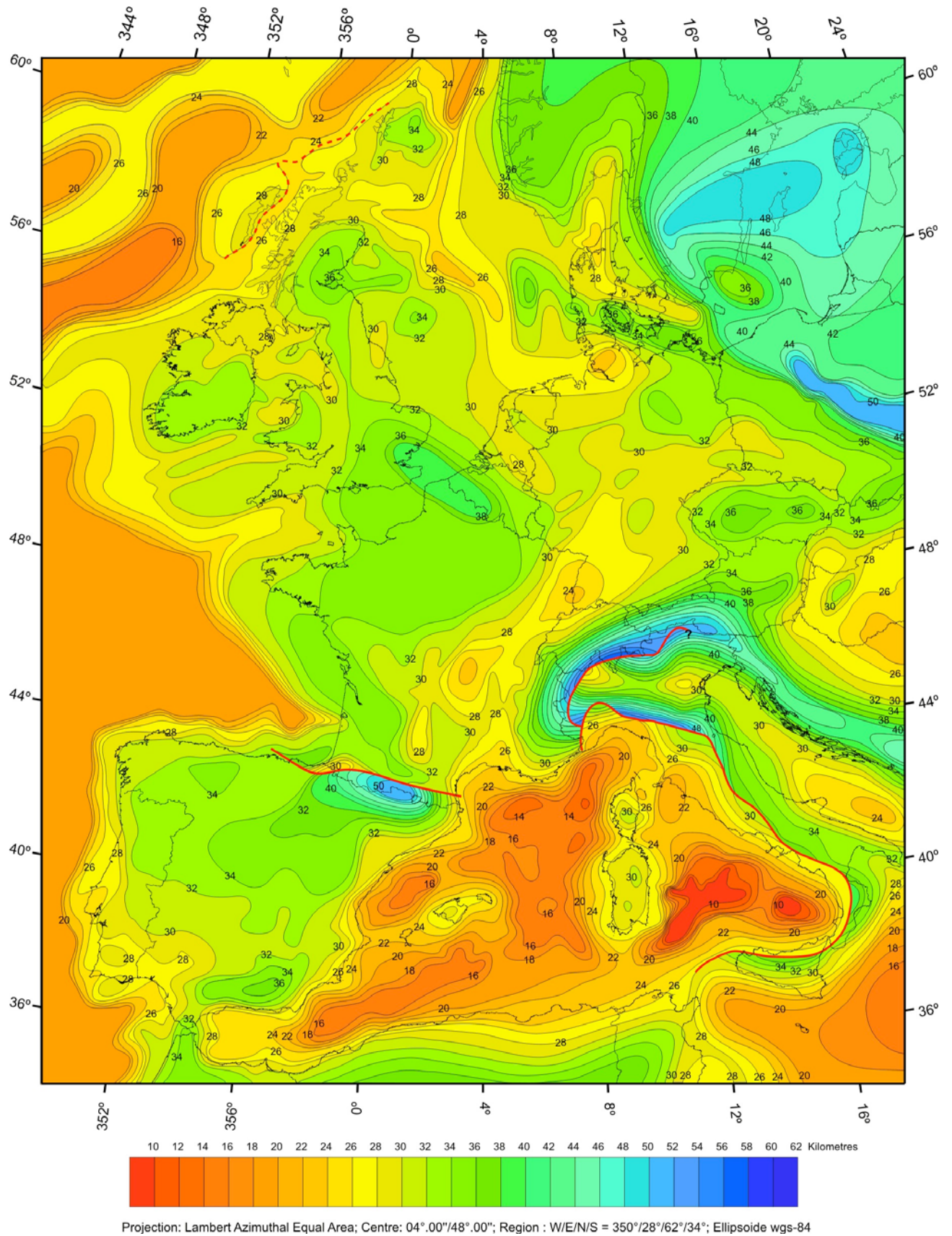
Fig 12.3: Depth of the Mohorovich discontinuity compiled from Dèzes and Ziegler, 2001
http://comp1.geol.unibas.ch/downloads/Moho_net/euromoho1_3.pdf).

a relatively low velocity (Vs~2.85 km/s) upper crustal layer is observed that overlies an about 20 km thick lower crust with Vs of about 3.75 km/s; the total crustal thickness is around 33 km.

In cells g1 and g2 both the upper and the lower crust are characterized by relatively higher velocities (see Tab. A2.2). In the upper crust, reaching a depth of about 20 km, the velocity is as high as ~ 3.55 km/s and the lower crust, with average Vs ~ 4.10 km/s, reaches a depth of about 35 km.

Following the Insubric Line, from the Western to the Eastern Alps (cells d-4, d-3, e-4, e-3, and from cell f-3 to cell f3), it is observed the presence of an about 15-20 km thick upper crust with the presence of an about 10-15 km thick layer where Vs ranges from about 2.65 km/s in the south-western part (cell d-3) to about 3.40 km/s in the north-eastern part (cell f2).

This layer overlies a lower crust, with a velocity in the range 3.85-4.00 km/s, reaching depths greater than 40 km. The South-Eastern Alps (cells from e-2 to e1) show a positive velocity gradient in their about 40 km thick crust (see Tab. A2.2), with the exception of cell e0 where the crust is about 34 km deep. The upper crust, with Vs reaching a value of about 3.15 km/s, overlies a high velocity lower crust with Vs in the range 3.75-4.00 km/s.

To the West, the Alpine Arc joins the Northern Apennines chain and similar crustal characteristics can be observed moving from cell d-4 and d-3 to d-2 and d-1: in the upper crust, that reaches a depth of about 15 km, Vs increases with depth (see Tab. A2.2) and in the lower crust the average Vs is about 4.00 km/s. The crustal thickness is greater than about 40 km.

More to the East, in the Po Basin (cells e2 and e3) a high velocity lower crust seems to be absent. Here, in the sediments a positive velocity gradient is observed (see Tab. A2.2). At a depth of ~7-8 km, an about 20 km thick layer, with Vs of about 3.40-3.45 km/s, starts. The crust is as deep as about 27-28 km.

Approximately along the Adria Dinarides front (cell e5, c6 and c7) a high velocity lower crust, with Vs in the range 3.75-4.00 km/s is observed, but while in cell e5 it starts at a depth of about 8 km and reaches a depth of about 32 km, in cell c6 and c7 the lower crust starts at a depth of about 20 km and reaches a depth of about 36-40 km. In all these cells a positive velocity gradient characterizes the sediments layers till a depth of about 8 km (see Tab. A2.2) below which, in cells c6 and c7, a layer, with Vs of about 3.30 km/s is seen. Similar characteristics can be observed in cell e4 (see description in chapter 3.3.2). In cell d5 (see Fig. 11.14 c) the crust is about 30 km thick and the high velocity lower crust seems to be absent.

In the eastern part of the Dinarides chain (cells d6 and d7) till a depth of about 6-7 km a positive velocity gradient is observed (see Tab. A2.2). Below a layer, with Vs in the range 3.65-3.80 km/s appears. It reaches a depth of about 12 km and it overlies a slower layer with Vs in the range 3.30-3.50 km/s. In cell d8 the velocity increases with increasing depth (see Tab. A2.2) till about 7 km below which a ~12 km thick layer, with Vs of about 3.55 km/s, occupies the deeper crust. The

Moho is at a depth of about 24 km in cell d6 and of about 29 km in cell d7 and d8. Cell c8 shows a rather complicate layering. At a depth of about 6 km a very fast and thin layer, with Vs of about 4.25 km/s is observed till a depth of about 9 km where a slower layer, with Vs of about 3.00 km/s starts. At the bottom of this layer, at a depth of about 18 km, a fast lower crust, with Vs of about 3.75 km/s is seen till a depth of about 40 km. This Vs - depth sequence seems to be consistent with a lithospheric doubling or with the presence of a shallow layer of consolidated magma. All the other hedgehog solutions, for cell c8, show a high velocity layer (Vs greater that 3.90 km/s) at a depth of about 6 km on the top of a slower layer (see Fig. 11.13b).

To the South of the Po basin, in cells d0 and d1, the velocity of the sediments increases with increasing depth (see Tab. A2.2). A fast lower crust seems to be absent and the Moho is as deep as about 19 km in cell d0 and 24 km in cell d1. In cell d2 a positive velocity gradient (see Tab. A2.2) is seen till a depth of about 8 km where a 6 km thick layer with Vs of about 3.30 km/s starts. At the bottom of this layer a relatively low velocity lower crust starts, with Vs of about 3.55 km/s and reaching a depth of about 34 km. In cell d3 the velocity still increases with increasing depth and an about 12 km thick and fast lower crust can be observed starting at a depth of about 25 km. Cell d4 shows the same velocity pattern as cell c3, till a depth of about 27 km, where the Moho can be placed.

More to the South, along the Tyrrhenian coastline, cells c0 and c1, b0 and b1 show a positive velocity gradient in the sediments (see Tab. A2.2). The crustal thickness varies from about 19 km in cell b0 to 22 km in cells c1 and b1, and about 27 km in cell c0. In cell c0 a high velocity lower crust, with Vs of about 3.75-3.80 km/s, starts at a depth of about 15 km, while it is not detected in cells c1, b0 and b1 where the deeper crustal layer has Vs in the range $3.35 \leq Vs \leq 3.45$ km/s.

A crustal thickness of about 35-40 km characterizes the North and Central Apennines. In cells c2 and c3 the sediments has Vs increasing with depth till a depth of about 4-6 km (see Tab. A2.2) where the upper crust begins with Vs at about 2.70 km/s in cell c2 and ~3.35 km/s in cell c3. The upper crust (in cell c2) is about 6 km and it overlies a lower crust with Vs of about 3.60 km/s that reaches a depth of about 34 km. In cell c3, the upper crust layer reaches a depth of about 22 km and it overlies a fast lower crust, 20 km thick, with Vs of about 3.95 km/s. The crustal structure of cell b2 is similar to that of cell c2, the thickness is the same but the lower crust is relatively faster, showing Vs of about 3.75 km/s. In cell b3 a positive velocity gradient is seen till a depth of about 5 km (see Tab. A2.2) where a low velocity layer starts, with Vs of about 3.15 km/s, and reaches a depth of about 19 km where the Moho has been located.

To the East, along the Adriatic coastline (cells c4, c5, b4 and b5) the crust is about 35 km thick and it is characterized by an about 15-20 km thick lower crust with an average Vs ~ 3.90 km/s. In cell b4 a positive velocity gradient is detected above the lower crust, while in the other cells the velocity

increases till a depth of about 6-9 km (see Tab. A2.2) and a low velocity layer, with Vs in the range 3.00-3.30 km/s, extends from this depth to the top of the fast lower crust.

In the central Adriatic Sea (cells b6, b7 and b8) the crust is no more than 25 km. An about 3 km thick layer, with a relatively high velocity of about 3.55 km/s, reaching a depth of about 7 km (see Tab. A2.2), overlies a layer with Vs in the range 3.10≤Vs≤3.30 km/s, whose thickness varies from about 8 km in cell b6 (where it overlies a relatively high velocity lower crust with Vs of about 3.60 km/s), to about 15 km in the other cells.

More to the South, in front of Latium coasts, in cell a1, the crust-mantle transition is rather complex. At a depth of about 6 km it is observed the presence of an 8 km thick layer with Vs ~4.40 km/s, underlined by an about 6 km thick layer with Vs ~ 3.15 km/s. This velocity sequence seems to be consistent with a lithospheric doubling or with the presence of a shallow layer of consolidated magma where the deeper Moho is at a depth of about 20 km.

In most of the Southern Tyrrhenian Basin, Vs values, which are usually observed in the crust (V_s~ 4.0 km/s and below), can be interpreted as mantle material (Panza et al., 2003; Panza and Pontevivo, 2004), with a relatively high percentage of partial melting (Bottinga and Steinmetz, 1979; Green and Falloon, 2005). This fact makes it difficult the identification of the crust-mantle transition as it happens in cell a2. Therefore it has been decided to study the cell as a special case using the seismic energy distribution to settle the uncertainties (see chapter 13).

In cells a3 and a4 a negative velocity gradient is observed in the crust (see Tab. A2.2): a high velocity layer, with Vs of about 3.85 km/s, is present at a depth of about 6 km overlying a slower crustal layer. However, in cell a3, that has a total crustal thickness of about 21 km, the fast layer is about 6 km thick and it overlies an about 10 km thick layer with Vs of about 3.45 km/s, while, in cell a4, the 3.85 km/s fast layer is about 2 km thick and it overlies a relatively slow layer, reaching a depth of about 13 km, with Vs ~ 2.85 km/s. Only in cell a4, at the bottom of this slow layer a lower crust, with Vs of about 3.90 km/s can be seen till a depth of 37 km. The crustal thickness decreases moving to the east: in cell a5, the crust is about 27 km thick, and it is possible to observe an upper crust with a maximum Vs of about 3.25 km/s and a lower crust with Vs of about 3.70 km/s; in cell a6, the crust is shallower reaching a depth of about 20 km and it is not observed a fast lower crust. The lower crust seems to be absent also in cell A5 where the Moho is present at a depth of about 20 km at the bottom of an about 10 km thick layer, with Vs of about 3.25 km/s.

In the Adriatic Sea and around the Otranto channel (cells a7 a8, a9, A6, A7, A8, A9, B7, B8, B9) the crustal thickness varies from about 20-25 km in the Sea area (cells a8, A6, A7, A8, A9, B7, and B8) to about 30-35 km near the coasts (cells a9, A9, and B9). Here the crust is characterized by a positive velocity gradient (see Tab. A2.2) with a slow lower crust (Vs in the range 3.10-3.30 km/s), with the exception of cells a7 and A9. In cell a7 the upper crust ends with a 13 km thick layer

having Vs of about 3.30 km/s which overlies a fast, 10 km thick, lower crust with Vs of about 3.95 km/s; near the Hellenic coasts, in cell A9, the Moho is at a depth of about 30 km and the velocity sequence sees an increase of Vs with increasing depth (see Tab. A2.2). At a depth of about 8 km a fast, 5 km thick layer starts, with Vs of about 3.90 km/s, which underlines a slower layer with Vs of about 3.50 km/s.

More to the South, in the Ionian Sea (cells C7, C8, C9, D7, D8 and D9) the crustal thickness is of about 25 km, reaching a depth of about 30 km in cell D9. The velocity of the sediments increases with increasing depth but, at a depth of 8 km, a negative gradient in the velocity distribution, is observed and the lower crustal layers have Vs in the range 3.00-3.30 km/s (see Tab. A2.2).

Moving to the west (see Fig. 11.14f), in Sardinia (cells A-2, A-1, B-2 and B-1), the crust is about 15-20 km thick and, while in the lower crust of the western coasts (cells A-2 and B-2) Vs is about 3.40 km/s, in the eastern coasts a high velocity lower crust is observed, with Vs ~ 3.90 km/s. This high velocity lower crust is present in cells A0 and B0, as well, where the crust is about 20 km thick. The Tyrrhenian basin (cells A1, A2, A3, and A4) is characterised by an about 25 km thick crust whose lower part has Vs in the range 3.50-3.70 km/s. An anomalous crust-mantle transition can be observed in cell A3 where, similarly to what observed in cells a1 and c8, at a depth of about 6 km, an about 5 km thick layer with a typical mantle-material Vs of about 4.40 km/s is observed, overlying a 10 km thick layer, with a typical crustal Vs of about 3.50 km/s. The velocity sequence seems to be consistent with a lithospheric doubling or with the presence of a shallow layer of consolidated magma. In Fig. 3.18a, b the Moho depth is represented considering, for cells c8, a1 and A3 both the shallowest and the deeper Moho position.

The Southern Tyrrhenian Basin (cells B1, B2, B3 and B4) is characterized by a very thin sedimentary layer, followed by a layering consistent with the standard schematic oceanic crustal models (e.g. Panza, 1984); the crust is about 6 km thick. Approaching Calabria the crustal thickness increases to about 24 km in cell B5, where the velocity of the sediments increases with increasing depth (see Tab. A2.2) and the lower crust has Vs ~ 3.50 km/s, and it is about 35 km in cell B6 (Calabria), where the velocity still increases with depth and the lower crust has Vs ~ 3.70 km/s. In cells from C1 to C6, with the exception of cells C3 and C4, a high velocity layer, just above the Moho, with Vs in the range 3.60-3.95 km/s, is observed, even though the crustal thickness varies from a minimum of about 20 km in cell C1 to a maximum of about 44 km in cell C5 (Messina Strait). In cells C3 and C4 the lower crustal layer has Vs in the range 3.05-3.30 km/s.

More to the South, in Sicily and its offshore regions (cells D1, D2, D3, D4, D5 and D6) the crust is about 20-25 km thick, with the exception of cell D1 where the crust is only about 15 km thick, and the lower crustal layer has Vs in the range 3.10-3.60 km/s.

In the Northern (Alps) and Eastern (Dinaridi) part of the studied area, the crust shows a typical continental character, the crustal thickness is in the range 30-40 km and in almost all the cells a clear distinction between a (slow) upper crust and a (fast) lower crust can be observed. In the central-southern part of the Adriatic Sea, the crustal models present, in general, a thickness of about 20-25 km and a lower crustal layer with Vs in the range 3.10-3.80 km/s, consistent with a graben-like character, accordingly with the models proposed by Mueller (1978).

13. Special cases.

For some cells the identification of the crust-mantle transition and the seismological definition of the nature of the crust require the use of independent information, like the seismic energy distribution.

A clear example where the identification of the crust-mantle transition on the base of Vs alone is questionable is observed in cell e4. Here, at a depth of about 23 km, a relatively high velocity layer (Vs ~ 4.0 km/s), about 30 km thick, is seen (see Fig. 11.14b). If this layer is entirely assigned to the lower crust, the Moho turns out to be about 53 km deep, i.e. deeper than what indicated by Nicolich and Dal Piaz (1990), Dèzes and Ziegler (2001) and Marone et al. (2003, 2004), as can be seen from Fig. 12.1, Fig. 12.2 and Fig. 12.3. The velocity of this layer, considered with its variability ranges (see table A2.2), can be considered either representative of the lower crust or a soft mantle. To settle the question, the seismic energy distribution versus depth has been analyzed. All the seismic events registered in cell e4, collected using the ISC (2004) online bulletin, in the period range 1904-2004, have been considered. The relation between the event magnitude and the released energy can be calculated starting from the hypothesis that the elastic energy radiated by an earthquake propagates uniformly in all directions. To calculate the seismic energy of the single event, the most used relation is that proposed by Gutenberg and Ricther (1956 a,b):

$$\log\big(E_i\,(\mathrm{erg})\big) = \big(11.4 + \big(1.5 \cdot M_s\big)\big) \tag{13.1}$$

where E_i is the energy associated to the i-th event. Where necessary, magnitudes m_b and m_l have been transformed into M_s using Peishan and Haitong (1989) relations. This is a rough procedure, but fully satisfactory for our purposes.

The Gutenberg-Richter (GR) magnitude-frequency relation, is a log–linear relation which correlates the magnitude, M, of earthquakes and their relative numbers:

$$\log N(M) = a - bM \tag{13.2}$$

The cumulative count of seismic events shown in (Fig. 13.1) indicates a significant deviation from GR relation. This fact is usually considered an indication of data uncompleteness, therefore to be conservative, in the following analysis of seismicity versus depth we group the hypocenters in 10 km intervals, instead of the 5 km interval routinely used.
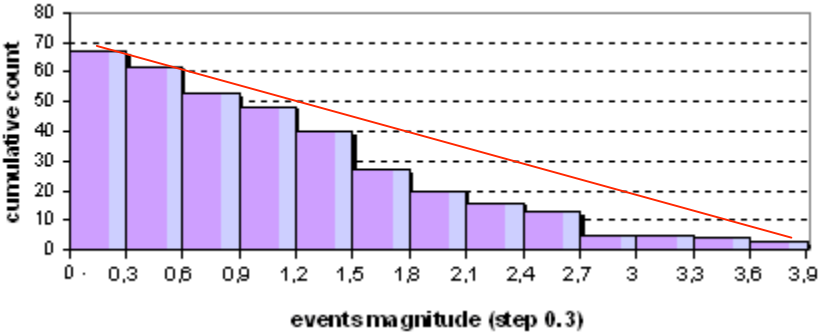
Fig. 13.1: Cumulative count of seismic events recorded in cell e4, accordingly to the ISC online bulletin and grouped in magnitude interval $\Delta M=0.3$.

The seismic energy versus depth has been calculated, grouping the events with hypocentres falling in the depth intervals (open to the right) 0-10; 10-20; 20-30; 30-40 and 40-50:

$$E_n(\text{erg}) = \sum_{i=1}^{m} E_i(\text{erg})$$

(13.3)

where m is the number of events of n-th interval and it has been represented as $\log(E_n/A_{min})$ where A_{min} (erg) is the minimum E_n, computed in one of the considered depth intervals. In this case the minimum energy (i.e. 2.37×10^{15} erg) lies in the depth interval 30-40 km.
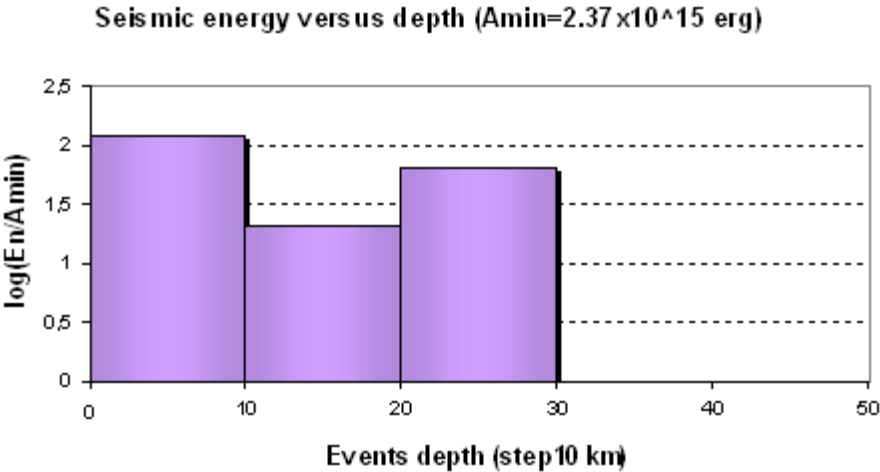
Fig. 13.2: Seismic energy distribution in cell e4, represented as $\log(E_n/A_{min})$ vs. depth: $A_{min}(\text{erg})= 2.37 \times 10^{15}$ erg is the minim energy, registered in the depth interval 30-40 km.

The seismic energy distribution, for cell e4, is shown in Fig. 13.2, where it can be seen that seismicity terminates below the depth of 40 km. Therefore, it can be reasonable to assign the first 17 km of the analysed layer to the brittle continental crust, placing the Moho at a depth of 40 km, in excellent agreement with Nicolich and Dal Piaz (1990), Dèzes and Ziegler (2001), Marone et al. (2003, 2004).
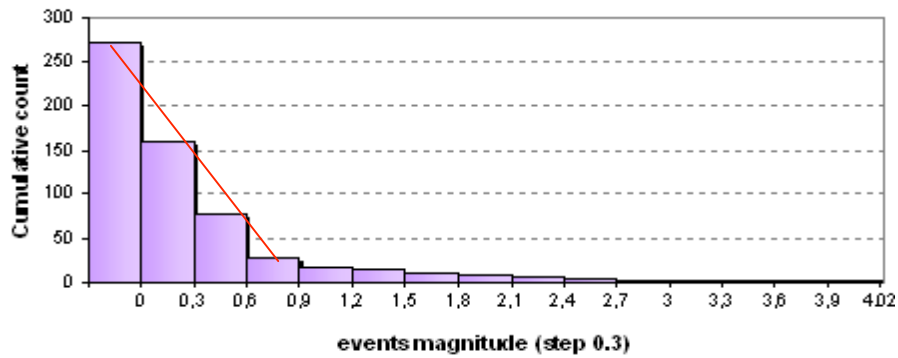
Fig. 13.3: Cumulative count of seismic events collected in cell a2 by the ISC online bulletin (1904-2004) and grouped every 0.3 M_s interval.
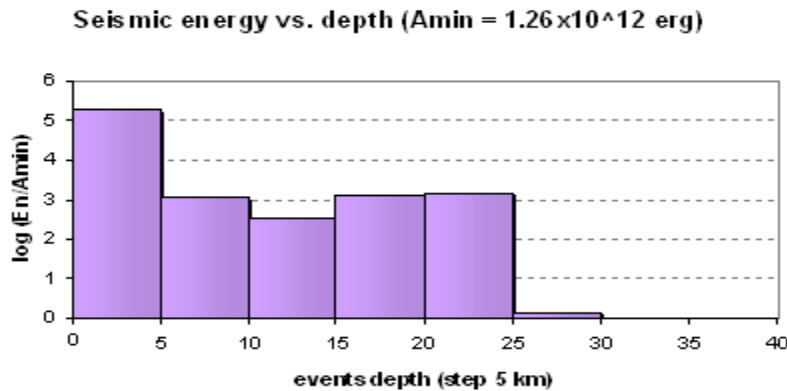
Fig. 13.4: Seismic energy distribution in cell a2, represented as $\log(E_n/A_{min})$ vs. depth: $A_{min}(erg)$= 1.26×10^{12} erg is the minim energy, registered in the depth interval 30-35 km.
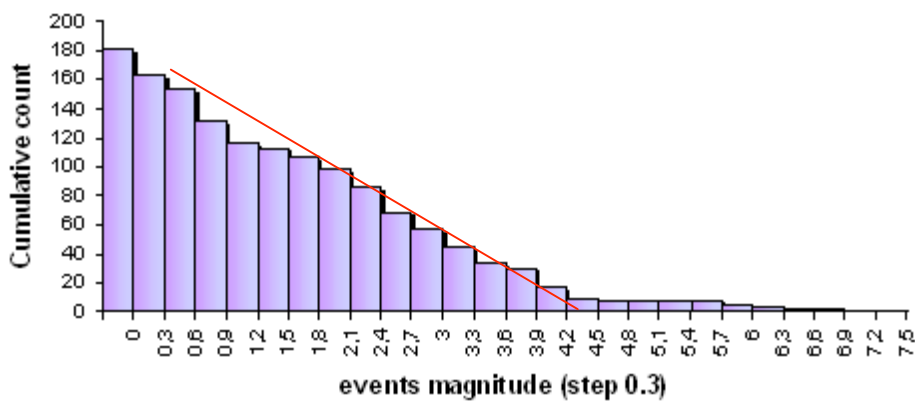
Fig. 13.5: Cumulative count of seismic events collected in cell C5 by the ISC online bulletin (1904-2004) and grouped every 0.3 M_s interval.
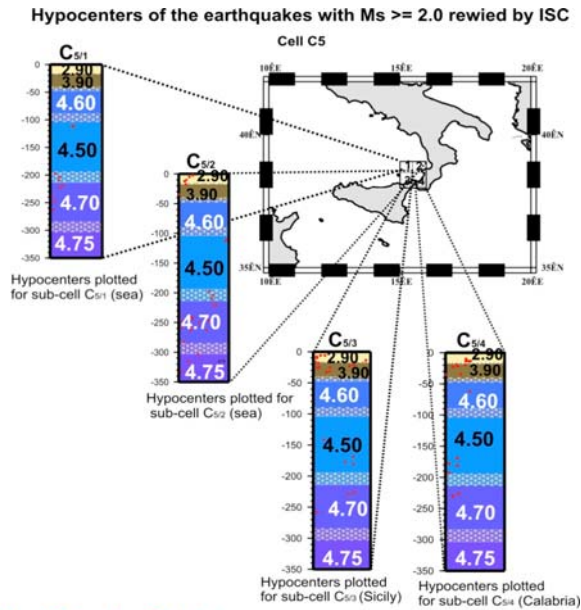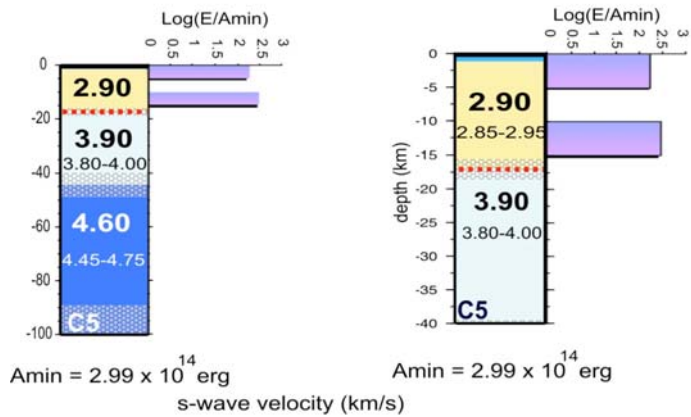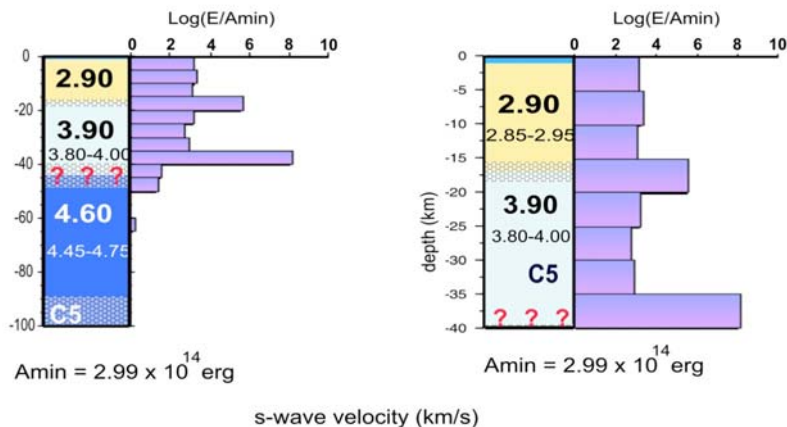
Fig. 13.6: Seismic energy vs. depth for all events with magnitude above the completeness threshold, defined by means of an exploratory analysis of the Gutemberg-Richter relation of the earthquake catalogue extracted from the ISC catalogue. Cell C5 (containing Stromboli) is divided into a northern (sub-cell C5/1 + sub-cell C5/2) and a southern (sub-cell C5/3 + sub-cell C5/4) part in order to highlight the seismicity space distribution and its contribution to the seismic energy, as shown in the lower panel. From the distribution of seismic energy, we can conclude that the crust-mantle transition is quite sharp (red brocken line) in the northern part, while it is broad (? ? ?) in the southern part of cell C5, where it reaches a depth of around 40 km.

The remaining 13 km are thus interpreted as a very soft mantle layer. A similar case is encountered in the Tyrrhenian Basin.

In this area and particularly in most of the Southern Tyrrhenian Sea, V_s values that are usually observed in the crust ($V_s \sim$ 4.0 km/s and below), can be interpreted as mantle material (Panza et al., 2003; Panza and Pontevivo, 2004), with a relatively high percentage of partial melting (Bottinga and Steinmetz, 1979; Green and Falloon, 2005). This fact makes it difficult the identification of the crust-mantle transition as it happens in cell a2 (see Fig. 11.14d) where an upper crust reaching a depth of about 7 km, with Vs ~ 3.30 km/s, overlies a 20 km thick layer with Vs ~ 3.90 km/s, reaching a depth of about 37 km. The cumulative count of seismic events for cell a2 is shown in Fig. 13.3. On account of the regular shape visible in Fig. 13.3, fairly consistent with the GR law, at small magnitudes, all the events registered in cell a2, collected using the ISC (2004) online bulletin, in the period range 1904-2004, have been considered and grouped, in depth, every 5 km.

Cell e-1N (9.5; 45.5) NORTH			Cell e-1S (9.5; 45.5) SOUTH			Cell e-1 (9.5; 45.5)		
h	V_S	V_P	h	V_S	V_P	h	V_S	V_P
(km)	(km/s)	(km/s)	(km)	(km/s)	(km/s)	(km)	(km/s)	(km/s)
1	2.75	4.80	1	1.45	2.50	3	2.30	4.00
1	3.00	5.20	1	1.80	3.20	3	2.60	4.50
1	3.35	5.80	1	2.30	4.00	----	----	----
1	3.45	6.00	1	2.40	4.20	----	----	----
----	----	----	1	2.75	4.80	----	----	----
P6	P1	P1x1.73	P6	P1	P1x1.73	P6	P1	P1x1.73
P7	P2	P2x1.73	P7	P2	P2x1.73	P7	P2	P2x1.73
P8	P3	P3x1.73	P8	P3	P3x1.73	P8	P3	P3x1.73
P9	P4	P4x1.73	P9	P4	P4x1.73	P9	P4	P4x1.73
P10	P5	P5x1.73	P10	P5	P5x1.73	P10	P5	P5x1.73
h	Step	Range	h	Step	Range	h	Step	Range
(km)	(km)	(km)	(km)	(km)	(km)	(km)	(km)	(km)
P6	3	4-13	P6	3.5	8-15	P6	5	10-20
P7	8	16-32	P7	6	7-25	P7	8	9-25
P8	30	32-62	P8	15	17-62	P8	30	30-80
P9	40	70-110	P9	40	70-110	P9	35	40-100
P10	40	70-110	P10	40	70-110	P10	40	40-110
V_S	Step	Range	V_S	Step	Range	V_S	Step	Range
(km/s)	(km/s)	(km/s)	(km/s)	(km/s)	(km/s)	(km/s)	(km/s)	(km/s)
P1	0.30	2.15-3.50	P1	0.10	3.45-3.95	P1	0.25	2.50-4.00
P2	0.20	3.30-4.10	P2	0.25	3.05-4.05	P2	0.25	2.40-4.05
P3	0.30	3.50-4.70	P3	0.20	3.70-4.60	P3	0.25	3.70-5.20
P4	0.25	3.80-4.80	P4	0.20	4.00-4.80	P4	0.30	3.80-5.20
P5	0.40	3.70-4.90	P5	0.30	3.80-5.00	P5	0.40	3.85-5.20

Tab. 13.1: Parameterization used in the non-linear inversion. Grey area: h (thickness), Vs, Vp of each layer. The uppermost layers are fixed on the basis of available literature (Cassinis et al., 1990). The variable parameters are Pi, with i=1, .., 5 for thickness and i=6, 10 for Vs. White area: step and variability range for each parameter Pi.

According to the distribution of seismic energy versus depth (see Fig. 13.4) and the seismic refraction data (e.g. Nicolich and Dal Piaz, 1990) the discussed layer can been reasonably assigned to the crust only till a depth of about 25 km, where the recorded seismicity stops, and the Moho depth, in cell a2, has been set at this depth.

In the area from Stromboli, Messina strait to Southern Calabria (cell C5, see Fig. 3.14f) it is difficult to define the nature of the crust, since a layer with V_s in the range 3.80-4.00 km/sec and reaching a depth of about 44 km, is detected above high velocity mantle material. The analysis of the seismicity in cell C5 has been done as follows. The cumulative count of seismic events is shown in Fig.13.5. On account of the shape visible in Fig. 13.5, from the ISC (2004) online bulletin, for the period range 1904-2004, we have selected all the events with magnitude above the completeness threshold registered in cell C5, Ms~2, and grouped them, in depth, every 5 km.

The analysis of the seismic energy distribution leads two distinct interpretations for this layer (two-faced "Janus"). If we plot the hypocenters at sea, the layer is totally aseismic and therefore it can be reasonably assigned to the partially molten mantle. On the other side, if all events in cell C5 are considered, the "Janus" layer is occupied only by hypocenters of events located either in Sicily and Calabria (continental area) or close to their shoreline (as shown in Fig. 13.6). In such a case the layer can be reasonably assigned to the brittle continental crust.
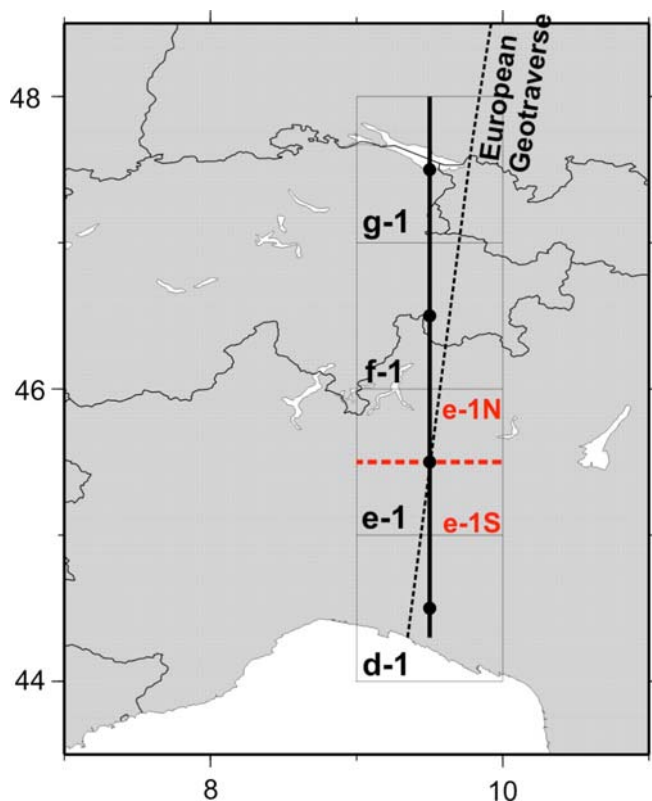
Fig. 13.7: Plot of the studied profile (solid line) through the Central Alps, the Po Plain and the Ligurian Apennines. Each dot corresponds to the centre of the 1°x1° cell. A part of the European Geotraverse (dashed line) is also shown.

Another interesting case (cell e-1) is encountered in a geologically complex area, where the southern part of the Central Alps joins the Po Plain. In this case the cell has been divided in two sub-cells of 1° (longitude) x 0.5° (latitude) and the non-linear "hedgehog" inversion has been repeated twice using the same dispersion relations but different shallow crustal a priori constraints for the northern and southern part in order to take into account the different geological evidences (see Tab. 13.1). Let us label the northern sub-cell as e-1N and the southern one as e-1S.

Cell e-1N (9.5;45.5) NORTH		Cell e-1S (9.5;45.5) SOUTH		Cell e-1 (9.5;45.5)	
Vs	h	Vs	h	Vs	h
(km/s)	(km)	(km/s)	(km)	(km/s)	(km)
2.75	1	1.45	1	----	----
3.00	1	1.80	1	2.30	3
3.35	1	2.30	1	2.60	3
3.45	1	2.40	1	----	----
----	----	2.75	1	----	----
2.55-2.85	5.5-8.5	3.60-3.70	8-10	3.00-3.25	10-12.5
3.60-3.80	20-28	3.45-3.65	10-16	3.85-4.10	21-25
4.25-4.55	47-62	4.10-4.30	32-39.5	4.30-4.55	65-80
4.15-4.45	70-90	4.30-4.50	90-110	4.20-4.50	82.5-100
4.30-4.70	90-110	4.25-4.55	90-110	4.20-4.60	90-110
4.75	***	4.75	***	4.75	***
4.90	44	4.90	44	4.90	44

Tab. 13.2: Results of the inversion: range of variability of the parameters h (thickness) and V_s for each layer of the chosen solution.

From the set of retrieved solutions, the representative models have been chosen by applying the LSO to the cell crossed by the European Geotraverse (see Fig. 13.7). The results are reported in Tab. 13.2.
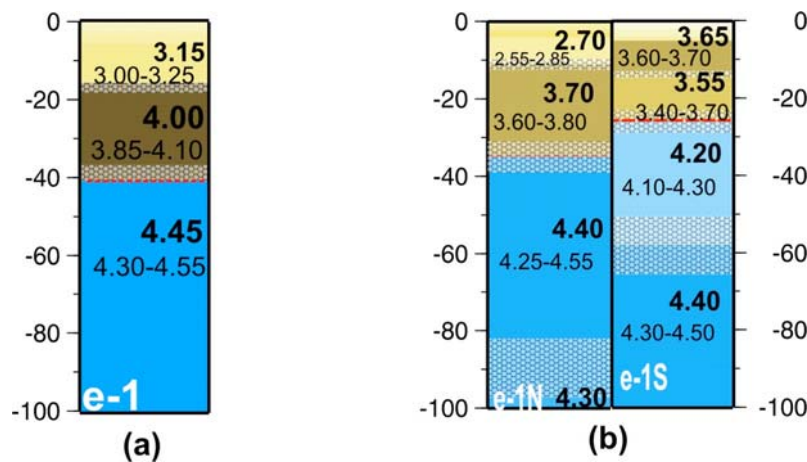
Fig. 13.8: Structural models, for the upper 100 km, for the chosen solution of cell e-1 (a) and of the two sub-cells e-1N and e-1S (b). The retrieved velocity (km/s) and its range of variability are shown. The variability range for the layer thickness is indicated by the shadowed area. This representation is used to evidence that the boundaries between layers can well be transition zones in their own right.

In Fig. 13.8 the structural models, down to 100 km, both for the 1° x 1° cell e-1 (a) and the 1° x 0.5° sub-cells e-1N and e-1S (b) are shown. We can see a Moho as deep as about 35 km in the northern part (e-1N) and a shallower Moho, which reaches a depth of about 26 km in the southern part (E-1s). In the northern part the velocity increases in the uppermost 4 km (see Tab. 13.1), below this depth a relatively low velocity layer, with Vs~2.70 km/s, is present till a depth of about 11 km overlying a fast lower crust with Vs~3.70 km/s.
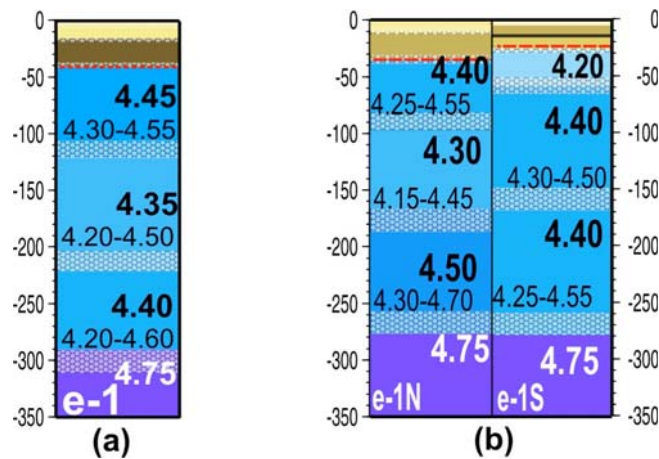
Fig. 13.9: Structural models, down to a depth of 350 km, for the chosen solution of cell e-1 (a) an of the two sub-cells e-1N and e-1S (b). The retrieved velocity (km/s) and its range of variability are shown. The variability range for the layer thickness is marked by the shadowed area. This representation is used to evidence that the boundaries between layers can well be transition zones in their own right.

In the southern part, the velocity increases with depth (see Tab. 13.1), at a depth of about 5 km a relatively fast layer, with Vs~3.65 km/s, is present till a depth of about 13 km overlying an about 13 km thick layer, with Vs~3.55 km/s.

In Fig. 13.9 the structural models, down to a depth of 350 km, are shown both for the 1° x 1° cell e-1 and the two sub-cells e-1N and e-1S. While in the northern part (e-1N) the Vs sequence in the mantle is similar to that observed in the, 1° x 1° cell, e-1 and a lithosphere reaching a depth of about 95 km overlies an asthenosphere with Vs of about 4.30 km/s reaching a depth of about 170 km, in the southern part (cell e-1S) a low velocity uppermost mantle, with Vs of bout 4.20 km/s is seen just below the Moho reaching a depth of about 60 km. It overlies a mantle characterized by almost constant Vs of about 4.40 km/s.

14. Validation of inversion results with independent data: comparison between different maps of crustal thickness.

Having defined the Moho depth for all cells (104), it is possible, by smooth interpolation, to construct the map of crustal thickness represented in Fig. 14.1. In the figure the contours of the shallower Moho where a possible lithospheric doubling has been detected, are shown.
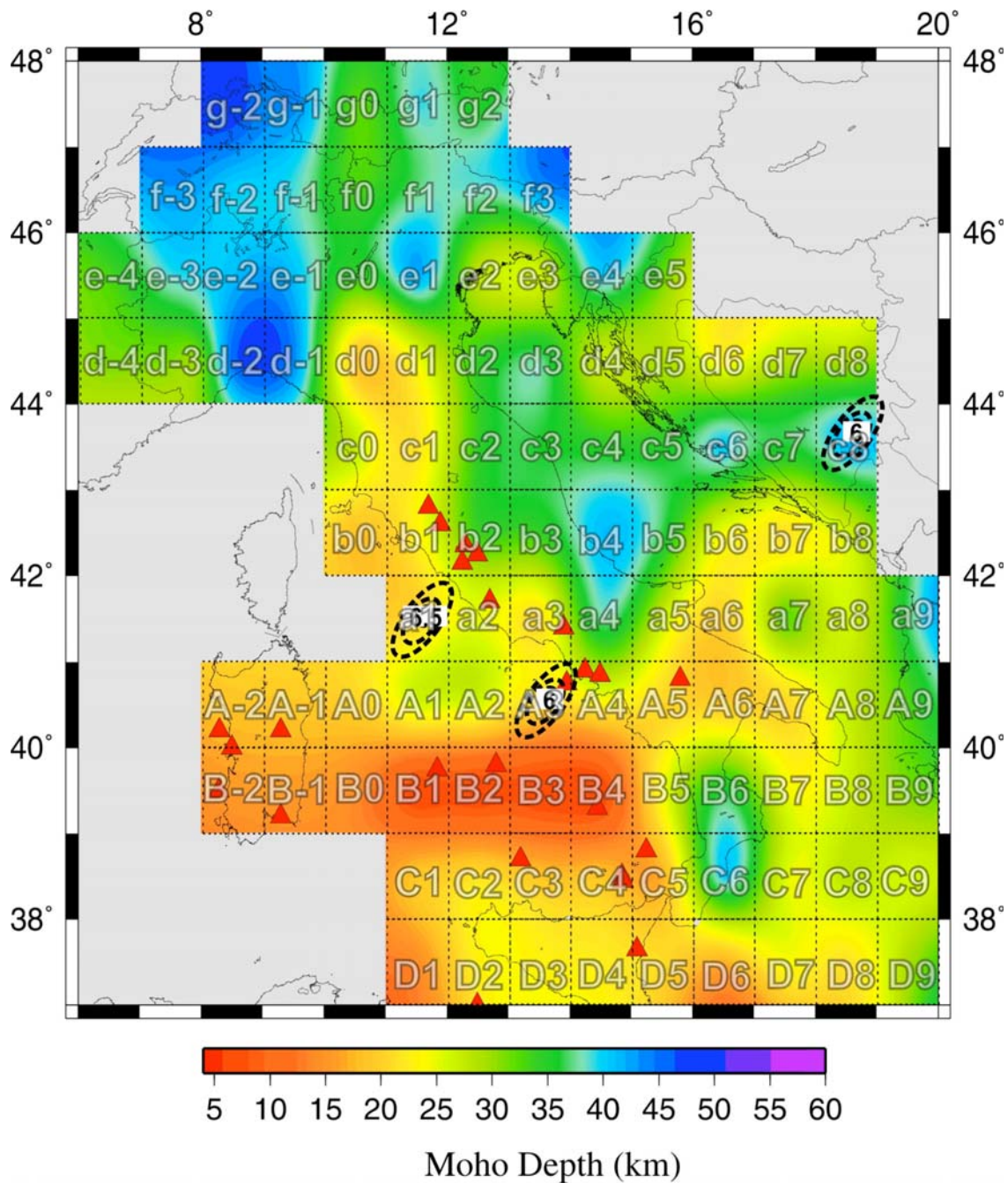
Fig. 14.1: Moho depth with contouring of the shallower Moho where lithospheric doubling has been detected. The map has been obtained with smooth interpolation of the 1° x 1° Moho depth data. On the map the cellular grid has been superimposed.

From Fig. 12.3, which represents the European crustal thickness determined from controlled source experiments (Dèzes and Ziegler, 2001), we can extract the part overlapping our study area (see Fig. 14.2). On the map the cellular grid, with the same notation used in Fig. 14.1 has been superimposed.
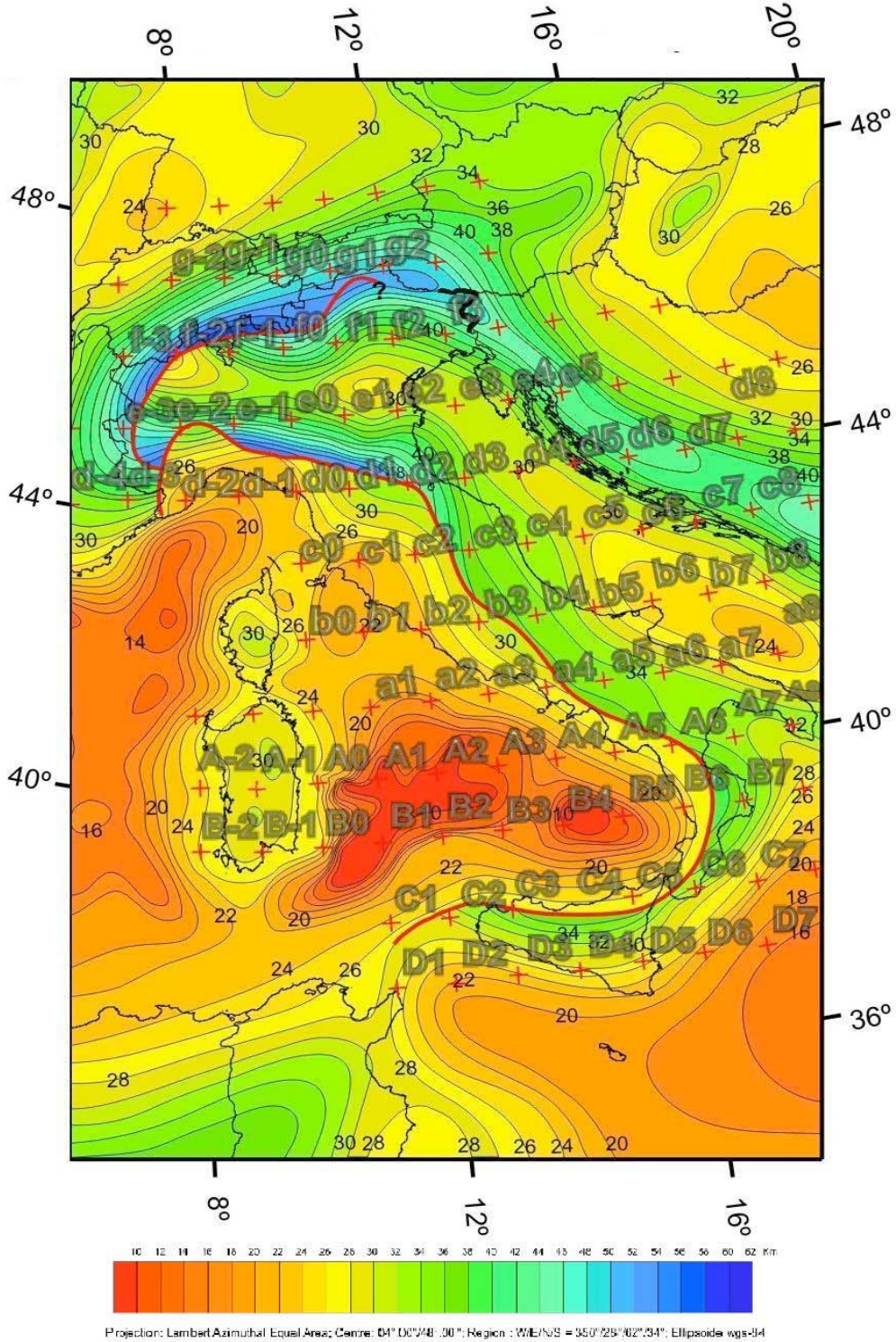
Fig. 14.2: Drawn out from Fig. 12.3: depth of the Mohorovich discontinuity compiled from Dèzes and Ziegler, 2001 http://comp1.geol.unibas.ch/downloads/Moho_net/euromoho1_3.pdf).

From this map the average cellular Moho depth (M_{CS}) has been determined in order to make a comparison between the crustal thickness determined from the surface wave tomography (M_{SW}) and controlled source experiments (M_{CS}). In Fig. 14.3 it is shown the map of M_p constructed with the same smooth interpolation and the same colour scale used in Fig. 14.1.
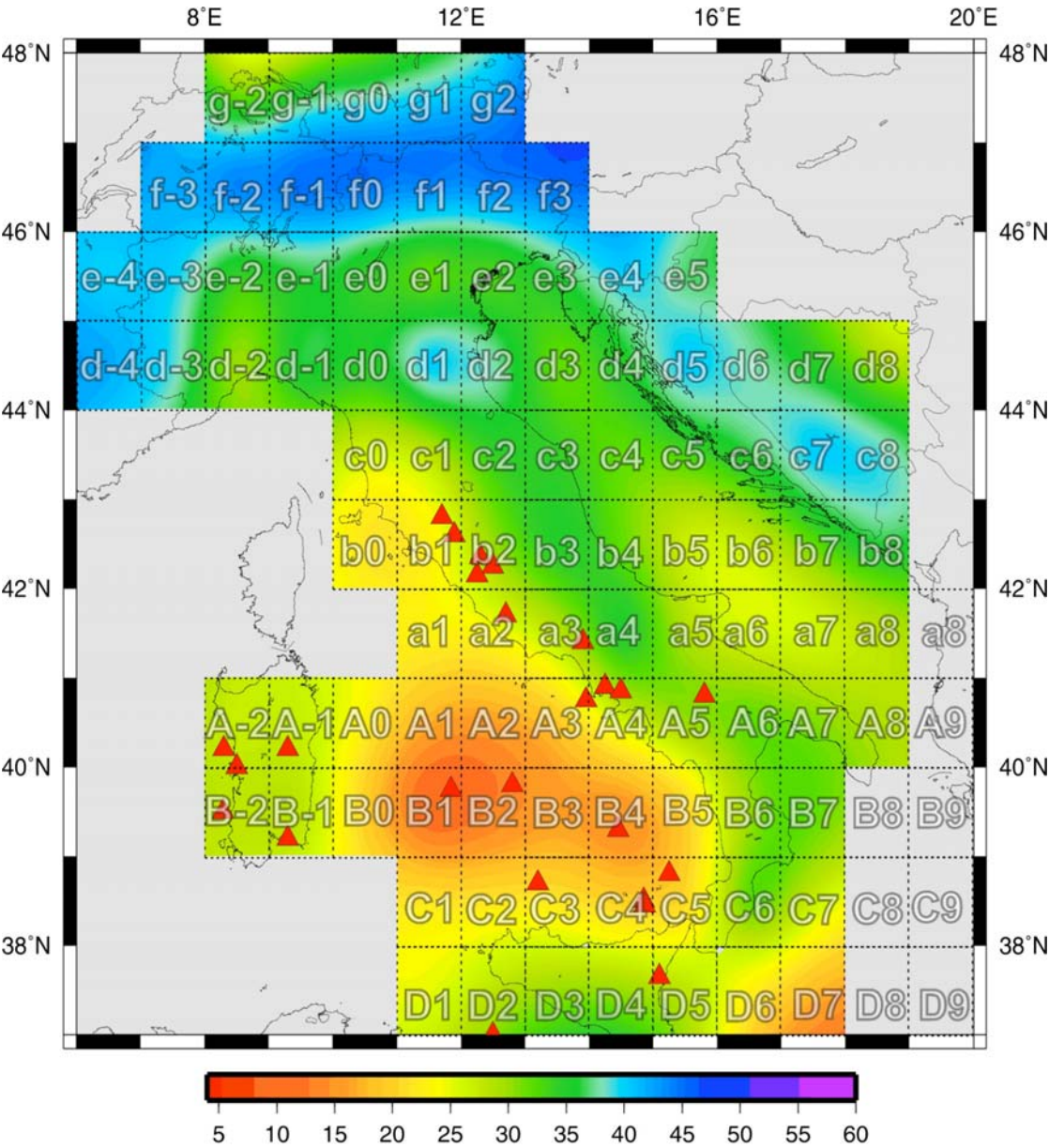
Fig. 14.3: Average Moho depth extracted from the map of the depth of the Mohorovich discontinuity compiled from Dèzes and Ziegler (2001) overlapping our study area. The map has been obtained with the same smoothing interpolation, used fro Fig. 14.1, of the 1° x 1° data. On the map the cellular grid has been superimposed.

The crustal thickness resulting from surface waves tomography is quite nicely validated by the comparison with the results of controlled source experiments (Dèzes and Ziegler, 2001). The major

differences are encountered in limited zones and the absolute difference does not exceed about 16 km (see Fig. 14.4). Where the difference is less than about 7 km the two Moho definitions cannot be considered different, within errors.
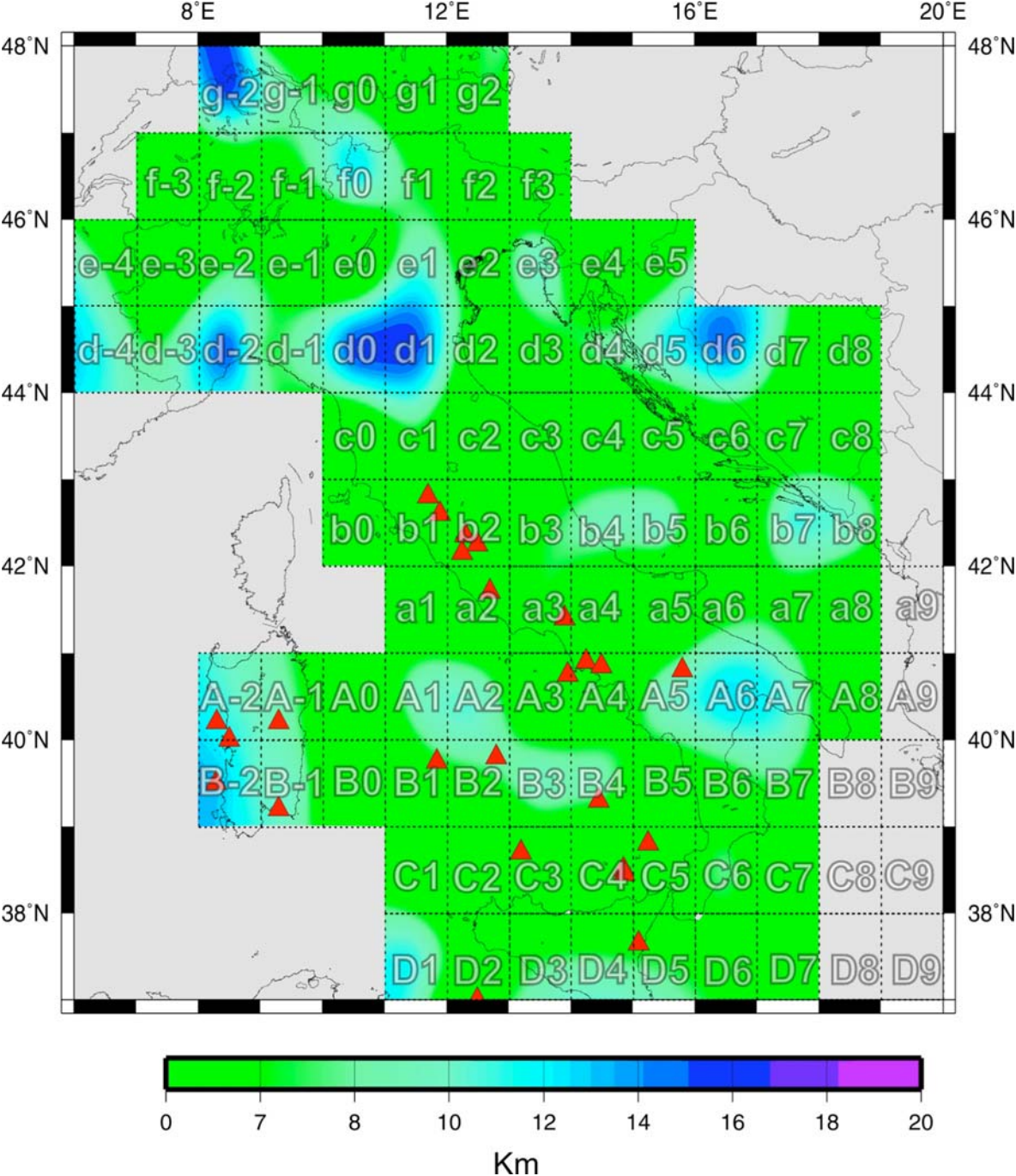
Fig. 14.4: Absolute value of the differences ($|M_{SW} - M_{CS}|$) between crustal thicknesses determined from surface wave tomography, M_{SW}, and controlled source experiment, M_{CS}, (Dèzes and Ziegler, 2001). Significant discrepancy, between the two estimations of the Moho depth, evidenced in isolated areas, outlines zones for future investigations.

15. The lithosphere asthenosphere system.

In the western part of the Molasse Basin (Fig. 11.14 a, b), near to the junction with the Jura belt (cells g-2 and g-1), below the Moho, at a depth greater than 45 km, a fast lid, reaching a depth of about 75-80 km is observed, with Vs of about 4.65 km/s. While in cell g-2 the lid overlies a ~100 km thick, relatively fast asthenosphere, with Vs ~ 4.30 km/s, the top of the asthenospheric layer in cell g-1, with Vs ~ 4.25 km/s is at a depth of about 185 km and extends to a depth of about 295 km. Moving to the East, in the northern part of the Eastern Alps (cells g0 and g1), the Moho depth becomes shallow and the lithosphere (Vs of about 4.45 km/s) reaches a depth of about 175 km in cell g0 and 190 km in cell g1. At this depth it is possible to observe the top of the asthenosphere with Vs ~ 4.35 km/s in cell g0 and about 4.25 km/s in cell g1. In both cells the asthenosphere reaches a depth of about 250 km. In cell g2 the uppermost mantle layer has Vs ~ 4.25 km/s and it overlies a relatively fast lid (Vs ~ 4.55 km/s) that starts at a depth of about 65 km and reaches a depth of about 165 km.

Along the Alpine Arc (cells d-4, d-3, d-2, d-1, e-4, e-3, f-3, f-2, f-1, f0, f1, f2 and f3) the Moho depth is in the range 35-40 km. In cell f-3 a slow, about 35 km thick lid, with Vs ~ 4.45 km/s overlies an about 110 km thick asthenosphere, with Vs ~ 4.35 km/s. In cell f-2 a fast lid is present just below the Moho and reaches a depth of about 75 km, where an about 110 km thick asthenosphere (Vs ~ 4.30 km/s), starts. In cells f-1 and f1 the lithosphere, with Vs ~ 4.50 km/s reaches a depth of about 120 km in cell f-1 and about 85 km in cell f1 and, at greater depths, the velocity is almost constant, as fast as about 4.40-4.45 km/s, till a depth of about 295 km in cell f-1 and 250 km in cell f1. The lithosphere reaches a depth of about 180 km in cell f0 and the uppermost mantle has average Vs ~ 4.50 km/s. At the bottom of the lithosphere, a low velocity asthenosphere, with Vs ~ 4.00 km/s, reaches a depth of about 250 km. In cell f2, a relatively slow lithospheric layer, about 30 km thick, with Vs ~ 4.35 km/s, starts at a depth of about 39 km. For greater depths the Vs is almost constant (as fast as about 4.50 km/s) down to a depth of about 245 km. In the mantle of cell f3 the velocity is almost constant at about 4.40 km/s, in the depth range 43-243 km. In cell e-4 the lithosphere reaches a depth of about 170 km and a fast lid, with Vs ~ 4.60 km is detected in the depth range 110-170 km overlaying the asthenosphere (Vs about 4.35 km/s) which extends till a depth of about 280 km. In cell d-4, an almost constant Vs ~ 4.40 km/s, is observed in the upper mantle, till a depth of about 270 km.

In cells d-3, d-2 and d-1, considering the range of variability of the detected velocities (see Fig. II a in Appendix II), it is possible to notice the presence of lithosphere till a depth of about 120-130 km. Below this depth a relatively fast asthenosphere, with Vs of about 4.35 km/s, about 100 km thick is seen in cells d-2 and d-3, while in cell d-1 the asthenosphere is slower (Vs ~4.25 km/s) and thinner (as think as about 70 km). In cells e-3, just below the Moho a fast lid is observed with Vs ~ 4.55 km/s, reaching a depth of about 125 km. The lid is underlain by a relatively fast asthenosphere with Vs ~ 4.30 km/s reaching a depth of about 220 km.

In the Southern-Central Alps (cells e-2 and e-1), the uppermost mantle has Vs ~ 4.45 km/s and the lithosphere reaches a depth of about 120 km/s overlaying an about 100 km thick asthenospheric layer where Vs ~ 4.35 km/s. In cell e0 an about 70 km thick asthenospheric layer, with Vs ~ 4.00 km/s is present at a depth of about 175 km at the bottom of a relatively fast, about 50 km thick, lid with Vs ~ 4.50 km/s.

Moving to the Po Plain (cell e1), below the Moho, at a depth of about 40 km, a fast lid, about 40 km thick, is observed with Vs ~ 4.75 km/s and, at a depth of about 150 km a low velocity asthenosphere, with Vs ~ 4.00 km/s, starts and reaches a depth of about 210 km. More to the east, in cells e2 and e3, a relatively low velocity layer is observed just below the Moho, with Vs ~ 4.25 km/s, no deeper than about 60 km. This layer overlies a fast lid, with Vs in the range 4.65-4.75 km/s and with a thickness of about 60 km.

The asthenosphere, with Vs ~ 4.20 km/s, extends to a depth of about 200 km, in cell e3 and it is observed in the depth range 160-210 km, with Vs ~ 4.00 km/s, in cell e2. In cell e4, as explained in chapter 3.5.1, the Moho has been fixed at a depth of about 40 km. Therefore, the fast lid, with Vs ~ 4.80 km/s, present in the depth range 53-83 km, is overlain by a soft uppermost mantle with Vs ~ 4.00 km/s. At the bottom of the lid a gentle velocity gradient can be noticed in the asthenospheric mantle. In cell e5 the lithosphere reaches a depth of about 117 km and a relatively fast lid, with Vs ~ 4.55 km/s can be seen in the depth range 57-117 overlaying the asthenosphere (Vs ~ 4.30 km/s,)which extends to a depth of about 205 km.

Panza et al. (2003) and Panza and Pontevivo (2004) have used the term "mantle wedge" to indicate the low velocity zone (Vs ≤ 4.20 km/s) in the uppermost mantle, where the amout of partial melting can be greater than 1%, according to Bottinga and Steinmetz (1979) and Green et al., 1991 models, overlying a lid with V_s generally greater than about 4.35 km/s. In the north-western part of the Apennines chain (cells d0 and d1) (Fig. 11.14 c, d), just below the Moho it is detected a relatively soft mantle, with Vs ~ 4.15 km/s and thickness of about 40 km in cell d0 and 30 km in cell d1, which overlies a fast lid, with Vs

~ 4.80 km/s and reaching a depth of about 85 km. This Vs sequence versus depth appears to be consistent with the presence of a *mantle wedge*.

More to the east, in cell d2 the lithosphere reaches a depth of about 170 km with a Vs almost constant (about 4.45 km/s). At the bottom of the lithosphere a low velocity asthenospheric layer, as thick as about 60 km, with Vs ~ 4.00 km/s is detected. In the neighbouring cell d3 the lithosphere is thinner, reaching a depth of about 120km and a fast lid, with Vs ~ 4.60 km/s can be seen in the depth range 70-120 km, overlying an about 100 km thick asthenosphere with Vs ~ 4.20 km/s.

In the northern part of Dinarides chain, in cell d4, a low velocity layer, with Vs ~ 4.15 km/s is seen between the Moho and a fast lid (Vs ~ 4.85 km/s) present in the depth range 65-115 km and overlain by an about 100 km thick asthenosphere with Vs ~ 4.20 km/s. In cell d5 the fast lid, as thick as about 30 km, with Vs ~ 4.60 km/s starts at a depth of about 60 km. At the bottom of the lid the Vs is almost constant at about 4.40 km/s till a depth of about 250km. The uppermost mantle of cell d6 has a low velocity layer, with Vs ~ 4.20 km/s, below the Moho on the top of a 60 km thick lid with Vs ~ 4.50 km/s and the asthenosphere seems to be absent. The fast lid seems to be absent in cells d7 and d8, where a gentle velocity gradient is observed in the upper mantle even though in cell d8 a low velocity uppermost mantle, with Vs ~ 4.20 km/s, reaching a depth of about 45 km can be seen.

To the South, in cell c8, where a lithospheric doubling is consistent with the Vs sequence, below the deeper Moho, almost constant Vs (~ 4.40 km/s) is observed in the upper mantle. In cells c6 an about 30 km thick lid, with Vs of about 4.60 km/s is sitting on a mantle characterized by a Vs of about 4.40 km/s till a depth of about 230 km, while the relatively fast lid, with Vs ~ 4.50 km/s, reaching a depth of about 95 km, is seen on the top of an about 55 km thick asthenospheric layer, with Vs of about 4.30 km/s. In the Adriatic Sea, while in cell c5 the upper mantle is characterized by an almost constant Vs ~ 4.40 km/s reaching a depth of about 235 km, in cell c4 the uppermost mantle layer has Vs ~ 4.40 km/s till a depth of about 95 km where the top of a fast lid, with Vs ~ 4.60 km/s and reaching a depth of about 145 km, is detected.

In the Northern Apennines area, cell c0 shows an upper mantle with almost constant Vs around 4.40 km/s till a depth of about 300 km while in cell c1 a thin (about 18 km) and low velocity uppermost mantle layer, with Vs ~ 4.10km/s overlies a relatively fast lid with Vs ~ 4.55 km/s and about 35 km thick. This fast layer, which has a thickness that varies from about 35 km in cell c2 and about 50 km in cell c3, starts just below the Moho, which is at a depth of about 35 km, in cell c2 and at a depth of about 40 km in cell c3 Below the lid, in

cells c1 and c2, the mantle exhibits almost constant Vs ~ 4.40 km/s till a depth of about 280 km, while in cell c3 the asthenosphere is present with Vs ~ 4.35 km/s till a depth of about 190 km.

Going to the South, near the Tuscany coasts, in cell b0 a mantle wedge, about 8 km thick, with Vs ~ 3.95 km/s is observed just below the Moho overlying an upper mantle, characterized by a gentle positive velocity gradient. The Vs increases from 4.25 km/s to 4.45 km/s till a depth of about 290 km. Similar characteristics can be observed in cell b1, where the uppermost mantle layer, starting at a depth of about 23 km, has Vs ~ 4.20 km/s, and cell b2 where the relatively low velocity uppermost mantle layer seems to be absent, while the gentle increase of Vs with increasing depth is still observed.

In the Central Apennines and near the coasts of Abruzzo, in cells b3 and b4 a relatively high velocity lid, with Vs in the range 4.50-4.60 km/s, is observed just below the Moho and reaches a depth of about 100 km, where an asthenospheric layer starts, with Vs of about 4.25-4.30 km/s. In cell b5 the lithosphere, with Vs ~ 4.45 km/s, reaches a depth of about 165 km and overlies an about 100 km thick asthenosphere with Vs ~ 4.40 km/s.

More to the East, in cell b6 a relatively low velocity uppermost mantle layer, with Vs ~ 4.20 km/s, is observed till a depth of about 38 km (see also table A2.2 and Fig. 11.14c) overlying a layer with Vs constant at about 4.40 km/s which reaches the depth of about 230 km. A low velocity layer is present just below the Moho also in cell b7 where Vs is about 3.95 km/s (see also Table A 2.2), and in cell b8 where it is about 4.20km/s. This layer is on the top of a 30 km thick layer with a high velocity of about 4.60 km/s. This high velocity lid is sits on top of an about 70 km thick asthenosphere, with Vs ~ 4.35 km/s.

In front of Latium coasts, in cell a1 a lithospheric doubling is consistent with the presence of a layer with mantle-material (Vs ~ 4.40 km/s), about 8 km thick, between two layers characterized by a typical crustal velocity. The shallower crust-mantle boundary can be observed at a depth of about 6.5 km, while, the deeper one is at about 20 km where the Moho depth is located by seismic refraction data (e.g. Nicolich and Dal Piaz, 1990), local, regional and teleseismic data (e.g. Marone et al., 2003). The Moho is on top of a ~ 20 km thick high velocity lid, with Vs ~ 4.50 km/s which overlies an about 90 km thick asthenosphere, with Vs ~ 4.20 km/s. In cell a2 the shut-down of the distribution of seismicity vs. depth within the cell, as shown in Fig. 13.4, at a depth of about 25 km, leaves room for an about 12 km thick aseismic, low velocity, mantle wedge, with a percentage of partial melting of about 2-3%, accordingly with Bottinga and Steinmetz (1979). At the bottom of this soft mantle a fast lid, with Vs ~ 4.70 km/s reaches a depth of about 55 km and it overlies a relatively slow asthenosphere, with Vs ~ 4.10 km/s that extends till a depth

of about 115 km. In cell a3, just below the Moho, a relatively low velocity uppermost mantle with $V_s \sim 4.20$ km/sec and a thickness of about 30 km is present. Below this layer V_s increases with depth.

In cell a4 the lithosphere reaches a depth of about 110 km, and Vs of about 4.40-4.45 km/s characterize the upper mantle, while in cell a5 a gentle positive velocity gradient is observed. Similar features are seen in cell a6 where a relatively low velocity (Vs ~ 4.20 km/s) uppermost mantle layer overlies a lid with Vs of about 4.45 km/s reaching a depth of about 115 km, where the top of a relatively fast asthenosphere (Vs of about 4.40 km/s) is detected. In cell a7, just below the Moho an about 90 km thick lid, with Vs ~ 4.50 km/s, is observed overlying a relatively fast asthenosphere, with Vs of about 4.40 km/s, that extends to a depth of about 240 km. In cell a8 the lithosphere reaches a depth of about 115 km and a lid with Vs of about 4.50 km/s can be noticed in the depth range 55-115 km, sitting on a relatively fast asthenosphere, about 60 km thick, with Vs of about 4.40 km/s. In cell a9 an about 50 km thick lid is seen just below the Moho, with Vs ~ 4.55 km/s. At the bottom of the lid, the asthenosphere (Vs ~ 4.30 km/s) is seen till a depth of about 115 km.

In the Southern Apennines and around the Otranto Channel, cells A5, A6 and A7 exhibit a lithosphere as deep as about 90-100 km characterized by a low velocity layer, with Vs in the range 4.10-4.25 km/s present just below the Moho and sitting on a fast lid, with Vs in the range 4.60-4.80 km/s. Only in cells A5 and A6 the presence of an asthenospheric layer, with Vs of about 4.30-4.35 km/s in clearly detected. Similar features can be seen in cells B5, B6 and B7 but the lithosphere is deeper: it reaches a depth of about 165-175 km even though the presence of a slower uppermost mantle over the fast lid is observed. In cells A8 and A9 the lid is present just below the Moho, but while it is as deep as about 90 km, with Vs ~ 4.55 km/s, in cell A9, it is shallower (~ 70 km deep), with Vs of about 4.60 km/s, in cell A8. The underlying asthenosphere has a relatively high average Vs of about 4.45 km/s, with a minimum value ~ 4.30 km/s in cell A8. Similarly, in cell B9 the lid, with Vs ~ 4.60 km/s, as deep as about 80 km, overlies an about 60 km thick slow mantle layer (Vs~4.35 km/s). At greater depth the velocity increases (Vs~4.70 km/s) till a depth of about 220 km, below which a low velocity asthenosphere (Vs~4.20 km/s) is present. In cell B8 the Vs in the lid is as high as about 4.70 km, in the depth range 75-110 km, and it overlies a fast asthenosphere with Vs ~ 4.50 km/s, that reaches a depth of about 320 km.

In cells C5 and C6 the observed velocity in the upper mantle is, in general, high both in the lithosphere and in the asthenosphere. In cell C7 a fast lid, with Vs of about 4.80 km/s is seen in the depth range 53-83 overlain by relatively soft layer with Vs of about 4.25 km/s.

The upper mantle, in cell C8 shows almost constant Vs ~ 4.50 km/s till a depth of about 300 km. To the north, from cell A5 to cell A9, the lithospheric thickness does not exceed about 100 km, even if a soft mantle layer in cells A5, A6 and A7 surmounts the high velocity lid. A thicker lithosphere is seen in cells from B5 to B9, with thickness increasing from about 90 km to about 175 km going from East to West. The soft layer on top of the high velocity lid is seen in cells B5, B6 and B7. The velocity sequence seen in cell B9 outlines a well-defined layering in the mantle, with clear alternations of low and high velocity layers.

More to the south, in cell C9 an uppermost mantle layer, with Vs of about 4.35 km/s overlies a fast lid with Vs of about 4.60 km/s reaching a depth of about 150 km and the asthenosphere, with Vs ~4.45 km/s, terminates at about 285 km of depth.

In cells D6, D7, D8 and D9 the lithosphere is as deep as about 160 km in cell D6 and about 180 km elsewhere. In cells D6 a low velocity layer, with Vs of about 4.00 km/s is present just below the Moho and in the lid, Vs increase with increasing depth from about 4.50 km/s to about 4.80 km/s, starting at a depth of about 100 km.. A gradient is seen in the lid of cells D7 and D8, where Vs reaches about 4.60 km/s at a depth of about 85 km and 50 km, respectively. While in cell D7 the presence of a slow asthenospheric layer, with Vs of about 4.25 km/s is observed at a depth of about 185 km, in cells D6, D8 and D9 the asthenosphere appears to be as fast as about 4.40 km/s and extends below ~ 250 km of depth.

To the west, in Sardinia region (cells A-2, A-1, B-2 and B-1) a fast but thin lid, on top a relatively slow and shallow asthenosphere is present just below the Moho. In the western cells the lid is faster and thinner (~ 15 km thick with Vs ~ 4.55 km/s in cell A-2 and ~ 4.80 km/s in cell B-2) than in the eastern cells (~ 40 km thick with Vs ~ 4.40 km/s). The uppermost asthenospheric layer is faster and thicker in the western part (Vs ~ 4.20 km/s in a layer about 30-35 km thick) than in the eastern part (Vs ~ 4.00 km/s in a layer ~ 15 km thick). In the lower asthenosphere, that extends to a depth of more than 250 km, the Vs is ~ 4.35 km/s.

In the Central area of the Tyrrhenian Sea, the uppermost mantle layer, reaching a depth of about 70 km in cell A0, ~ 50 km in cell A1, and ~ 80 km in cell B0, is relatively slow, with Vs of about 4.30 km/s and it represents the Tyrrhenian young lithosphere according to Panza and Calcagnile (1979) and Bottinga and Steinmetz (1979). The low velocity asthenosphere is shallow, with Vs ~t 4.20-4.25 km/s till a depth of about 150 km in cell A0, ~ 160 km in B0 and ~ 110 km in cell A1. In cell A2 the lithosphere ends at a depth of about 40 km and it overlies an about 60 km thick low velocity asthenosphere, with Vs ~ 4.15

km/s. At greater depths Vs ~ 4.40 km/s is present in all the Central area of the Tyrrhenian Sea. To the West, in cell A3, the crust-mantle transition is rather complex (see chapter 3.3.1) and seems to be consistent with a lithospheric doubling where the deeper Moho is at about 20 km and sits on mantle wedge, with a 2-3% of partial melting (Vs ~ 4.00 km/s). The mantle wedge is present also in cell A4, Vs ~ 4.20 km/s and reaches a depth of about 75 km. The presence of the mantle wedge in cells A3 and A4 has been originally detected by Calcagnile and Panza (1981) and Panza et al. (1980b) and confirmed by the geochemical analysis by Locardi (1986).

In the Southern Tyrrhenian Basin (cells B1, B2, B3 and B4), the uppermost upper mantle has Vs varying in the range 3.15 – 4.05 km/s (see table A 2.2) and overlies a layer with Vs ~ 4.2 km/s. These extremely low velocities are consistent with a high percentage of partial melting - in the range 5-10% accordingly with Bottinga and Steinmetz (1979). At depths greater than about 100 km the Vs in the asthenosphere is ~ 4.30-4.40 km/s; in cell B4 a low velocity layer (Vs ~ 4.05 km/s) about 30 km thick is seen in the depth range from 55 to 85 km.

The structural models of cells C1, C2, C3 and C4 are different from these of cells B1, B2, B3 and B4. The Moho is at about 20 km of depth and the uppermost upper mantle Vs varies in the range 3.85-4.10 km/s. This low velocity layer is about 10 km in thick in cells C3 and C4 and thicker, about 30 km, in cells C1 and C3. The lowest velocity is observed in the uppermost mantle layer of cell C4 where the mantle wedge with a degree of partial melting of about 5% is present. Below about 70 km, the Vs in the asthenosphere of cells C1, C2 and C3 is ~ 4.40 km/s, while some layering is seen in cell C4.

To the South, the Moho deepens from about 14 km in cell D1 to about 23 km in cells D2, D3, D4 and D5. A low velocity layer, with Vs in the range 4.00-4.10 km/s, is present just below the Moho in cells D1 and D2 overlying a relatively fast lid, with Vs in the range 4.50-4.60 km/s, and about 25 km thick. The uppermost mantle in cells D3, D4 and D5 is characterized by a layer about 30 km thick, with Vs ~ 4.30 km/s, that overlies a lid, Vs in the range 4.40-4.50 km/s. At greater depths, in the lower asthenosphere, Vs varies in the range 4.40-4.50 km/s.

In many of the analyzed cells, the presence of almost constant Vs in the upper mantle makes it difficult the identification of the lithosphere-asthenosphere transition. The solidus of a pyrolite-like composition approximates that of the mantle, therefore it may constitute an important constrain on the depth of possible melting, therefore we use it as tracer of the lithosphere-asthenosphere transition.

In Fig. 15.1 it is shown the summary of the phase relation in pyrolite after Green and Ringwood, (1967) (http://www.le.ac.uk/geology/art/gl209/lecture1-7.html). Shaded strips correspond to different shear-wave velocities of 4.1 (1), 4.2 (2), 4.3 (3), 4.4 (4), 4.5 (5), 4.6 (6), 4.7 km/s (7) in a single mantle layer made of peridotite (Ahrens, 1973; Bottinga and Allègre, 1976) (lower bound) and of olivine (Fo_{90}, Fa_{10}) (Graham, 1970) (upper bound); dashed lines correspond to the different values of heat flow, labelling each line, after Della Vedova et al. (1991). According to Fig. 15.1, in the cells characterized by almost constant Vs~4.40 km/s in the upper mantle, the lithosphere-asthenosphere transition (Fig. 15.3) is fixed at a depth of about 90 km. Other constraints on the physical state of the upper mantle can be supplied by a comparison of Fig. 15.1 with Fig. 15.2.
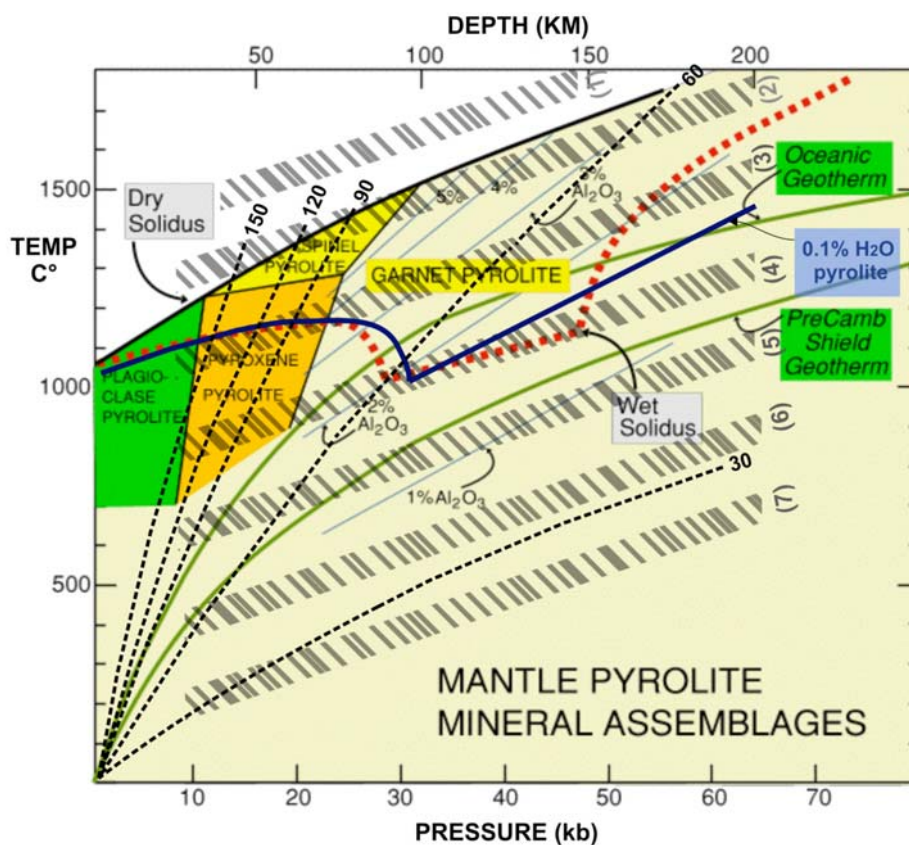
Fig. 15.1: Summary of phase relations in pyrolite (after Green and Ringwood, 1967), appropriate to upper mantle conditions (modified from http://www.le.ac.uk/geology/art/gl209/lecture1-7.html). Wet solidus is calculated for small amount of hornblende breakdown. Dashed lines correspond to the different surface heat flow values, expressed in mW/m^2, labelling each line. Shaded strips correspond to different shear-wave velocities of 4.1 (1), 4.2 (2), 4.3 (3), 4.4 (4), 4.5 (5), 4.6 (6), 4.7 km/s (7) in a single mantle layer of simple composition (after Della Vedova et al., 1991).
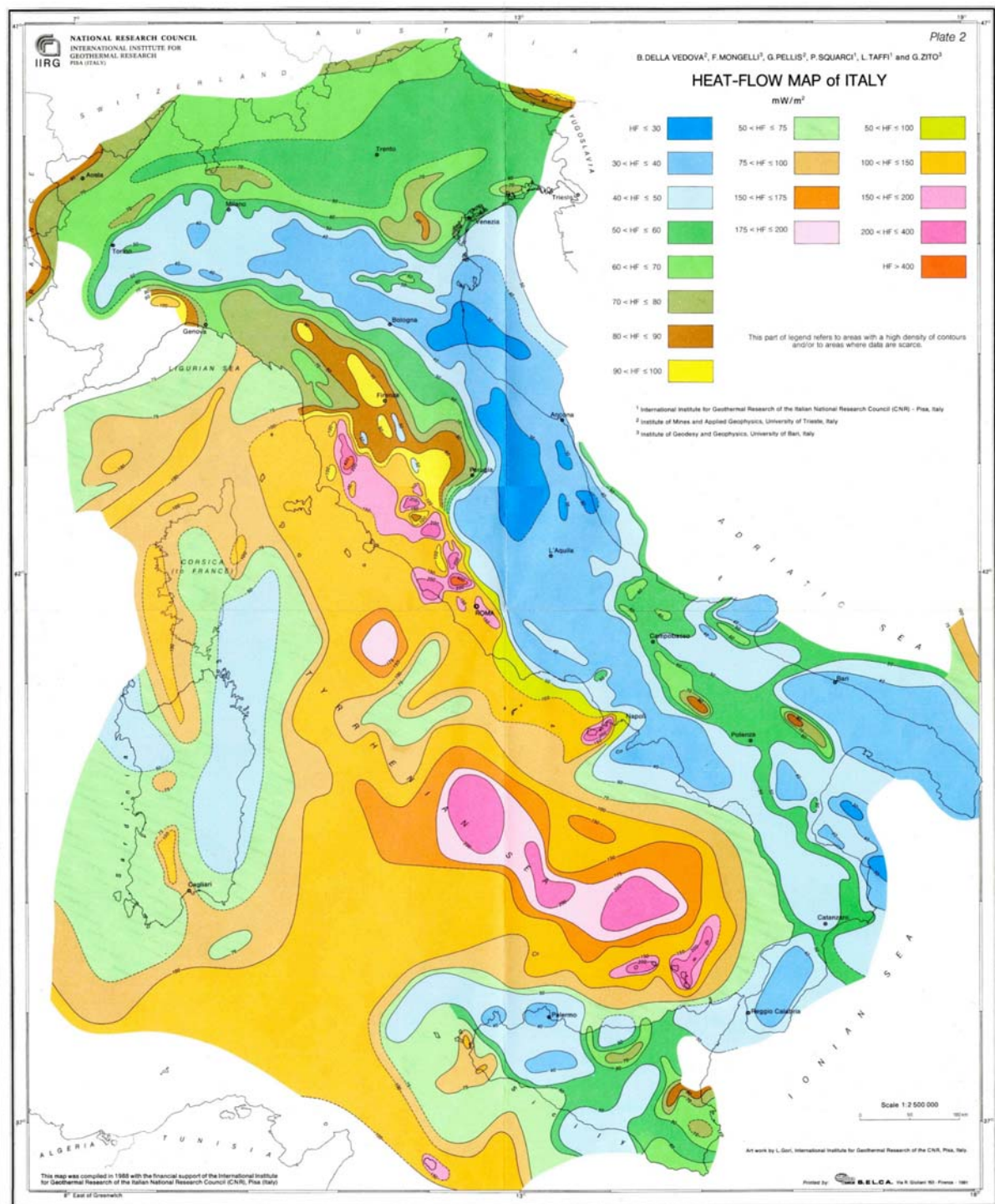
Fig. 15.2: Heat flow map of Italy and surrounding seas. (Della Vedova et al., 1991). A comparison of Fig. 15.1 with Fig. 15.2 can supply constraints on the physical state of the upper mantle.

Having defined the lithosphere-asthenosphere transition for all cells, it is possible, by smooth interpolation, to construct the map of the lithospheric thickness shown in Fig. 15.3. In Fig.15.4, instead, the bottom of the asthenosphere, below which the Vs velocity is fixed

according to the already published data (Du et al., 1998), corresponds to the maximum penetration depth of our data.
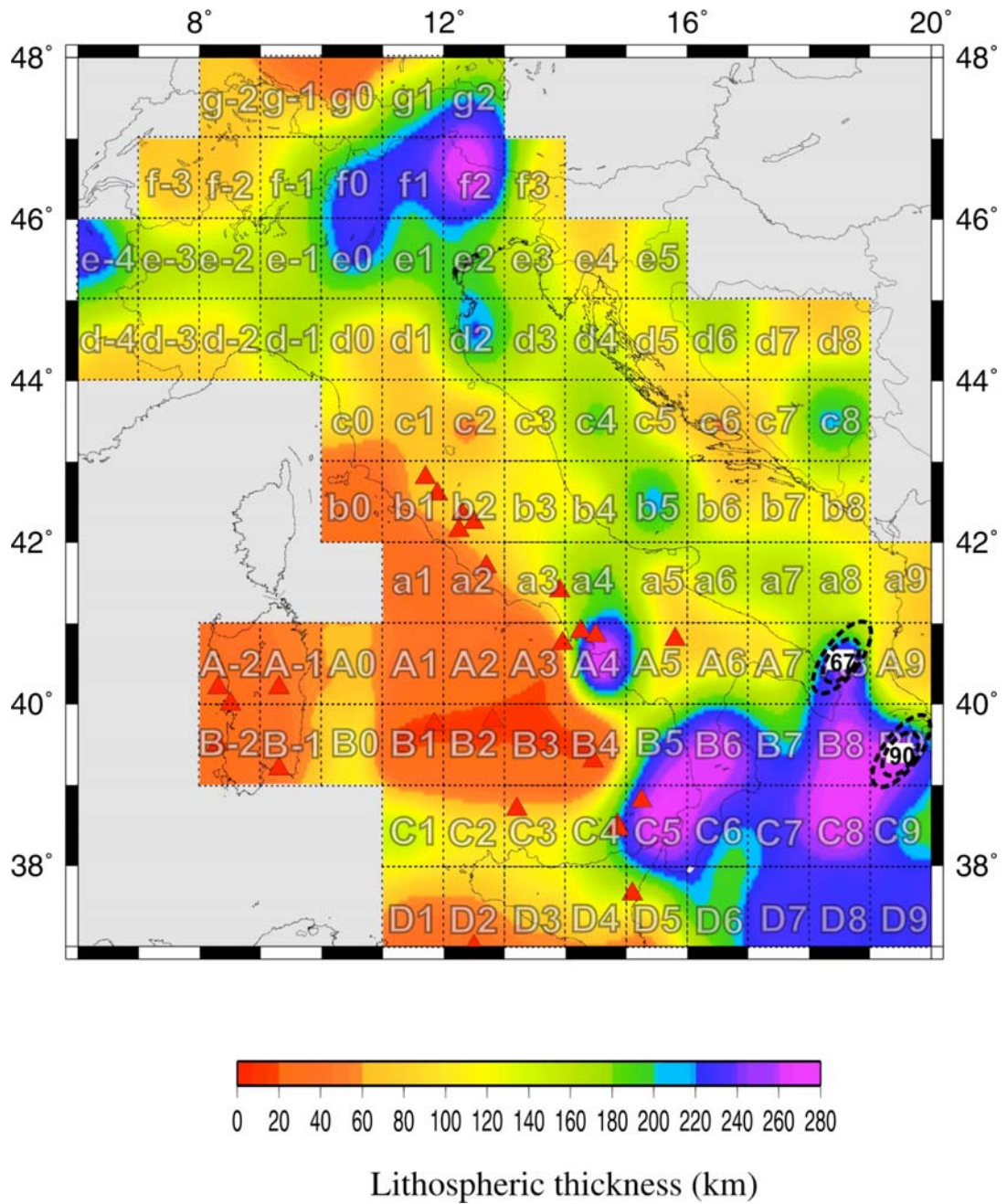
Fig. 15.3: Lithospheric thickness (km) with cellular grid superimposed and with contouring of the shallower lithosphere-asthenosphere transition in the cells where a possible lithospheric doubling has been detected. The map has been obtained with smooth interpolation of the 1° x 1° lithospheric thickness data.
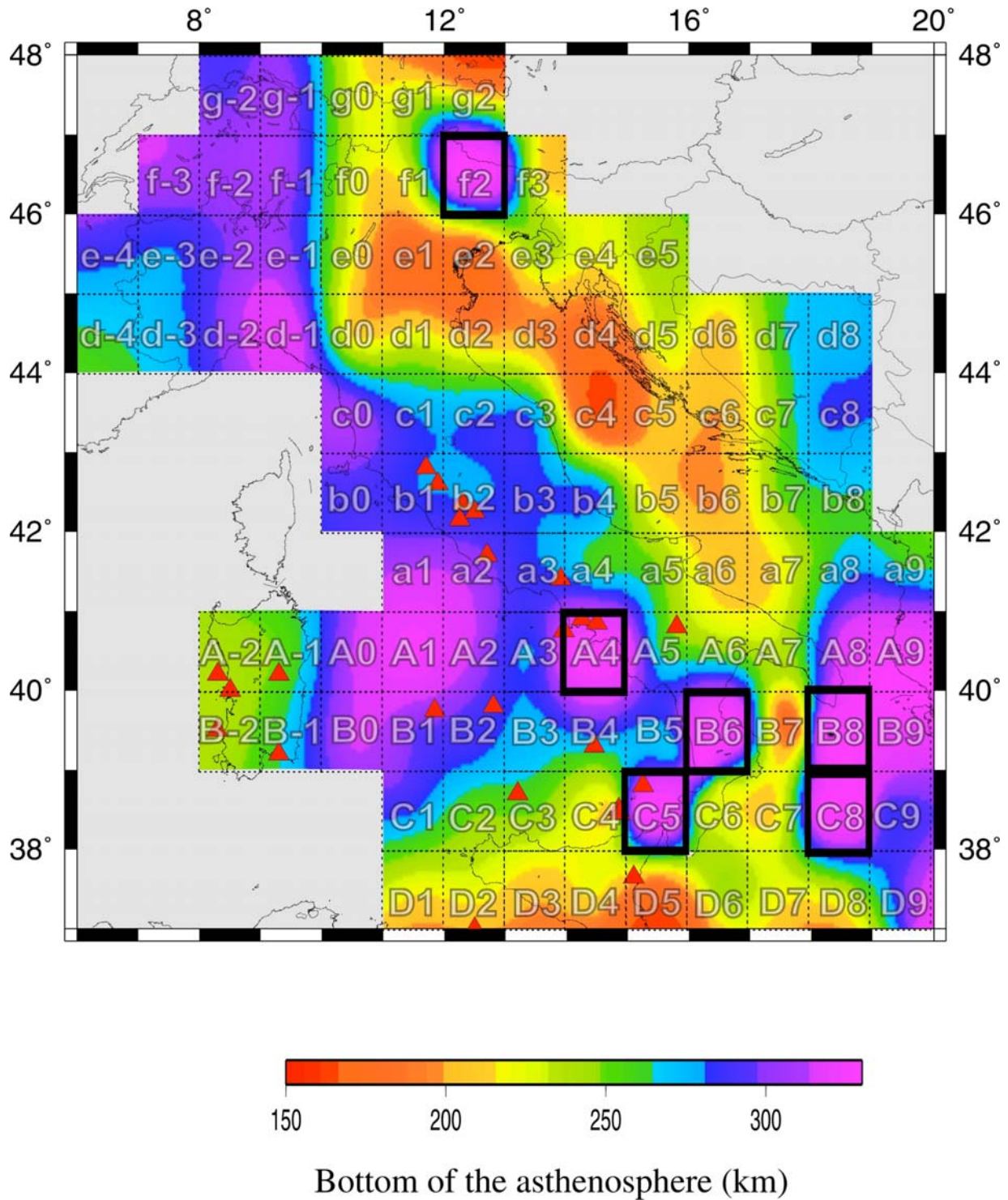
Fig. 15.4: Bottom of the asthenosphere (km) with the cellular grid superimposed. In the cells contoured with heavy line, the asthenosphere bottom cannot be defined because of the presence of slab or lithospheric roots that extend to depths greater than the vertical penetration of our data set. The map has been obtained with smooth interpolation of the 1° x 1° data on the depth of the bottom of the asthenosphere.

References

Ahrens, T.J., 1973. Petrologic properties of the upper 670 km of the Earth's mantle; geophysical implications. Phys. Earth Planet. Inter., 7: 167-186.

Aljinovic, B., and Blaskovic, I., 1987. Some characteristics of the carbonate complex in the offshore Adriatic area. Mem. Soc. Geol. It., 40: 327-334.

Ansorge, J., Lippitsch, R., and Kissling, E., 2003. Lithosphere structure of the Alpine arc: new evidence from high-resolution teleseismic tomography. Mem. Sc. Geol. 54: 53-54.

Backus, G., and Gilbert, J.F., 1968. Resolving power of gross earth data. Geophys. J. R. Astr. Soc., 16: 168-205.

Backus, G., and Gilbert, J.F., 1970. Uniqueness in the inversion of inaccurate gross earth data. Phil. Trans. R. Soc. A., 266: 123-192.

Bally, A.W., Burbi, L., Cooper, C., and Ghelardoni, R., 1986. Balanced sections and seismic reflection profiles across the Central Apennines. Mem. Soc. Geol. It., 35: 257-310.

Barchi, M.R., De Feyter, A., Magnani, M.B., Minelli, G., Pialli, G., and Sotera, B.M., 1998. The structural style of the Umbria-Marche fold and thrust belt. Mem. Soc. Geol. It., 52: 557-578.

Blundell, P., Freeman, R., and Mueller, St., (eds), 1992. Cambridge Univ. Press. A continental revealed. The European Geotraverse. University Press, Cambridge, 275p.

Bondar, I., Zoltan, B., Zivcic, Z., Costa, G., and Levhin, A., 1996. Rayleigh wave group and phase velocity measurements in the Pannonian Basin. Proc. XV Congress of the Carpatho-Balcan Geological Association, Athens, September, 1995.

Bottinga, Y., and Steinmetz, L., 1979. A geophysical, geochemical, petrological model of the sub-marine lithosphere. Tectonophysics, 55: 311-347.

Bryson, A. E., and Ho Yu-Chi, 1975. Applied optimal control. Taylor & Francis, 480p.

Calcagnile, G., D'Ingeo, F., Farrugia, P., and Panza, G.F., 1982. The lithosphere in the central-eastern Mediterranean area. Pure Appl. Geophys., 120: 389-406.

Calcagnile, G., and Panza, G.F., 1981. The main characteristics of the lithosphere-asthenosphere system in Italy and surrounding regions. Pure Appl. Geophys., 119: 865-879.

Carminati, E., Doglioni, C., and Scrocca, D., 2004. Alps vs. Apennines. Special Volume of the Italian Geological Society for the IGC 32 Florence 2004.

Catalano, R., Di Stefano, P., Sulli, A., and Vitale, F.P., 1996. Paleogeography and structure of the central Mediterranean: Sicily and its offshore area. Tectonophysics, 260: 291-323.

Catalano, R., Doglioni, C., and Merlini, S., 2001. On the Mesozoic Ionian Basin. Geophys. J. Int., 144: 49-64.

Cernobori, L., Hirn, A., McBride, J.H., Nicolich, R., Petronio, L., Romanelli, M., and STREAMERS/PROFILES Working Groups, 1996. Crustal image of the Ionian basin and its Calabrian margin. Tectonophysics, 264: 175-189.

Chamot-Rooke, N., Jestin, F., and Gaulier, J. M., 1997. Constrain on Moho depth and crustal thickness in the Ligurian-Provençal Basin from 3D gravity inversion: geodynamic implication. Reveu de l'Institute Francais du Petrole V.52, N. 6.

Chimera, G., Aoudia, A., Saraò, A., and Panza, G.F., 2003. Active tectonics in central Italy: constraint from surface wave tomography and source moment tensor inversion. Phys. Earth Planet. Inter., 138: 241-262.

Cristofolini, R., Ghisetti, F., Scarpa, R., and Vezzani, L., 1985. Character of the stress field in the Calabrian Arc and Southern Apennines (Italy) as deducted by geological, seismologica and volcanologica information. Tectonophysics, 117: 39-58.

De Gori, P, Cimini, G.B., Chiarabba, C., De Natale, G., Troise, C., and Deschamps, A., 2001. Teleseismic tomography of the Campanian volcanic area and surrounding Apenninic belt. J. Volc. and Geoth. Res., 109: 55-75.

De Groot-Hedlin, C., and Constable, S., 1990. Occam's inversion to generate smooth, two-dimensional models from magnetotelluric data. Geophysics, 55: 1613-1624.

Della Vedova, B., Marson, I., Panza, G.F., and Suhadolc, P., 1991. Upper mantle properties of the Tuscan-Tyrrhenian area: a framework for its recent tectonic evolution. Tectonophysics, 195: 311-318.

Della Vedova B., F. Mongelli, G. Pellis, P. Squarci, L. Taffi and G. Zito, 1991. Heat flow map of Italy. Scale 1: 2 500 000. National Research Council, Int. Institute for Geothermal Research, Pisa, SELCA, Firenze. In: R. Cataldi, F. Mongelli, P. Squarci, L. Taffi, G. Zito and C. Calore. Geothermal ranking of italian territory. Geothermics, 24(1): 115-129.

Della Vedova, B., Pellis, G., and Pinna, E., 1989. Studio geofisico dell'area di transizione tra il Mar Pelagico e la piana abissale dello Ionio. Atti 8° Convegno Annuale G.N.G.T.S., Roma, 543-558.

De Matteis, R., Latorre, D., Zollo, A., and Virieux, J., 2000. 1D P-velocity models of Mt. Vesuvio Volcano from the Inversion of TomoVes96 first arrival time data. Pure Appl. Geophys., 157: 1643-1661.

De Voggd, B., Truffert, C., Chamot-Rooke, N., Huchon, P., Lallermant, S. and Le Pichon, X., 1992. Two-ship deep seismic soundings in the basins of the Eastern Mediterranean Sea (Pasiphae cruise). Geophys. J. Int., 109: 536-552.

Dèzes and Ziegler, 2001. Map of the European Moho. EUCOR-URGENT: http://comp1.geol.unibas.ch/downloads/Moho_net/euromoho1_3.pdf

Ditmar, P.G., and Yanovskaya, T.B., 1987. A generalization of the Backus-Gilbert method for estimation of lateral variations of surface wave velocity. Izv. AN SSSR, Fiz. Zemli (Physics of the Solid Earth), 23 (6): 470-477.

Doglioni, C., Innocenti, F., and Mariotti, G., 1998a. On the geodynamic origin of Mt. Etna. Proceedings XVII Convegno Gruppo Nazionale Geofisica Terra Solida, Roma, 1133-1145.

Du, Z.J., Michelini, A., and Panza, G.F., 1998. EurID: a regionalised 3-D seismological model of Europe. Phys. Earth Planet. Inter., 105: 31-62.

Dziewonski, A.M., and Anderson, D.L., 1981. Preliminary reference Earth model. Phys. Earth Planet. Int., 60: 297-356.

Fantoni, R., Della Vedova, B., Giustiniani, M., Nicolich, R., Barbieri, C., Del Ben, A., Finetti, I., and Catellarin, A., 2003. Deep aseismic profiles through the Venetian and Adriatic foreland (Northern Italy). Mem. Sci. Geol., 54: 131-134.

Ferrucci, F., Gaudiosi, G., Hirn, A., and Nicolich, R., 1991. Ionian Basin and Calabrian Arc: some new elements from DSS data. Tectonophysics, 195: 411-419.

Finetti, I., 1982. Structure, stratigraphy and evolution of central Mediterranean. Boll. Geof. Teor. Appl., 24, N. 96.

Finetti, I.R., Boccaletti, M., Bonini, M., Del Ben, A., Geletti, R., Pipan, M., and Sani, F., 2001. Crustal section based on CROP seismic data across the North Tyrrhenian - Northern Apennines - Adriatic Sea. Tectonophysics, 343: 135-163.

Finetti, I., Bricchi, G., Del Ben, A., Pipan, M., and Xuan, Z., 1987. Geophysical study of the Adria plate. Mem. Soc. Geol. It., 40: 335-344.

Finetti, I., and Del Ben, A., 1986. Geophysical study of the Tyrrhenian opening. Boll. Geofis. Teor. Appl., 28, 110: 75-156.

Fowler, C.M.R., 1995. The Solid Earth. An introduction to Global Geophysics. Cambridge Univ. Press.

Graham, E.K., 1970. Elasticity and composition of the upper mantle. Geophys. J. R. Astr. Soc., 20: 285-302.

Green, D.H., and Falloon, T.J., 2005. Primary magmas at mid-ocean ridges, "horspots", and other intraplate settings: Constraints on mantle potential temperature. In: In: Foulger G.R., Nathland G.H., Presnall D.C., Anderson D.L. (editors), Plates, plumes, and paradigms. Geol. Soc. Am. Spec. Paper 388, pp. 215-247.

Gutenberg, B. and Richter, C. F. 1956a. The energy of earthquakes. Q. J. Geol. Soc. London, 112, 1–14.

Gutenberg, B., and Richter, C.F., 1956b. Earthquake magnitude, intensity, energy and acceleration. Bull. Seismol. Soc. Am., 46: 105-145.

Improta, L., Iannaccone, G., Capuano, P., Zollo, A., and Scandone, P., 2000. Inferences on the upper crustal structure of Southern Apennines (Italy)

from seismic refraction investigations and surface data. Tectonophysics, 317: 273-297.

Karagianni, E.E., Panagiotopoulos, D.G., Panza, G.F., Suhadolc, P., Papazachos, C.B., Papazachos, B.C., Kiratzi, A., Hatzfeld, D., Makropoulos, K., Priestley, K., and Vuan, A., 2002. Rayleigh Wave Group Velocity Tomography in the Aegean area. Tectonophysics, 358: 187-209.

Keilis-Borok, V.I., and Yanovskaya, T.B., 1967. Inverse problems of seismology (structural review). Geophys. J. R. Astr. Soc., 13:223-234.

Kern, H., and Schenk, V., 1988. A model of velocity structure beneath Calabria, southern Italy, based on laboratory data. Earth and Pla. Sc. Lett., 87: 325-337.

Knopoff, L., 1972. Observations and inversion of surface-wave dispersion. In: The Upper Mantle. Tectonophysics, Ritsema A.R. ed., 13: 497-519.

Knopoff, L., and Panza, G.F., 1977. Resolution of Upper Mantle Structure using higher modes of Rayleigh waves. Ann. Geof., 30: 491-505.

Levshin, A.L., Pisarenko, V.F., and Pogrebinsky, G.A., 1972. On a frequency time analysis of oscillations. Annales Geophysicae, 28: 211-218.

Levshin, A.L., Ratnikova, L., and Berger, J., 1992. Peculiarities of surface wave propagation across Central Eurasia. Bull. Seismol. Soc. Am., 82: 2464-2493.

Locardi, E., 1986. Tyrrhenian volcanic arcs: volcano-tectonics, petrogenesis and economic aspects. In: The origin of the arcs, F.C. Wezel Ed., Elsevier, 351-373.

Ludwig, W.J., Nafe, J.E., and Drake, C.L., 1970. Seismic refraction. In: The Sea, Wiley-Intersci., New York. Vol. 4, Part 1: 53-84.

Mantovani, E., Nolet, G., and Panza, G.F., 1985. Lateral heterogeneity in the crust of the Italian region from regionalized Rayleigh-wave group velocities. Annales Geophysicae, 3: 519-530.

Markusic, S., Herak, D., Ivancic, I., Sovic, I., Herak, M., and Prelogovic, E., 1998. Seismicity of Croatia in the period 1993-1996 and the Ston-Slao earthquake of 1996. Geofizika, Vol. 15: 83-101.

Marone, F., Van der Mejiede, M. Van der Lee, S., and Giardini, D., 2003. Joint inversion of local, regional and teleseismic data for crustal thickness in the Eurasia-Africa plate boundary region. Geophys. J. Int., 154: 499-514

Marone, F., Van der Lee, and Giardini, D., 2004. Three-dimensional upper-mantle S-velocity model for the Eurasia-Africa plate boundary region. Geophys. J. Int., 158: 109-130

Marson, I., Panza, G.F., and Suhadolc, P., 1995. Crust and upper mantle models along the active Tyrrhenian rim. Terra Nova, 7: 348-357.

Martinez, M.D., Lana, X., Badal, J., Canas, J.A., and Pujades, L., 1997. Preliminary objective regionalization of the Mediterranean basin derived from surface-wave tomography. Annali di Geofis., XL, 1: 43-59.

Martinez, M.D., Lana, X., Canas, J.A., Badal, J., and Pujades, L., 2000. Shear-wave velocity tomography of the lithosphere-asthenosphere system beneath the Mediterranean area. Phys. Earth and Plan. Int., 122: 33-54.

Martinez, M.D., Canas, J.A., Lana, X., and Badal, J., 2001. Objective regionalization of Rayleigh wave dispersion data by clustering algorithms: an application to the Mediterranean basin. Tectonophysics, 330: 245-266.

Meletti, C., Patacca, E., and Scandone, P., 2000. Construction of a Seismotectonic Model: The Case of Italy. Pure Appl. Geophys., 157: 11-35.

Merlini, S., Doglioni, C., Fantoni, R., and Ponton, M., 2002. Analisi strutturale lungo un rprofilo geologico tra la linea Fella-Sava e l'avampaese adriatico (Friuli-Venezia-Giulia Italia). Mem. Soc. Geol. It., 57: 293-300.

Morelli, C., 1998. Lithospheric structure and geodynamics of the Italian peninsula derived from geophysical data: a review. Mem. Soc. Geol. It., 52: 113-122.

Moritz, H., 1995. Science, mind and the universe, Wichmann, 298pp.

Mostaanpour, M.M., 1984. Einheitliche Auswertung krustenseismicher daten in Westeuropa. Darstellung von Krustenparametern und Laufzeitanomalien. Verlag von Dirtrich Reimer in Berlin.

Mueller, S., 1978. The evolution of the Earth Crust. In: Tectonics and Geophysics of Continental Rifts. Ramberg, I.B. and Neuman, E.R., Eds, 11-28, Reidel, Dordrecht.

Nicolich, R., and Dal Piaz, R., 1990. Moho isobaths. In: Structural model of Italy and Gravity Map. Sheet2. Consiglio Nazionale delle Ricerche.

Panza G.F., 1976. Phase velocity determination of fundamental Love and Rayleigh waves. Pageoph, 114: 753-764.

Panza, G.F., 1981. The resolving power of seismic surface waves with respect to crust and upper mantle structural models. In: The solution of the inverse problem in geophysical interpretation. Cassinis R. ed., Plenum Publ. Corp., 39-77.

Panza, G.F., 1984. Contributi geofisici alla geologia: stato attuale dell'arte e prospettive future. In: Cento anni di geologia italiana. Vol. giub. I Centenario S.G.I., 363-376, Bologna.

Panza, G.F., and Calcagnile, G., 1979. The upper mantle structure in Balearic and Tyrrhenian bathyal plains and the messinian salinity crisis. Palaeogeo. Palaeoclim. Palaeoeco., 29: 3-14.

Panza, G.F., Mueller, S., and Calcagnile, G., 1980a. The gross features of the lithosphere-asthenosphere system in Europe from seismic surface waves and body waves. Pure Appl. Geoph., 118: 1209-1213.

Panza, G.F., Calcagnile, G., Scandone, P., and Mueller, S., 1980b. La struttura profonda dell'area mediterranea. Le Scienze, 141: 60-69.

Panza, G.F., and Pontevivo, A., 2004. The Calabrian Arc: a detailed structural model of the lithosphere-asthenosphere system. Acc. Naz. XL V. XXVIII: 51-88.

Panza, G.F., Pontevivo, A., Chimera, G., Raykova, R., and Aoudia, A., 2003b. The lithosphere-asthenosphere: Italy and surroundings. Episodes, 26: 169-174.Panza, G.F., and Pontevivo, A., 2004. The Calabrian Arc: a detailed structural model of the lithosphere-asthenosphere system. Acc. Naz. XL V. XXVIII: 51-88.

Panza, G.F., Raykova, R., Chimera, G., and Aoudia, A., 2003a. Multiscale surface wave tomography in the Alps. Mem. Sc. Geol., 54: 55-56.

Parker, R.L., 1994. Geophysical Inverse Theory. Princeton Press, 386 pp

Pasyanos, M.E., Walter, W.R., and Hazler, S.E., 2001. A surface wave dispersion study of the Middle East and North Africa for Monitoring the Compressive Nuclear-Test-Ban Treaty. Pure Appl. Geophys., 158: 1445-1474.

Paul, A., Cattaneo, M., Thouvenot, F., Spallarossa, D., Béthoux, N., and Fréchet, J., 2001. A three-dimensional crustal velocità model of the southwestern Alps from local earthquake tomography. J. G. R., 106: 19,367-19,389.

Peishan, C., and Haitong, C., 1989. Scaling law and its applications to earthquake statistical relations. Tectonophysics, 166: 53-72.

Pepe, F., Bertotti, G., Cella, F., and Marsella, E., 2000. Rifted margin formation in the south Tyrrhenian Sea: a high-resolution seismic profile across the north Sicily passive continental margin. Tectonics, 19, 2: 241-257.

Pfiffnerr, O.A., Schlunegger, F., and Buiter, S.J.H., 2002. The Swiss Alps and their peripheral basin: stratigraphic response to the deep crustal processes. Tectonics, 21 (2): 3-1, 3-17.

Pialli, G., Alvarez, W., and Minelli, G., 1995. Geodinamica dell'Appennino settentrionale e sue ripercussioni nella evoluzione tettonica miocenica. Studi geol. Camerti, Volume speciale 1995/1: 523-536.

Pontevivo, A., 2003. Surface-wave tomography and non-linear inversion in Italy and surrounding areas, Ph.D. thesis, University of Trieste (XV ciclo – tutor: G.F. Panza).

Pontevivo, A., and Panza, G.F., 2002. Group Velocity Tomography and Regionalization in Italy and bordering areas. Phys. Earth Planet. Inter., 134: 1-15.

Pontevivo, A. and Panza, G.F., 2006. The Lithosphere-Asthenosphere System in the Calabrian Arc and surrounding seas – Southern Italy. Pageoph, in press.

Press, F., 1968. Earth models obtained by Monte-Carlo inversion. J. G. R., 73: 5223-5234.

Raykova, R., Chimera, G., Farina, B., and Panza, G. F., 2004. S-wave velocity structure of the lithosphere-asthenosphere system in Mediterranean region. 32th International Geological Congress - August, 2004, Florence, Italy, Abs. Vol., Pt.2, abs.208-5 , p.970.

Ringwood, A.E., 1966. Mineralogy of the mantle. In: Advances in Earth Science. P.M. Hurley ed., MIT Press, 357-399.

Ritzwoller, M.H., and Levshin, A.L., 1998. Eurasian surface wave tomography: Group velocities. J. Geophys. Res., 103, B3: 4839-4878.

Russell, B., 1946. History of western philosophy. George Allen and Unwind, Ltd.

Scarascia, S., and Cassinis, R., 1992. Profili sismici a grande angolo esplorati in prossimità del tracciato del profilo Crop01: una raccolta dei risultati e qualche revisione. Studi geol. Camerti, volume speciale CROP 1-1A: 17-26.

Scarascia, S., and Cassinis, R., 1997. Crustal structures in the central-eastern Alpine sector: a revision of the available DSS data. Tectonophysics, 271: 157-188.

Scarascia, S., Lozej, A., and Cassinis, R., 1994. Crustal structures of the Ligurian, Tyrrhenian and Ionian Seas and adjacent onshore areas interpreted from wide-angle seismic profiles. Boll. Geof. Teor. Appl., 36: 141-144.

Shapiro, N.M. and M.H. Ritzwoller, Monte-Carlo inversion for a global shear velocity model of the crust and upper mantle, *Geophys. J. Int.*, 151, 88-105, 2002.

Tarantola, A., 1987. Inverse problem theory, methods for data fitting and model parameter estimation Elsevier, New-York, 630 pp.

Transalp Working Group, 2002. First deep seismic reflection images of the Eastern Alps reveal giant crustal wedges and transcrustal ramps. Geophys. Res. Lett., 29 (10): 92.1-92.4.

Turcotte, D.L., and Schubert, G., 1982. Geodynamics: applications of continuum physics to geological problems. Eds. J. Wiley and Sons, New York.

Urban, L., Cichowicz, A., and Vaccari, F., 1993. Computation of analytical partial derivatives of phase and group velocities for Rayleigh waves with respect to structural parameters. Studia geoph. et geod., 37: 14-36.

Valyus, V.P., 1972. Determining seismic profiles from a set of observations. In: Computational Seismology. Keilis-Borok ed., Consult. Bureau, New-York, 114-118.

Valyus, V.P., Keilis-Borok, V.I., and Levshin, A., 1969. Determination of the upper-mantle velocity cross-section for Europe. Proc. Acad. Sci. USSR, 185, 3.

Venisti, N., Calcagnile, G., Pontevivo, A., and Panza, G.F., 2005. Surface wave and body wave tomography combined study of the Apulian Plate. PAGEOPH, 162, 311-329.

Yanovskaya, T.B., 2003. Inverse problems of geophysics, International Centre for Theoretical Physics, IC/2003/54, p. 172.

Yanovskaya, T.B., and Antonova, L.M., 2000. Lateral variations in the structure of the crust and upper mantle in the Asian region from data on the group velocities of Rayleigh waves. Izv., Physics of the Solid Earth, 36, 2: 121-128.

Yanovskaya, T.B., Antonova, L.M., and Kozhevnikov, V.M., 2000. Lateral variations of the upper mantle structure in Eurasia from group velocities of surface waves. Phys. Earth Planet. Inter., 122: 19-32.

Yanovskaya, T.B., and Ditmar, P.G., 1990. Smoothness criteria in surface-wave tomography. Geophys. J. Int., 102: 63-72.

Yanovskaya, T.B., Kizima, E.S., and Antonova, L.M., 1998. Structure of the crust in the Black Sea and adjoining regions from surface wave data. J. Seismol., 2: 303-316.

Yanovskaya, T.B., Maaz, R., Ditmar, P.G., and Neunhofer, H., 1988. A method for joint interpretation of the phase and group surface-wave velocities to estimate lateral variations of the Earth's structure. Phys. Earth Plan. Inter., 51: 59-67.

Zhdanov, M., 2002. Geophysical inverse theory and regularization problems, Elsevier, 628pp.

Zivcic, M., Bondar, I., and Panza, G.F., 2000. Upper crustal velocity structure in Slovenia from Rayleigh wave dispersion. Pure Appl. Geophys., 157: 131-146.

APPENDIX I

DATA USED IN THE CELLULAR NON-LINEAR INVERSION: GROUP AND PHASE VELOCITY DATA

In the following tables, A1.1, group and phase mean velocity data, their single point error and r.m.s used in the non-linear inversion, are tabled for each 1° x 1° cell (see Chapter 3). The data base of the group velocity dispersion curve has been extended, for period longer than 80 sec, with data collected from global studies, available at the Center for Imaging the Earth's Interior in the University of Colorado at Boulder (http://ciei.colorado.edu/~nshapiro/MODEL/index.html), while, the group velocity value, at 80 sec, has been calculated as an average between the improved Raykova (2004) database (U_r) and the Boulder database (U_b). Since the two measurements are independent, the associated error is:

$$\rho_g(U) = \sqrt{\rho_g(U_r)^2 + \rho_g(U_b)^2} = \sqrt{(0.90)^2 + (0.83)^2} \approx 0.120$$

Table A1.1: Group (U) and phase (C) velocity values at different periods (the maximum investigated range is from T=7s to T=150s and from T=15s to T=150s, respectively) with the single point error (ρ_g, ρ_{ph}) and the r.m.s. values (for U and C) for each cell.

Period	Cell g-2 (8.5; 47.5)				Cell g-1 (9.5; 47.5)				Cell g0 (10.5; 47.5)				Cell g1 (11.5; 47.5)			
	U	ρ_g	C	ρ_{ph}	U	ρ_g	C	ρ_{ph}	U	ρ_g	C	ρ_{ph}	U	ρ_g	C	ρ_{ph}
(s)	(km/s)	(km/s)	(km/s)	(km/s)	(km/s)	(km/s)	(km/s)	(km/s)	(km/s)	(km/s)	(km/s)	(km/s)	(km/s)	(km/s)	(km/s)	(km/s)
7	2.927	0.150			2.894	0.160			2.827	0.150			2.724	0.155		
10	2.634	0.120			2.670	0.130			2.709	0.140			2.718	0.135		
15	2.692	0.100			2.742	0.105			2.774	0.105			2.749	0.105		
20	2.902	0.090	3.605	0.150	2.967	0.095	3.586	0.150	2.980	0.090	3.569	0.150	2.916	0.100	3.557	0.150
25	3.142	0.090	3.705	0.110	3.142	0.095	3.658	0.110	3.142	0.090	3.680	0.110	3.098	0,100	3.667	0.110
30	3.482	0.090	3.749	0.090	3.425	0.095	3.747	0.090	3.362	0.090	3.749	0.090	3.291	0.100	3.742	0.090
35	3.610	0.090	3.799	0.080	3.548	0.095	3.801	0.080	3.472	0.090	3.804	0.080	3.412	0..095	3.799	0.080
50	3.792	0.090	3.874	0.060	3.817	0.095	3.889	0.060	3.800	0.090	3.901	0.060	3.770	0.090	3.896	0.060
80	3.842	0.120	3.945	0.060	3.807	0.120	3.966	0.060	3.801	0.120	3.984	0.060	3.780	0.125	3.986	0.060
100	3.825	0.080	4.013	0.080	3.800	0.081	4.016	0.080	3.777	0.080	4.016	0.080	3.762	0.081	4.016	0.080
125	3.735	0.080	4.069	0.240	3.720	0.081			3.707	0.080			3.702	0.081		
150	3.680	0.080			3.677	0.081			3.672	0.080			3.670	0.081		
r.m.s.		0.064		0.071		0.062		0.054		0.067		0.059		0.065		0.056

Cell g2 (12.5; 47.5) — Cell f-3 (7.5; 46.5) — Cell f-2 (8.5; 46.5) — Cell f-1 (9.5; 46.5)

Period (s)	U (km/s)	ρ_g (km/s)	C (km/s)	ρ_{ph} (km/s)	Period (s)	U (km/s)	ρ_g (km/s)	C (km/s)	ρ_{ph} (km/s)	Period (s)	U (km/s)	ρ_g (km/s)	C (km/s)	ρ_{ph} (km/s)	Period (s)	U (km/s)
7	2.637	0.160			7	2.637	0.160			7	2.637	0.160			7	2.637
10	2.717	0.120			10	2.717	0.120			10	2.717	0.120			10	2.717
15	2.700	0.100			15	2.700	0.100			15	2.700	0.100			15	2.700
20	2.854	0.100			20	2.854	0.100			20	2.854	0.100			20	2.854
25	3.062	0.100			25	3.062	0.100			25	3.062	0.100			25	3.062
30	3.258	0.100			30	3.258	0.100			30	3.258	0.100			30	3.258
35	3.384	0.100			35	3.384	0.100			35	3.384	0.100			35	3.384
50	3.745	0.090			50	3.745	0.090			50	3.745	0.090			50	3.745
80	3.770	0.120			80	3.770	0.120			80	3.770	0.120			80	3.770
100	3.745	0.080			100	3.745	0.080			100	3.745	0.080			100	3.745
125	3.697	0.080			125	3.697	0.080			125	3.697	0.080			125	3.697
150	3.670	0.080			150	3.670	0.080			150	3.670	0.080			150	3.670
r.m.s.		0.068		0.000	r.m.s.		0.068		0.000	r.m.s.		0.068		0.000	r.m.s.	

Cell f0 (10.5; 46.5) — Cell f1 (11.5; 46.5) — Cell f2(12.5; 46.5) — Cell f3 (13.5; 46.5)

Period (s)	U (km/s)	ρ_g (km/s)	C (km/s)	ρ_{ph} (km/s)	U (km/s)	ρ_g (km/s)	C (km/s)	ρ_{ph} (km/s)	U (km/s)	ρ_g (km/s)	C (km/s)	ρ_{ph} (km/s)	U (km/s)	ρ_g (km/s)	C (km/s)	ρ_{ph} (km/s)
7	2.597	0.190			2.554	0.170			2.513	0.155			2.517	0.150		
10	2.728	0.130			2.750	0.130			2.680	0.130			2.628	0.120		
15	2.771	0.100			2.736	0.105			2.672	0.100			2.667	0.100		
20	2.912	0.100	3.640	0.110	2.833	0.100	3.519	0.150	2.782	0.095			2.807	0.100		
25	3.057	0.100	3.702	0.090	2.975	0.100	3.627	0.110	2.932	0.095			2.946	0.100		
30	3.252	0.100	3.764	0.080	3.170	0.100	3.699	0.090	3.134	0.095			3.139	0.100		
35	3.419	0.100	3.881	0.060	3.331	0.100	3.761	0.080	3.277	0.095			3.289	0.095		
50	3.762	0.090	3.974	0.060	3.730	0.095	3.869	0.060	3.710	0.095			3.697	0.095		
80	3.786	0.120	4.011	0.080	3.783	0.125	3.971	0.060	3.783	0.120			3.732	0.120		
100	3.745	0.080	4.069	0.120	3.725	0.081	4.011	0.080	3.705	0.080			3.690	0.080		
125	3.670	0.080			3.662	0.081			3.655	0.080			3.650	0.080		
150	3.630	0.080			3.627	0.081			3.625	0.080			3.627	0.080		
r.m.s.		0.067		0.056		0.078		0.063		0.067		0.000		0.067		0.000

Cell e-4 (6.5; 45.5) — Cell e-3 (7.5; 45.5) — Cell e-2 (8.5; 45.5) — Cell e-1 (9.5; 45.5)

Period (s)	U (km/s)	ρ_g (km/s)	C (km/s)	ρ_{ph} (km/s)	U (km/s)	ρ_g (km/s)	C (km/s)	ρ_{ph} (km/s)	U (km/s)	ρ_g (km/s)	C (km/s)	ρ_{ph} (km/s)	U (km/s)	ρ_g (km/s)	C (km/s)	ρ_{ph} (km/s)
7													2.301	0.170		
10	2.288	0.125			2.267	0.125			2.304	0.130			2.391	0.140		
15	2.575	0.100			2.597	0.100			2.626	0.105			2.632	0.110		
20	2.820	0.096	3.608	0.150	2.865	0.096	3.561	0.150	2.874	0.095	3.519	0.150	2.833	0.100		
25	3.097	0.096	3.682	0.110	3.067	0.096	3.650	0.110	3.045	0.095	3.632	0.110	2.991	0.100	3.621	0.220
30	3.374	0.096	3.729	0.090	3.311	0.096	3.702	0.090	3.254	0.095	3.682	0.090	3.191	0.100	3.672	0.090
35	3.455	0.096	3.774	0.080	3.447	0.096	3.751	0.080	3.419	0.095	3.739	0.080	3.374	0.095	3.736	0.080
50	3.572	0.096	3.874	0.060	3.627	0.096	3.864	0.060	3.665	0.095	3.861	0.060	3.692	0.095	3.864	0.060
80	3.801	0.125	3.949	0.060	3.801	0.120	3.956	0.060	3.792	0.120	3.964	0.060	3.776	0.120	3.964	0.060
100	3.792	0.081	4.011	0.080	3.802	0.081	4.011	0.080	3.775	0.080	4.011	0.080	3.740	0.081	4.008	0.080
125	3.695	0.081			3.697	0.081			3.675	0.080	4.069	0.120	3.650	0.081	4.069	0.120
150	3.610	0.081			3.612	0.081			3.600	0.080			3.587	0.081		
r.m.s.		0.063		0.058		0.063		0.058		0.063		0.061		0.064		0.061

Cell e0 (10.5; 45.5) — Cell e1 (11.5; 45.5) — Cell e2 (12.5; 45.5) — Cell e3 (13.5; 45.5)

Period (s)	U (km/s)	ρg (km/s)	C (km/s)	ρph (km/s)	Period (s)	U (km/s)	ρg (km/s)	C (km/s)	ρph (km/s)	Period (s)	U (km/s)	ρg (km/s)	C (km/s)	ρph (km/s)	Period (s)	U (km/s)
7	2.210	0175			7	2.210	0175			7	2.210	0175			7	2.210
10	2.451	0.150			10	2.451	0.150			10	2.451	0.150			10	2.451
15	2.619	0.115			15	2.619	0.115			15	2.619	0.115			15	2.619
20	2.763	0.100			20	2.763	0.100			20	2.763	0.100			20	2.763
25	2.905	0.100	3.596	0.110	25	2.905	0.100	3.596	0.110	25	2.905	0.100	3.596	0.110	25	2.905
30	3.116	0.095	3.659	0.090	30	3.116	0.095	3.659	0.090	30	3.116	0.095	3.659	0.090	30	3.116
35	3.327	0.095	3.729	0.00	35	3.327	0.095	3.729	0.00	35	3.327	0.095	3.729	0.00	35	3.327
50	3.707	0.095	3.856	0.060	50	3.707	0.095	3.856	0.060	50	3.707	0.095	3.856	0.060	50	3.707
80	3.771	0.125	3.961	0.060	80	3.771	0.125	3.961	0.060	80	3.771	0.125	3.961	0.060	80	3.771
100	3.715	0.081	4.003	0.080	100	3.715	0.081	4.003	0.080	100	3.715	0.081	4.003	0.080	100	3.715
125	3.635	0.081	4.069	0.240	125	3.635	0.081	4.069	0.240	125	3.635	0.081	4.069	0.240	125	3.635
150	3.585	0.081			150	3.585	0.081			150	3.585	0.081			150	3.585
r.m.s.		0.070		0.067	r.m.s.		0.070		0.067	r.m.s.		0.070		0.067	r.m.s.	

Cell e4 (14.5; 45.5) — Cell e5 (15.5; 45.5) — Cell d-4 (6.5; 44.5) — Cell d-3 (7.5; 44.5)

Period (s)	U (km/s)	ρg (km/s)	C (km/s)	ρph (km/s)	U (km/s)	ρg (km/s)	C (km/s)	ρph (km/s)	U (km/s)	ρg (km/s)	C (km/s)	ρph (km/s)	U (km/s)	ρg (km/s)	C (km/s)	ρph (km/s)
7	2.535	0.150														
10	2.633	0.130			2.744	0.155			2.292	0.130			2.226	0.130		
15	2.697	0.110	3.222	0.200	2.757	0.105			2.671	0.120			2.653	0.120		
20	2.789	0.099	3.479	0.150	2.825	0.100	3.461	0.150	2.978	0.120			2.966	0.120	3.556	0.150
25	2.861	0.099	3.616	0.110	2.933	0.100	3.603	0.110	3.167	0.100	3.645	0.220	3.152	0.120	3.623	0.110
30	3.003	0.099	3.719	0.090	3.085	0.100	3.709	0.090	3.369	0.100	3.709	0.180	3.333	0.120	3.687	0.090
35	3.196	0.099	3.779	0.080	3.263	0.100	3.771	0.080	3.488	0.100	3.766	0.160	3.486	0.120	3.741	0.080
50	3.627	0.099	3.859	0.060	3.612	0.100	3.859	0.060	3.587	0.100	3.871	0.120	3.617	0.120	3.854	0.060
80	3.780	0.120	3.949	0.060	3.785	0.150			3.780	0.120	3.949	0.120	3.784	0.120	3.954	0.060
100	3.657	0.081	4.008	0.080	3.665	0.080	4.013	0.160	3.760	0.080	4.011	0.160	3.770	0.080	4.006	0.160
125	3.612	0.081	4.088	0.120	3.617	0.080			3.667	0.080			3.667	0.080		
150	3.592	0.081	4.180	0.120	3.597	0.080			3.580	0.080			3.580	0.080		
r.m.s.		0.068		0.070		0.072		0.070		0.063		0.104		0.062		0.066

Cell d-2 (8.5; 44.5) — Cell d-1 (9.5; 44.5) — Cell d0 (10.5; 44.5) — Cell d1 (11.5; 44.5)

Period (s)	U (km/s)	ρg (km/s)	C (km/s)	ρph (km/s)	U (km/s)	ρg (km/s)	C (km/s)	ρph (km/s)	U (km/s)	ρg (km/s)	C (km/s)	ρph (km/s)	U (km/s)	ρg (km/s)	C (km/s)	ρph (km/s)
7	2.136	0.165			2.088	0.160			2.013	0.155			2.019	0.155		
10	2.230	0.125			2.257	0.120			2.269	0.125			2.297	0.120		
15	2.599	0.105			2.560	0.100	3.123	0.200	2.532	0.105	3.113	0.200	2.495	0.100		
20	2.895	0.100	3.504	0.150	2.818	0.100	3.466	0.150	2.728	0.097	3.439	0.150	2.639	0.095		
25	3.093	0.100	3.613	0.110	2.993	0.100	3.593	0.110	2.883	0.097	3.558	0.110	2.799	0.095	3.538	0.110
30	3.263	0.100	3.669	0.090	3.164	0.100	3.652	0.090	3.082	0.097	3.630	0.090	3.022	0.095	3.623	0.090
35	3.426	0.100	3.726	0.080	3.347	0.095	3.716	0.080	3.307	0.097	3.701	0.080	3.295	0.095	3.699	0.080
50	3.632	0.090	3.841	0.060	3.652	0.095	3-.836	0.060	3.685	0.097	3.831	0.060	3.717	0.095	3.816	0.060
80	3.771	0.120	3.956	0.060	3.760	0.125	3.954	0.060	3.759	0.120	3.951	0.060	3.759	0.120	3.946	0.060
100	3.740	0.081	4.003	0.080	3.712	0.080	3.998	0.080	3.659	0.080	3.993	0.080	3.677	0.080	3.991	0.160
125	3.640	0.081			3.617	0.080			3.602	0.080			3.595	0.080		
150	3.565	0.081			3.552	0.080			3.547	0.080			3.547	0.080	4.167	0.240
r.m.s.		0.068		0.062		0.062		0.062		0.066		0.074		0.067		0.074

	Cell d2 (12.5; 44.5)				Cell d3 (13.5; 44.5)					Cell d4 (14.5; 44.5)					Cell d5 (15.5; 44.5)	
Period	U	ρ_g	C	ρ_{ph}	Period	U	ρ_g	C	ρ_{ph}	Period	U	ρ_g	C	ρ_{ph}	Period	U
(s)	(km/s)	(km/s)	(km/s)	(km/s)	(s)	(km/s)	(km/s)	(km/s)	(km/s)	(s)	(km/s)	(km/s)	(km/s)	(km/s)	(s)	(km/s)
7	2.134	0.160			7	2.134	0.160			7	2.134	0.160			7	2.134
10	2.344	0.125			10	2.344	0.125			10	2.344	0.125			10	2.344
15	2.499	0.105			15	2.499	0.105			15	2.499	0.105			15	2.499
20	2.605	0.095			20	2.605	0.095			20	2.605	0.095			20	2.605
25	2.770	0.095	3.553	0.110	25	2.770	0.095	3.553	0.110	25	2.770	0.095	3.553	0.110	25	2.770
30	2.982	0.095	3.647	0.090	30	2.982	0.095	3.647	0.090	30	2.982	0.095	3.647	0.090	30	2.982
35	3.254	0.095	3.724	0.080	35	3.254	0.095	3.724	0.080	35	3.254	0.095	3.724	0.080	35	3.254
50	3.705	0.095	3.836	0.060	50	3.705	0.095	3.836	0.060	50	3.705	0.095	3.836	0.060	50	3.705
80	3.763	0.120	3.942	0.060	80	3.763	0.120	3.942	0.060	80	3.763	0.120	3.942	0.060	80	3.763
100	3.662	0.080	3.991	0.080	100	3.662	0.080	3.991	0.080	100	3.662	0.080	3.991	0.080	100	3.662
125	3.592	0.080	4.075	0.120	125	3.592	0.080	4.075	0.120	125	3.592	0.080	4.075	0.120	125	3.592
150	3.550	0.080	4.167	0.120	150	3.550	0.080	4.167	0.120	150	3.550	0.080	4.167	0.120	150	3.550
r.m.s.		0.067		0.059	r.m.s.		0.067		0.059	r.m.s.		0.067		0.059	r.m.s.	

Period	Cell d6 (16.5; 44.5)				Cell d7 (17.5; 44.5)				Cell d8 (18.5; 44.5)				Cell c0 (10.5; 43.5)			
	U	ρ_g	C	ρ_{ph}	U	ρ_g	C	ρ_{ph}	U	ρ_g	C	ρ_{ph}	U	ρ_g	C	ρ_{ph}
(s)	(km/s)	(km/s)	(km/s)	(km/s)	(km/s)	(km/s)	(km/s)	(km/s)	(km/s)	(km/s)	(km/s)	(km/s)	(km/s)	(km/s)	(km/s)	(km/s)
7	2.646	0.165			2.654	0.160			2.588	0.160			2.000	0.155		
10	2.830	0.165			2.771	0.155			2.613	0.135			2.305	0.130		
15	2.761	0.115			2.771	0.115			2.675	0.115			2.614	0.115	3.113	0.200
20	2.789	0.105	3.421	0.060	2.817	0.10	3.404	0.150	2.798	0.110	3.392	0.150	2.873	0.115	3.434	0.150
25	2.964	0.095	3.578	0.080	2.979	0.105	3.561	0.110	2.946	0.110	3.549	0.110	3.060	0.115	3.548	0.110
30	3.129	0.095	3.697	0.090	3.156	0.097	3.689	0.090	3.12	0.105	3.682	0.090	3.212	0.110	3.615	0090
35	3.295	0.095	3.764	0.110	3.322	0.097	3.759	0.080	3.314	0.095	3.756	0.080	3.417	0.105	3.691	0.080
50	3.595	0.095	3.874	0.150	3.597	0.097	3.876	0.060	3.612	0.095	3.879	0.060	3.687	0.090	3.819	0.060
80	3.766	0.120			3.772	0.120			3.785	0.120			3.745	0.120	3.942	0.060
100	3.652	0.080			3.660	0.080			3.670	0.080			3.677	0.080	3.986	0.080
125	3.607	0.080			3.620	0.080			3.640	0.080			3.580	0.080		
150	3.509	0.080			3.605	0.080			3.627	0.080			3.522	0.080	4.167	0.140
r.m.s.		0.072		0.064		0.070		0.064		0.070		0.064		0.071		0.077

Period	Cell c1 (11.5; 43.5)				Cell c2 (12.5; 43.5)				Cell c3 (13.5; 43.5)				Cell c4 (14.5; 43.5)			
	U	ρ_g	C	ρ_{ph}	U	ρ_g	C	ρ_{ph}	U	ρ_g	C	ρ_{ph}	U	ρ_g	C	ρ_{ph}
(s)	(km/s)	(km/s)	(km/s)	(km/s)	(km/s)	(km/s)	(km/s)	(km/s)	(km/s)	(km/s)	(km/s)	(km/s)	(km/s)	(km/s)	(km/s)	(km/s)
7	2.056	0.155			2.150	0.155			2.199	0.150			2.202	0.150		
10	2.351	0.125			2.352	0.125			2.314	0.125			2.298	0.125		
15	2.526	0.110	3.098	0.200	2.480	0.105	3.078	0.200	2.447	0.100			2.440	0.100		
20	2.751	0.110	3.401	0.150	2.660	0.105	3.381	0.150	2.584	0.098			2.570	0.096		
25	2.949	0.110	3.531	0.110	2.859	0.105	3.541	0.110	2.781	0.098	3.566	0.110	2.765	0.096	3.588	0.220
30	3.135	0.110	3.603	0.090	3.069	0.105	3.615	0.090	3.008	0.098	3.649	0.090	2.91	0.096	3.682	0.180
35	3.369	0.096	3.686	0.080	3.304	0.094	3.696	0.080	3.209	0.098	3.726	0.080	3.174	0.096	3.754	0.160
50	3.697	0.096	3.819	0.060	3.670	0.094	3.834	0.060	3.635	0.098	3.859	0.060	3.630	0.096	3.874	0.120
80	3.750	0.120	3.942	0.060	3.762	0.120	3.942	0.060	3.766	0.120	3.946	0.060	3.760	0.120	3.949	0.120
100	3.670	0.080	3.983	0.080	3.662	0.080	3.983	0.080	3.657	0.080			3.657	0.080		
125	3.580	0.080	4.066	0.120	3.582	0.080	4.074	0.120	3.582	0.080	4.078	0.120	3.590	0.080	4.080	0.240
150	3.525	0.080	4.162	0.120	3.532	0.080	4.165	0.120	3.542	0.080	4.172	0.120	3.555	0.080	4.175	0.240
r.m.s.		0.069		0.070		0070		0.070		0.067		0.060		0.066		0.119

Cell c5 (15.5; 43.5) — Cell c6 (16.5; 43.5) — Cell c7 (17.5; 43.5) — Cell c8 (18.5; 43.5)

Period (s)	U (km/s)	ρ_g (km/s)	C (km/s)	ρ_{ph} (km/s)	Period (s)	U (km/s)	ρ_g (km/s)	C (km/s)	ρ_{ph} (km/s)	Period (s)	U (km/s)	ρ_g (km/s)	C (km/s)	ρ_{ph} (km/s)	Period (s)	U (km/s)
7	2.297	0.160			7	2.297	0.160			7	2.297	0.160			7	2.297
10	2.379	0.140			10	2.379	0.140			10	2.379	0.140			10	2.379
15	2.508	0.110			15	2.508	0.110			15	2.508	0.110			15	2.508
20	2.631	0.100	3.414	0.150	20	2.631	0.100	3.414	0.150	20	2.631	0.100	3.414	0.150	20	2.631
25	2.853	0.100	3.596	0.110	25	2.853	0.100	3.596	0.110	25	2.853	0.100	3.596	0.110	25	2.853
30	3.075	0.100	3.697	0.090	30	3.075	0.100	3.697	0.090	30	3.075	0.100	3.697	0.090	30	3.075
35	3.250	0.100	3.766	0.080	35	3.250	0.100	3.766	0.080	35	3.250	0.100	3.766	0.080	35	3.250
50	3.632	0.100	3.881	0.060	50	3.632	0.100	3.881	0.060	50	3.632	0.100	3.881	0.060	50	3.632
80	3.754	0.120	3.949	0.060	80	3.754	0.120	3.949	0.060	80	3.754	0.120	3.949	0.060	80	3.754
100	3.660	0.080			100	3.660	0.080			100	3.660	0.080			100	3.660
125	3.602	0.080	4.080	0.120	125	3.602	0.080	4.080	0.120	125	3.602	0.080	4.080	0.120	125	3.602
150	3.570	0.080	4.175	0.120	150	3.570	0.080	4.175	0.120	150	3.570	0.080	4.175	0.120	150	3.570
r.m.s.		0.069		0.064	r.m.s.		0.069		0.064	r.m.s.		0.069		0.064	r.m.s.	

Cell b0 (11.5; 42.5) — Cell b1 (11.5; 42.5) — Cell b2 (12.5; 42.5) — Cell b3 (13.5; 42.5)

Period (s)	U (km/s)	ρ_g (km/s)	C (km/s)	ρ_{ph} (km/s)	U (km/s)	ρ_g (km/s)	C (km/s)	ρ_{ph} (km/s)	U (km/s)	ρ_g (km/s)	C (km/s)	ρ_{ph} (km/s)	U (km/s)	ρ_g (km/s)	C (km/s)	ρ_{ph} (km/s)
7									2.267	0.170			2.270	0.165		
10	2.441	0.130			2.527	0.135			2.599	0.155			2.438	0.165		
15	2.728	0.110			2.642	0.115			2.595	0.125	3.056	0.200	2.539	0.125	3.035	0.200
20	3.069	0.105	3.469	0.150	2.964	0.115	3.419	0.150	2.863	0.125	3.371	0.150	2.736	0.125	3.339	0.150
25	3.299	0.105	3.553	0.110	3.209	0.115	3.558	0.110	3.079	0.125	3.561	0.110	2.916	0.1115	3.551	0.110
30	3.442	0.105	3.598	0.090	3.396	0.115	3.595	0.090	3.310	0.120	3.603	0.090	3.175	0.115	3.625	0.090
35	3.579	0.100	3.686	0.080	3.534	0.110	3.684	0.080	3.445	0.115	3.684	0.080	3.299	0.110	3.699	0.080
50	3.715	0.100	3.824	0.060	3.717	0.100	3.824	0.060	3.685	0.095	3.834	0.060	3.655	0.095	3.854	0.060
80	3.727	0.120	3.927	0.060	3.739	0.120	3.935	0.060	3.758	0.120	3.945	0.060	3.766	0.120	3.949	0.060
100	3.657	0.080	3.986	0.080	3.660	0.080	3.983	0.080	3.665	0.080	3.983	0.080	3.670	0.080	3.986	0.080
125	3.562	0.080	4.061	0.120	3.565	0.080	4.064	0.120	3.575	0.080	4.071	0.240	3.587	0.080	4.074	0.120
150	3.500	0.080	4.165	0.120	3.505	0.080	4.160	0.120	3.515	0.080	4.162	0.240	3.532	0.080	4.165	0.120
r.m.s.		0.068		0.063		0.068		0.063		0.075		0.085		0.078		0.070

Cell b4 (14.5; 42.5) — Cell b5 (15.5; 42.5) — Cell b6 (16.5; 42.5) — Cell b7 (17.5; 42.5)

Period (s)	U (km/s)	ρ_g (km/s)	C (km/s)	ρ_{ph} (km/s)	U (km/s)	ρ_g (km/s)	C (km/s)	ρ_{ph} (km/s)	U (km/s)	ρ_g (km/s)	C (km/s)	ρ_{ph} (km/s)	U (km/s)	ρ_g (km/s)	C (km/s)	ρ_{ph} (km/s)
7	2.246	0.160			2.275	0.160			2.337	0.160			2.446	0.165		
10	2.288	0.125			2.251	0.125			2.273	0.125			2.333	0.130		
15	2.490	0.110	3.020	0.200	2.469	0.105	3.032	0.200	2.438	0.105	3.065	0.200	2.410	0.110	3.086	0.400
20	2.666	0.105	3.326	0.150	2.646	0.098	3.341	0.150	2.612	0.095	3.359	0.150	2.572	0.105	3.356	0.150
25	2.844	0.097	3.541	0.110	2.879	0.098	3.548	0.110	2.922	0.095	3.548	0.110	2.850	0.105	3.533	0.110
30	3.123	0.097	3.645	0.090	3.191	0.098	3.664	0.090	3.247	0.095	3.677	0.090	3.161	0.105	3.672	0.090
35	3.245	0.097	3.719	0.080	3.329	0.098	3.741	0.080	3.424	0.095	3.754	0.080	3.369	0.105	3.751	0.080
50	3.660	0.097	3.871	0.060	3.660	0.098	3.884	0.060	3.632	0.095	3.886	0.060	3.582	0.095	3.881	0.060
80	3.760	0.120	3.949	0.060	3.750	0.120	3.949	0.060	3.739	0.120	3.946	0.060	3.724	0.120	3.945	0.060
100	3.680	0.080	3.986	0.080	3.690	0.080	3.986	0.080	3.700	0.080	3.988	0.080	3.712	0.080	3.991	0.080
125	3.602	0.080	4.074	0.120	3.617	0.080	4.074	0.120	3.625	0.080	4.071	0.120	3.652	0.080	4.066	0.120
150	3.552	0.080	4.162	0.120	3.572	0.080	4.162	0.120	3.595	0.080	4.160	0.120	3.620	0.080	4.150	0.120
r.m.s.		0.068		0.070		0.068		0.070		0.067		0.070		0.070		0.083

Cell b8 (18.5; 42.5) / Cell a1 (11.5; 41.5) / Cell a2 (12.5; 41.5) / Cell a3 (13.5; 41.5)

	Cell b8 (18.5; 42.5)				Cell a1 (11.5; 41.5)				Cell a2 (12.5; 41.5)				Cell a3 (13.5; 41.5)	
Period	U	ρ_g	C	ρ_{ph}	Period	U	ρ_g	C	ρ_{ph}	Period	U	ρ_g	C	ρ_{ph}	Period	U
(s)	(km/s)	(km/s)	(km/s)	(km/s)	(s)	(km/s)	(km/s)	(km/s)	(km/s)	(s)	(km/s)	(km/s)	(km/s)	(km/s)	(s)	(km/s)
7	2.553	0.180			7	2.553	0.180			7	2.553	0.180			7	2.553
10	2.447	0.135			10	2.447	0.135			10	2.447	0.135			10	2.447
15	2.454	0.110	3.113	0.400	15	2.454	0.110	3.113	0.400	15	2.454	0.110	3.113	0.400	15	2.454
20	2.560	0.100	3.351	0.150	20	2.560	0.100	3.351	0.150	20	2.560	0.100	3.351	0.150	20	2.560
25	2.729	0.100	3.521	0.110	25	2.729	0.100	3.521	0.110	25	2.729	0.100	3.521	0.110	25	2.729
30	3.002	0.100	3.662	0.090	30	3.002	0.100	3.662	0.090	30	3.002	0.100	3.662	0.090	30	3.002
35	3.218	0.100	3.749	0.080	35	3.218	0.100	3.749	0.080	35	3.218	0.100	3.749	0.080	35	3.218
50	3.545	0.095	3.876	0.060	50	3.545	0.095	3.876	0.060	50	3.545	0.095	3.876	0.060	50	3.545
80	3.721	0.120	3.945	0.060	80	3.721	0.120	3.945	0.060	80	3.721	0.120	3.945	0.060	80	3.721
100	3.725	0.080	3.991	0.080	100	3.725	0.080	3.991	0.080	100	3.725	0.080	3.991	0.080	100	3.725
125	3.667	0.080	4.061	0.120	125	3.667	0.080	4.061	0.120	125	3.667	0.080	4.061	0.120	125	3.667
150	3.645	0.080	4.141	0.120	150	3.645	0.080	4.141	0.120	150	3.645	0.080	4.141	0.120	150	3.645
r.m.s.		0.070		0.083	r.m.s.		0.070		0.083	r.m.s.		0.070		0.083	r.m.s.	

Cell a4 (14.5; 41.5) / Cell a15 (15.5; 41.5) / Cell a6 (16.5; 41.5) / Cell a7 (17.5; 41.5)

	Cell a4 (14.5; 41.5)				Cell a15 (15.5; 41.5)				Cell a6 (16.5; 41.5)				Cell a7 (17.5; 41.5)			
Period	U	ρ_g	C	ρ_{ph}	U	ρ_g	C	ρ_{ph}	U	ρ_g	C	ρ_{ph}	U	ρ_g	C	ρ_{ph}
(s)	(km/s)	(km/s)	(km/s)	(km/s)	(km/s)	(km/s)	(km/s)	(km/s)	(km/s)	(km/s)	(km/s)	(km/s)	(km/s)	(km/s)	(km/s)	(km/s)
7	2.387	0.160							2.321	0.155						
10	2.370	0.135			2.254	0.125			2.249	0.125			2.287	0.125		
15	2.605	0.110	3.000	0.200	2.471	0.105	3.000	0.200	2.367	0.105	3.008	0.200	2.340	0.105	3.037	0.400
20	2.828	0.105	3.302	0.150	2.699	0.097	3.304	0.150	2.599	0.099	3.311	0.150	2.532	0.098	3.319	0.300
25	2.969	0.105	3.541	0.110	2.905	0.097	3.516	0.110	2.860	0.099	3.503	0.110	2.803	0.098	3.493	0.220
30	3.219	0.095	3.652	0.090	3.212	0.097	3.654	0.090	3.244	0.099	3.667	0.090	3.234	0.098	3.669	0.180
35	3.277	0.095	3.719	0.080	3.296	0.097	3.726	0.080	3.396	0.099	3.739	0.080	3.444	0.098	3.744	0.160
50	3.662	0.095	3.859	0.060	3.647	0.097	3.874	0.060	3.615	0.095	3.881	0.060	3.570	0.098	3.879	0.120
80	3.762	0.120	3.945	0.060	3.753	0.120	3.945	0.060	3.740	0.120	3.942	0.060	3.727	0.120	3.937	0.060
100	3.697	0.080	3.986	0.080	3.712	0.081	3.986	0.080	3.727	0.081	3.986	0.080	3.745	0.080	3.986	0.160
125	3.620	0.080	4.066	0.120	3.637	0.080	4.064	0.120	3.657	0.081	4.064	0.120	3.677	0.080	4.059	0.120
150	3.557	0.080	4.152	0.120	3582	0.080	4.150	0.120	3.607	0.080	4.147	0.120	3.632	0.080	4.141	0.240
r.m.s.		0.068		0.070		0.064		0.070		0.068		0.070		0.064		0.127

Cell a8 (18.5; 41.5) / Cell a9 (19.5; 41.5) / Cell A0 (10.5; 40.5) / Cell A1 (11.5; 40.5)

	Cell a8 (18.5; 41.5)				Cell a9 (19.5; 41.5)				Cell A0 (10.5; 40.5)				Cell A1 (11.5; 40.5)			
Period	U	ρ_g	C	ρ_{ph}	U	ρ_g	C	ρ_{ph}	U	ρ_g	C	ρ_{ph}	U	ρ_g	C	ρ_{ph}
(s)	(km/s)	(km/s)	(km/s)	(km/s)	(km/s)	(km/s)	(km/s)	(km/s)	(km/s)	(km/s)	(km/s)	(km/s)	(km/s)	(km/s)	(km/s)	(km/s)
7																
10	2.368	0.125			2.582	0.150			2.552	0.130			2.583	0.135		
15	2.425	0.110	3.085	0.400	2.591	0.115	3.125	0.300	2.986	0.110			2.909	0.105		
20	2.535	0.105	3.326	0.300	2.609	0.100	3.331	0.300	3.314	0.090			3.236	0.096		
25	2.749	01.05	3.488	0.220	2.737	0.100	3.488	0.220	3.557	0.090	3.635	0.220	3.474	0.096	3.630	0.110
30	3.133	0.105	3.664	0.180	3.023	0.100	3.659	0.180	3.615	0.090	3.652	0.180	3.544	0.096	3.659	0.090
35	3.366	0.105	3.746	0.160	3.234	0.100	3.749	0.160	3.692	0.090	3.719	0.160	3.637	0.096	3.716	0.080
50	3.542	0.105	3.869	0.120	3.532	0.100	3.864	0.120	3.712	0.090	3.829	0.120	3.694	0.096	3.819	0.060
80	3.724	0.120	3.935	0.120	3.726	0.120			3.705	0.130	3.922	0.120	3.723	0.120	3.920	0.060
100	3.762	0.082	3.986	0.160	3.777	0.080	3.986	0.160	3.635	0.080			3.652	0.080		
125	3.695	0.082	4.054	0.240	3.715	0.080	4.049	0.240	3.560	0.080			3.575	0.080		
150	3.657	0.082	4.131	0.240	3.680	0.080	4.123	0.240	3.500	0.080			3.515	0.080		
r.m.s.		0.067		0.139		0.068		0.132		0.058		0.096		0.064		0.052

	Cell A2 (12.5; 40.5)				Cell A3 (13.5; 40.5)					Cell A4 (14.5; 40.5)					Cell A5 (15.5; 40.5)	
Period	U	ρg	C	ρph	Period	U	ρg	C	ρph	Period	U	ρg	C	ρph	Period	U
(s)	(km/s)	(km/s)	(km/s)	(km/s)	(s)	(km/s)	(km/s)	(km/s)	(km/s)	(s)	(km/s)	(km/s)	(km/s)	(km/s)	(s)	(km/s)
7					7					7					7	
10	2.650	0.130			10	2.650	0.130			10	2.650	0.130			10	2.650
15	2.865	0.105			15	2.865	0.105			15	2.865	0.105			15	2.865
20	3.165	0.095			20	3.165	0.095			20	3.165	0.095			20	3.165
25	3.367	0.095	3.621	0.120	25	3.367	0.095	3.621	0.120	25	3.367	0.095	3.621	0.120	25	3.367
30	3.442	0.095	3.664	0.060	30	3.442	0.095	3.664	0.060	30	3.442	0.095	3.664	0.060	30	3.442
35	3.536	0.095	3.716	0.080	35	3.536	0.095	3.716	0.080	35	3.536	0.095	3.716	0.080	35	3.536
50	3.659	0.095	3.814	0.090	50	3.659	0.095	3.814	0.090	50	3.659	0.095	3.814	0.090	50	3.659
80	3.739	0.120	3.922	0.110	80	3.739	0.120	3.922	0.110	80	3.739	0.120	3.922	0.110	80	3.739
100	3.675	0.080			100	3.675	0.080			100	3.675	0.080			100	3.675
125	3.597	0.080			125	3.597	0.080			125	3.597	0.080			125	3.597
150	3.535	0.080			150	3.535	0.080			150	3.535	0.080			150	3.535
r.m.s.		0.065		0.060	r.m.s.		0.065		0.060	r.m.s.		0.065		0.060	r.m.s.	

	Cell A6 (16.5; 40.5)				Cell A7 (17.5; 40.5)				Cell A8 (18.5; 40.5)				Cell A9 (19.5; 40.5)			
Period	U	ρg	C	ρph	U	ρg	C	ρph	U	ρg	C	ρph	U	ρg	C	ρph
(s)	(km/s)	(km/s)	(km/s)	(km/s)	(km/s)	(km/s)	(km/s)	(km/s)	(km/s)	(km/s)	(km/s)	(km/s)	(km/s)	(km/s)	(km/s)	(km/s)
7	2.244	0.160			2.310	0.170			2.475	0.160						
10	2.254	0.125			2.298	0.125			2.410	0.130			2.579	0.135		
15	2.321	0.105	2.983	0.400	2.331	0.105	3.016	0.200	2.451	0.105	3.050	0.200	2.565	0.110	3.075	0.200
20	2.615	0.098	3.294	0.300	2.527	0.105	3.306	0.150	2.522	0.095	3.314	0.150	2.558	0.100	3.319	0.150
25	2.770	0.098	3.498	0.220	2.754	0.105	3.473	0.110	2.810	0.095	3.458	0.100	2.764	0.100	3.453	0.110
30	3.102	0.098	3.672	0.180	3.131	0.105	3.677	0.090	3.184	0.095	3.677	0.090	3.103	0.100	3.674	0.090
35	3.271	0.098	3.739	0.160	3.346	0.105	3.744	0.080	3.409	0.095	3.746	0.080	3.312	0.100	3.749	0.080
50	3.595	0.098	3.864	0.060	3.600	0.095	3.864	0.060	3.602	0.095	3.856	0.060	3.592	0.100	3.854	0.060
80	3.758	0.120	3.930	0.060	3.759	0.120	3.927	0.060	3.759	0.120	3.925	0.060	3.753	0.120	3.925	0.060
100	3.755	0.081	3.983	0.160	3.775	0.080	3.981	0.080	3.797	0.081	3.981	0.080	3.820	0.080	3.981	0.080
125	3.687	0.081	4.056	0.240	3.710	0.080	4.049	0.120	3.730	0.081	4.044	0.120	3.750	0.080	4.039	0.120
150	3.625	0.081	4.138	0.240	3.650	0.080	4.131	0.120	3.675	0.081	4.121	0.120	3.700	0.080	4.116	0.120
r.m.s.		0.067		0.131		0.067		0.070		0.066		0.070		0.068		0.070

	Cell B1 (11.5; 39.5)				Cell B2 (12.5; 39.5)				Cell B3 (13.5; 39.5)				Cell B4 (14.5; 39.5)			
Period	U	ρg	C	ρph	U	ρg	C	ρph	U	ρg	C	ρph	U	ρg	C	ρph
(s)	(km/s)	(km/s)	(km/s)	(km/s)	(km/s)	(km/s)	(km/s)	(km/s)	(km/s)	(km/s)	(km/s)	(km/s)	(km/s)	(km/s)	(km/s)	(km/s)
7																
10	2.409	0.130			2.468	0.135			2.430	0.135			2.328	0.125		
15	2.838	0.110			2.7994	0.105			2.718	0.110			2.551	0.115		
20	3.148	0.100			3.063	0.100			2.980	0.100			2.873	0.110		
25	3.382	0.100	3.670	0.220	3.291	0.100	3.652	0.060	3.195	0.100	3.627	0.110	3.040	0.110		
30	3.455	0.100	3.707	0.10	3.369	0.100	3.704	0.060	3.320	0.095	3.702	0.090	3.246	0.096		
35	3.517	0.100	3.751	0.160	3.425	0.100	3.746	0.080	3.367	0.095	3.746	0.080	3.309	0.096		
50	3.162	0.095	3.824	0.120	3.567	0.095	3.812	0.090	3.537	0.095	3.819	0.060	3.525	0.096	3.834	0.060
80	3.670	0.120	3.913	0.120	3.735	0.120	3.912	0.110	3.747	0.120	3.915	0.120	3.755	0.120	3.915	0.060
100	3.650	0.080			3.675	0.080			3.702	0.080			3.727	0.080		
125	3.590	0.080			3.612	0.080			3.637	0.080			3.665	0.080		
150	3.532	0.080			3.555	0.080			3.580	0.080			3.600	0.080		
r.m.s.		0.063		0.104		0.065		0.052		0.065		0.060		0.066		0.039

	Cell B5 (15.5; 39.5)				Cell B6 (16.5; 39.5)				Cell B7 (17.5; 39.5)					Cell B8 (18.5; 39.5)		
Period	U	ρ_g	C	ρ_{ph}	Period	U	ρ_g	C	ρ_{ph}	Period	U	ρ_g	C	ρ_{ph}	Period	U
(s)	(km/s)	(km/s)	(km/s)	(km/s)	(s)	(km/s)	(km/s)	(km/s)	(km/s)	(s)	(km/s)	(km/s)	(km/s)	(km/s)	(s)	(km/s)
7					7					7					7	
10	2.236	0.125			10	2.236	0.125			10	2.236	0.125			10	2.236
15	2.354	0.120			15	2.354	0.120			15	2.354	0.120			15	2.354
20	2.744	0.110			20	2.744	0.110			20	2.744	0.110			20	2.744
25	2.824	0.110			25	2.824	0.110			25	2.824	0.110			25	2.824
30	3.096	0.110			30	3.096	0.110			30	3.096	0.110			30	3.096
35	3.226	0.097			35	3.226	0.097			35	3.226	0.097			35	3.226
50	3.517	0.097	3.841	0.060	50	3.517	0.097	3.841	0.060	50	3.517	0.097	3.841	0.060	50	3.517
80	3.760	0.120	3.917	0.060	80	3.760	0.120	3.917	0.060	80	3.760	0.120	3.917	0.060	80	3.760
100	3.752	0.081			100	3.752	0.081			100	3.752	0.081			100	3.752
125	3.692	0.081			125	3.692	0.081			125	3.692	0.081			125	3.692
150	3.622	0.081			150	3.622	0.081			150	3.622	0.081			150	3.622
r.m.s.		0.067		0.039	r.m.s.		0.067		0.039	r.m.s.		0.067		0.039	r.m.s.	

Period	Cell B9 (19.5; 39.5)				Cell C1 (11.5; 38.5)				Cell C2 (12.5; 38.5)				Cell C3 (13.5; 38.5)			
	U	ρ_g	C	ρ_{ph}	U	ρ_g	C	ρ_{ph}	U	ρ_g	C	ρ_{ph}	U	ρ_g	C	ρ_{ph}
(s)	(km/s)	(km/s)	(km/s)	(km/s)	(km/s)	(km/s)	(km/s)	(km/s)	(km/s)	(km/s)	(km/s)	(km/s)	(km/s)	(km/s)	(km/s)	(km/s)
7																
10	2.474	0.140			2.309	0.125			2.324	0.125			2.309	0.125		
15	2.445	0.110	3.062	0.200	2.800	0.105			2.734	0.105			2.611	0.115		
20	2.490	0.095	3.319	0.150	2.994	0.105			2.920	0.098			2.842	0.100		
25	2.789	0.095	3.436	0.110	3.248	0.097	3.710	0.060	3.184	0.098	3.690	0.060	3.079	0.100	3.658	0.060
30	3.114	0.095	3.682	0.090	3.359	0.097	3.752	0.080	3.312	0.098	3.747	0.060	3.269	0.095	3.732	0.060
35	3.354	0.095	3.749	0.080	3.402	0.097	3.784	0.090	3.350	0.098	3.781	0.080	3.322	0.095	3.772	0.080
50	3.665	0.095	3.844	0.060	3.592	0.097	3.710	0.110	3.550	0.098	3.829	0.090	3.520	0.095	3.826	0.090
80	3.811	0.120	3.920	0.060	3.680	0.120			3.700	0.120	3.910	0.110	3.717	0.120	3.910	0.100
100	3.857	0.081	3.976	0.080	3.655	0.080			3.677	0.080			3.705	0.080		
125	3.795	0.081	4.029	0.120	3.612	0.080			3.630	0.080			3.652	0.080		
150	3.720	0.081	4.111	0.120	3.560	0.080			3.577	0.080			3.600	0.080		
r.m.s.		0.065		0.070		0.063		0.056		0.065		0.052		0.064		0.052

Period	Cell C4 (14.5; 38.5)				Cell C5 (15.5; 38.5)				Cell C6 (16.5; 38.5)				Cell C7 (17.5; 38.5)			
	U	ρ_g	C	ρ_{ph}	U	ρ_g	C	ρ_{ph}	U	ρ_g	C	ρ_{ph}	U	ρ_g	C	ρ_{ph}
(s)	(km/s)	(km/s)	(km/s)	(km/s)	(km/s)	(km/s)	(km/s)	(km/s)	(km/s)	(km/s)	(km/s)	(km/s)	(km/s)	(km/s)	(km/s)	(km/s)
7																
10	2.242	0.130			2.183	0.125			2.165	0.120			2.125	0.125		
15	2.431	0.120			2.240	0.115			2.152	0.105			2.159	0.105		
20	2.742	0.110			2.644	0.100			2.556	0.096			2.456	0.096		
25	2.906	0.110			2.719	0.100			2.627	0.096			2.642	0.096		
30	3.173	0.097			3.045	0.098			2.976	0.096			3.001	0.096		
35	3.259	0.097			3.189	0.098			3.189	0.096			3.254	0.096		
50	3.502	0.097	3.834	0.060	3.497	0.098			3.537	0.096			3.614	0.096		
80	3.735	0.120	3.910	0.060	3.760	0.120			3.780	0.120			3.811	0.120		
100	3.732	0.080			3.757	0.080			3.785	0.080			3.815	0.080		
125	3.680	0.080			3.710	0.080			3.742	0.080			3.772	0.080		
150	3.620	0.080			3.642	0.080			3.667	0.080			3.692	0.080		
r.m.s.		0.066		0.039		0.065		0.000		0.076		0.000		0.064		0.00

	Cell C8 (18.5; 38.5)				Cell C9 (19.5; 38.5)				Cell D1 (11.5; 37.5)					Cell D2 (12.5; 37.5)	
Period	U	ρ_g	C	ρ_{ph}	Period	U	ρ_g	C	ρ_{ph}	Period	U	ρ_g	C	ρ_{ph}	Period	U
(s)	(km/s)	(km/s)	(km/s)	(km/s)	(s)	(km/s)	(km/s)	(km/s)	(km/s)	(s)	(km/s)	(km/s)	(km/s)	(km/s)	(s)	(km/s)
7					7					7					7	
10	2.148	0.140			10	2.148	0.140			10	2.148	0.140			10	2.148
15	2.198	0.115			15	2.198	0.115			15	2.198	0.115			15	2.198
20	2.381	0.096			20	2.381	0.096			20	2.381	0.096			20	2.381
25	2.689	0.096			25	2.689	0.096			25	2.689	0.096			25	2.689
30	3.057	0.096			30	3.057	0.096			30	3.057	0.096			30	3.057
35	3.337	0.096			35	3.337	0.096			35	3.337	0.096			35	3.337
50	3.690	0.096			50	3.690	0.096			50	3.690	0.096			50	3.690
80	3.841	0.120			80	3.841	0.120			80	3.841	0.120			80	3.841
100	3.845	0.080			100	3.845	0.080			100	3.845	0.080			100	3.845
125	3.800	0.080			125	3.800	0.080			125	3.800	0.080			125	3.800
150	3.717	0.080			150	3.717	0.080			150	3.717	0.080			150	3.717
r.m.s.		0.065		0.000	r.m.s.		0.065		0.000	r.m.s.		0.065		0.000	r.m.s.	

	Cell D3 (13.5; 37.5)				Cell D4 (14.5; 37.5)				Cell D5 (15.5; 37.5)				Cell D6 (16.5; 37.5)			
Period	U	ρ_g	C	ρ_{ph}	U	ρ_g	C	ρ_{ph}	U	ρ_g	C	ρ_{ph}	U	ρ_g	C	ρ_{ph}
(s)	(km/s)	(km/s)	(km/s)	(km/s)	(km/s)	(km/s)	(km/s)	(km/s)	(km/s)	(km/s)	(km/s)	(km/s)	(km/s)	(km/s)	(km/s)	(km/s)
7																
10	2.198	0.125			2.133				2.290	0.150						
15	2.457	0.120			2.286				2.150	0.115			2.100	0.130		
20	2.721	0.098			2.694				2.685	0.115			2.670	0.130		
25	3.001	0.098			2.891				2.835	0.115			2.844	0.130		
30	3.257	0.095			3.196				3.173	0.110			3.196	0.125		
35	3.347	0.095			3.294				3.292	0.105			3.365	0.115		
50	3.575	0.095			3.555				3.569	0.095			3.626	0.097		
80	3.732	0.120			3.751				3.766	0.120			3.791	0.120		
100	3.705	0.80			3.730				3.755	0.80			3.782	0.080		
125	3.670	0.080			3.692				3.720	0.080			3.750	0.080		
150	3.622	0.080			3.640				3.660	0.080			3.682	0.080		
r.m.s.		0.065		0.000		0.064		0.000		0.069		0.000		0.071		0.000

	Cell D7 (17.5; 37.5)				Cell D8 (18.5; 37.5)				Cell D9 (19.5; 37.5)			
Period	U	ρ_g	C	ρ_{ph}	U	ρ_g	C	ρ_{ph}	U	ρ_g	C	ρ_{ph}
(s)	(km/s)	(km/s)	(km/s)	(km/s)	(km/s)	(km/s)	(km/s)	(km/s)	(km/s)	(km/s)	(km/s)	(km/s)
7												
10	2.040	0.130			2.045	0.120			2.095	0.125		
15	2.097	0.130			2.115	0.120			2.176	0.105		
20	2.607	0.130			2.460	0.120			2.385	0.105		
25	2.854	0.130			2.812	0.120			2.756	0.105		
30	3.216	0.125			3.194	0.115			3.110	0.105		
35	2.432	0.115			3.441	0.110			3.367	0.105		
50	3.689	0.095			3.737	0.095			3.770	0.095		
80	3.819	0.120			3.850	0.120			3.884	0.120		
100	3.810	0.080			3.840	0.080			3.870	0.080		
125	3.780	0.080			3.810	0.080			3.837	0.080		
150	3.707	0.080			3.732	0.080			3.775	0.080		
r.m.s.		0.067		0.000		0.065		0.000		0.065		0.000

APPENDIX II

(part 1)

PARAMETERIZATION USED IN THE CELLULAR NON-LINEAR INVERSION AND RESULTS OF THE INVERSION

Table A2.1: Parameterization used in the non-linear inversion. *Grey area*: h (thickness), V_s and V_p of each layer. The uppermost layers are fixed on the base of available literature (see details in Chapter 3). The variable parameters are Pi, with i= 1, … 5 for thickness and i= 6, … 10 for V_s. *White area*: used step and allowed variability range for each parameter Pi. The explored parameter space, in some cases, exceeds physical boundaries even though all the retrieved solutions respect the accepted rules (see chapter 3.2.1).

Cell g-2 (8.5; 47.5)			Cell g-1 (9.5; 47.5)			Cell g0 (10.5; 47.5)			Cell g1 (11.5; 47.5)		
h	V_S	V_P	h	V_S	V_P	h	V_S	V_P	h	V_S	V_P
(km)	(km/s)	(km/s)	(km)	(km/s)	(km/s)	(km)	(km/s)	(km/s)	(km)	(km/s)	(km/s)
0.5	2.30	4.00									
0.5	2.65	4.60									
1	2.90	5.00									
2	3.45	6.00	2	2.75	4.75	3	3.40	5.80	3	2.70	4.65
2	3.40	5.90	5	3.40	5.88	2	3.50	6.05	3	3.00	5.20
P6	P1	P1x1.73	P6	P1	P1x1.73	P6	P1	P1x1.73	P6	P1	P1x1.73
P7	P2	P2x1.73	P7	P2	P2x1.73	P7	P2	P2x1.73	P7	P2	P2x1.73
P8	P3	P3x1.73	P8	P3	P3x1.73	P8	P3	P3x1.73	P8	P3	P3x1.73
P9	P4	P4x1.73	P9	P4	P4x1.73	P9	P4	P4x1.73	P9	P4	P4x1.73
P10	P5	P5x1.73	P10	P5	P5x1.73	P10	P5	P5x1.73	P10	P5	P5x1.73
h	Step	Range	h	Step	Range	h	Step	Range	h	Step	Range
(km)	(km)	(km)	(km)	(km)	(km)	(km)	(km)	(km)	(km)	(km)	(km)
P6	3	4-19	P6	4.5	8-17	P6	5	7.5-17.5	P6	6	6-24
P7	20	30-50	P7	9	20-38	P7	14	20-48	P7	10	15-35
P8	30	30-60	P8	20	30-50	P8	20	35-55	P8	40	50-90
P9	40	60-100	P9	40	70-110	P9	40	70-110	P9	35	60-95
P10	40	70-110	P10	40	70-110	P10	40	70-110	P10	40	60-100
V_S	Step	Range	V_S	Step	Range	V_S	Step	Range	V_S	Step	Range
(km/s)	(km/s)	(km/s)	(km/s)	(km/s)	(km/s)	(km/s)	(km/s)	(km/s)	(km/s)	(km/s)	(km/s)
P1	0.05	3.15-3.40	P1	0.20	2.70-4.10	P1	0.30	2.40-3.90	P1	0.20	2.75-4.00
P2	0.20	3.00-4.60	P2	0.30	2.90-4.70	P2	0.30	3.15-4.65	P2	0.30	2.80-4.05
P3	0.25	3.85-4.90	P3	0.20	4.00-4.90	P3	0.30	3.85-5.05	P3	0.20	4.00-5.20
P4	0.15	3.90-4.90	P4	0.25	4.00-5.15	P4	0.35	4.00-4.80	P4	0.40	4.00-5.20
P5	0.45	4.00-4.90	P5	0.50	4.00-4.80	P5	0.35	4.00-5.10	P5	0.50	4.00-5.20

Cell g2 (12.5; 47.5)

h (km)	V_S (km/s)	V_P (km/s)
1.8	2.20	3.80
3.2	3.20	5.55
P6	P1	P1x1.73
P7	P2	P2x1.73
P8	P3	P3x1.73
P9	P4	P4x1.73
P10	P5	P5x1.73

h	Step (km)	Range (km)
P6	7	10-24
P7	13	13-39
P8	30	30-60
P9	40	60-100
P10	40	70-110

V_S	Step (km/s)	Range (km/s)
P1	0.15	3.15-3.90
P2	0.50	2.65-4.65
P3	0.35	3.55-4.95
P4	0.35	3.95-4.85
P5	0.35	4.00-5.10

Cell f-3 (7.5; 46.5)

h (km)	V_S (km/s)	V_P (km/s)
1	2.85	5.00
2	3.10	5.40
2	3.45	6.00
P6	P1	P1x1.73
P7	P2	P2x1.73
P8	P3	P3x1.73
P9	P4	P4x1.73
P10	P5	P5x1.73

h	Step (km)	Range (km)
P6	3	3-15
P7	8	10-44
P8	25	35-60
P9	40	70-110
P10	40	70-110

V_S	Step (km/s)	Range (km/s)
P1	0.10	2.90-3.90
P2	0.30	3.05-4.55
P3	0.25	3.95-4.80
P4	0.15	4.00-4.90
P5	0.50	4.00-5.00

Cell f-2 (8.5; 46.5)

h (km)	V_S (km/s)	V_P (km/s)
1	2.85	5.00
1	3.10	5.40
2	3.45	6.00
P6	P1	P1x1.73
P7	P2	P2x1.73
P8	P3	P3x1.73
P9	P4	P4x1.73
P10	P5	P5x1.73

h	Step (km)	Range (km)
P6	4	7-19
P7	6	6-36
P8	35	35-70
P9	40	70-110
P10	40	70-110

V_S	Step (km/s)	Range (km/s)
P1	0.30	2.45-3.94
P2	0.15	3.10-4.60
P3	0.30	3.70-4.90
P4	0.30	4.00-4.90
P5	0.50	4.00-5.10

Cell f-1 (9.5; 46.5)

h (km)	V_S (km/s)	V_P (km/s)
0.1	1.20	2.20
7.9	3.30	5.75
P6	P1	P1x1.73
P7	P2	P2x1.73
P8	P3	P3x1.73
P9	P4	P4x1.73
P10	P5	P5x1.73

h	Step (km)	Range (km)
P6	2	4-13
P7	8	10-33
P8	30	50-80
P9	35	65-100
P10	40	70-110

V_S	Step (km/s)	Range (km/s)
P1	0.25	2.10-4.00
P2	0.15	2.40-4.20
P3	0.15	3.705.20
P4	0.40	3.80-5.20
P5	0.45	3.95-5.00

Cell f0 (10.5; 46.5)

h (km)	V_S (km/s)	V_P (km/s)
3	3.20	5.50
2	3.50	6.10
P6	P1	P1x1.73
P7	P2	P2x1.73
P8	P3	P3x1.73
P9	P4	P4x1.73
P10	P5	P5x1.73

h	Step (km)	Range (km)
P6	2	2-12
P7	10	12-42
P8	30	35-65
P9	40	70-110
P10	40	70-110

V_S	Step (km/s)	Range (km/s)
P1	0.10	2.55-3.55
P2	0.20	3.10-4.30
P3	0.25	3.85-4.85
P4	0.30	3.90-4.80
P5	0.50	4.00-5.10

Cell f1 (11.5; 46.5)

h (km)	V_S (km/s)	V_P (km/s)
0.1	1.20	2.10
0.9	3.35	5.80
3	3.15	5.45
P6	P1	P1x1.73
P7	P2	P2x1.73
P8	P3	P3x1.73
P9	P4	P4x1.73
P10	P5	P5x1.73

h	Step (km)	Range (km)
P6	3	5-12
P7	7	11-32
P8	30	45-75
P9	35	65-100
P10	40	70-110

V_S	Step (km/s)	Range (km/s)
P1	0.20	2.50-4.00
P2	0.20	2.40-4.25
P3	0.25	3.75-500
P4	0.30	4.00-5.05
P5	0.45	4.00-5.05

Cell f2 (12.5; 46.5)

h (km)	V_S (km/s)	V_P (km/s)
0.5	3.50	6.05
6.5	2.85	4.90
P6	P1	P1x1.73
P7	P2	P2x1.73
P8	P3	P3x1.73
P9	P4	P4x1.73
P10	P5	P5x1.73

h	Step (km)	Range (km)
P6	7	7.5-21.5
P7	9	17-35
P8	20	35-55
P9	40	70-110
P10	50	70-110

V_S	Step (km/s)	Range (km/s)
P1	0.20	2.80-4.00
P2	0.35	2.90-4.55
P3	0.35	4.00-5.05
P4	0.35	4.00-4.85
P5	0.50	4.00-5.10

Cell f3 (13.5; 46.5)

h (km)	V_S (km/s)	V_P (km/s)
0.25	1.70	2.80
1	2.40	3.80
6.8	3.15	5.80
P6	P1	P1x1.73
P7	P2	P2x1.73
P8	P3	P3x1.73
P9	P4	P4x1.73
P10	P5	P5x1.73

h	Step (km)	Range (km)
P6	8	10-26
P7	25	25-50
P8	20	30-50
P9	40	60-100
P10	40	70-110

V_S	Step (km/s)	Range (km/s)
P1	0.30	3.10-3.85
P2	0.40	2.90-4.85
P3	0.40	3.45-4.80
P4	0.40	4.00-4.90
P5	0.35	4.00-4.75

Cell e-4 (6.5; 45.5)			Cell e-3 (7.5; 45.5)			Cell e-2 (8.5; 45.5)			Cell e-1 (9.5; 45.5)		
h	V_S	V_P	h	V_S	V_P	h	V_S	V_P	h	V_S	V_P
(km)	(km/s)	(km/s)	(km)	(km/s)	(km/s)	(km)	(km/s)	(km/s)	(km)	(km/s)	(km/s)
0.5	1.20	2.10	0.1	1.20	2.10	3	2.43	4.20	3	2.30	4.00
4.5	2.90	5.00	5.9	2.80	4.75	3	2.90	5.00	3	2.60	4.50
P6	P1	P1x1.73	P6	P1	P1x1.73	P6	P1	P1x1.73	P6	P1	P1x1.73
P7	P2	P2x1.73	P7	P2	P2x1.73	P7	P2	P2x1.73	P7	P2	P2x1.73
P8	P3	P3x1.73	P8	P3	P3x1.73	P8	P3	P3x1.73	P8	P3	P3x1.73
P9	P4	P4x1.73	P9	P4	P4x1.73	P9	P4	P4x1.73	P9	P4	P4x1.73
P10	P5	P5x1.73	P10	P5	P5x1.73	P10	P5	P5x1.73	P10	P5	P5x1.73
h	Step	Range	h	Step	Range	h	Step	Range	h	Step	Range
(km)	(km)	(km)	(km)	(km)	(km)	(km)	(km)	(km)	(km)	(km)	(km)
P6	2	4-16	P6	2	7-12	P6	4	6-18	P6	5	10-20
P7	6	8-26	P7	7	9-33	P7	8	9-33	P7	8	9-25
P8	20	35-75	P8	30	55-85	P8	30	40-80	P8	30	30-80
P9	35	40-100	P9	55	45-100	P9	40	60-100	P9	35	40-100
P10	45	40-110	P10	55	55-110	P10	40	70-110	P10	40	40-110
V_S	Step	Range	V_S	Step	Range	V_S	Step	Range	V_S	Step	Range
(km/s)	(km/s)	(km/s)	(km/s)	(km/s)	(km/s)	(km/s)	(km/s)	(km/s)	(km/s)	(km/s)	(km/s)
P1	0.10	2.50-4.00	P1	0.20	2.50-4.00	P1	0.25	2.50-4.15	P1	0.25	2.50-4.00
P2	0.40	2.40-4.35	P2	0.15	2.40-4.00	P2	0.20	2.40-4.40	P2	0.25	2.40-4.05
P3	0.05	3.70-4.80	P3	0.15	3.70-5.20	P3	0.20	3.70-4.85	P3	0.25	3.70-5.20
P4	0.20	3.80-5.20	P4	0.50	3.60-5.20	P4	0.30	4.00-4.95	P4	0.30	3.80-5.20
P5	0.35	3.65-5.20	P5	0.50	3.85-5.20	P5	0.40	4.00-4.80	P5	0.40	3.85-5.20

Cell e0 (10.5; 45.5)			Cell e1 (11.5; 45.5)			Cell e2 (12.5; 45.5)			Cell e3 (13.5; 45.5)		
h	V_S	V_P	h	V_S	V_P	h	V_S	V_P	h	V_S	V_P
(km)	(km/s)	(km/s)	(km)	(km/s)	(km/s)	(km)	(km/s)	(km/s)	(km)	(km/s)	(km/s)
									1	2.10	3.60
1	2.00	3.50	4.5	2.55	4.40	1	2.10	3.60	4	2.60	4.50
2	2.56	4.40	1.5	3.18	5.50	4	2.50	4.30	1	3.00	5.20
3	3.01	5.20	1	3.30	5.70	2	2.90	5.00	2	3.20	5.55
P6	P1	P1x1.73	P6	P1	P1x1.73	P6	P1	P1x1.73	P6	P1	P1x1.73
P7	P2	P2x1.73	P7	P2	P2x1.73	P7	P2	P2x1.73	P7	P2	P2x1.73
P8	P3	P3x1.73	P8	P3	P3x1.73	P8	P3	P3x1.73	P8	P3	P3x1.73
P9	P4	P4x1.73	P9	P4	P4x1.73	P9	P4	P4x1.73	P9	P4	P4x1.73
P10	P5	P5x1.73	P10	P5	P5x1.73	P10	P5	P5x1.73	P10	P5	P5x1.73
h	Step	Range	h	Step	Range	h	Step	Range	h	Step	Range
(km)	(km)	(km)	(km)	(km)	(km)	(km)	(km)	(km)	(km)	(km)	(km)
P6	2	5-13	P6	3	4-10	P6	7	7-28	P6	6	12-24
P7	6	9-33	P7	7	12-35	P7	20	20-60	P7	5	10-35
P8	40	50-90	P8	40	40-80	P8	30	30-60	P8	30	30-90
P9	40	50-90	P9	40	70-110	P9	40	50-90	P9	40	50-90
P10	40	70-110	P10	45	60-105	P10	50	50-100	P10	40	50-90
V_S	Step	Range	V_S	Step	Range	V_S	Step	Range	V_S	Step	Range
(km/s)	(km/s)	(km/s)	(km/s)	(km/s)	(km/s)	(km/s)	(km/s)	(km/s)	(km/s)	(km/s)	(km/s)
P1	0.20	2.50-4.00	P1	0.25	2.30-3.80	P1	0.10	2.70-4.50	P1	0.10	3.00-4.10
P2	0.15	2.40-4.05	P2	0.25	2.80-4.55	P2	0.35	3.20-4.60	P2	0.30	4.00-4.90
P3	0.20	3.70-5.20	P3	0.25	4.00-5.10	P3	0.25	4.00-4.90	P3	0.10	4.00-4.85
P4	0.50	3.80-5.00	P4	0.30	4.00-5.10	P4	0.30	4.00-5.00	P4	0.15	4.00-4.80
P5	0.75	4.00-4.75	P5	0.50	4.00-5.10	P5	0.45	4.00-4.90	P5	0.50	4.00-5.10

Top group

Cell e4 (14.5; 45.5)			Cell e5 (15.5; 45.5)			Cell d-4 (6.5; 44.5)			Cell d-3 (7.5; 44.5)		
h	V_S	V_P	h	V_S	V_P	h	V_S	V_P	h	V_S	V_P
(km)	(km/s)	(km/s)	(km)	(km/s)	(km/s)	(km)	(km/s)	(km/s)	(km)	(km/s)	(km/s)
4	2.30	4.00							1	2.75	4.80
1.5	3.25	5.60	4	2.10	3.65	2	2.75	4.80	1	2.85	5.00
1.5	3.35	5.80	1.5	3.30	5.70	2	3.00	5.20	1	3.00	5.20
1	3.45	6.00	2.5	3.60	6.20	1	3.15	5.45	2	3.10	5.40
P6	P1	P1x1.73	P6	P1	P1x1.73	P6	P1	P1x1.73	P6	P1	P1x1.73
P7	P2	P2x1.73	P7	P2	P2x1.73	P7	P2	P2x1.73	P7	P2	P2x1.73
P8	P3	P3x1.73	P8	P3	P3x1.73	P8	P3	P3x1.73	P8	P3	P3x1.73
P9	P4	P4x1.73	P9	P4	P4x1.73	P9	P4	P4x1.73	P9	P4	P4x1.73
P10	P5	P5x1.73	P10	P5	P5x1.73	P10	P5	P5x1.73	P10	P5	P5x1.73
h	Step	Range	h	Step	Range	h	Step	Range	h	Step	Range
(km)	(km)	(km)	(km)	(km)	(km)	(km)	(km)	(km)	(km)	(km)	(km)
P6	10	15-35	P6	8	8-32	P6	3	5-14	P6	4	6-18
P7	15	15-45	P7	25	25-50	P7	5	7-27	P7	20	20-40
P8	20	30-50	P8	30	30-60	P8	30	40-70	P8	35	50-85
P9	40	60-100	P9	40	50-90	P9	50	60-110	P9	40	60-100
P10	50	60-110	P10	50	50-100	P10	50	60-110	P10	40	60-100
V_S	Step	Range	V_S	Step	Range	V_S	Step	Range	V_S	Step	Range
(km/s)	(km/s)	(km/s)	(km/s)	(km/s)	(km/s)	(km/s)	(km/s)	(km/s)	(km/s)	(km/s)	(km/s)
P1	0.10	3.10-4.40	P1	0.20	2.95-4.55	P1	0.25	2.15-3.65	P1	0.25	2.40-3.55
P2	0.40	2.80-4.80	P2	0.35	2.70-4.65	P2	0.25	2.85-4.40	P2	0.30	2.25-4.85
P3	0.20	4.00-4.80	P3	0.35	3.85-4.90	P3	0.15	4.00-4.80	P3	0.20	3.90-4.95
P4	0.40	4.00-4.80	P4	0.30	4.00-4.90	P4	0.30	3.90-4.95	P4	0.30	3.75-4.95
P5	0.45	4.00-4.95	P5	0.50	4.00-5.10	P5	0.40	4.00-4.80	P5	0.50	3.70-4.90

Bottom group

Cell d-2 (8.5; 44.5)			Cell d-1 (9.5; 44.5)			Cell d0 (10.5; 44.5)			Cell d1 (11.5; 44.5)		
h	V_S	V_P	h	V_S	V_P	h	V_S	V_P	h	V_S	V_P
(km)	(km/s)	(km/s)	(km)	(km/s)	(km/s)	(km)	(km/s)	(km/s)	(km)	(km/s)	(km/s)
						3	2.00	3.45	2	2.00	3.45
						1.4	2.20	3.80	2.4	2.15	3.70
3	2.30	4.00	2	2.30	4.00	1.6	2.80	4.80	1.6	2.80	4.80
4	2.50	4.30	4	2.50	4.30	1	3.25	5.60	1	3.25	5.60
P6	P1	P1x1.73	P6	P1	P1x1.73	P6	P1	P1x1.73	P6	P1	P1x1.73
P7	P2	P2x1.73	P7	P2	P2x1.73	P7	P2	P2x1.73	P7	P2	P2x1.73
P8	P3	P3x1.73	P8	P3	P3x1.73	P8	P3	P3x1.73	P8	P3	P3x1.73
P9	P4	P4x1.73	P9	P4	P4x1.73	P9	P4	P4x1.73	P9	P4	P4x1.73
P10	P5	P5x1.73	P10	P5	P5x1.73	P10	P5	P5x1.73	P10	P5	P5x1.73
h	Step	Range	h	Step	Range	h	Step	Range	h	Step	Range
(km)	(km)	(km)	(km)	(km)	(km)	(km)	(km)	(km)	(km)	(km)	(km)
P6	4	4-14	P6	5	5-15	P6	1	4-15	P6	8	9-25
P7	9	11-38	P7	8	12-28	P7	20	20-60	P7	10	10-40
P8	30	30-80	P8	30	55-85	P8	30	30-60	P8	20	30-50
P9	40	60-100	P9	35	70-105	P9	50	50-100	P9	40	60-100
P10	40	70-110	P10	40	70-110	P10	50	50-100	P10	40	60-100
V_S	Step	Range	V_S	Step	Range	V_S	Step	Range	V_S	Step	Range
(km/s)	(km/s)	(km/s)	(km/s)	(km/s)	(km/s)	(km/s)	(km/s)	(km/s)	(km/s)	(km/s)	(km/s)
P1	0.30	2.10-4.00	P1	0.30	2.10-4.00	P1	0.05	2.65-4.45	P1	0.15	2.65-4.45
P2	0.30	2.40-4.70	P2	0.25	2.40-4.50	P2	0.20	3.25-4.75	P2	0.35	2.75-4.85
P3	0.20	3.70-4.80	P3	0.20	3.70-4.80	P3	0.35	3.75-4.80	P3	0.30	3.40-4.80
P4	0.25	3.80-4.80	P4	0.35	3.90-5.85	P4	0.45	4.00-4.90	P4	0.35	4.00-5.05
P5	0.50	4.00-5.10	P5	0.50	4.00-5.20	P5	0.40	4.00-5.10	P5	0.45	4.00-4.90

Cell d2 (12.5; 44.5)			Cell d3 (13.5; 44.5)			Cell d4 (14.5; 44.5)			Cell d5 (15.5; 44.5)		
h	V_S	V_P	h	V_S	V_P	h	V_S	V_P	h	V_S	V_P
(km)	(km/s)	(km/s)	(km)	(km/s)	(km/s)	(km)	(km/s)	(km/s)	(km)	(km/s)	(km/s)
			0.05	0.00	1.52						
0.4	0.00	1.52	2.95	1.76	3.05	0.05	0.00	1.52			
3.6	2.00	3.45	1	2.25	3.90	2.95	1.76	3.05	4	2.10	3.65
2	3.30	5.70	1	3.45	6.00	1	2.25	3.90	1.5	3.30	5.70
2	3.50	6.05	1	3.50	6.05	2	3.40	5.90	2.5	3.60	6.20
P6	P1	P1x1.73	P6	P1	P1x1.73	P6	P1	P1x1.73	P6	P1	P1x1.73
P7	P2	P2x1.73	P7	P2	P2x1.73	P7	P2	P2x1.73	P7	P2	P2x1.73
P8	P3	P3x1.73	P8	P3	P3x1.73	P8	P3	P3x1.73	P8	P3	P3x1.73
P9	P4	P4x1.73	P9	P4	P4x1.73	P9	P4	P4x1.73	P9	P4	P4x1.73
P10	P5	P5x1.73	P10	P5	P5x1.73	P10	P5	P5x1.73	P10	P5	P5x1.73
h	Step	Range	h	Step	Range	h	Step	Range	h	Step	Range
(km)	(km)	(km)	(km)	(km)	(km)	(km)	(km)	(km)	(km)	(km)	(km)
P6	6	6-18	P6	7	12-26	P6	3.5	4.50-18.5	P6	8	13-29
P7	12	20-44	P7	4	8-16	P7	3.5	6.5-22.5	P7	10	10-40
P8	30	30-60	P8	15	15-60	P8	1	20-45	P8	20	30-50
P9	50	55-105	P9	30	50-110	P9	3	26-86	P9	40	60-100
P10	50	60-110	P10	40	70-110	P10	10	50-140	P10	60	60-120
V_S	Step	Range	V_S	Step	Range	V_S	Step	Range	V_S	Step	Range
(km/s)	(km/s)	(km/s)	(km/s)	(km/s)	(km/s)	(km/s)	(km/s)	(km/s)	(km/s)	(km/s)	(km/s)
P1	0.15	2.70-4.35	P1	0.10	3.05-4.25	P1	0.05	2.35-4.55	P1	0.05	3.00-4.10
P2	0.40	2.75-4.75	P2	0.50	2.85-4.10	P2	0.05	3.15-4.75	P2	0.50	2.80-4.80
P3	0.30	4.00-4.80	P3	0.20	4.00-4.80	P3	0.05	3.55-4.75	P3	0.05	4.00-4.80
P4	0.45	4.00-4.90	P4	0.20	4.00-4.80	P4	0.05	4.00-4.95	P4	0.30	4.00-4.80
P5	0.45	4.00-4.90	P5	0.20	4.00-4.80	P5	0.05	4.00-4.80	P5	0.40	4.00-4.80

Cell d6 (16.5; 44.5)			Cell d7 (17.5; 44.5)			Cell d8 (18.5; 44.5)			Cell c0 (10.5; 43.5)		
h	V_S	V_P	h	V_S	V_P	h	V_S	V_P	h	V_S	V_P
(km)	(km/s)	(km/s)	(km)	(km/s)	(km/s)	(km)	(km/s)	(km/s)	(km)	(km/s)	(km/s)
4	2.20	3.80	3	2.20	3.80						
1	2.30	4.00	1	2.30	4.00	4	2.30	4.00	4	2.20	3.80
1.5	3.30	5.70	1	3.30	5.70	1.5	3.25	5.60	1	2.65	4.60
1.5	3.45	6.00	1	3.50	6.05	1.5	3.45	6.00	1.5	3.00	5.20
P6	P1	P1x1.73	P6	P1	P1x1.73	P6	P1	P1x1.73	P6	P1	P1x1.73
P7	P2	P2x1.73	P7	P2	P2x1.73	P7	P2	P2x1.73	P7	P2	P2x1.73
P8	P3	P3x1.73	P8	P3	P3x1.73	P8	P3	P3x1.73	P8	P3	P3x1.73
P9	P4	P4x1.73	P9	P4	P4x1.73	P9	P4	P4x1.73	P9	P4	P4x1.73
P10	P5	P5x1.73	P10	P5	P5x1.73	P10	P5	P5x1.73	P10	P5	P5x1.73
h	Step	Range	h	Step	Range	h	Step	Range	h	Step	Range
(km)	(km)	(km)	(km)	(km)	(km)	(km)	(km)	(km)	(km)	(km)	(km)
P6	4	4.5-12.5	P6	4	6.5-18-5	P6	11	11-33	P6	7	7.5-21.5
P7	8	12-30	P7	6	10-22	P7	15	15-45	P7	13	13.5-39.5
P8	30	40-70	P8	30	40-70	P8	34	40-74	P8	30	30-60
P9	50	60-110	P9	50	65-110	P9	40	50-90	P9	50	50-100
P10	50	60-110	P10	60	60-120	P10	50	50-100	P10	50	60-110
V_S	Step	Range	V_S	Step	Range	V_S	Step	Range	V_S	Step	Range
(km/s)	(km/s)	(km/s)	(km/s)	(km/s)	(km/s)	(km/s)	(km/s)	(km/s)	(km/s)	(km/s)	(km/s)
P1	0.15	3.00-4.05	P1	0.25	3.15-4.65	P1	0.15	3.10-4.15	P1	0.20	2.70-4.00
P2	0.20	3.00-4.45	P2	0.25	2.75-4.50	P2	0.55	2.55-4.75	P2	0.40	3.00-4.60
P3	0.20	3.90-4.85	P3	0.20	3.80-4.80	P3	0.30	3.50-5.10	P3	0.15	3.95-4.80
P4	0.20	4.00-4.90	P4	0.30	4.00-5.10	P4	0.40	4.00-4.80	P4	0.30	3.80-5.10
P5	0.40	4.00-4.80	P5	0.50	4.00-5.10	P5	0.50	4.00-5.10	P5	0.45	4.00-4.90

Cell c1 (11.5; 43.5)			Cell c2 (12.5; 43.5)			Cell c3 (13.5; 43.5)			Cell c4 (14.5; 43.5)		
h	V_S	V_P	h	V_S	V_P	h	V_S	V_P	h	V_S	V_P
(km)	(km/s)	(km/s)	(km)	(km/s)	(km/s)	(km)	(km/s)	(km/s)	(km)	(km/s)	(km/s)
			0.5	1.60	2.65	1.1	1.55	2.65	0.15	0.00	1.52
4	2.20	3.80	1.5	2.30	3.60	2.4	3.60	3.60	2.85	1.76	3.05
1	2.65	4.60	1	3.00	5.50	1.5	3.18	5.50	1	2.25	3.90
2	3.20	5.55	1.5	3.50	6.10	1	3.50	6.10	2	3.45	6.00
P6	P1	P1x1.73	P6	P1	P1x1.73	P6	P1	P1x1.73	P6	P1	P1x1.73
P7	P2	P2x1.73	P7	P2	P2x1.73	P7	P2	P2x1.73	P7	P2	P2x1.73
P8	P3	P3x1.73	P8	P3	P3x1.73	P8	P3	P3x1.73	P8	P3	P3x1.73
P9	P4	P4x1.73	P9	P4	P4x1.73	P9	P4	P4x1.73	P9	P4	P4x1.73
P10	P5	P5x1.73	P10	P5	P5x1.73	P10	P5	P5x1.73	P10	P5	P5x1.73
h	Step	Range	h	Step	Range	h	Step	Range	h	Step	Range
(km)	(km)	(km)	(km)	(km)	(km)	(km)	(km)	(km)	(km)	(km)	(km)
P6	6	8-24	P6	2	4-10	P6	6	10-22	P6	6	9-21
P7	10	18-38	P7	3.5	16-32	P7	7	13-27	P7	14	14-42
P8	30	35-65	P8	30	35-65	P8	30	30-60	P8	30	30-60
P9	40	65-105	P9	40	60-100	P9	40	70-110	P9	50	40-100
P10	50	50-100	P10	50	60-110	P10	40	70-110	P10	50	40-100
V_S	Step	Range	V_S	Step	Range	V_S	Step	Range	V_S	Step	Range
(km/s)	(km/s)	(km/s)	(km/s)	(km/s)	(km/s)	(km/s)	(km/s)	(km/s)	(km/s)	(km/s)	(km/s)
P1	0.20	2.30-3.80	P1	0.20	2.30-3.40	P1	0.15	2.90-3.80	P1	0.10	2.40-4.40
P2	0.30	3.10-4.70	P2	0.15	3.00-4.55	P2	0.30	3.00-4.25	P2	0.35	3.20-4.70
P3	0.20	3.80-4.85	P3	0.20	4.00-4.80	P3	0.30	4.00-4.80	P3	0.40	4.00-5.10
P4	0.30	4.00-4.70	P4	0.30	3.80-4.70	P4	0.25	4.00-4.85	P4	0.30	4.00-4.90
P5	0.40	4.00-4.90	P5	0.40	4.00-4.80	P5	0.45	4.00-4.90	P5	0.40	4.00-4.80

Cell c5 (15.5; 43.5)			Cell c6 (16.5; 43.5)			Cell c7 (17.5; 43.5)			Cell c8 (18.5; 43.5)		
h	V_S	V_P	h	V_S	V_P	h	V_S	V_P	h	V_S	V_P
(km)	(km/s)	(km/s)	(km)	(km/s)	(km/s)	(km)	(km/s)	(km/s)	(km)	(km/s)	(km/s)
0.2	0.00	1.52				2	2.20	3.80			
2.8	1.96	3.38	4	2.10	3.65	2	2.25	3.90	4	2.20	3.80
1	2.28	4.00	1.5	3.30	5.70	1.5	3.40	5.90	1	3.25	5.60
2	3.45	6.00	2.5	3.60	6.20	2.5	3.60	6.20	1	3.45	6.00
P6	P1	P1x1.73	P6	P1	P1x1.73	P6	P1	P1x1.73	P6	P1	P1x1.73
P7	P2	P2x1.73	P7	P2	P2x1.73	P7	P2	P2x1.73	P7	P2	P2x1.73
P8	P3	P3x1.73	P8	P3	P3x1.73	P8	P3	P3x1.73	P8	P3	P3x1.73
P9	P4	P4x1.73	P9	P4	P4x1.73	P9	P4	P4x1.73	P9	P4	P4x1.73
P10	P5	P5x1.73	P10	P5	P5x1.73	P10	P5	P5x1.73	P10	P5	P5x1.73
h	Step	Range	h	Step	Range	h	Step	Range	h	Step	Range
(km)	(km)	(km)	(km)	(km)	(km)	(km)	(km)	(km)	(km)	(km)	(km)
P6	6	8-20	P6	6	6-24	P6	4.5	6.5-20	P6	2.4	2.5-12
P7	8	15-31	P7	10	10-40	P7	17	17-34	P7	3	3-15
P8	30	40-70	P8	30	30-60	P8	30	30-60	P8	11.5	12-58
P9	50	50-100	P9	50	50-100	P9	40	60-95	P9	60	60-120
P10	50	60-110	P10	50	60-110	P10	50	60-110	P10	60	60-120
V_S	Step	Range	V_S	Step	Range	V_S	Step	Range	V_S	Step	Range
(km/s)	(km/s)	(km/s)	(km/s)	(km/s)	(km/s)	(km/s)	(km/s)	(km/s)	(km/s)	(km/s)	(km/s)
P1	0.20	2.70-4.10	P1	0.15	3.00-3.90	P1	0.15	2.45-4.45	P1	0.30	3.05-4.45
P2	0.35	2.90-43.0	P2	0.30	3.00-4.80	P2	0.40	2.95-4.55	P2	0.25	2.60-4.45
P3	0.30	3.90-4.70	P3	0.25	3.85-4.85	P3	0.40	3.70-4.90	P3	0.30	3.45-4.95
P4	0.40	4.00-4.80	P4	0.30	3.80-5.10	P4	0.25	4.00-5.05	P4	0.15	4.00-4.90
P5	0.40	4.00-4.80	P5	0.40	4.00-4.80	P5	0.50	4.00-5.10	P5	0.30	4.00-4.80

Cell b0 (10.5; 42.5)			Cell b1 (11.5; 42.5)			Cell b2 (12.5; 42.5)			Cell b3 (13.5; 42.5)		
h	V_S	V_P	h	V_S	V_P	h	V_S	V_P	h	V_S	V_P
(km)	(km/s)	(km/s)	(km)	(km/s)	(km/s)	(km)	(km/s)	(km/s)	(km)	(km/s)	(km/s)
						1.2	1.60	2.75	1.2	1.55	2.65
0.5	0.00	1.52	0.25	3.00	5.50	0.8	2.08	3.60	0.8	2.13	3.70
0.5	3.00	5.50	0.75	3.50	6.10	1.5	3.00	5.20	1.5	3.10	5.35
6	2.65	5.00	6	2.65	5.00	1	3.30	5.70	1	3.60	6.25
P6	P1	P1x1.73	P6	P1	P1x1.73	P6	P1	P1x1.73	P6	P1	P1x1.73
P7	P2	P2x1.73	P7	P2	P2x1.73	P7	P2	P2x1.73	P7	P2	P2x1.73
P8	P3	P3x1.73	P8	P3	P3x1.73	P8	P3	P3x1.73	P8	P3	P3x1.73
P9	P4	P4x1.73	P9	P4	P4x1.73	P9	P4	P4x1.73	P9	P4	P4x1.73
P10	P5	P5x1.73	P10	P5	P5x1.73	P10	P5	P5x1.73	P10	P5	P5x1.73
h	Step	Range	h	Step	Range	h	Step	Range	h	Step	Range
(km)	(km)	(km)	(km)	(km)	(km)	(km)	(km)	(km)	(km)	(km)	(km)
P6	5.5	6-25.5	P6	4	4-20	P6	5	5-15	P6	5	9-19
P7	4	7.5-15.5	P7	16	17.5-49.5	P7	5	9-29	P7	14	14.-42
P8	30	30-60	P8	30	30-60	P8	25	30-55	P8	30	30-60
P9	40	70-110	P9	50	60-110	P9	40	70-110	P9	50	60-110
P10	60	60-120	P10	50	50-100	P10	50	70-120	P10	50	60-110
V_S	Step	Range	V_S	Step	Range	V_S	Step	Range	V_S	Step	Range
(km/s)	(km/s)	(km/s)	(km/s)	(km/s)	(km/s)	(km/s)	(km/s)	(km/s)	(km/s)	(km/s)	(km/s)
P1	0.15	2.85-4.05	P1	0.20	2.85-4.05	P1	0.15	2.75-3.80	P1	0.10	2.85-3.45
P2	0.55	2.85-4.50	P2	0.15	3.60-4.50	P2	0.30	2.55-4.35	P2	0.30	2.95-4.75
P3	0.05	4.00-4.50	P3	0.20	3.95-4.75	P3	0.15	3.70-4.90	P3	0.40	3.70-4.90
P4	0.10	4.00-4.80	P4	0.15	4.00-4.90	P4	0.20	4.00-4.90	P4	0.25	4.00-5.10
P5	0.40	4.00-4.80	P5	0.45	4.00-4.90	P5	0.40	4.00-4.90	P5	0.45	4.00-4.90

Cell b4 (14.5; 42.5)			Cell b5 (15.5; 42.5)			Cell b6 (16.5; 42.5)			Cell b7 (17.5; 42.5)		
h	V_S	V_P	h	V_S	V_P	h	V_S	V_P	h	V_S	V_P
(km)	(km/s)	(km/s)	(km)	(km/s)	(km/s)	(km)	(km/s)	(km/s)	(km)	(km/s)	(km/s)
						0.2	0.00	1.52			
0.2	0.00	1.52	0.15	0.00	1.52	3.7	1.90	3.30	0.5	0.00	1.52
3.8	2.08	3.60	3.9	1.90	3.30	1.6	3.55	6.15	3.3	1.90	3.30
3	3.20	3.20	1.95	3.55	6.15	2.5	3.50	6.07	3.7	3.55	6.15
P6	P1	P1x1.73	P6	P1	P1x1.73	P6	P1	P1x1.73	P6	P1	P1x1.73
P7	P2	P2x1.73	P7	P2	P2x1.73	P7	P2	P2x1.73	P7	P2	P2x1.73
P8	P3	P3x1.73	P8	P3	P3x1.73	P8	P3	P3x1.73	P8	P3	P3x1.73
P9	P4	P4x1.73	P9	P4	P4x1.73	P9	P4	P4x1.73	P9	P4	P4x1.73
P10	P5	P5x1.73	P10	P5	P5x1.73	P10	P5	P5x1.73	P10	P5	P5x1.73
h	Step	Range	h	Step	Range	h	Step	Range	h	Step	Range
(km)	(km)	(km)	(km)	(km)	(km)	(km)	(km)	(km)	(km)	(km)	(km)
P6	3	4-13	P6	2	3-7	P6	4.5	-21	P6	3	5-20
P7	10	14-34	P7	3.5	6.5-18	P7	8	9-25	P7	9.5	9.5-38
P8	30	30-60	P8	8	13-37	P8	10	14-44	P8	30	30-60
P9	40	70-110	P9	50	80-130	P9	40	70-110	P9	40	50-90
P10	50	70-120	P10	60	70-130	P10	50	70-110	P10	60	60-120
V_S	Step	Range	V_S	Step	Range	V_S	Step	Range	V_S	Step	Range
(km/s)	(km/s)	(km/s)	(km/s)	(km/s)	(km/s)	(km/s)	(km/s)	(km/s)	(km/s)	(km/s)	(km/s)
P1	0.20	2.75-3.95	P1	0.40	2.60-4.40	P1	0.10	2.70-3.70	P1	0.10	2.90-3.80
P2	0.30	2.70-4.50	P2	0.25	2.60-4.10	P2	0.35	2.75-4.65	P2	0.40	3.15-4.75
P3	0.40	3.40-5.10	P3	0.20	3.40-4.65	P3	0.40	3.80-4.80	P3	0.25	3.90-4.90
P4	0.30	4.00-4.90	P4	0.15	4.00-4.85	P4	0.15	3.95-4.85	P4	0.35	4.00-5.05
P5	0.50	4.00-5.10	P5	0.40	4.00-4.80	P5	0.30	3.90-5.10	P5	0.50	4.00-5.10

Cell b8 (18.5; 42.5) | Cell a1 (11.5; 41.5) | Cell a2 (12.5; 41.5) | Cell a3 (13.5; 41.5)

h (km)	V_S (km/s)	V_P (km/s)	h (km)	V_S (km/s)	V_P (km/s)	h (km)	V_S (km/s)	V_P (km/s)	h (km)	V_S (km/s)	V_P (km/s)
			1	0.00	1.52	0.4	0.00	1.52			
0.2	0.00	1.52	2.5	1.33	2.30	2.1	1.32	2.30	2.5	1.87	3.25
3.3	1.90	3.30	1.1	2.90	5.00	1	3.06	5.30	1.5	2.19	3.80
3.5	3.55	6.15	1.9	3.30	5.70	3.2	3.30	5.70	1.4	3.26	5.65
P6	P1	P1x1.73	P6	P1	P1x1.73	P6	P1	P1x1.73	P6	P1	P1x1.73
P7	P2	P2x1.73	P7	P2	P2x1.73	P7	P2	P2x1.73	P7	P2	P2x1.73
P8	P3	P3x1.73	P8	P3	P3x1.73	P8	P3	P3x1.73	P8	P3	P3x1.73
P9	P4	P4x1.73	P9	P4	P4x1.73	P9	P4	P4x1.73	P9	P4	P4x1.73
P10	P5	P5x1.73	P10	P5	P5x1.73	P10	P5	P5x1.73	P10	P5	P5x1.73

h (km)	Step (km)	Range (km)	h (km)	Step (km)	Range (km)	h (km)	Step (km)	Range (km)	h (km)	Step (km)	Range (km)
P6	3.5	12-22.5	P6	1.2	4.5-11.5	P6	2	25-33	P6	6	6-18
P7	12	22-34	P7	3	5.5-17.5	P7	6	12-24.5	P7	6	10-32
P8	30	30-60	P8	10	10-30	P8	20	20-60	P8	30	30-60
P9	40	70-110	P9	40	50-90	P9	40	70-110	P9	50	60-110
P10	50	60-110	P10	40	60-180	P10	40	70-110	P10	50	70-120

V_S (km/s)	Step (km/s)	Range (km/s)	V_S (km/s)	Step (km/s)	Range (km/s)	V_S (km/s)	Step (km/s)	Range (km/s)	V_S (km/s)	Step (km/s)	Range (km/s)
P1	0.10	2.90-4.00	P1	0.20	3.05-4.60	P1	0.05	3.75-4.40	P1	0.20	2.95-4.65
P2	0.30	3.60-4.80	P2	0.30	2.55-4.35	P2	0.20	3.90-4.90	P2	0.25	3.10-4.80
P3	0.30	4.00-4.90	P3	0.20	3.80-4.90	P3	0.10	4.00-4.60	P3	0.15	4.00-4.75
P4	0.25	4.00-4.85	P4	0.05	4.00-4.80	P4	0.15	4.00-4.90	P4	0.30	4.00-4.95
P5	0.50	4.00-5.10	P5	0.10	4.00-4.80	P5	0.30	4.00-4.90	P5	0.40	4.00-4.80

Cell a4 (14.5; 41.5) | Cell a5 (15.5; 41.5) | Cell a6 (16.5; 41.5) | Cell a7 (17.5; 41.5)

h (km)	V_S (km/s)	V_P (km/s)	h (km)	V_S (km/s)	V_P (km/s)	h (km)	V_S (km/s)	V_P (km/s)	h (km)	V_S (km/s)	V_P (km/s)
2.5	2.25	3.90	3	2.00	3.50						
2	2.45	4.25	2	2.28	3.95	0.2	0.00	1.52	1.3	0.00	1.52
0.5	2.55	4.40	3	3.00	5.20	4.3	2.22	3.85	3.7	2.08	3.60
1.5	3.06	5.30	2	3.25	5.60	1.4	3.20	5.55	4	3.06	5.30
P6	P1	P1x1.73	P6	P1	P1x1.73	P6	P1	P1x1.73	P6	P1	P1x1.73
P7	P2	P2x1.73	P7	P2	P2x1.73	P7	P2	P2x1.73	P7	P2	P2x1.73
P8	P3	P3x1.73	P8	P3	P3x1.73	P8	P3	P3x1.73	P8	P3	P3x1.73
P9	P4	P4x1.73	P9	P4	P4x1.73	P9	P4	P4x1.73	P9	P4	P4x1.73
P10	P5	P5x1.73	P10	P5	P5x1.73	P10	P5	P5x1.73	P10	P5	P5x1.73

h (km)	Step (km)	Range (km)	h (km)	Step (km)	Range (km)	h (km)	Step (km)	Range (km)	h (km)	Step (km)	Range (km)
P6	2	2-8	P6	8.5	8.5-25.5	P6	2.5	4-9	P6	6	8-26
P7	5	5-20	P7	20	25-45	P7	3.5	6.5-13.5	P7	5	9-19
P8	11	13-57	P8	30	30-60	P8	12	14-38	P8	30	30-60
P9	40	70-110	P9	40	50-100	P9	40	70-110	P9	40	60-100
P10	40	40-120	P10	50	50-100	P10	50	70-120	P10	50	70-120

V_S (km/s)	Step (km/s)	Range (km/s)	V_S (km/s)	Step (km/s)	Range (km/s)	V_S (km/s)	Step (km/s)	Range (km/s)	V_S (km/s)	Step (km/s)	Range (km/s)
P1	0.40	3.05-4.65	P1	0.20	3.10-4.30	P1	0.05	2.80-4.00	P1	0.15	3.00-4.00
P2	0.40	2.45-4.05	P2	0.30	3.40-4.90	P2	0.20	2.25-3.45	P2	0.45	3.05-4.85
P3	0.20	3.60-4.70	P3	0.30	4.00-4.70	P3	0.30	3.00-4.80	P3	0.15	4.00-4.80
P4	0.15	4.00-4.90	P4	0.40	4.00-4.80	P4	0.10	4.00-4.85	P4	0.10	4.00-4.80
P5	0.35	4.00-5.10	P5	0.50	4.00-5.10	P5	0.20	4.00-4.80	P5	0.30	4.00-5.10

Cell a8 (18.5; 41.5) · Cell a9 (19.5; 41.5) · Cell A-2 (8.5; 40.5) · Cell A-1 (7.5; 40.5)

h (km)	V_S (km/s)	V_P (km/s)	h (km)	V_S (km/s)	V_P (km/s)	h (km)	V_S (km/s)	V_P (km/s)	h (km)	V_S (km/s)	V_P (km/s)
						2	1.85	3.20	1.5	1.85	3.20
1.1	0.00	1.52	4.5	1.85	3.20	1	2.66	4.60	1.5	2.78	4.80
3.9	2.08	3.60	1	3.50	6.10	0.8	2.90	5.00	0.5	2.90	5.00
2	3.03	5.25	0.5	3.56	6.20	0.7	3.35	5.80	1.5	3.35	5.80
P6	P1	P1x1.73	P6	P1	P1x1.73	P6	P1	P1x1.73	P6	P1	P1x1.73
P7	P2	P2x1.73	P7	P2	P2x1.73	P7	P2	P2x1.73	P7	P2	P2x1.73
P8	P3	P3x1.73	P8	P3	P3x1.73	P8	P3	P3x1.73	P8	P3	P3x1.73
P9	P4	P4x1.73	P9	P4	P4x1.73	P9	P4	P4x1.73	P9	P4	P4x1.73
P10	P5	P5x1.73	P10	P5	P5x1.73	P10	P5	P5x1.73	P10	P5	P5x1.73
h (km)	Step (km)	Range (km)	h (km)	Step (km)	Range (km)	h (km)	Step (km)	Range (km)	h (km)	Step (km)	Range (km)
P6	6	13-31	P6	2.5	25-37.5	P6	1	12-25	P6	4	4-14
P7	20	30-50	P7	20	30-50	P7	20	10-40	P7	5	10-20
P8	30	30-60	P8	20	30-50	P8	35	45-80	P8	30	40-70
P9	40	60-100	P9	50	50-100	P9	35	55-90	P9	35	45-80
P10	40	60-100	P10	50	55-105	P10	40	70-110	P10	70	90-160
V_S (km/s)	Step (km/s)	Range (km/s)	V_S (km/s)	Step (km/s)	Range (km/s)	V_S (km/s)	Step (km/s)	Range (km/s)	V_S (km/s)	Step (km/s)	Range (km/s)
P1	0.20	3.10-3.90	P1	0.10	2.35-4.45	P1	0.10	2.30-4.00	P1	0.30	2.30-4.00
P2	0.40	3.60-4.80	P2	0.20	3.65-4.75	P2	0.10	2.40-4.85	P2	0.25	2.40-4.10
P3	0.30	3-80-4.80	P3	0.30	4.00-4.90	P3	0.20	3.70-5.00	P3	0.15	3.70-4.80
P4	0.30	4.00-4.70	P4	0.35	4.00-4.85	P4	0.20	3.80-4.90	P4	0.20	4.00-4.90
P5	0.50	4.00-5.20	P5	0.50	4.00-5.10	P5	0.30	3.90-4.90	P5	0.35	3.90-5.10

Cell A0 (10.5; 40.5) · Cell A1 (11.5; 40.5) · Cell A2 (12.5; 40.5) · Cell A3 (13.5; 40.5)

h (km)	V_S (km/s)	V_P (km/s)	h (km)	V_S (km/s)	V_P (km/s)	h (km)	V_S (km/s)	V_P (km/s)	h (km)	V_S (km/s)	V_P (km/s)
1.8	0.00	1.52									
1.2	1.16	2.00	2.5	0.00	1.52	2.5	0.00	1.52	1.5	0.00	1.52
2	3.01	5.20	0.7	1.38	2.40	0.7	1.20	2.05	2.2	1.20	2.05
2	3.12	5.40	1	3.45	6.00	1	3.45	6.00	1	3.45	6.00
1	3.24	5.60	1.8	3.52	6.10	1.8	3.95	6.85	1.3	3.95	6.85
P6	P1	P1x1.73	P6	P1	P1x1.73	P6	P1	P1x1.73	P6	P1	P1x1.73
P7	P2	P2x1.73	P7	P2	P2x1.73	P7	P2	P2x2.00	P7	P2	P2x2.00
P8	P3	P3x1.73	P8	P3	P3x1.73	P8	P3	P3x2.00	P8	P3	P3x2.00
P9	P4	P4x1.73	P9	P4	P4x1.73	P9	P4	P4x2.00	P9	P4	P4x2.00
P10	P5	P5x1.73	P10	P5	P5x1.73	P10	P5	P5x2.00	P10	P5	P5x2.00
h (km)	Step (km)	Range (km)	h (km)	Step (km)	Range (km)	h (km)	Step (km)	Range (km)	h (km)	Step (km)	Range (km)
P6	8	12-20	P6	4	4-24	P6	10	10-40	P6	2.6	5-15
P7	20	30-50	P7	24	25-50	P7	10	13-33	P7	10	10-30
P8	30	50-80	P8	30	30-60	P8	30	30-60	P8	30	40-70
P9	35	50-85	P9	40	60-100	P9	40	60-100	P9	40	60-110
P10	40	65-105	P10	40	70-110	P10	50	50-100	P10	40	60-110
V_S (km/s)	Step (km/s)	Range (km/s)	V_S (km/s)	Step (km/s)	Range (km/s)	V_S (km/s)	Step (km/s)	Range (km/s)	V_S (km/s)	Step (km/s)	Range (km/s)
P1	0.20	2.30-4.10	P1	0.10	3.00-4.30	P1	0.10	3.05-4.25	P1	0.35	3.00-4.75
P2	0.25	3.60-4.90	P2	0.20	3.80-4.90	P2	0.40	3.60-4.80	P2	0.20	2.80-4.60
P3	0.25	3.90-4.95	P3	0.20	4.00-4.80	P3	0.10	4.00-4.85	P3	0.30	3.70-4.90
P4	0.55	3.80-5.00	P4	0.35	4.00-4.75	P4	0.30	4.00-4.95	P4	0.15	4.00-4.80
P5	0.55	3.80-5.20	P5	0.45	4.00-4.90	P5	0.40	4.00-4.80	P5	0.40	4.00-4.80

Cell A4 (14.5; 40.5)			Cell A5 (15.5; 40.5)			Cell A6 (16.5; 40.5)			Cell A7 (17.5; 40.5)		
h	V_S	V_P	h	V_S	V_P	h	V_S	V_P	h	V_S	V_P
(km)	(km/s)	(km/s)	(km)	(km/s)	(km/s)	(km)	(km/s)	(km/s)	(km)	(km/s)	(km/s)
0.5	0.00	1.52	1.1	1.50	2.65	1.1	1.50	2.65			
1	2.60	4.50	2.4	2.10	3.60	2.4	2.10	3.60			
1.5	3.00	5.20	1.5	2.90	5.00	1.5	2.90	5.00	4.6	2.25	3.90
3	3.35	5.80	4	3.50	6.05	4	3.50	6.05	2.9	3.06	5.30
P6	P1	P1x1.73	P6	P1	P1x1.73	P6	P1	P1x1.73	P6	P1	P1x1.73
P7	P2	P2x1.73	P7	P2	P2x1.73	P7	P2	P2x1.73	P7	P2	P2x1.73
P8	P3	P3x1.73	P8	P3	P3x1.73	P8	P3	P3x1.73	P8	P3	P3x1.73
P9	P4	P4x1.73	P9	P4	P4x1.73	P9	P4	P4x1.73	P9	P4	P4x1.73
P10	P5	P5x1.73	P10	P5	P5x1.73	P10	P5	P5x1.73	P10	P5	P5x1.73
h	Step	Range	h	Step	Range	h	Step	Range	h	Step	Range
(km)	(km)	(km)	(km)	(km)	(km)	(km)	(km)	(km)	(km)	(km)	(km)
P6	3	4-13	P6	4	7.5-15.5	P6	5	5.5-1.5.5	P6	2	5-17
P7	10	13-33	P7	20	30-50	P7	10	20-40	P7	8	14-38
P8	20	30-50	P8	20	20-50	P8	30	30-60	P8	30	50-80
P9	40	70-110	P9	50	60-110	P9	50	60-110	P9	40	60-100
P10	50	70-120	P10	50	60-110	P10	40	70-110	P10	40	60-100
V_S	Step	Range	V_S	Step	Range	V_S	Step	Range	V_S	Step	Range
(km/s)	(km/s)	(km/s)	(km/s)	(km/s)	(km/s)	(km/s)	(km/s)	(km/s)	(km/s)	(km/s)	(km/s)
P1	0.30	2.25-3.45	P1	0.20	2.25-3.85	P1	0.40	2.30-4.00	P1	0.10	2.70-4.30
P2	0.40	2.70-4.30	P2	0.20	3.35-4.65	P2	0.20	3.35-4.35	P2	0.10	3.60-4.70
P3	0.20	3.80-4.60	P3	0.40	4.00-4.80	P3	0.30	4.00-4.80	P3	0.15	4.00-4.90
P4	0.25	4.00-4.70	P4	0.30	4.00-4.90	P4	0.35	4.00-4.70	P4	0.15	4.00-4.90
P5	0.40	4.00-4.80	P5	0.45	4.00-4.90	P5	0.35	4.00-4.85	P5	0.40	4.00-4.80

Cell A8 (18.5; 40.5)			Cell A9 (19.5; 40.5)			Cell B-2 (8.5; 39.5)			Cell B-1 (9.5; 39.5)		
h	V_S	V_P	h	V_S	V_P	h	V_S	V_P	h	V_S	V_P
(km)	(km/s)	(km/s)	(km)	(km/s)	(km/s)	(km)	(km/s)	(km/s)	(km)	(km/s)	(km/s)
0.35	0.00	1.52				2	1.85	3.20	2	1.85	3.20
2.45	2.25	3.90	0.8	1.85	3.20	1	2.66	4.60	1.5	2.78	4.80
1.9	2.60	4.50	4.2	1.95	3.40	0.8	2.89	5.00	0.5	2.89	5.00
2.3	3.03	5.25	3	3.50	6.07	0.7	3.35	5.80	1.5	3.35	5.80
P6	P1	P1x1.73	P6	P1	P1x1.73	P6	P1	P1x1.73	P6	P1	P1x1.73
P7	P2	P2x1.73	P7	P2	P2x1.73	P7	P2	P2x1.73	P7	P2	P2x1.73
P8	P3	P3x1.73	P8	P3	P3x1.73	P8	P3	P3x1.73	P8	P3	P3x1.73
P9	P4	P4x1.73	P9	P4	P4x1.73	P9	P4	P4x1.73	P9	P4	P4x1.73
P10	P5	P5x1.73	P10	P5	P5x1.73	P10	P5	P5x1.73	P10	P5	P5x1.73
h	Step	Range	h	Step	Range	h	Step	Range	h	Step	Range
(km)	(km)	(km)	(km)	(km)	(km)	(km)	(km)	(km)	(km)	(km)	(km)
P6	2	10-22	P6	4	5.5-13.5	P6	2	11-20	P6	2	4-10
P7	20	20-60	P7	7	7-33	P7	10	15-45	P7	5	9-22
P8	20	30-50	P8	30	30-60	P8	30	20-60	P8	30	20-70
P9	30	50-105	P9	40	80-120	P9	35	25-90	P9	30	30-80
P10	40	60-105	P10	40	70-110	P10	40	70-110	P10	50	60-160
V_S	Step	Range	V_S	Step	Range	V_S	Step	Range	V_S	Step	Range
(km/s)	(km/s)	(km/s)	(km/s)	(km/s)	(km/s)	(km/s)	(km/s)	(km/s)	(km/s)	(km/s)	(km/s)
P1	0.10	3.00-3.80	P1	0.40	2.75-4.70	P1	0.15	2.30-4.10	P1	0.40	2.30-4.00
P2	0.10	3.70-4.80	P2	0.30	2.80-4.20	P2	0.20	2.40-4.85	P2	0.20	2.40-4.10
P3	0.30	3.70-4.90	P3	0.20	3.95-4.95	P3	0.20	3.70-5.00	P3	0.20	3.70-4.80
P4	0.30	4.00-4.80	P4	0.15	4.00-4.90	P4	0.25	3.70-4.90	P4	0.40	3.70-4.90
P5	0.40	4.00-4.80	P5	0.30	4.00-5.10	P5	0.30	4.00-5.00	P5	0.25	3.90-5.20

Cell B0 (10.5; 39.5)			Cell B1 (11.5; 39.5)			Cell B2 (12.5; 39.5)			Cell B3 (13.5; 39.5)		
h	V_S	V_P	h	V_S	V_P	h	V_S	V_P	h	V_S	V_P
(km)	(km/s)	(km/s)	(km)	(km/s)	(km/s)	(km)	(km/s)	(km/s)	(km)	(km/s)	(km/s)
2.3	0.00	1.52									
0.7	1.16	2.00	3	0.00	1.52	3	0.00	1.52	0.00	1.52	0.00
2	3.01	5.20	0.7	1.20	2.05	0.7	1.20	2.05	1.20	2.05	1.20
2	3.12	5.40	1	3.45	6.00	1	3.45	6.00	3.45	6.00	3.45
1	3.24	5.60	2	3.95	6.85	2	3.95	6.85	3.95	6.85	3.95
P6	P1	P1x1.73	P6	P1	P1x1.73	P6	P1	P1x1.73	P6	P1	P1x1.73
P7	P2	P2x1.73	P7	P2	P2x2.00	P7	P2	P2x2.00	P7	P2	P2x2.00
P8	P3	P3x1.73	P8	P3	P3x2.00	P8	P3	P3x2.00	P8	P3	P3x2.00
P9	P4	P4x1.73	P9	P4	P4x2.00	P9	P4	P4x2.00	P9	P4	P4x2.00
P10	P5	P5x1.73	P10	P5	P5x2.00	P10	P5	P5x2.00	P10	P5	P5x2.00
h	Step	Range	h	Step	Range	h	Step	Range	h	Step	Range
(km)	(km)	(km)	(km)	(km)	(km)	(km)	(km)	(km)	(km)	(km)	(km)
P6	4	3-20	P6	2.5	4-11.5	P6	3	6-15	P6	4	7-19
P7	25	20-60	P7	6	11-29	P7	3	5-23	P7	3	5-17
P8	30	30-80	P8	15	15-60	P8	30	40-70	P8	20	20-60
P9	30	35-80	P9	40	60-100	P9	40	60-110	P9	40	70-110
P10	40	40-100	P10	60	60-120	P10	60	60-120	P10	50	70-120
V_S	Step	Range	V_S	Step	Range	V_S	Step	Range	V_S	Step	Range
(km/s)	(km/s)	(km/s)	(km/s)	(km/s)	(km/s)	(km/s)	(km/s)	(km/s)	(km/s)	(km/s)	(km/s)
P1	0.20	2.30-4.10	P1	0.45	3.10-4.80	P1	0.35	3.00-4.75	P1	0.40	3.20-4.60
P2	0.15	3.60-4.90	P2	0.20	3.00-4.60	P2	0.30	2.25-4.05	P2	0.40	2.10-4.10
P3	0.30	3.90-4.95	P3	0.10	3.60-4.60	P3	0.20	3.75-4.75	P3	0.20	3.50-4.80
P4	0.40	4.80-5.00	P4	0.20	4.00-4.70	P4	0.15	3.90-4.90	P4	0.20	4.00-4.90
P5	0.80	3.60-5.20	P5	0.40	4.00-4.90	P5	0.40	4.00-4.90	P5	0.40	4.00-4.90

Cell B4 (14.5; 39.5)			Cell B5 (15.5; 39.5)			Cell B6 (16.5; 39.5)			Cell B7 (17.5; 39.5)		
h	V_S	V_P	h	V_S	V_P	h	V_S	V_P	h	V_S	V_P
(km)	(km/s)	(km/s)	(km)	(km/s)	(km/s)	(km)	(km/s)	(km/s)	(km)	(km/s)	(km/s)
2.5	0.00	1.52									
0.5	1.30	2.05	0.9	0.00	1.52				1.5	0.00	1.52
2	3.45	6.00	2.10	1.15	1.98	4	2.45	4.25	1.5	2.90	5.00
1.5	3.95	6.85	3.00	2.90	5.00	9	2.80	4.85	2	3.52	6.10
P6	P1	P1x1.73	P6	P1	P1x1.73	P6	P1	P1x1.73	P6	P1	P1x1.73
P7	P2	P2x2.00	P7	P2	P2x1.73	P7	P2	P2x1.73	P7	P2	P2x1.73
P8	P3	P3x2.00	P8	P3	P3x1.73	P8	P3	P3x1.73	P8	P3	P3x1.73
P9	P4	P4x2.00	P9	P4	P4x1.73	P9	P4	P4x1.73	P9	P4	P4x1.73
P10	P5	P5x2.00	P10	P5	P5x1.73	P10	P5	P5x1.73	P10	P5	P5x1.73
h	Step	Range	h	Step	Range	h	Step	Range	h	Step	Range
(km)	(km)	(km)	(km)	(km)	(km)	(km)	(km)	(km)	(km)	(km)	(km)
P6	4	5-21	P6	8	10-34	P6	6.5	8-21	P6	2	3-12
P7	30	30-60	P7	5	8-23	P7	10	15.35	P7	6	8-32
P8	30	30-60	P8	20	20-60	P8	30	30-60	P8	30	3-60
P9	40	50-90	P9	40	70-110	P9	50	60-110	P9	40	70-110
P10	40	70-110	P10	40	70-110	P10	50	60-110	P10	50	60-110
V_S	Step	Range	V_S	Step	Range	V_S	Step	Range	V_S	Step	Range
(km/s)	(km/s)	(km/s)	(km/s)	(km/s)	(km/s)	(km/s)	(km/s)	(km/s)	(km/s)	(km/s)	(km/s)
P1	0.20	2.60-4.65	P1	0.05	3.30-3.90	P1	0.15	3.10-4.00	P1	0.10	2.05-3.60
P2	0.20	2.50-4.80	P2	0.40	3.10-.70	P2	0.40	2.90-4.50	P2	0.30	2.60-4.10
P3	0.30	3.75-4.80	P3	0.15	3.85-4.75	P3	0.40	3.50-4.80	P3	0.40	3.40-4.80
P4	0.40	4.00-4.80	P4	0.20	4.00-4.80	P4	0.35	4.00-4.95	P4	0.20	4.00-4.80
P5	0.40	4.00-4.80	P5	0.40	4.00-4.80	P5	0.50	4.00-5.10	P5	0.40	4.00-4.80

Cell B8 (18.5; 39.5)

h (km)	V_S (km/s)	V_P (km/s)
1	0.00	1.52
3.1	2.25	3.90
3.9	3.05	5.30
P6	P1	P1x1.73
P7	P2	P2x1.73
P8	P3	P3x1.73
P9	P4	P4x1.73
P10	P5	P5x1.73

h (km)	Step (km)	Range (km)
P6	2.5	8.5-21
P7	20	30-50
P8	25	35-60
P9	40	50-90
P10	60	60-120

V_S (km/s)	Step (km/s)	Range (km/s)
P1	0.10	2.30-4.25
P2	0.30	3.70-4.90
P3	0.25	3.95-4.95
P4	0.35	4.00-4.85
P5	0.50	4.00-5.10

Cell B9 (19.5; 39.5)

h (km)	V_S (km/s)	V_P (km/s)
1.7	0.00	1.52
3.3	2.30	4.00
2	3.00	5.20
P6	P1	P1x1.73
P7	P2	P2x1.73
P8	P3	P3x1.73
P9	P4	P4x1.73
P10	P5	P5x1.73

h (km)	Step (km)	Range (km)
P6	4	9-28
P7	20	20-60
P8	20	20-60
P9	20	50-90
P10	40	40-100

V_S (km/s)	Step (km/s)	Range (km/s)
P1	0.10	3.00-4.10
P2	0.10	4.00-4.80
P3	0.35	4.00-4.90
P4	0.20	4.00-4.90
P5	0.20	4.00-4.80

Cell C1 (11.5; 38.5)

h (km)	V_S (km/s)	V_P (km/s)
1.5	0.00	1.52
0.9	1.10	1.90
0.4	2.31	4.00
4.2	2.90	5.00
P6	P1	P1x1.73
P7	P2	P2x1.73
P8	P3	P3x1.73
P9	P4	P4x1.73
P10	P5	P5x1.73

h (km)	Step (km)	Range (km)
P6	6	6-18
P7	16	10-48
P8	30	30-60
P9	40	60-100
P10	50	50-110

V_S (km/s)	Step (km/s)	Range (km/s)
P1	0.30	3.00-4.20
P2	0.20	3.15-4.75
P3	0.15	4.00-4.90
P4	0.30	4.00-4.90
P5	0.45	4.00-4.90

Cell C2 (12.5; 38.5)

h (km)	V_S (km/s)	V_P (km/s)
1	0.00	1.52
1.5	1.11	1.91
0.4	2.20	3.80
3.6	2.63	4.55
P6	P1	P1x1.73
P7	P2	P2x1.73
P8	P3	P3x1.73
P9	P4	P4x1.73
P10	P5	P5x1.73

h (km)	Step (km)	Range (km)
P6	10	15-35
P7	15	20-50
P8	30	30-60
P9	40	60-100
P10	50	50-100

V_S (km/s)	Step (km/s)	Range (km/s)
P1	0.20	3.50-4.60
P2	0.15	3.40-4.80
P3	0.10	3.40-4.90
P4	0.15	4.00-4.80
P5	0.40	4.00-4.80

Cell C3 (13.5; 38.5)

h (km)	V_S (km/s)	V_P (km/s)
2	0.00	1.52
0.4	1.10	1.90
0.4	2.31	4.00
3.2	2.90	5.00
P6	P1	P1x1.73
P7	P2	P2x1.73
P8	P3	P3x1.73
P9	P4	P4x1.73
P10	P5	P5x1.73

h (km)	Step (km)	Range (km)
P6	3	4-22
P7	12	12-46
P8	30	30-60
P9	40	50-90
P10	40	60-110

V_S (km/s)	Step (km/s)	Range (km/s)
P1	0.10	2.90-3.80
P2	0.10	2.90-4.80
P3	0.20	3.80-4.80
P4	0.20	4.00-4.80
P5	0.40	4.00-4.80

Cell C4 (14.5; 38.5)

h (km)	V_S (km/s)	V_P (km/s)
2.36	0.00	1.52
0.04	1.00	1.75
0.4	2.31	4.00
3.2	3.35	6.15
P6	P1	P1x1.73
P7	P2	P2x1.73
P8	P3	P3x1.73
P9	P4	P4x1.73
P10	P5	P5x1.73

h (km)	Step (km)	Range (km)
P6	4	5-17
P7	12	12-36
P8	30	30-60
P9	40	60-100
P10	40	80-120

V_S (km/s)	Step (km/s)	Range (km/s)
P1	0.15	2.60-3.65
P2	0.40	2.65-4.35
P3	0.25	3.80-4.80
P4	0.25	4.00-4.80
P5	0.40	4.00-4.80

Cell C5 (15.5; 38.5)

h (km)	V_S (km/s)	V_P (km/s)
1	0.00	1.52
2	2.60	4.50
P6	P1	P1x1.73
P7	P2	P2x1.73
P8	P3	P3x1.73
P9	P4	P4x1.73
P10	P5	P5x1.73

h (km)	Step (km)	Range (km)
P6	3	5-17
P7	9	9-36
P8	30	30-60
P9	40	70-110
P10	40	70-110

V_S (km/s)	Step (km/s)	Range (km/s)
P1	0.15	2.30-3.55
P2	0.20	3.30-4.50
P3	0.30	3.70-4.90
P4	0.20	4.00-4.90
P5	0.35	4.00-5.05

Cell C6 (16.5; 38.5)

h (km)	V_S (km/s)	V_P (km/s)
3.8	2.45	4.25
1	2.74	4.75
P6	P1	P1x1.73
P7	P2	P2x1.73
P8	P3	P3x1.73
P9	P4	P4x1.73
P10	P5	P5x1.73

h (km)	Step (km)	Range (km)
P6	6	8-20
P7	12	12-32
P8	30	30-60
P9	40	70-110
P10	40	70-110

V_S (km/s)	Step (km/s)	Range (km/s)
P1	0.15	3.00-4.10
P2	0.20	3.15-4.75
P3	0.30	4.00-4.80
P4	0.25	4.00-4.90
P5	0.40	4.00-4.80

Cell C7 (17.5; 38.5)

h (km)	V_S (km/s)	V_P (km/s)
2.4	0.00	1.52
2.1	2.10	3.63
0.7	2.25	3.90
1.8	3.25	5.62
P6	P1	P1x1.73
P7	P2	P2x1.73
P8	P3	P3x1.73
P9	P4	P4x1.73
P10	P5	P5x1.73

h (km)	Step (km)	Range (km)
P6	5	8.5-24
P7	11	17-50
P8	30	30-60
P9	40	60-100
P10	40	60-100

V_S (km/s)	Step (km/s)	Range (km/s)
P1	0.15	2.40-4.50
P2	0.25	3.35-4.80
P3	0.30	3.10-4.80
P4	0.30	4.00-4.90
P5	0.45	4.00-4.90

Cell C8 (18.5; 38.5)

h (km)	V_S (km/s)	V_P (km/s)
2.9	0.00	1.52
1.2	2.25	3.90
1.1	2.35	4.05
2.8	3.32	5.75
P6	P1	P1x1.73
P7	P2	P2x1.73
P8	P3	P3x1.73
P9	P4	P4x1.73
P10	P5	P5x1.73

h (km)	Step (km)	Range (km)
P6	6	8-26
P7	20	30-50
P8	20	30-50
P9	40	50-100
P10	40	70-110

V_S (km/s)	Step (km/s)	Range (km/s)
P1	0.20	2.65-3.85
P2	0.40	3.70-4.90
P3	0.45	4.05-4.95
P4	0.45	4.05-4.95
P5	0.50	4.00-5.10

Cell C9 (19.5; 38.5)

h (km)	V_S (km/s)	V_P (km/s)
2.8	0.00	1.52
1.2	2.02	3.50
P6	P1	P1x1.73
P7	P2	P2x1.73
P8	P3	P3x1.73
P9	P4	P4x1.73
P10	P5	P5x1.73

h (km)	Step (km)	Range (km)
P6	6	6-18
P7	9	10-37
P8	30	15-60
P9	40	70-110
P10	40	80-120

V_S (km/s)	Step (km/s)	Range (km/s)
P1	0.25	2.60-4.10
P2	0.40	2.60-4.60
P3	0.20	3.95-4.95
P4	0.20	4.00-4.80
P5	0.35	4.00-4.80

Cell D1 (11.5; 37.5)

h (km)	V_S (km/s)	V_P (km/s)
0.6	0.00	1.52
2.5	1.73	3.00
2	2.90	5.02
4.4	3.40	5.90
P6	P1	P1x1.73
P7	P2	P2x1.73
P8	P3	P3x1.73
P9	P4	P4x1.73
P10	P5	P5x1.73

h (km)	Step (km)	Range (km)
P6	2.5	5.5-9.5
P7	4	11.5-31.5
P8	10	15-45
P9	40	40-120
P10	60	60-120

V_S (km/s)	Step (km/s)	Range (km/s)
P1	0.30	2.50-4.30
P2	0.10	3.60-4.50
P3	0.15	4.00-4.90
P4	0.05	4.00-4.80
P5	0.15	4.10-4.85

Cell D2 (12.5; 37.5)

h (km)	V_S (km/s)	V_P (km/s)
0.5	0.00	1.52
2.5	1.85	3.20
2	2.65	4.60
2	2.89	5.00
P6	P1	P1x1.73
P7	P2	P2x1.73
P8	P3	P3x1.73
P9	P4	P4x1.73
P10	P5	P5x1.73

h (km)	Step (km)	Range (km)
P6	6	6-22
P7	12	12-36
P8	30	30-60
P9	40	70-110
P10	40	70-110

V_S (km/s)	Step (km/s)	Range (km/s)
P1	0.25	2.85-4.35
P2	0.40	3.30-4.90
P3	0.10	4.00-4.80
P4	0.05	4.00-4.80
P5	0.30	4.00-5.10

Cell D3 (13.5; 37.5)

h (km)	V_S (km/s)	V_P (km/s)
2.5	1.73	3.00
2.5	2.60	4.50
5	2.90	5.00
P6	P1	P1x1.73
P7	P2	P2x1.73
P8	P3	P3x1.73
P9	P4	P4x1.73
P10	P5	P5x1.73

h (km)	Step (km)	Range (km)
P6	12	13-37
P7	20	30-50
P8	30	30-60
P9	40	50-90
P10	40	60-100

V_S (km/s)	Step (km/s)	Range (km/s)
P1	0.25	3.30-4.30
P2	0.30	3.70-4.90
P3	0.45	4.05-4.95
P4	0.40	4.00-4.80
P5	0.50	4.00-5.10

Cell D4 (14.5; 37.5)

h (km)	V_S (km/s)	V_P (km/s)
3	1.73	3.00
2	2.60	4.50
5	2.90	5.00
P6	P1	P1x1.73
P7	P2	P2x1.73
P8	P3	P3x1.73
P9	P4	P4x1.73
P10	P5	P5x1.73

h (km)	Step (km)	Range (km)
P6	5	7.5-22.5
P7	20	30-50
P8	30	30-60
P9	40	60-100
P10	40	60-100

V_S (km/s)	Step (km/s)	Range (km/s)
P1	0.15	3.20-4.10
P2	0.15	3.85-4.75
P3	0.40	3.60-4.80
P4	0.45	4.00-4.90
P5	0.50	4.00-5.10

Cell D5 (15.5; 37.5)

h (km)	V_S (km/s)	V_P (km/s)
1.5	0.00	1.52
2.4	2.22	3.85
1.3	2.31	4.00
1.8	3.15	5.45
P6	P1	P1x1.73
P7	P2	P2x1.73
P8	P3	P3x1.73
P9	P4	P4x1.73
P10	P5	P5x1.73

h (km)	Step (km)	Range (km)
P6	1	5-18
P7	20	30-50
P8	20	30-50
P9	40	70-110
P10	40	70-110

V_S (km/s)	Step (km/s)	Range (km/s)
P1	0.10	2.80-3.70
P2	0.15	3.50-4.75
P3	0.30	3.85-4.75
P4	0.30	4.00-4.75
P5	0.50	3.75-4.75

Cell D6 (16.5; 37.5)			Cell D7 (17.5; 37.5)			Cell D8 (18.5; 37.5)			Cell D9 (19.5; 37.5)		
h	V_S	V_P	h	V_S	V_P	h	V_S	V_P	h	V_S	V_P
(km)	(km/s)	(km/s)	(km)	(km/s)	(km/s)	(km)	(km/s)	(km/s)	(km)	(km/s)	(km/s)
			3.1	0.00	1.52						
2.7	0.00	1.52	0.9	2.08	3.60	2.9	0.00	1.52	2.9	0.00	1.52
1.4	2.25	3.90	0.2	2.22	3.85	1.2	2.25	3.90	1.2	2.25	3.90
1.1	2.31	4.00	1.1	2.31	4.00	1.1	2.31	4.00	1.1	2.31	4.00
2.8	3.32	5.75	2.7	3.31	5.75	2.8	3.31	5.75	2.8	3.31	5.75
P6	P1	P1x1.73	P6	P1	P1x1.73	P6	P1	P1x1.73	P6	P1	P1x1.73
P7	P2	P2x1.73	P7	P2	P2x1.73	P7	P2	P2x1.73	P7	P2	P2x1.73
P8	P3	P3x1.73	P8	P3	P3x1.73	P8	P3	P3x1.73	P8	P3	P3x1.73
P9	P4	P4x1.73	P9	P4	P4x1.73	P9	P4	P4x1.73	P9	P4	P4x1.73
P10	P5	P5x1.73	P10	P5	P5x1.73	P10	P5	P5x1.73	P10	P5	P5x1.73
h	Step	Range	h	Step	Range	h	Step	Range	h	Step	Range
(km)	(km)	(km)	(km)	(km)	(km)	(km)	(km)	(km)	(km)	(km)	(km)
P6	4	5-21	P6	1	7-20	P6	3	5-23	P6	4	5-21
P7	20	20-60	P7	30	30-60	P7	20	30-50	P7	6	10-28
P8	30	30-60	P8	30	30-60	P8	25	30-55	P8	20	30-50
P9	40	60-100	P9	40	60-100	P9	40	60-100	P9	40	60-100
P10	40	60-100	P10	40	60-100	P10	40	70-110	P10	50	60-110
V_S	Step	Range	V_S	Step	Range	V_S	Step	Range	V_S	Step	Range
(km/s)	(km/s)	(km/s)	(km/s)	(km/s)	(km/s)	(km/s)	(km/s)	(km/s)	(km/s)	(km/s)	(km/s)
P1	0.25	2.60-3.85	P1	0.05	3.00-3.95	P1	0.15	2.70-3.75	P1	0.40	2.65-4.25
P2	0.20	3.80-4.80	P2	0.10	3.80-4.80	P2	0.30	3.70-4.90	P2	0.35	2.45-4.45
P3	0.30	3.90-4.80	P3	0.30	3.85-4.75	P3	0.30	3.90-4.90	P3	0.30	4.00-4.90
P4	0.40	4.00-4.80	P4	0.30	4.00-4.90	P4	0.30	3.90-4.85	P4	0.20	4.00-4.80
P5	0.45	4.00-4.90	P5	0.50	4.00-4.75	P5	0.35	4.00-5.10	P5	0.45	4.00-4.90

APPENDIX II

(part 2)

Table A2.2: Results of the inversion: range of variability of the parameters h (thickness) and V_s for each layer of the chosen solution. In the table the inverted quantities are rounded off to 0.5 km or to 0.05km/s and we take into account the a priori information used to constrain the inversion, therefore the chosen solution does not necessarily fall in the centre of the range that can be smaller than the step used in the inversion. In most of the cells of the study area, one and the same relation between V_s, V_p has been used for all the dependent parameters in the inversion $\left(\frac{V_p}{V_s} = \sqrt{3} \right)$. In the cells marked by * the value of $\left(\frac{V_p}{V_s} = 2.0 \right)$ has been used, in agreement with the geophysical, geochemical and petrological model of the sub-marine lithosphere proposed by Bottinga and Steinmetz (1979).

The thickness marked by *** is not a truly inverted parameter, but it satisfies the condition that the total thickness from the free surface to the top of the fixed upper mantle is equal to a predefined quantity H. In this study H=349 km. The structur, deeper that H, is the same for all the considered cells and it has been fixed accordingly with already published models (Du et al, 1998).

Cell g-2 (8.5;47.5)		Cell g-1 (9.5;47.5)		Cell g0 (10.5;47.5)		Cell g1 (11.5;47.5)		Cell g2 (12.5;47.5)	
Vs	h	Vs	h	Vs	h	Vs	h	Vs	h
(km/s)	(km)	(km/s)	(km)	(km/s)	(km)	(km/s)	(km)	(km/s)	(km)
----	----	----	----	----	----	----	----	----	----
2.30	0.5	2.75	2	3.40	3	2.70	3	2.20	1.8
2.65	0.5	3.40	5	3.50	2	3.00	3	3.20	3.2
2.90	1.0	----	----	----	----	----	----	----	----
3.45	2.0	----	----	----	----	----	----	----	----
3.40	2.0	----	----	----	----	----	----	----	----
3.15-3.35	11.5-14.5	3.00-3.20	8-10	2.70-3.00	7.5-10	3.45-3.65	15-21	3.25-3.45	13.5-20.5
4.10-4.30	30-40	3.95-4.25	24.5-33.5	3.60-3.90	20-27	3.85-4.05	15-20	3.85-4.35	13-19.5
4.55-4.75	30-45	4.55-4.75	30-40	4.30-4.60	35-45	4.35-4.55	70-90	4.05-4.45	30-45
4.25-4.35	80-100	4.35-4.55	90-110	4.25-4.65	90-110	4.20-4.60	60-77.5	4.35-4.75	80-100
4.25-4.65	90-110	4.00-4.50	90-110	4.10-4.50	70-90	4.00-4.50	60-80	4.25-4.65	70-90
4.75	***	4.75	***	4.75	***	4.75	***	4.75	***
4.90	44	4.90	44	4.90	44	4.90	44	4.90	44

Cell f-3 (7.5;46.5)		Cell f-2 (8.5;46.5)		Cell f-1 (9.5;46.5)		Cell f0 (10.5;46.5)		Cell f1 (11.5;46.5)	
Vs	h	Vs	h	Vs	h	Vs	h	Vs	h
(km/s)	(km)	(km/s)	(km)	(km/s)	(km)	(km/s)	(km)	(km/s)	(km)
----	----	----	----	----	----	----	----	----	----
2.85	1	2.85	1	1.20	0.1	3.20	3	1.20	0.1
3.10	2	3.10	1	3.30	7.9	3.50	2	3.35	0.9
3.45	2	3.45	2	----	----	----	----	3.15	3
2.95-3.05	10.5-13.5	2.85-3.25	9-13	2.70-2.90	5-7	2.80-2.90	5-7	2.90-3.10	6.5-9.5
3.80-4.10	22-30	3.75-3.95	21-27	3.85-4.05	21-29	3.60-3.80	17-27	3.60-3.80	21.5-28.5
4.35-4.55	35-47.5	4.45-4.75	35-52.5	4.45-4.55	65-80	4.35-4.55	35-50	4.35-4.65	45-60
4.25-4.45	90-110	4.15-4.45	90-110	4.20-4.60	47.5-82.5	4.35-4.65	90-110	4.30-4.60	82.5-100
4.25-4.75	90-110	4.25-4.75	90-110	4.20-4.60	90-110	4.00-4.25	70-90	4.25-4.65	70-90
4.75	***	4.75	***	4.75	***	4.75	***	4.75	***
4.90	44	4.90	44	4.90	44	4.90	44	4.90	44

Cell f2 (12.5;46.5)		Cell f3 (13.5;46.5)		Cell e-4 (6.5;45.5)		Cell e-3 (7.5;45.5)		Cell e-2 (8.5;45.5)	
Vs	h	Vs	h	Vs	h	Vs	h	Vs	h
(km/s)	(km)	(km/s)	(km)	(km/s)	(km)	(km/s)	(km)	(km/s)	(km)
----	----	----	----	----	----	----	----	----	----
3.50	0.5	1.70	0.25	1.20	0.5	1.20	0.1	2.43	3
2.85	6.5	2.40	1	2.90	4.5	2.80	5.9	2.90	3
----	----	3.15	6.8	----	----	----	----	----	----
3.30-3.50	11-18	3.00-3.30	10-14	2.80-2.90	7-9	2.75-2.95	7-8	3.05-3.25	8-12
3.65-4.05	21.5-30.5	3.65-4.05	25-37.5	3.75-4.15	17-23	3.90-4.10	22.5-29.5	3.90-4.10	21-29
4.15-4.55	35-45	4.20-4.60	30-40	4.40-4.50	65-75	4.50-4.60	70-85	4.35-4.55	70-80
4.35-4.65	90-110	4.20-4.60	80-100	4.50-4-.70	47.5-82.5	4.05-4.55	72.5-100	4.20-4.50	80-100
4.25-4.75	60-85	4.25-4.55	70-90	4.15-4.55	85.5-110	4.25-4.75	82.5-110	4.20-4.60	70-90
4.75	***	4.75	***	4.75	***	4.75	***	4.75	***
4.90	44	4.90	44	4.90	44	4.90	44	4.90	44

Cell e-1 (9.5;45.5)		Cell e0 (10.5;45.5)		Cell e1 (11.5;45.5)		Cell e2 (12.5;45.5)		Cell e3 (13.5;45.5)	
Vs	h	Vs	h	Vs	h	Vs	h	Vs	h
(km/s)	(km)	(km/s)	(km)	(km/s)	(km)	(km/s)	(km)	(km/s)	(km)
----	----	----	----	----	----	----	----	----	----
2.30	3	2.00	1	2.55	4.5	2.10	1	2.10	1
2.60	3	2.56	2	3.18	1.5	2.50	4	2.60	4
----	----	3.01	3	3.30	1	2.90	2	3.00	1
----	----	----	----	----	----	----	----	3.20	2
3.05-3.25	10-12.5	3.05-3.25	6-8	2.95-3.15	5.5-8.5	3.40-3.50	17.5-24.5	3.35-3.45	15-21
3.85-4.15	21-25	3.65-3.85	18-24	3.65-3.95	24.5-31.5	4.05-4.45	20-30	4.10-4.40	27.5-32.5
4.35-4.55	65-80	4.35-4.55	70-90	4.65-4.85	40-60	4.55-4.75	45-60	4.70-4.80	45-75
4.20-4.50	82.5-100	4.25-4.75	50-70	4.25-4.55	70-90	4.25-4.55	50-70	4.15-4.25	70-90
4.20-4.60	90-110	4.00-4.35	70--90	4.00-4.25	60-82.5	4.00-4.20	50-75	4.25-4.75	50-70
4.75	***	4.75	***	4.75	***	4.75	***	4.75	***
4.90	44	4.90	44	4.90	44	4.90	44	4.90	44

Cell e4 (14.5;45.5)		Cell e5 (15.5;45.5)		Cell d-4 (6.5;44.5)		Cell d-3 (7.5;44.5)		Cell d-2 (8.5;44.5)	
Vs	h	Vs	h	Vs	h	Vs	h	Vs	h
(km/s)	(km)	(km/s)	(km)	(km/s)	(km)	(km/s)	(km)	(km/s)	(km)
----	----	----	----	----	----	----	----	----	----
2.30	4	2.10	4	2.75	2	2.75	1	2.30	3
3.25	1.5	3.30	1.5	3.00	2	2.85	1	2.50	4
3.35	1.5	3.60	2.5	3.15	1	3.00	1	----	----
3.45	1	----	----	----	----	3.10	2	----	----
3.45-3.55	15-20	3.65-3.85	20-28	2.75-3.05	6.5-9.5	2.55-2.75	6-8	3.20-3.50	8-12
3.80-4.20	22.5-37.5	4.15-4.45	25-37.5	3.75-4.05	14.5-19.5	3.70-4.00	20-30	3.95-4.25	24.5-33.5
4.70-4.80	30-40	4.35-4.75	45-60	4.25-4.45	55-70	4.30-4.50	67.5-85	4.30-4.50	65-80
4.20-4.60	80-100	4.15-4.45	70-90	4.20-4.50	60-85	4.20-4.50	80-100	4.25-4.45	80-100
4.25-4.75	60-85	4.25-2.75	50-75	4.20-4.60	85-110	4.25-4.75	60-80	4.25-4.75	70-90
4.75	***	4.75	***	4.75	***	4.75	***	4.75	***
4.90	44	4.90	44	4.90	44	4.90	44	4.90	44

Cell d-1 (9.5;44.5)		Cell d0 (10.5;44.5)		Cell d1 (11.5;44.5)		Cell d2 (12.5;44.5)		Cell d3 (13.5;44.5)	
Vs	h	Vs	h	Vs	h	Vs	h	Vs	h
(km/s)	(km)	(km/s)	(km)	(km/s)	(km)	(km/s)	(km)	(km/s)	(km)
----	----	----	----	----	----	0.00	0.4	0.00	0.05
2.30	2	2.00	3	2.00	2	2.00	3.6	1.76	2.95
2.50	4	2.20	1.4	2.15	2.4	3.30	2	2.25	1
----	----	2.80	1.6	2.80	1.6	3.50	2	3.45	1
----	----	3.25	1	3.25	1	----	----	3.50	1
3.15-3.45	7.5-12.5	3.30-3.40	11.5-12.5	3.35-3.45	13-21	3.25-3.35	6-9	3.50-3.60	16-23
3.85-4.15	24-32	4.05-4.25	30-50	3.95-4.35	25-35	3.35-3.75	20-26	3.60-4.10	10-14
4.35-4.55	60-85	4.60-4.80	30-45	4.65-4.80	30-40	4.35-4.65	30-45	4.30-4.50	22.5-37.5
4.05-4.45	70-87.5	4.25-4.65	75-100	4.15-4.55	80-100	4.25-4.65	80-105	4.50-4.70	50-65
4.25-4.75	90-110	4.00-4.20	50-75	4.00-4.25	60-80	4.00-4.25	60-85	4.10-4.30	90-110
4.75	***	4.75	***	4.75	***	4.75	***	4.75	***
4.90	44	4.90	44	4.90	44	4.90	44	4.90	44

Cell d4 (14.5;44.5)		Cell d5 (15.5;44.5)		Cell d6 (16.5;44.5)		Cell d7 (17.5;44.5)		Cell d8 (18.5;44.5)	
Vs	h	Vs	h	Vs	h	Vs	h	Vs	h
(km/s)	(km)	(km/s)	(km)	(km/s)	(km)	(km/s)	(km)	(km/s)	(km)
0.00	0.05	----	----	----	----	----	----	----	----
1.76	2.95	2.10	4	2.20	4	2.20	3	2.30	4
2.25	1	3.30	1.5	2.30	1	2.30	1	3.25	1.5
3.40	2	3.60	2.5	3.30	1.5	3.30	1	3.45	1.5
----	----	----	----	3.45	1.5	3.50	1	----	----
3.55-3.65	9.5-13	3.45-3.55	17-25	3.75-3.85	4.5-6.5	3.55-3.75	6.5-8	3.45-3.65	15.5-26.5
3.50-3.60	7.5-11	4.05-4.55	25-35	3.20-3.40	12-16	3.35-3.65	13-19	3.95-4.45	15-22.5
4.10-4.20	36.5-37.5	4.55-4.65	30-40	4.10-4.30	40-55	4.30-4.50	55-70	4.25-4.55	57-74
4.80-4.90	48.5-51.5	4.25-4.55	80-100	4.40-4.60	60-85	4.25-4.55	85-110	4.20-4.60	70-90
4.15-4.25	95-105	4.20-4.60	60-90	4.20-4.60	85-110	4.25-4.75	60-90	4.25-4.75	50-75
4.75	***	4.75	***	4.75	***	4.75	***	4.75	***
4.90	44	4.90	44	4.90	44	4.90	44	4.90	44

Cell c0 (10.5;43.5)		Cell c1 (11.5;43.5)		Cell c2 (12.5;43.5)		Cell c3 (13.5;43.5)		Cell c4 (14.5;43.5)	
Vs	h	Vs	h	Vs	h	Vs	h	Vs	h
(km/s)	(km)	(km/s)	(km)	(km/s)	(km)	(km/s)	(km)	(km/s)	(km)
----	----	----	----	----	----	----	----	0.00	0.15
2.20	4.0	2.20	4.0	1.60	0.5	1.55	1.1	1.76	2.85
2.65	1.0	2.65	1.0	2.30	1.0	2.08	2.4	2.25	1
3.00	1.5	3.20	2.0	3.00	1.0	3.18	1.5	3.45	2
----	----	----	----	3.50	1.5	3.50	1.0	----	----
3.10-3.30	7.5-11	3.25-3.45	11.5-17.5	2.60-2.80	5-7	3.25-3.40	10-13	3.20-3.30	12-18
3.60-4.00	13.5-20	3.95-4.25	18-23	3.55-3.65	22-25.5	3.50-3.80	16.5-23.5	3.65-4.05	14-21
4.35-4.45	45-60	4.45-4.65	35-50	4.50-4.70	35-50	4.35-4.65	45-60	4.20-4.60	45-60
4.25-4.55	75-100	4.25-4.55	85-105	4.25-4.55	80-100	4.25-4.45	90-110	4.45-4.75	50-75
4.25-4.65	85-110	4.20-4.60	75-100	4.20-4.60	85-110	4.25-4.65	70-90	4.00-4.20	50-75
4.75	***	4.75	***	4.75	***	4.75	***	4.75	***
4.90	44	4.90	44	4.90	44	4.90	44	4.90	44

Cell c5 (15.5;43.5)		Cell c6 (16.5;43.5)		Cell c7 (17.5;43.5)		Cell c8 (18.5;43.5)		Cell b0 (10.5;42.5)	
Vs	h	Vs	h	Vs	h	Vs	h	Vs	h
(km/s)	(km)	(km/s)	(km)	(km/s)	(km)	(km/s)	(km)	(km/s)	(km)
0.00	0.2	----	----	----	----	----	----	0.00	0.5
1.96	2.8	2.10	4	2.20	2	2.20	4	3.00	0.5
2.28	1	3.30	1.5	2.25	2	3.25	1	2.65	6.0
3.45	2	3.60	2.5	3.40	1.5	3.45	1	----	----
----	----	----	----	3.60	2.5	----	----	----	----
3.20-3.40	11-17	3.25-3.35	9-15	3.25-3.45	8.5-13	4.10-4.40	2.5-4	3.35-3.55	8.5-14
3.75-4.15	15-19	3.75-4.05	15-25	3.55-.3.95	17-25.5	2.90-3.10	7.5-10.5	3.65-4.25	7.5-9.5
4.25-4.55	40-55	4.45-4.75	30-45	4.30-4.70	45-60	3.50-3.90	17.5-29	4.20-4.30	30-45
4.20-4.60	75-100	4.25-4.55	75-100	4.15-4.45	55-75	4.35-4.55	90-120	4.25-4.35	90-110
4.20-4.60	60-85	4.20-4.60	60-85	4.25-4.75	85-110	4.25-4.55	60-90	4.20-4.60	90-120
4.75	***	4.75	***	4.75	***	4.75	***	4.75	***
4.90	44	4.90	44	4.90	44	4.90	44	4.90	44

Cell b1 (11.5;42.5)		Cell b2 (12.5;42.5)		Cell b3 (13.5;42.5)		Cell b4 (14.5;42.5)		Cell b5 (15.5;42.5)	
Vs	h	Vs	h	Vs	h	Vs	h	Vs	h
(km/s)	(km)	(km/s)	(km)	(km/s)	(km)	(km/s)	(km)	(km/s)	(km)
----	----	----	----	----	----	0.00	0.2	0.00	0.15
3.00	0.25	1.60	1.2	1.55	1.2	2.08	3.8	1.90	3.9
3.50	0.75	2.30	0.8	2.13	0.8	3.20	3	3.55	1.95
2.65	6.0	3.00	1.5	3.10	1.5	----	----	----	----
----	----	3.30	1.0	3.61	1.0	----	----	----	----
3.35-3.55	14-18	3.25-3.45	7.5-12.5	3.00-3.10	9-11.5	3.25-3.45	8.5-11.5	3.30-3.70	3-4
4.15-4.25	17.5-25.5	3.60-3.90	16.5-21.5	3.70-4.00	21-35	3.75-4.05	19-29	2.85-3.15	6.5-8
4.25-4.45	30-45	4.25-4.45	42.5-55	4.30-4.70	45-60	4.40-4.80	45-60	3.80-4.10	17-25
4.20-4.40	85-110	4.20-4.40	70-90	4.15-4.35	60-85	4.15-4.45	90-110	4.35-4.55	105-130
4.25-4.65	75-100	4.20-4.60	95-120	4.25-4.65	85-110	4.25-4.75	70-95	4.20-4.60	70-100
4.75	***	4.75	***	4.75	***	4.75	***	4.75	***
4.90	44	4.90	44	4.90	44	4.90	44	4.90	44

Cell b6 (16.5;42.5)		Cell b7 (17.5;42.5)		Cell b8 (18.5;42.5)		Cell a1 (11.5;41.5)		Cell a2 (12.5;41.5)	
Vs	h	Vs	h	Vs	h	Vs	h	Vs	h
(km/s)	(km)	(km/s)	(km)	(km/s)	(km)	(km/s)	(km)	(km/s)	(km)
0.00	0.2	0.00	0.5	0.00	0.2	0.00	1.0	0.00	0.4
1.90	3.7	1.90	3.3	1.90	3.3	1.33	2.5	1.32	2.1
3.55	1.6	3.55	3.7	3.55	3.5	2.90	1.1	3.06	1.0
3.50	2.5	----	----	----	----	3.30	1.9	3.30	3.2
3.05-3.15	7.5-9.5	3.15-3.25	12.5-15.5	3.25-3.35	17-20.5	4.30-4.50	7.5-9	3.85-3.95	30-32
3.45-3.75	9-13	3.75-4.15	9.5-14	4.05-4.35	28-34	3.00-3.30	5.5-7.0	4.60-4.80	15.5-21.5
4.00-4.40	14-19	4.25-4.55	45-60	4.45-4.75	30-45	4.40-4.60	10-15	4.05-4.15	50-60
4.35-4.45	70-90	4.15-4.55	50-70	4.25-4.45	70-90	4.10-4.20	70-90	4.35-4.45	70-90
4.25-4.55	95-120	4.25-4.75	90-120	4.25-4.75	85-110	4.25-4.35	160-180	4.15-4.45	90-110
4.75	***	4.75	***	4.75	***	4.75	***	4.75	***
4.90	44	4.90	44	4.90	44	4.90	44	4.90	44

Cell a3 (13.5;41.5)		Cell a4 (14.5;41.5)		Cell a5 (15.5;41.5)		Cell a6 (16.5,41.5)		Cell a7 (17.5,41.5)	
Vs	h	Vs	h	Vs	h	Vs	h	Vs	h
(km)	(km)	(km/s)	(km)	(km/s)	(km)	(km/s)	(km)	(km/s)	(km)
----	----	----	----	----	----	0.00	0.2	0.00	1.3
1.87	2.5	2.25	2.45	2.00	3.00	2.22	4.3	2.08	3.7
2.19	1.1	2.45	2.05	2.28	2.00	3.20	1.4	3.06	4
3.26	1.4	2.55	0.5	3.00	3.00	----	----	----	----
----	----	3.06	1.5	3.25	2.00	----	----	----	----
3.75-3.95	6-9	3.65-4.05	2-3	3.60-3.80	12.5-21	3.20-3.30	4-5	3.20-.3.40	11-17
3.35-3.55	10-13	2.65-3.05	5-7.5	4.15-4.45	25-35	3.05-3.25	8-11.5	3.70-4.20	9-11.5
4.15-4.25	30-45	3.80-4.00	18.5-29.5	4.25-4.55	45-60	4.05-4.35	20-32	4.40-4.60	30-45
4.20-4.50	85-110	4.35-4.55	90-110	4.20-4.60	80-100	4.40-4.50	70-90	4.45-.455	60-80
4.20-4.60	95-120	4.25-4.65	100-120	4.25-4.75	50-75	4.30-4.50	95-120	4.25-4.65	95-120
4.75	***	4.75	***	4.75	***	4.75	***	4.75	***
4.90	44	4.90	44	4.90	44	4.90	44	4.90	44

Cell a8 (18.5;41.5)		Cell a9 (19.5;41.5)		Cell A-2 (8.5;40.5)		Cell A-1 (9.5,40.5)		Cell A0 (10.5,40.5)	
Vs	h	Vs	h	Vs	h	Vs	h	Vs	h
(km)	(km)	(km/s)	(km)	(km/s)	(km)	(km/s)	(km)	(km/s)	(km)
0.00	1.1	----	----	----	----	----	----	0.00	1.8
2.08	3.9	1.85	4.5	1.85	2.00	1.85	1.5	1.16	1.2
3.03	2	3.50	1	2.66	1.00	2.78	1.5	3.01	2.0
----	----	3.56	0.5	2.89	0.80	2.89	0.5	3.12	1.0
----	----	----	----	3.35	0.70	3.35	1.5	3.24	1.0
3.20-3.40	16-22	3.65-.375	28.5-31	3.45-3.55	12-12.5	2.90-3.20	4-6	3.75-3.95	8-16
4.20-4.60	30-40	4.45-4.65	40-50	4.50-4.60	20-30	3.65-3.95	10-12.5	4.15-4.45	40-50
4.35-4.65	45-60	4.15-4.45	30-40	4.10-4.30	62.5-80	4.35-4.55	40-55	4.05-4.35	75-80
4.25-4.55	60-80	4.35-4.65	50-75	4.20-4.40	37.5-72.5	4.00-4.10	45.62.5	4.15-4.65	67.5-85
4.25-4.75	80-120	4.25-4.75	80-105	4.15-4.45	90-110	4.15-4.55	125-160	4.15-4.65	65-85
4.75	***	4.75	***	4.75	***	4.75	***	4.75	***
4.90	44	4.90	44	4.90	44	4.90	44	4.90	44

Cell A1 (11.5;40.5)		Cell A2 (12.5;40.5)		Cell A3 (13.5;40.5)		Cell A4 (14.5;40.5)		Cell A5 (15.5;40.5)	
Vs	h	Vs	h	Vs	h	Vs	h	Vs	h
(km)	(km)	(km/s)	(km)	(km/s)	(km)	(km/s)	(km)	(km/s)	(km)
0.00	2.5	0.00	2.5	0.00	1.5	0.00	0.5	----	----
1.38	0.7	1.20	0.7	1.20	2.2	2.60	1.0	1.50	1.1
3.45	1.0	3.45	1.0	3.45	1.0	3.00	1.5	2.10	2.4
3.52	1.8	3.95	1.8	3.95	1.3	3.35	3.0	2.90	1.5
----	----	----	----	----	----	----	----	3.49	4.0
3.65-3.75	18-22	3.60-3.70	15-25	4.25-4.55	3.5-8.5	2.40-2.70	4-5.5	3.15-3.35	9.5-13.5
4.20-4.40	25-37	4.20-4.60*	13-18	3.40-3.60*	10-15	3.30-3.70	13-18	4.15-4.35	40-50
4.10-4.30	45-60	4.10-4.20*	45-60	3.85-4.15*	40-45	4.10-4.30	40-50	4.60-4.80	30-40
4.25-4.55	80-100	4.20-4.50*	80-100	4.25-4.45*	90-110	4.35-4.55	70-90	4.15-4.45	60-85
4.25-4.65	90-110	4.20-4.60*	75-100	4.20-4.45*	90-110	4.20-4.60	70-95	4.25-4.65	85-110
4.75	***	4.75	***	4.75	***	4.75	***	4.75	***

4.90	44	4.90	44	4.90	44	4.90	44	4.90	44

Cell A6 (16.5;40.5)		Cell A7 (17.5;40.5)		Cell A8 (18.5;40.5)		Cell A9 (19.5;40.5)		Cell B-2 (8.5,39.5)	
Vs	h	Vs	h	Vs	h	Vs	h	Vs	h
(km)	(km)	(km/s)	(km)	(km/s)	(km)	(km/s)	(km)	(km/s)	(km)
----	----	----	----	0.00	0.35	----	----	----	----
1.50	1.1	2.25	4.6	2.25	2.45	1.85	0.8	1.85	2.0
2.10	2.4	3.06	2.9	2.60	1.9	1.95	4.2	2.66	1.0
2.90	1.5	----	----	3.03	2.3	3.50	3	2.89	0.8
3.49	4.0	----	----	----	----	----	----	3.35	0.7
2.90-3.30	8-13	3.05-3.15	12-14	3.25-3.35	19-21	3.70-4.10	5.5-7.5	3.35-3.45	11-12
4.05-4.25	35-45	4.05-4.15	18-26	4.55-4.65	30-50	3.35-3.65	15.5-22.5	4.70-4.80	15-20
4.65-4.80	30-45	4.55-4.65	50-65	4.15-4.45	30-40	4.45-4.65	45-60	4.10-4.30	45-60
4.15-4.55	60-85	4.35-4.55	80-100	4.35-4.65	90-105	4.35-4.55	100-120	4.15-4.45	37.5-72.5
4.35-4.65	90-110	4.20-4.60	60-80	4.20-4.60	85-105	4.25-4.55	90-110	4.15-4.45	90-110
4.75	***	4.75	***	4.75	***	4.75	***	4.75	***
4.90	44	4.90	44	4.90	44	4.90	44	4.90	44

CellB-1 (9.5,39.5)		Cell B0 (10.5,39.5)		Cell B1 (11.5;39.5)		Cell B2 (12.5;39.5)		Cell B3 (13.5;39.5)	
Vs	h	Vs	h	Vs	h	Vs	h	Vs	h
(km)	(km)	(km/s)	(km)	(km/s)	(km)	(km/s)	(km)	(km/s)	(km)
----	----	0.00	2.3	0.00	3.0	0.00	3.0	0.00	3.0
1.85	1.5	1.16	0.7	1.20	0.7	1.20	0.7	1.20	0.7
2.78	1.5	3.01	2.0	3.45	1.0	3.45	1.0	3.45	1.0
2.89	0.5	3.12	2.0	3.95	2.0	3.95	2.0	3.95	2.0
3.35	1.5	3.24	1.0	----	----	----	----	----	----
2.60-3.00	4-5	3.75-3.95	10-14	3.65-4.15	5.5-8.5	3.85-4.25	7.5-10.5	3.60-4.00	9-13
3.80-4.00	9-11.5	4.25-4.35	47.5-60	3.50-3.70*	11-15	3.00-3.30*	6.5-9.5	2.90-3.30*	6.5-9.5
4.30-4.50	40-55	4.10-4.40	65-80	4.15-4.25*	53.5-67.5	4.10-4.30*	55-70	4.10-4.30*	50-06
3.80-4.20	45-60	4.20-4.60	65-80	4.20-4.40*	80-100	4.25-4.35*	70-90	4.20-4.40*	70-90
4.25-4.45	135-160	4.00-4.80	60-80	4.20-4.60*	60-90	4.20-4.60*	90-120	4.20-4.60*	95-120
4.75	***	4.75	***	4.75	***	4.75	***	4.75	***
4.90	44	4.90	44	4.90	44	4.90	44	4.90	44

Cell B4 (14.5;39.5)		Cell B5 (15.5;39.5)		Cell B6 (16.5;39.5)		Cell B7 (17.5;39.5)		Cell B8 (18.5;39.5)	
Vs	h	Vs	h	Vs	h	Vs	h	Vs	h
(km)	(km)	(km/s)	(km)	(km/s)	(km)	(km/s)	(km)	(km/s)	(km)
0.00	2.5	0.00	0.9	----	----	0.00	1.5	0.00	1
1.30	0.5	1.15	2.1	2.45	4.0	2.90	1.5	2.25	3.1
3.45	2.0	2.90	3.0	2.80	9.0	3.52	2	3.05	3.9
3.95	1.5	----	----	----	----	----	----	----	----
3.20-3.40	15-19	3.45-3.55	14-22	3.35-3.45	8-11	2.55-.265	5-7	3.20-3.30	17-19.5
4.10-4.30*	30-45	3.70-4.10	10.5-15.5	3.50-3.90	15-20	3.05-3.35	11-17	4.45-4.75	40-50
3.90-4.20*	30-45	4.25-4.35	50-60	4.20-4.60	30-45	4.00-4.40	30-45	4.50-4.90	35-47.5
4.20-4.60*	70-90	4.50-4.70	70-90	4.45-4.75	85-110	4.50-4.70	90-110	4.35-4.65	70-90
4.20-4.60*	90-110	4.20-4.60	90-110	4.25-4.75	60-85	4.20-4.60	60-85	4.25-4.75	90-120
4.75	***	4.75	***	4.75	***	4.75	***	4.75	***
4.90	44	4.90	44	4.90	44	4.90	44	4.90	44

Cell B9 (19.5;39.5)		Cell C1 (11.5;38.5)		Cell C2 (12.5;38.5)		Cell C3 (13.5;38.5)		Cell C4 (14.5;38.5)	
Vs	h	Vs	h	Vs	h	Vs	h	Vs	h
(km)	(km)	(km/s)	(km)	(km/s)	(km)	(km/s)	(km)	(km/s)	(km)
0.00	1.7	0.00	1.5	0.00	1.0	0.00	2.0	0.00	2.36
2.30	3.3	1.10	0.9	1.11	1.5	1.10	0.4	1.00	0.04
3.00	2	2.31	0.4	2.20	0.4	2.31	0.4	2.31	0.4
----	----	2.90	4.2	2.63	3.6	2.90	3.2	3.55	3.20
3.35-3.45	22-26	3.45-3.75	9-15	3.65-3.85	15-20	3.25-3.35	11.5-14.5	2.95-3.15	11-15
4.55-4.65	50-60	4.05-4.25	24-40	4.05-4.15	20-27.5	4.05-4.15	12-18	3.65-4.05	12-18
4.15-4.55	50-60	4.35-4.55	45-60	4.35-4.45	45-60	4.10-4.30	30-45	3.95-4.15	30-45
4.60-4.80	60-80	4.15-4.45	60-80	4.30-4.50	60-80	4.30-4.50	70-90	4.45-4.65	60-80
4.10-43.0	80-100	4.25-4.65	85-110	4.20-4.60	75-100	4.20-4.60	90-110	4.20-4.60	100-120
4.75	***	4.75	***	4.75	***	4.75	***	4.75	***
4.90	44	4.90	44	4.90	44	4.90	44	4.90	44

Cell C5 (15.5,38.5)		Cell C6 (16.5;38.5)		Cell C7 (17.5;38.5)		Cell C8 (18.5;38.5)		Cell C9 (19.5;38.5)	
Vs	h	Vs	h	Vs	h	Vs	h	Vs	h
(km)	(km)	(km/s)	(km)	(km/s)	(km)	(km/s)	(km)	(km/s)	(km)
0.00	1.0	----	----	0.00	2.4	0.00	2.9	0.00	2.8
2.60	2.0	2.45	3.8	2.10	2.1	2.25	1.2	2.02	1.2
----	----	2.74	1.0	2.25	0.7	2.35	1.1	----	----
----	----	----	----	3.25	1.8	3.32	2.8	----	----
2.85-2.95	12.5-15.5	3.50-3.70	11-17	3.15-3.25	16-21	3.15-3.35	17-23	2.85-3.15	9-15
3.80-4.00	22.5-31.5	3.85-4.05	12-18	4.15-4.35	23.5-33.5	4.30-4.70	30-40	2.80-3.20	10-14.5
4.45-4.75	45-60	4.35-4.65	30-45	4.65-4.80	30-45	4.25-4.75	30-40	4.25-4.45	30-45
4-40-4.60	90-110	4.55-4.75	90-110	4.35-4.65	80-100	4.25-4.75	80-100	4.50-4.70	90-110
4.55-4.85	70-90	4.20-4.60	70-90	4.25-4.65	60-80	4.25-4.75	90-110	4.25-4.65	100-120
4.75	***	4.75	***	4.75	***	4.75	***	4.75	***
4.90	44	4.90	44	4.90	44	4.90	44	4.90	44

Cell D1 (11.5;37.5)		Cell D2 (12.5;37.5)		Cell D3 (13.5;37.5)		Cell D4 (14.5,37.5)		Cell D5 (15.5;37.5)	
Vs	h	Vs	h	Vs	h	Vs	h	Vs	h
(km)	(km)	(km/s)	(km)	(km/s)	(km)	(km/s)	(km)	(km/s)	(km)
0.00	0.6	0.00	0.5	----	----	----	----	0.00	1.5
1.73	2.5	1.85	2.5	1.73	2.5	1.73	3.0	2.22	2.4
2.90	2.0	2.65	2.0	2.60	2.5	2.60	2.0	2.31	1.3
3.40	4.4	2.89	1.0	2.90	5.0	2.90	5.0	3.15	1.8
2.95-3.25	4.5-5.5	3.45-3.75	13-19	3.45-3.65	13-19	3.45-3.55	10-15	3.05-3.15	13.5-14.5
3.95-4.05	21.5-25.5	3.90-4.30	12-18	4.15-4.45	30-40	4.25-4.35	30-40	4.25-4.35	30-40
4.55-4.65	20-30	4.45-4.55	30-45	4.25-4.75	30-45	4.20-4.60	30-45	4.30-4.60	40-60
4.35-4.45	100-120	4.35-4.45	70-90	4.20-4.60	70-110	4.25-4.65	80-100	4.30-4.60	90-110
4.35-4.45	60-90	4.25-4.55	90-110	4.25-4.75	60-80	4.25-4.75	60.80	4.50-4.75	90-110
4.75	***	4.75	***	4.75	***	4.75	***	4.75	***
4.90	44	4.90	44	4.90	44	4.90	44	4.90	44

Cell D6 (16.5;37.5)		Cell D7 (17.5;37.5)		Cell D8 (18.5;37.5)		Cell D9 (19.5,37.5)	
Vs	h	Vs	h	Vs	h	Vs	h
(km)	(km)	(km/s)	(km)	(km/s)	(km)	(km/s)	(km)
0.00	2.7	0.00	3.1	0.00	2.9	0.00	2.9
2.25	1.4	2.08	0.9	2.25	1.2	2.25	1.2
2.31	1.1	2.22	0.2	2.31	1.1	2.31	1.1
3.32	2.8	2.31	1.1	3.31	2.8	3.31	2.8
----	----	3.31	2.7	----	----	----	----
2.75-2.95	7-11	3.15-3.25	15.5-16.5	2.95-3.05	12-15	2.85-3.25	5-7
3.90-4.10	20-30	4.35-4.45	30-45	4.15-4.45	30-40	3.15-3.45	13-19
4.35-4.65	45-60	4.30-4.60	30-45	4.45-4.75	30-42.5	4.45-4.75	40-50
4.60-4.80	60-80	4.45-4.75	80-100	4.40-4.70	80-100	4.50-4.70	80-100
4.25-4.65	80-100	4.00-4.50	60-80	4.25-4.55	70-90	4.25-4.65	85-110
4.75	***	4.75	***	4.75	***	4.75	***
4.90	44	4.90	44	4.90	44	4.90	44

Cell C5 (15.5,38.5)		Cell C6 (16.5;38.5)		Cell C7 (17.5;38.5)		Cell C8 (18.5;38.5)		Cell C9 (19.5;38.5)	
Vs	h	Vs	h	Vs	h	Vs	h	Vs	h
(km)	(km)	(km/s)	(km)	(km/s)	(km)	(km/s)	(km)	(km/s)	(km)
0.00	1.0	----	----	0.00	2.4	0.00	2.9	0.00	2.8
2.60	2.0	2.45	3.8	2.10	2.1	2.25	1.2	2.02	1.2
----	----	2.74	1.0	2.25	0.7	2.35	1.1	----	----
----	----	----	----	3.25	1.8	3.32	2.8	----	----
2.85-2.95	12.5-15.5	3.50-3.70	11-17	3.15-3.25	16-21	3.15-3.35	17-23	2.85-3.10	9-15
3.80-4.00	22.5-31.5	3.85-4.05	12-18	4.15-4.35	23.5-33.5	4.30-4.70	30-40	2.80-3.20	10-14.5
4.45-4.75	45-60	4.35-4.65	30-45	4.65-4.80	30-45	4.25-4.75	30-40	4.25-4.45	30-45
4-40-4.60	90-110	4.57-4.75	90-110	4.35-4.65	80-100	4.25-4.75	80-100	4.50-4.70	90-110
4.55-4.85	70-90	4.20-4.60	70-90	4.25-4.65	60-80	4.25-4.75	90-110	4.25-4.60	100-120
4.75	***	4.75	***	4.75	***	4.75	***	4.75	***
4.90	44	4.90	44	4.90	44	4.90	44	4.90	44

Cell D1 (11.5;37.5)		Cell D2 (12.5;37.5)		Cell D3 (13.5;37.5)		Cell D4 (14.5,37.5)		Cell D5 (15.5;37.5)	
Vs	h	Vs	h	Vs	h	Vs	h	Vs	h
(km)	(km)	(km/s)	(km)	(km/s)	(km)	(km/s)	(km)	(km/s)	(km)
0.00	0.6	0.00	0.5	----	----	----	----	0.00	1.5
1.73	2.5	1.85	2.5	1.73	2.5	1.73	3.0	2.22	2.4
2.90	2.0	2.65	2.0	2.60	2.5	2.60	2.0	2.31	1.3
3.40	4.4	2.89	1.0	2.90	5.0	2.90	5.0	3.15	1.8
2.95-3.25	4.5-5.5	3.45-3.75	13-19	3.45-3.65	13-19	3.45-3.55	10-15	3.05-3.15	13.5-14.5
3.95-4.05	21.5-25.5	3.90-4.30	12-18	4.15-4.45	30-40	4.25-4.35	30-40	4.25-4.35	30-40
4.55-4.65	20-30	4.45-4.55	30-45	4.25-4.75	30-45	4.20-4.60	30-45	4.30-4.60	40-60
4.35-4.45	100-120	4.35-4.45	70-90	4.20-4.60	70-110	4.25-4.65	80-100	4.30-4.60	90-110
4.35-4.45	60-90	4.25-4.55	90-110	4.25-4.75	60-80	4.25-4.75	60.80	4.50-4.75	90-110
4.75	***	4.75	***	4.75	***	4.75	***	4.75	***
4.90	44	4.90	44	4.90	44	4.90	44	4.90	44

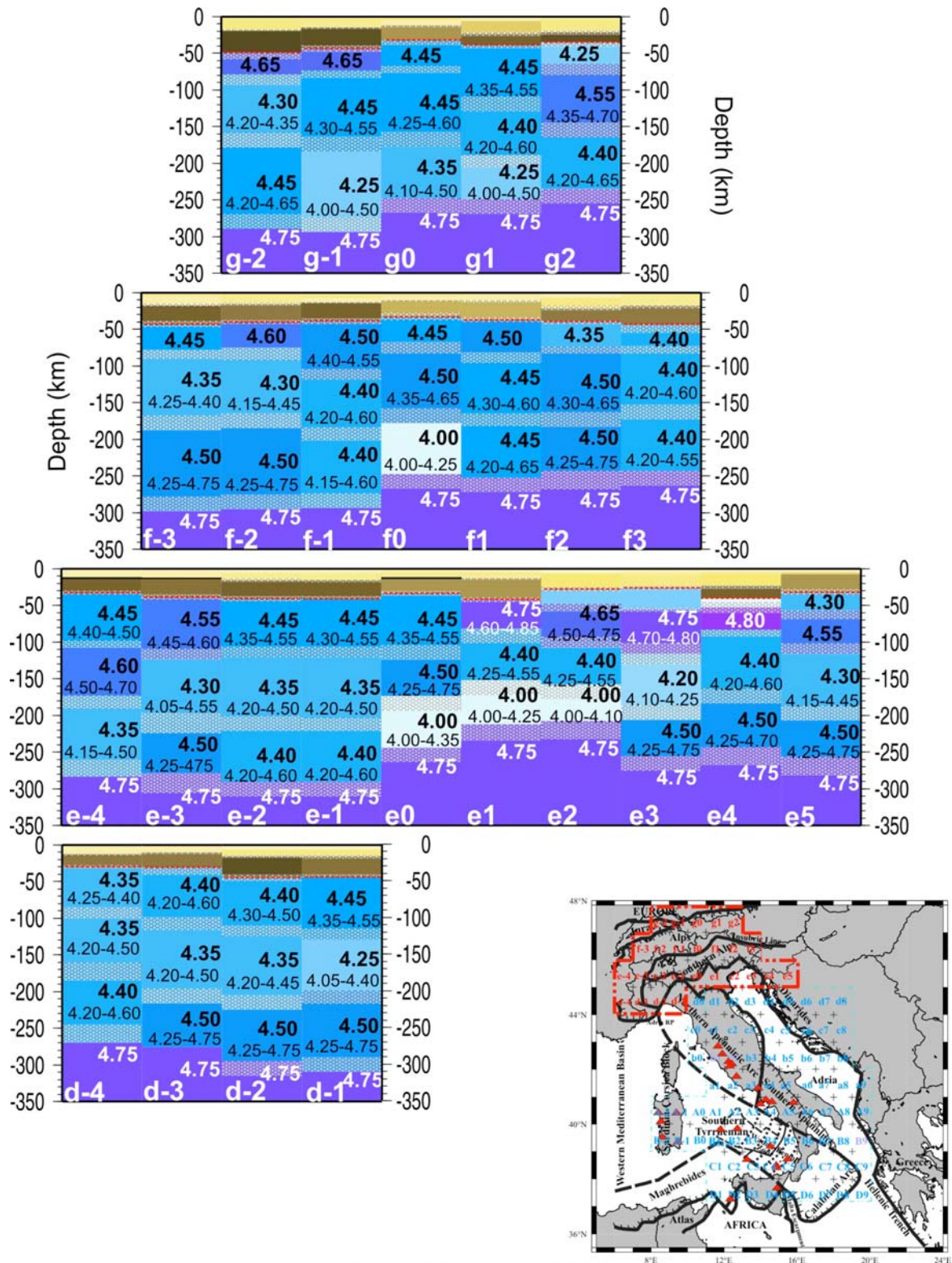| Cell D6 (16.5;37.5)		Cell D7 (17.5;37.5)		Cell D8 (18.5;37.5)		Cell D9 (19.5,37.5)	
Vs	h	Vs	h	Vs	h	Vs	h
(km)	(km)	(km/s)	(km)	(km/s)	(km)	(km/s)	(km)
0.00	2.7	0.00	3.1	0.00	2.9	0.00	2.9
2.25	1.4	2.08	0.9	2.25	1.2	2.25	1.2
2.31	1.1	2.22	0.2	2.31	1.1	2.31	1.1
3.32	2.8	2.31	1.1	3.31	2.8	3.31	2.8
----	----	3.31	2.7	----	----	----	----
2.75-2.95	7-11	3.15-3.25	15.5-16.5	2.95-3.05	12-15	2.85-3.25	5-7
3.90-4.10	20-30	4.35-4.45	30-45	4.15-4.45	30-40	3.15-3.45	13-19
4.35-4.65	45-60	4.30-4.60	30-45	4.45-4.75	30-42.5	4.45-4.75	40-50
4.60-4.80	60-80	4.45-4.75	80-100	4.40-4.70	80-100	4.50-4.70	80-100
4.25-4.65	80-100	4.00-4.50	60-80	4.25-4.55	70-90	4.25-4.65	85-110
4.75	***	4.75	***	4.75	***	4.75	***
4.90	44	4.90	44	4.90	44	4.90	44

Fig. II a: Structural models of the chosen solution, indicated by red line in Fig. 3.13b. For each cell of the study area, indicated by the red dashed line in the insert, the velocity value and its range of variability is specified for the mantle layers down to the investigated 350 km. The thickness range of variability is marked by the shadowed area. The boundaries between layers can well be transition zones in their own right.
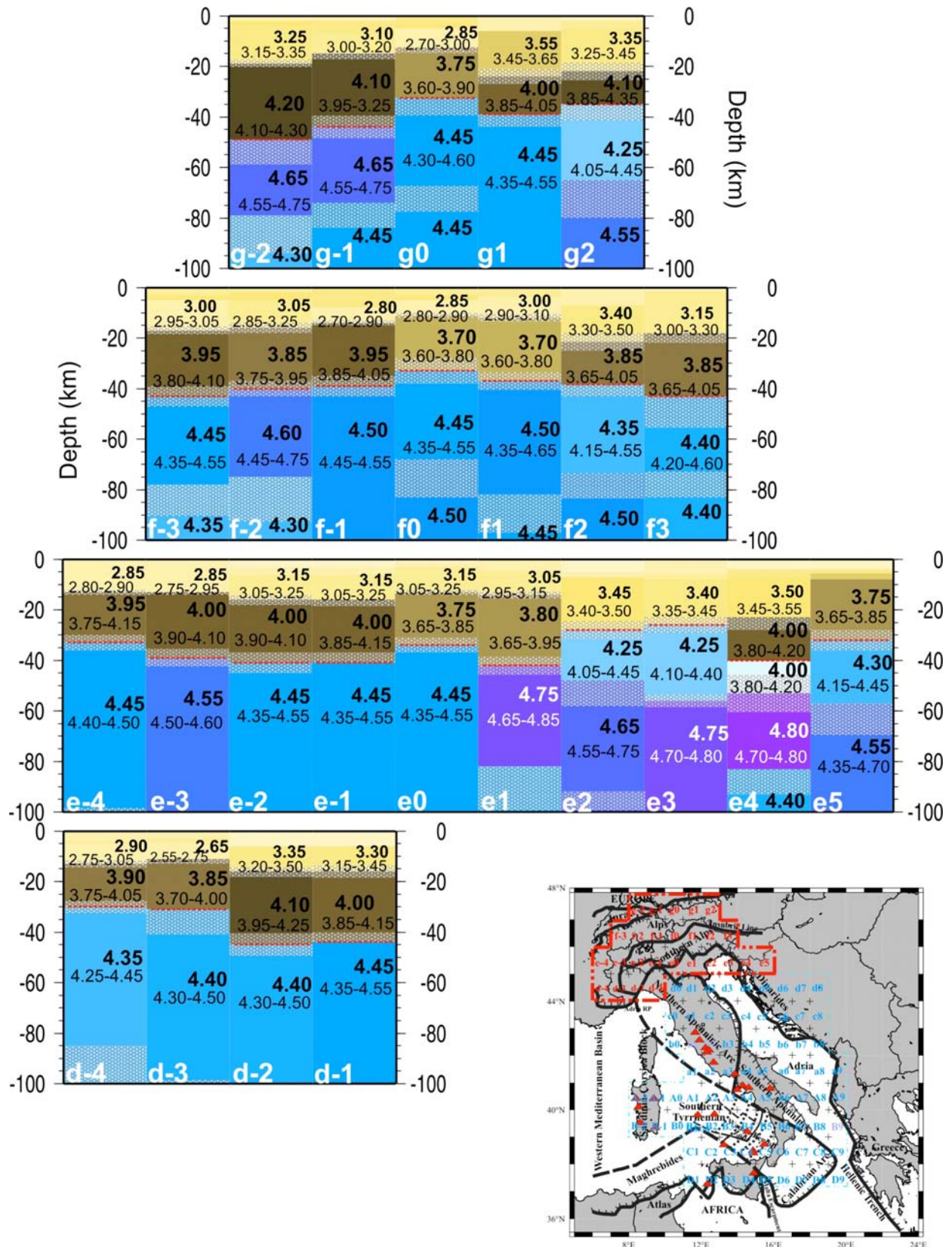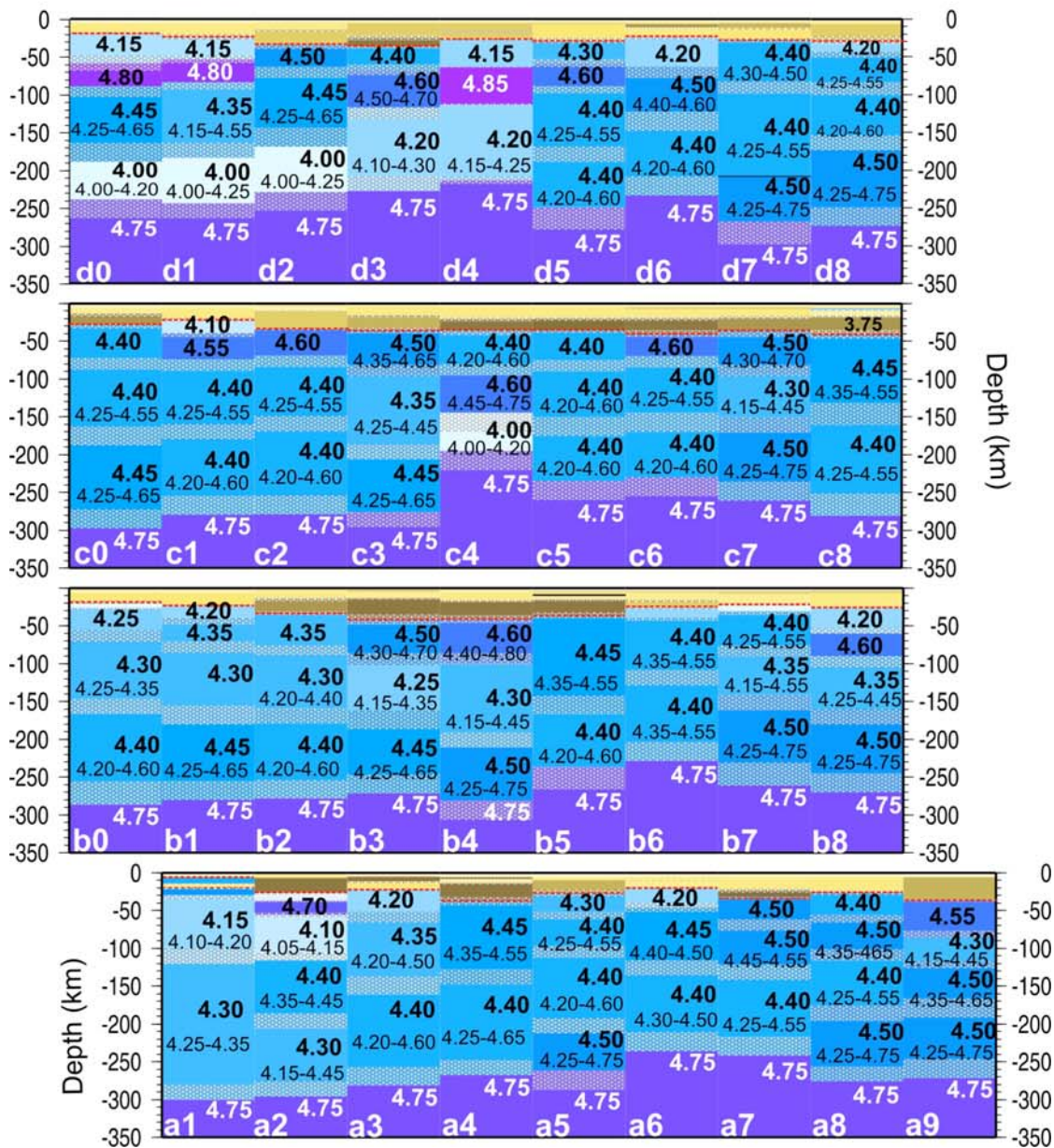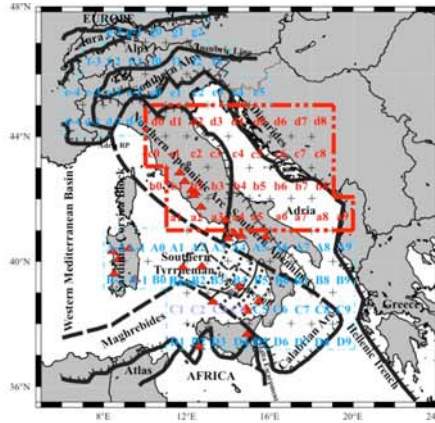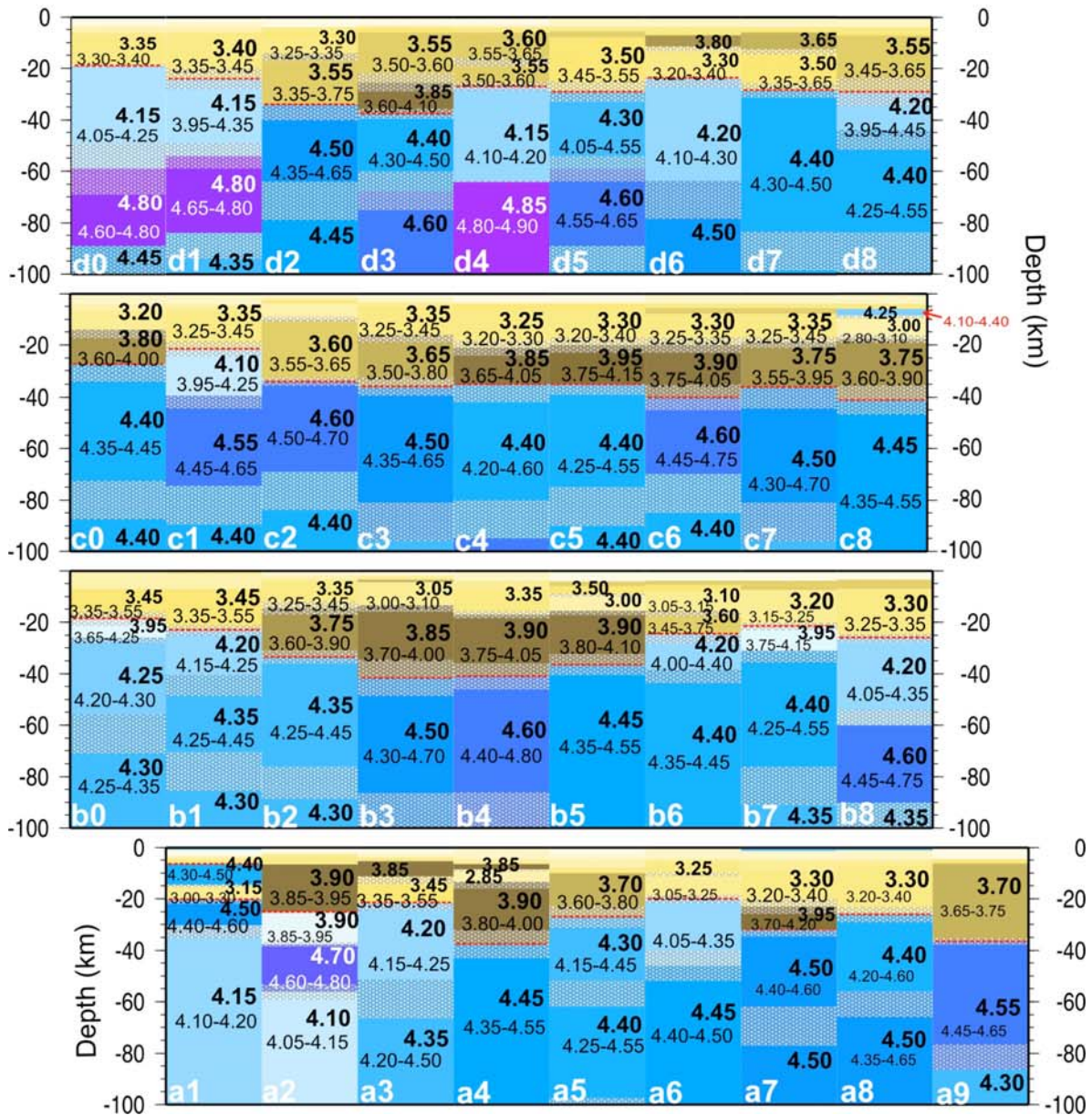
Fig. IIb: Structural models of the chosen solution, indicated by red line in Fig. 3.13b. For each cell of the study area, indicated by the red dashed line in the insert, the velocity value and its range of variability is specified for the crust and upper mantle layers down to 100 km. The thickness range of variability is marked by the shadowed area. The boundaries between layers can well be transition zones in their own right.
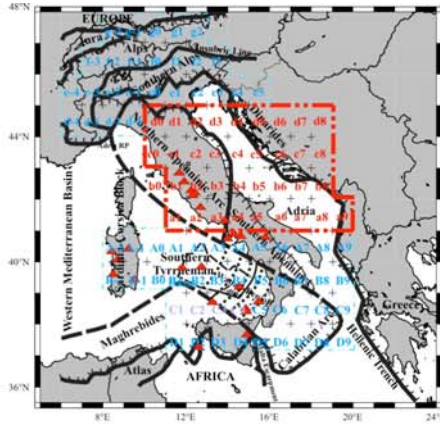
Fig. IIc: Structural models of the chosen solution, indicated by red line in Fig. 3.13b. For each cell of the study area, indicated by the red dashed line in the insert, the velocity value and its range of variability is specified for the mantle layers down to the investigated 350 km. The thickness range of variability is marked by the shadowed area. The boundaries between layers can well be transition zones in their own right.
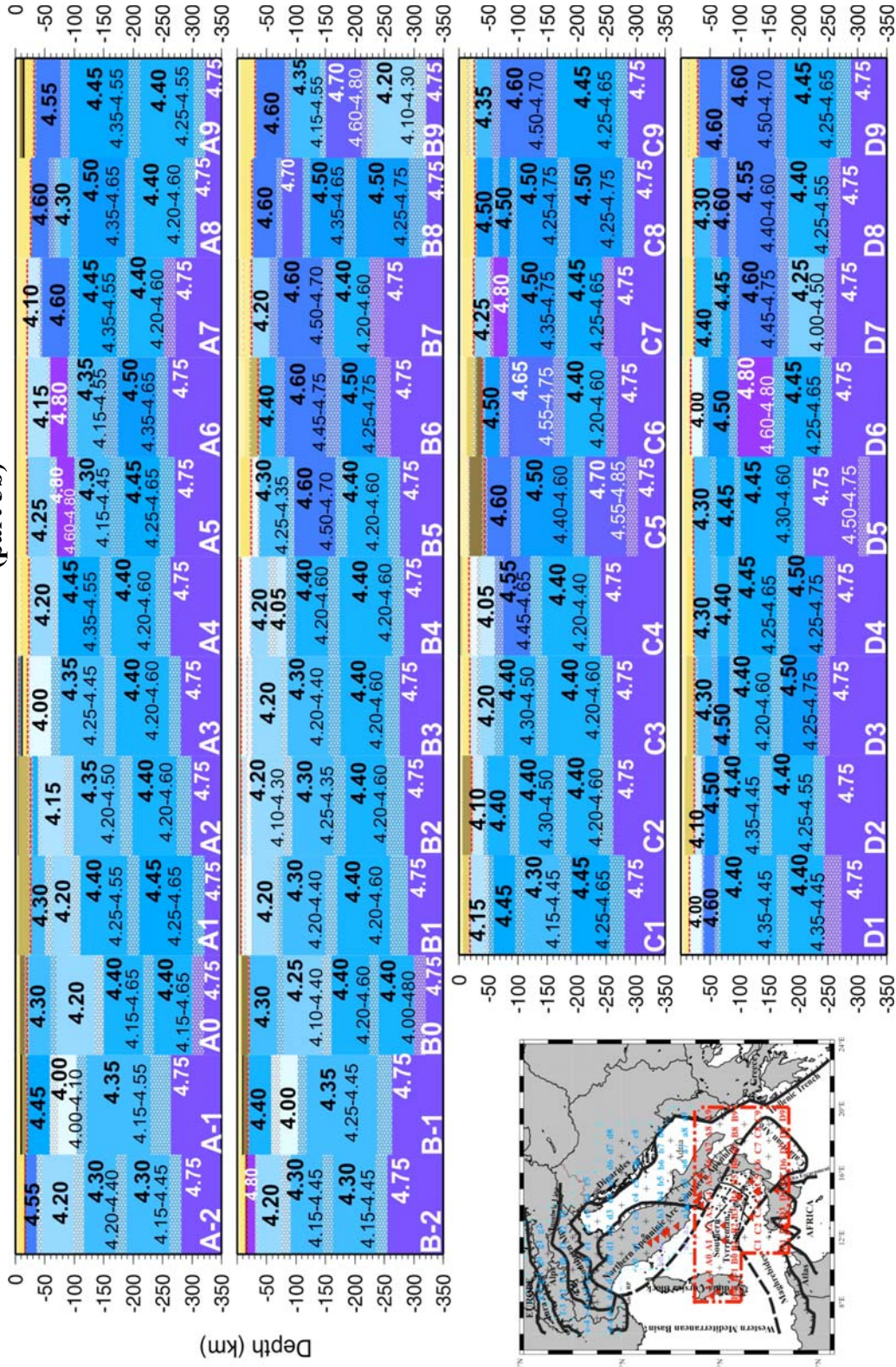
Fig. IId: Structural models of the chosen solution, indicated by red line in Fig. 3.1b. For each cell of the study area, indicated by the red dashed line in the insert, the velocity value and its range of variability is specified for the crust and upper mantle layers down to 100 km. The thickness range of variability is marked by the shadowed area. The boundaries between layers can well be transition zones in their own right.
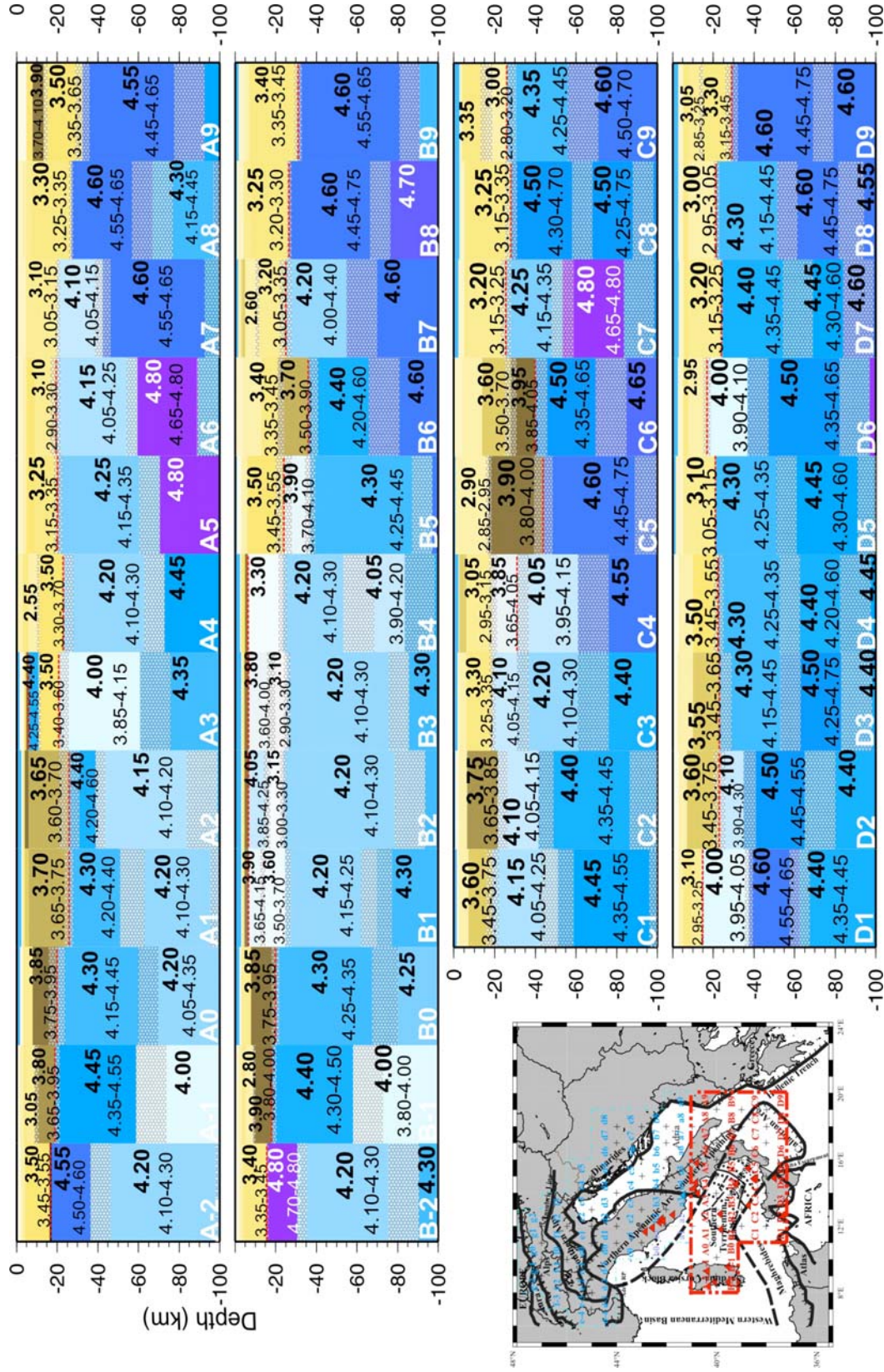
APPENDIX II
(part 3b)

Fig. II e: Structural models of the chosen solution, indicated by red line in Fig. 3.13a. For each cell of the study area, indicated by the red dashed line in Fig. 3.13a. For each cell of the study area, the velocity value and its range of variability is specified for the mantle layers down to the investigated 350 km. The thickness range of variability is marked by the shadowed area.

Fig. II f: Structural models of the chosen solution, indicated by the red dashed line in Fig. 3.13a. For each cell of the study area, indicated by red line in the insert, the velocity value and its range of variability is specified for the crust and upper mantle layers down to 100 km. The thickness range of variability is marked by the shadowed area.